

Elena Dal Martello

**Impurity distribution and
reduction behaviour of quartz
in the production of high purity
silicon**

Thesis for the degree of Philosophiae Doctor

Trondheim, September 2012

Norwegian University of Science and Technology
Faculty of Natural Sciences and Technology
Department of Materials Science and Engineering



NTNU

Norwegian University of
Science and Technology

NTNU

Norwegian University of Science and Technology

Thesis for the degree of philosophiae doctor

Faculty of Natural Sciences and Technology
Department of Materials Science and Engineering

© Elena Dal Martello

ISBN-nummer: 978-82-471-3658-4 (printed version)

ISBN-nummer: 978-82-471-3659-1 (electronic version)

ISSN-nummer: 1503-8181

Doctoral theses at NTNU, 2012:156

Printed by NTNU-trykk

To Gabriella and Lars

Preface

The work presented in this thesis has been carried out primarily at the Department of Materials Science and Engineering (Norwegian University of Science and Technology, NTNU) during the period from March 2009 to June 2012. September to December 2011 was spent at the School of Material Science and Engineering at the University of New South Wales in Sydney, Australia.

The thesis focuses on quartz feedstock for silicon solar cells and on the production of silicon via the metallurgical route. The thesis consists of two parts: the first part introduces to the topic and background literature, describes the experimental work and discusses the findings from an overall perspective. The second part consists of published/submitted articles which are the results of the experimental work that has been carried out.

Trondheim, June 2012

Elena Dal Martello

Acknowledgments

The completion of this PhD work has been possible thanks to the important contribution of many people. First of all I would like to thank my supervisors Gabriella and Lars.

Thanks Gabriella for always supporting my ideas, boosting my positivity of seeing things and passion of trying things. Thanks for having pushed me to the limits of work efficiency and motivation, I know my limits now 😊. Thanks for the very productive and enjoyable meetings. Thanks for contributing actively to all the papers. Thanks for giving me the opportunity to travel, I learned to look at things with a different perspective. Thanks for introducing me to the right people, all of them gave an important contribution to the research work. And.. thanks for being the perfect confident 😊😊.

Thanks Lars for your solid support and strong presence throughout all my PhD. Thanks for teaching me to be methodic and careful. Thanks for your selected questions during our meetings: you stimulated my creativity of solving problems. Thanks for the warm welcome, and thanks for caring of my situation during my difficult moments 😊.

I would like to thanks my co-supervisor Rune, for having introduced me to the complicated world of geology and for the interesting discussions on the behavior of the impurities in quartz.

A special thanks to Ola. Thanks for your intuitions and long discussions on the reaction mechanisms. You gave me an important direction in my PhD work.

Thanks Kai for contributing with the thermodynamic simulations and for the interesting and funny discussions ☺. Thanks Merete for being always available to answer my doubts. Thanks Sean for your valuable contribution in the beginning of my PhD, for your wise vision of life and for teasing me all the time ☺. Thanks Oleg, Guangqing, Xing, Emily and John: you have been the perfect combination of theoretical and technical support during my staying at UNSW. In particular Oleg: thanks for your warm welcome.

There are many technicians, PhDs, professors and students which contributed with technical help and productive discussions. Thanks Marisa, Rolf Arne, Gauthe, Morten, Kristian, Vegar, Edin, Kurt, Halvard, Arjan, Eli, Mari, Lars, Egil, Jeff, Bjørn, Chiara, Nelia, Tøril, Julien, Syverin, Kjell, Anne Maritt, Nicholas, Røar, Shawn, Korneliussen, Per Anders, Kari and Alexander. Thanks to the sweet secretaries Elin, Hilde and thanks to Stuart King.

Thanks to my sweet office mate Ingvild ☺ for our not-related to work discussions ☺ and for talking to me in Norwegian ☺.

There are then people that have supported me during these three years, and there are people that I met for a short time and that I hope to see again, and people that I met too early or too late, or just in time. I would like to thank all of them because they make me happy and make me experience an explosion of emotions. Thanks Pål, Eirik Antoine, Delphine, mine "chlorine-venniner" Ragnhild og Seher, Chiara, Maani, Albert, Raymond, John, Orestis, Thomáš, Matthias, Ralf, Julien, and my family.

List of Publications

The following journal articles are included in the second part:

Article I:

E. Dal Martello, G. Tranell, O. Raaness, L. Arnberg, ”*Combined XRD and XRF Technique for the quantification of the mass balance in a Si carbothermic production experiment*”, ISIJ International, **51**(9): 1492-1496, 2011.

Contributions

E. Dal Martello: experimental work, understanding of the experimental results, developing of the method, paper writing

G. Tranell: defining of the experimental setting, discussion of the experimental results

O. Raaness: discussion of the experimental results

L. Arnberg: discussion of the experimental results

Article II:

E. Dal Martello, G. Tranell, S. Gaal, O. Raaness, K. Tang, L. Arnberg, “*Study of pellets and lumps as raw materials in silicon production*”, Metallurgical and Materials Transactions B, **42**(5): 939-950, 2011.

Contributions

E. Dal Martello: experimental work, understanding of the experimental results, paper writing

G. Tranell: defining of the experimental setting, discussion of the experimental results

S. Gaal: defining of the experimental setting, discussion of the experimental results

O. Raaness: discussion of the experimental results

K. Tang: discussion of the experimental results, thermodynamic simulations

L. Arnberg: discussion of the experimental results

Article III:

E. Dal Martello, S. Bernardis, R.B. Larsen, G. Tranell, M.di Sabatino, L. Arnberg , " *Electrical fragmentation as novel route for the refinement of quartz raw materials for trace mineral impurities*", Powder Technology, **224**: 209-216, 2012.

Contributions

E. Dal Martello: defining of the experimental setting, experimental work, understanding of the experimental results, paper writing

S.Bernardis: defining of the experimental set-up

R. B. Larsen: discussion of the experimental results

G. Tranell: defining of the experimental setting, discussion of the experimental results

M di Sabatino : discussion of the experimental results

L. Arnberg: discussion of the experimental results

Article IV:

E. Dal Martello, G. Tranell, O. Ostrovski, G. Zhang, K. Tang, Ola Raaness, R.B. Larsen, P. Koshy " *Trace elements in the silicon furnace. Part 1: Behaviour of impurities in quartz during reduction*"; Metallurgical and Materials Transactions B, In press.

Contributions

E. Dal Martello: defining of the experimental setting, experimental work, understanding of the experimental results, paper writing

G. Tranell: defining of the experimental setting, discussion of the experimental results

O. Ostrovski: defining of the experimental setting, discussion of the experimental results

G.Zhang: defining of the experimental setting, discussion of the experimental results

K. Tang: discussion of the experimental results

O. Raaness: discussion of the experimental results

R.B.Larsen: discussion of the experimental results

P. Koshy: analytical work

Article V:

E. Dal Martello, G. Tranell, O. Ostrovski, G. Zhang, K. Tang, Ola Raaness, R.B. Larsen, P. Koshy “*Analysis of condensate in carbothermal reduction of quartz*”; Metallurgical and Materials Transactions B, In press.

Contributions

E. Dal Martello: defining of the experimental setting, experimental work, understanding of the experimental results, paper writing

G. Tranell: defining of the experimental setting, discussion of the experimental results

O. Ostrovski: defining of the experimental setting, discussion of the experimental results

G.Zhang: defining of the experimental setting, discussion of the experimental results

K. Tang: discussion of the experimental results, thermodynamic simulations

O. Raaness: discussion of the experimental results

R.B.Larsen: discussion of the experimental results

P. Koshy: analytical work

In addition to the included journal articles, the work has been presented in the following conferences:

E. Dal Martello and G. Tranell ”Effect of the raw material mixture in carbothermic silicon production experiments” Oral presentation at *TMS 2011 The Minerals, Metals & Materials Society*, San Diego, California, 27th February- 3rd March 2011.

E. Dal Martello, G. Tranell, S.Gaal, O. S. Raaness, M. Tangstad, R.Larsen, L. Arnberg "Study of pellets and lumps as raw material in Silicon production” Oral presentation at *CSSC 4th International Workshop on Science and Technology of Crystalline Silicon Solar Cells*, Taipei, Taiwan 27-29 October 2010.

E.Dal Martello, G.Tranell, O.Ostrovski, G.Zhang, O.Raaness “Impurities distribution between SiO(g) and reactant materials in a silicon furnace” oral

presentation at *TMS 2012 The Minerals, Metals & Materials Society*, Orlando, Florida 12-15th March 2012.

E. Dal Martello, G. Tranell, R.Larsen, O. Ostrovski, G. Zhang, O. Raaness, K. Tang “Study of removal of impurities in quartz silicon feedstock by means of selective fragmentation and heating in reducing atmosphere”
Poster at *Technoport Sharing Possibilities*, Trondheim 16-18 April 2012.

Abstract

The production of solar grade silicon is based on the use of expensive high purity carbon and quartz feedstock as well as various silicon refining techniques. Impurities in the feedstock materials enter the silicon during the carbothermic reduction of quartz. The knowledge of the impurity distribution/removal in the feedstock and in the carbothermic reduction process is necessary for targeting less pure and cheaper raw materials.

The aim of the present study is to investigate the impurity distribution and behavior in quartz feedstock throughout the metallurgical production of silicon; in particular four areas were investigated: 1) removal of mineral inclusions from quartz prior to carbothermic reduction by means of selective fragmentation; 2) effect of pellets, lumps on the silicon production reactions; 3) high temperature properties of quartz under reducing conditions; 4) distribution of contaminants from quartz to the gas phase during quartz reduction. Pellets and lumpy charge, hydrothermal quartz and quartzite were studied.

Because of the complex objective of this study, several experimental techniques as well as characterization methods were used: 1) a novel refining route for hydrothermal quartz based on electrical fragmentation, was tested in a laboratory scale to investigate the advantages of using electric fragmentation in terms of cracks distribution, mineral liberation and fragment morphology; 2) mixtures of quartz and silicon carbide in form of pellets or lumps were heated to 2000 °C for 1 h in graphite crucibles in an inductive furnace to compare the properties of pellets and lumps during the silicon production reaction; 3) quartz pieces were heated in CO(g) atmosphere in a sessile drop experiment to study the ability of different types of quartz to produce SiO(g); 4) mixtures of quartz and silicon and quartz and silicon carbide, in form of lumps or pellets, were heated in graphite crucibles to 1650 °C and 1850 °C to investigate which gaseous compounds form other than SiO(g) during quartz reduction, and to which extent.

EPMA was used to investigate the morphology of the reacted charge, XRD to identify different phases in a mixture, XRF to quantify elements in a mixture of phase. ICP-MS was used to investigate the impurity content in the charge and reaction products.

It was observed that electrical fragmentation efficiently liberates mineral inclusions in the quartz matrix, and that the use of an inexpensive separation technique such as sieving is well suited to separate these minerals.

Pellets and lumps behave differently when quartz and silicon carbide are heated to 2000°C in a reducing atmosphere. More silicon is produced with lumps, i.e. quartz reacts faster to SiO(g,) and more SiO(g) is lost when pellets are used.

The rate of formation of SiO(g) is enhanced when the quartz contains cracks and fluid inclusions.

It was found that during quartz reduction gaseous compounds leave the quartz but to various extents: the average measured volatility of B, P, K, Fe, Al, Mn, Zn, Pb is respectively 11 %, 25 %, 26 %, 45 %, 1 %, 38 %, 10 % and 36%. Liquid inclusions, common in lumps of hydrothermal quartz, enhance the distribution of the contaminants to the gas phase. The gaseous compounds which form may be entrapped by the condensation process, circulate in the furnace and eventually end up in the silicon.

List of abbreviations and Symbols

Abbreviations

Eg-Si	Electronic grade silicon
EPMA	Electron probe micro analyzer
ICP-MS	Inductively coupled plasma mass spectrometry
Mg-Si	Metallurgical grade silicon
ppm	Part per million
ppmw	Part per million weight
PTFE	Polytetrafluoroethylene
PV	photovoltaic
SEM	Scanning electron microscope
SoG-Si	Solar grade silicon
Wt%	Weight fraction
XRD	X-ray powder diffraction
XRF	X-ray fluorescence spectroscopy

Symbols

α -quartz	Low temperature quartz
α -SiC	Hexagonal and rhombohedral silicon carbide polytype
β -quartz	High temperature quartz
β -SiC	Cubic silicon carbide polytype
ϵ_r	Relative permittivity [-]

λ	Mean free path [μm]
$m_{\text{el,gasphase}}$	Impurity content by mass in the condensate [ppmw]
$m_{\text{el,chargemix}}$	Impurity content by mass in the charged quartz [ppmw]
ρ	Electrical resistivity [Ωm]
P_{CO}	Partial pressure CO [kPa]
P_{SiO}	Partial pressure SiO [kPa]
Δ	Change in the impurity concentration [%]
3C:SiC	Cubic silicon carbide polytype
6H:SiC	Hexagonal silicon carbide polytype
15R:SiC	Rhombohedral silicon carbide polytype

Table of contents

Preface.....	i
Acknowledgments.....	iii
List of publications.....	v
Abstract	ix
List of Abbreviations and Symbols.....	xi
1 IMPURITIES IN THE METALLURGICAL SOLAR SILICON VALUE CHAIN	1
1.1 Why the metallurgical route?	1
1.2 Why attention to the impurities?	3
1.3 Source of contamination in the silicon production	4
1.4 Aim of the research work	7
2 THEORETICAL BACKGROUND ON QUARTZ AND SILICON PRODUCTION	10
2.1 Production of silicon.....	10
2.1.1 Compounds in the silicon furnace.....	10
2.1.2 Main reactions in the silicon furnace under equilibrium conditions.....	13
2.1.3 High temperature zone: reactions involving SiO ₂ , SiC and Si ..	14
2.1.4 Low temperature zone: reactions involving SiO ₂ and C	16
2.1.5 Low temperature zone: condensation reactions.....	17
2.2 Impurity distribution in a silicon furnace.....	20
2.3 Requirements of quartz in the silicon production	24

2.4	Impurities in quartz.....	26
2.4.1	Structural impurities in quartz	26
2.4.2	Liquid inclusions in quartz.....	28
2.4.3	Mineral inclusions in quartz.....	30
2.5	High temperature properties of quartz	31
2.5.1	Silica polymorphs	31
2.5.2	Crack formation	34
2.5.3	Melted quartz	35
2.5.4	Minerals behavior when heating quartz.....	36
2.6	Diffusion of impurities in quartz.....	37
2.6.1	Diffusion of impurities in crystalline quartz.....	37
2.6.2	Diffusion of impurities in molten quartz	39
2.7	Quartz beneficiation	41
2.7.1	Electric fragmentation.....	42
2.7.2	Beneficiated quartz needs to be milled: mechanical activation of quartz and agglomeration.....	45
3	EXPERIMENTAL SETTING AND ANALYTICAL TECHNIQUES...	46
3.1	Materials	49
3.2	Analytical techniques	50
3.2.1	Electron Probe Micro Analyzer (EPMA)	51
3.2.2	X-ray diffraction (XRD)	51
3.2.3	X-ray fluorescence spectroscopy (XRF).....	51
3.2.4	Inductively Coupled Plasma –Mass Spectrometry (ICP-MS)...	52

3.3	Quartz beneficiation by electrical fragmentation (Experimental set 1).....	53
3.3.1	Method of analysis	55
3.4	Production of silicon from pellets and lumps (Experimental set 2)	55
3.4.1	Method of analysis	58
3.5	Quartz behaviour during heating (Experimental set 3).....	59
3.5.1	Method of analysis	60
3.6	Production of SiO(g) and CO(g) from quartz, silicon carbide and silicon (Experimental set 4)	60
3.6.1	Method of analysis	63
4	DISCUSSION OF RESULTS.....	66
4.1	Removal of mineral inclusions from quartz.....	66
4.1.1	Impurities in mineral inclusions in quartz diffuse out from the mineral to the surrounding quartz matrix when heating quartz.....	66
4.1.2	Mineral inclusions in quartz can be efficiently removed by means of electric fragmentation, sieving and magnetic separation	68
4.2	Effect of pellets and lumps on the silicon producing reactions	71
4.3	High temperature properties of quartz in reducing atmosphere....	76
4.3.1	Effect of pellets and lumps	76
4.3.2	Effect of the quartz morphology	78
4.4	Distribution of contaminants from quartz to the gas phase during quartz reduction.....	80
4.4.1	Gaseous compounds other than SiO(g) form during quartz reduction.....	80

4.4.2	Effect of pellets and lumps	82
4.4.3	Effect of the quartz type.....	83
5	SUGGESTIONS FOR FUTURE WORK.....	86
5.1.1	Further investigations.....	86
5.1.2	New method for charging lumpy quartz	87
5.1.3	New quartz refining route to be used in the pellets route	88
5.1.4	Production of silicon via a carbon-free metallurgical route	88
6	CONCLUSIONS	92
	REFERENCES	94
	ARTICLES	104

1 IMPURITIES IN THE METALLURGICAL SOLAR SILICON VALUE CHAIN

1.1 Why the metallurgical route?

The overall challenge and driving force for the research within the silicon PV industry is to lower the cost of solar electricity through a combination of reduced production cost and/or increased product performance. Over the past decade, the availability, quality and associated cost of silicon feedstock have been some of the most important and debated issues in the silicon-based solar cell industry (Tranell *et al.* 2010).

The Si photovoltaic industry was initially using rejected materials from integrated circuit poly-silicon and single-crystal production, mainly Cz ingot top and tails, pot scrap, and rejected wafers. This arrangement worked well until 1995 when solar electricity demand first exceeded the supply and a shortage of poly-silicon feedstock began to drive up the costs and limit the growth of the silicon PV industry. Many actions could have been taken: (1) maintaining the old route and increasing the capacity, or (Tsujo *et al.* 1998) (2) establish a dedicated solar grade silicon production route, (3) find new ways to use the rejected silicon that was not used. The second option seemed viable, since it enhances the independent growth of the expanding solar silicon market in the 1990', without depending on the price and availability of feedstock to the demand by the electronics industry. Two paths towards achieving solar grade silicon were followed: new and improved chemical route and the metallurgical route involving the direct purification of metallurgical grade silicon by metallurgical and pyrometallurgical processes.

The chemical route comprises the gasification of metallurgical silicon to trichlorosilane, followed by distillation and decomposition of trichlorosilane or mono-silane to pure silicon. Different companies have developed the chemical route: REC, WackerChemie's and Tokuyama Corporation. Many companies worked on the metallurgical production of silicon, including Bluestar/Elkem Solar, Fesil/Evonik, Photosil, Calisolar/Silicor Materials, Dow Chemical, Ferrosolar, Nippon Steel, JFE Steel Corporation, Crystal system, Jaco, Ferroatlantica, Clean silicon, and Norwegian silicon refinery.

The metallurgical route uses metallurgical processes, such as vacuum and plasma refining, slagging, filtering, leaching, etching, with a final stage consisting of a liquid/solid segregation. Silicon with impurities in a range of a few ppmw is produced and is denoted upgraded metallurgical silicon. (SEMI 2012).

The silicon produced by the chemical route is very energy intensive: 180 kWh/kg for the traditional combined MG-Si/Siemens route. The silicon produced by the metallurgical route on the contrary requires 40-50 kWh/kg SoG-Si (Tranell *et al.* 2010).

The purity of electronic grade silicon far exceeds the purity requirements of the PV industry. In addition, with environmental commitments becoming progressively more important, it is problematic that the chemical route produces large amounts of waste, including a mix of environmentally damaging chlorinated compounds (Tranell *et al.* 2010). Together these factors bring the metallurgical route to an advantage from an energy consumption and environmental point of view.

Table 1.1 summarizes the main impurity content in the silicon produced by Bluestar- Elkem Solar, Evonik, Photosil, Ningxia and Shanghai Propower.

Table 1.1- Dopants and metallic impurities in different metallurgically produced SOG-Si (Tranell *et al.* 2010). *= total Fe, Al, Ti and Cu

Company	Bppmw	Pppmw	Total metal
Bluestar/Elkem Solar	0.25	0.63	<1
Fesil/ Evonik	0.5	0.4	NA
Photosil	0.3	1.0	<8*
Ningxia	0.3	0.4-0.6	<1
Shanghai Propower	0.6	0.8	<1

Due to the economic crisis some producers of silicon have terminated their activities. The current approaches for the production of metallurgical solar grade silicon are summarized in Table 1.2. Evonik produces high purity silicon directly by using extremely pure raw materials that are prepared in the form of pellets. The other companies produce conventional metallurgical silicon which is subsequently refined by different refining techniques. The last refining step, common to all the routes, is the directional solidification. Directional solidification is very efficient in removing metal impurities, therefore the major purpose of the other techniques such as slag, plasma and vacuum refining is the removal of B and P from silicon.

Table 1.2- Production-refining of UMG-Si in the world (Tranell *et al.* 2010), (Nichol 2009) and (Sandberg 2012).

Company	Step1	Step 2	Step 3	Step 4
Evonik	SiC production and agglomeration of quartz, carbon black and SiC-fines	MG-Si production	C filtering	Directional solidification
Bluestar/Elkem Solar	Carbothermic MG-Si production	Slag refining	Leaching	Directional solidification
Photosil	Carbothermic MG-Si production	Metallurgical segregation	Plasma purification	Directional solidification
Silicor Materials	Carbothermic MG-Si production	Slag refining	Solvent refining	Directional solidification
Ningxia Yinxing Polycrystalline Silicon Co	Carbothermic MG-Si production	Slag refining and acid Leaching	EBM vacuum refining	Directional solidification
Shanghai Propower	Carbothermic MG-Si production	Oxidation refining and acid leaching	Vacuum refining	Directional solidification

1.2 Why attention to the impurities?

The challenge of the metallurgical route is to reach very low levels of impurities in a consistent process. The efficiency of a crystalline silicon solar cell is highly dependant on the impurity content. (Swanson 2005) described the losses in going from the thermodynamic limit to future practical cells. The conversion limit for a silicon solar cell having a band gap 1.15eV-1.12eV is 33%. Optical losses due to reflectance and recombination losses due to radiative and Auger recombination lower the limit to 29%. These losses are intrinsic to silicon and nothing can be done to improve this upper limit. Still, the actual efficiency of commercial cells is 25% for crystalline and 20% for multi-crystalline solar cells (Green *et al.* 2011). The gap to the 29% limit is due to recombination at defects, passivation and contact surfaces.

The contaminants can be divided into three major groups: metal elements, light elements and dopants. Metallic elements (Al, Ti, Fe, Cr, Cu, Zn, Mo and Ni) and light elements (O, C, N) in form of dissolved elements or precipitates are detrimental because they provide recombination sites for the charge carries. Dopants (B, P) determine the electronic properties of the

solar cell material, they should be carefully controlled because their levels affect the resistivity and therefore the electrical properties of the carriers. Solar grade silicon specifications were defined during the Crystal Clear Workshop in Amsterdam 2008 and are shown in Table 1.3 (Coletti 2011).

Table 1.3 - Solar grade silicon specification in ppmw (Panel discussion 2008). “Undoped Sog-Si” refers to relaxed electronic-grade silicon, nominally uncompensated; “compensated SoG-Si” refers to a UMG Si route and contains a higher concentration of B and P.

Element	SoG –Si Undoped	SoG-Si Compensated
B	<0.05	<0.45
P	<0.1	<0.6
Fe	<0.05	<5
Al	<0.05	<5
Zn	-	<2
Ti	<0.005	<0.05
Na	-	-
Cu	<0.01	<1
Ni	<0.01	<1
Cr	<0.05	<1

Solar grade silicon specifications are currently reached by a combination of high purity silicon feedstock and subsequent silicon purification processes. The major problem for most providers of UMG-Si is represented by P and B which have a relatively high segregation coefficient and are not easily removed by directional solidification.

1.3 Source of contamination in the silicon production

Silicon is produced from quartz and carbon materials in a submerged arc furnace. “Intermediate-purity quartz” (Norwegian Geological Survey 2012), which is the quartz used normally, comprises most of the known hydrothermal deposits. Hydrothermal quartz is the product of precipitation

of silica from hot aqueous solutions percolating through fractures in the Earth's crust. If the minerals precipitate before quartz crystallization, hydrothermal quartz may be very pure.

The carbonaceous materials used as reducing agents may be divided into two main categories: fossil carbon materials (coal, coke/char, petrol coke) and biological carbon materials- (wood chips, charcoal). A literature review of the charge mixtures for silicon production used in silicon smelters in different countries has been done by E. Myrhaug (Myrhaug 2003). A typical example of raw material mix is 26 wt% coal; 10 wt% charcoal; 52 wt% quartz; 12 wt% wood chips (Schei et al. 1998).



Fig. 1.1 – Common raw materials in the silicon production: quartz, wood chips, coke, coal, charcoal carbon.

There are three main sources of contamination in the silicon process (Amick *et al.* 1985): the first comes from the construction materials of the arc furnace, and from the stoking and tapping operations, the second is contamination during handling and preparation of the raw materials, the third is the base level of impurities in the raw materials and electrode.

Contamination from the raw materials can be minimized by choosing high purity or beneficiated middle raw material quartz. A core graphite electrode without an outer steel casing is used for the Si production in order to minimize the Fe content. The bottom of the furnace, where the silicon melt accumulates, may be lined with spectral-grade graphite. In order to get high purity silicon, it has been suggested (Amick *et al.* 1985) that the outlet gutter, should also be fabricated from spectral-grade graphite or from less pure graphite coated with CVDSiC. To reduce contamination, molten silicon must be constantly poured off into high-purity silica crucibles (Gribov *et al.* 2003).

The impurities present in quartz vary considerably depending on the location and geological characteristics of the mine. The impurities in carbon vary from the carbon source used. The range of impurity content in quartz, carbon and electrode for a Si and Fe-Si furnace is reported in Table 1.4

Table 1.4-Average impurity content in quartz carbon and electrode for a Fe-Si furnace (Myrhaug et al. 2000)(Aasly 2008). Values are in ppmw.

	Quartz	Carbon	Electrode
P	<5-50	<5-300	<5-170
B	<10-45	<10-100	<10
Fe	1000-1500	<100-9000	100-3500
Al	300-3200	<50-10000	<50-4000
Ca	<75-160	<75-4000	200-1500
Ti	20-200	<0.5-4000	100
Mn	3-600	1-270	50-3500
K	<75-1700	<75-1800	<75-250
Mg	20-140	70-1400	<15-500
Na	50-170	<50-2100	<50-300

The distribution of Fe, B and P between the electrode and the raw materials is shown in Fig. 1.2.

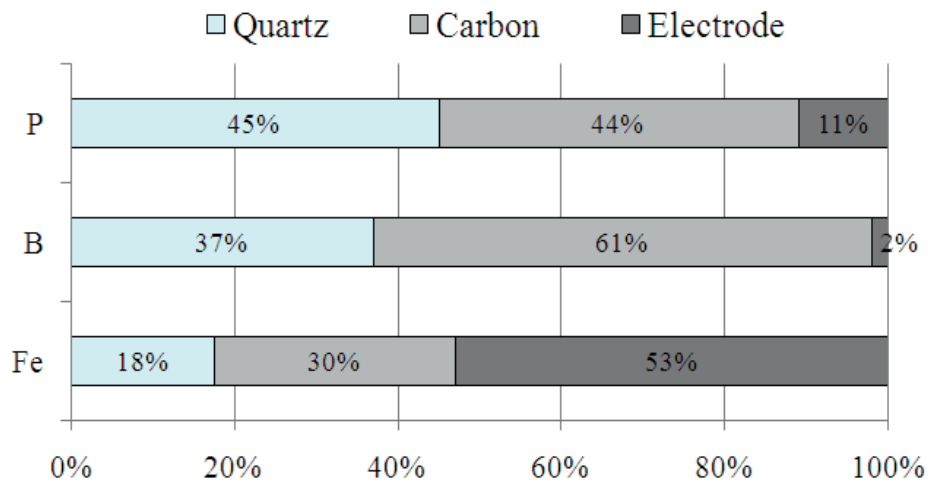


Fig. 1.2 - The distribution of P, B and Fe between the electrode and the raw materials. The values refer to a Si and Fe-Si production (Myrhaug et al. 2000).

1.4 Aim of the research work

Contaminants detrimental for solar cells are present in both silica and carbon feedstock and enter the silicon phase during the carbothermic reduction of silica. The aim of this research work was to investigate the impurity distribution from quartz feedstock to solar silicon produced via the metallurgical route. In particular four areas were investigated.

1. Removal of mineral impurities from quartz prior to carbothermic reduction by means of selective fragmentation.
2. Beneficiation of quartz produces a fine grained material which requires agglomeration and subsequent charging the quartz in form of pellets, which is different from the conventional lumpy charge. The second aim was therefore to investigate the effect of pellets and lumps on the silicon production reactions;
3. High temperature properties of quartz under reducing condition.
4. Distribution of contaminants from quartz to the gas phase during quartz reduction. Pellets and lumpy charge, hydrothermal quartz and quartzite were studied.

2 THEORETICAL BACKGROUND ON QUARTZ AND SILICON PRODUCTION

A literature review of the reaction mechanisms, the impurity distribution in the silicon electric arc furnace, the types and high temperature properties of quartz, the impurities in quartz and the available beneficiation techniques, was carried out and presented in the following sections.

2.1 Production of silicon

2.1.1 Compounds in the silicon furnace

Metallurgical grade silicon is produced conventionally by the reduction of silicon dioxide with carbon in a submerged electric arc furnace. The most common arc furnaces used for the silicon production consist of three electrodes delivering a three-phase alternating current. The process runs in cycles and the cycle time, varies from 30 to 70 min, depending on the operational conditions of the furnace. The charge materials, C and SiO₂, are charged to the furnace top and molten silicon ($T \cong 1600$ °C) is tapped out from the bottom through tap holes. Because a sticky condensate forms and glues the top charge, a stoking operation before charging is always necessary.

Various phases are present in the silicon furnace: solid (C, SiC, SiO₂ and Si), liquid (Si and SiO₂) and gaseous (primarily CO, SiO). The reactions take place under atmospheric pressure in a temperature interval of 1400–2000°C. The furnace bottom is the hottest area and the furnace top the coldest. The atmosphere in the furnace is strongly reducing, composed mainly by SiO(g) and CO(g). SiO₂ and C move downwards while SiO(g) and CO(g) move upwards. In presence of CO(g) quartz is reduced to SiO(g). Since the furnace is hotter at its bottom, the quartz melts descending downwards. In presence of SiO(g) carbonaceous materials react to CO(g) and SiC. Silicon carbide, in turn, is transformed to CO(g) and Si. The non reacted SiO(g) and the produced CO(g) move upwards. They partly react to form a condensate layer at the top of the furnace and partly oxidize above the furnace surface and leave the furnace as SiO₂ (called dust or microsilica) and CO₂.

Fig. 2.1 is a schematic view of the main phases present in the silicon furnace.

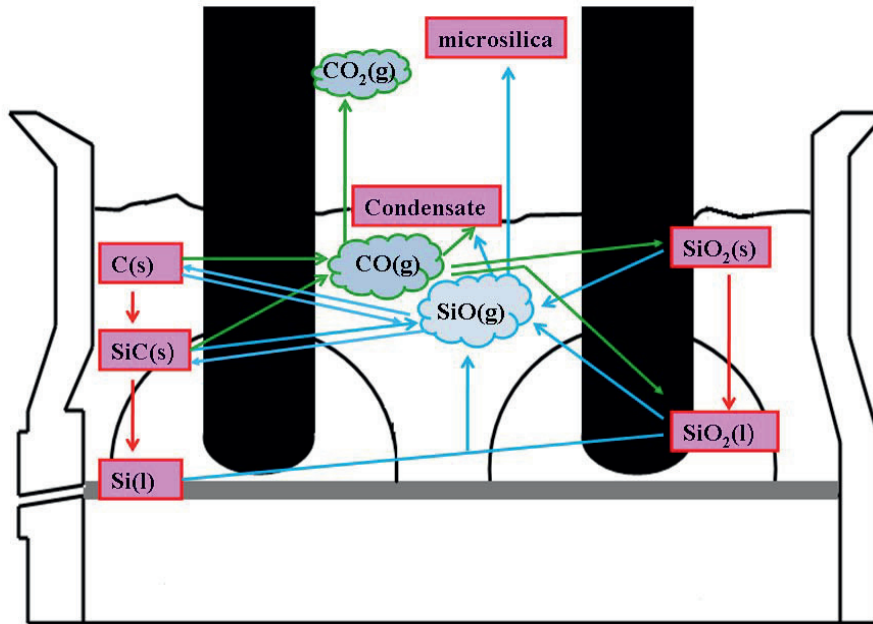


Fig. 2.1 Schematic view of the main solid (s), liquid (l) and gaseous phases (g) present in the silicon furnace. Carbon C and quartz SiO₂ are charged at the top of the furnace and descend downwards, while SiO(g) and CO(g) move upwards.

Fig. 2.2 shows the main phases found during the excavation of the Fe-Si furnace at Finnjord, Norway (Tranell et al. 2012). Furnace excavations are useful indirect qualitative observations of the inner operation of the furnace, since temperature and partial pressure are difficult to measure directly due to the combination of high temperature and aggressive chemical surroundings (Schei *et al.* 1998). The top 200-300 mm of the charge at Finnjord plant was loosely packed and appeared not notably transformed. Below the top charge, an approximately 500 mm thick horizontal zone of partly reacted raw materials, held together with glassy white condensates, was observed. Lumpy quartz was found only in the upper 200 mm of the charge mixture. Below this level, the quartz was generally disintegrated. Most of the quartz transformed to the polymorph cristobalite. One large cavity was found around each electrode. The crater walls had a dense structure, mainly built up of SiC and Si. Crater walls extended up through the top layer and allowed large quantities of raw material charge falling down to the region below the electrode. Gas channels formed on the crater walls, creating a layered structure. The

channels, typically 200 mm wide, started at the bottom of the crater, and narrow at the top. The existence of such gas channels illustrate the strong gas flows also outside the crater, resulting from vigorous reactions under the electrode. Outside the gas channels, brown and white condensates were found in a layered structure towards the furnace mantle, suggesting the presence of radial temperature zones in the furnace.

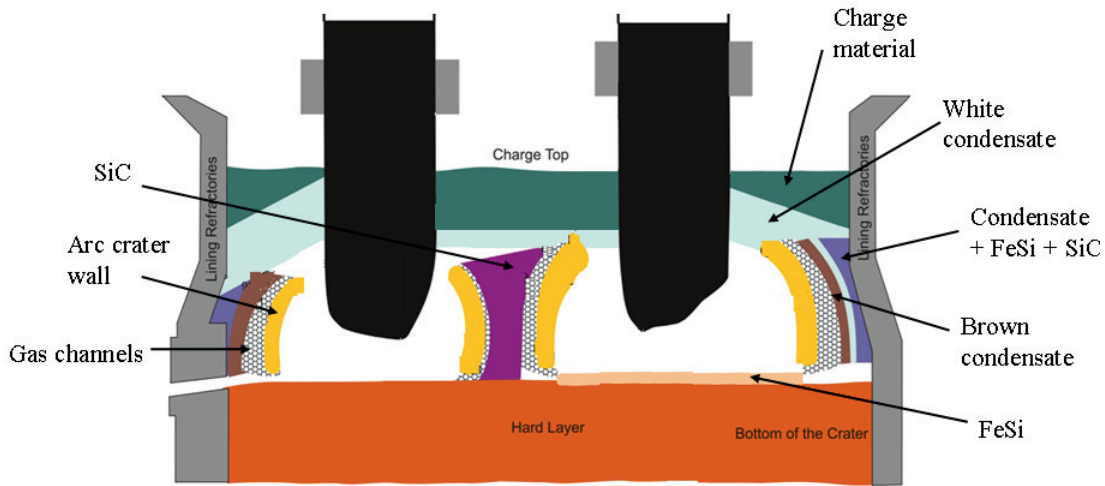


Fig. 2.2 Main features found during the excavation of the Fe-Si furnace at Finnjord, Norway (Tranell *et al.* 2012): the top charge was not notably transformed, below the top charge, an horizontal zone of partly reacted raw materials, held together with glassy white condensates was found. One large cavity, extending up through the top layer was found around each electrode. Gas channels formed within the crater walls. Outside the gas channels and towards the furnace mantle, brown and white condensates were found in a layered structure.

Jensen (Jensen 1986) recorded the reactions taking place in the crater zone of a 50 kW single electrode pilot scale furnace when lumpy charge materials were used. The crater appeared complex and dynamic: melted SiO_2 and solid SiC entered the crater cavity and a Si bath was present in the bottom. When quartz entered in contact with SiC, it reacted violently starting bubbling. When SiC entered in the crater zone it disappeared. When Si and SiO_2 entered in contact, SiO_2 started bubbling and the reactants quickly disappeared.

Another cavity, not found in the excavation of the Fe-Si plant at Finnjord, was reported during the pilot production of silicon in a 150 kW furnace (Myrhaug 2003). The cavity appeared right below the top charge and

formed because the condensate glued the top charge particles together preventing them from descending. A cavity in the charge top was also found in the small scale silicon production experiments run by Andersen and Ksiazek (Ksiazek *et al.* 2009).

2.1.2 Main reactions in the silicon furnace under equilibrium conditions

The main reactions taking place in the silicon furnace according to equilibrium are described by equations (2.1-2.9) (Schei *et al.* 1998). Schematically: equations (2.7), (2.8), and (2.9) occur in the high temperature “crater zone”. Reactions (2.1), (2.2), (2.3), (2.4), (2.5) and (2.6) occur in the upper, low temperature zone of the furnace.

In the low temperature zone of the furnace, carbon and quartz react to form SiO(g) and CO(g) according to (2.1). The ascending SiO(g) reacts with C to form SiC according to (2.2) or decomposes to Si and SiO₂ according to (2.3). Other condensation reactions can thermodynamically occur, they are (2.4), (2.5) and (2.6). In the hottest part of the furnace SiO₂ reacts with SiC to form SiO(g), CO(g) and Si according to equation (2.7) and (2.8). SiO(g) is also produced from the reaction of Si with molten SiO₂ (2.9).

In general, SiO(g) is formed at the SiO₂, SiC and Si surfaces, while CO(g) is formed at the C and SiC surfaces.

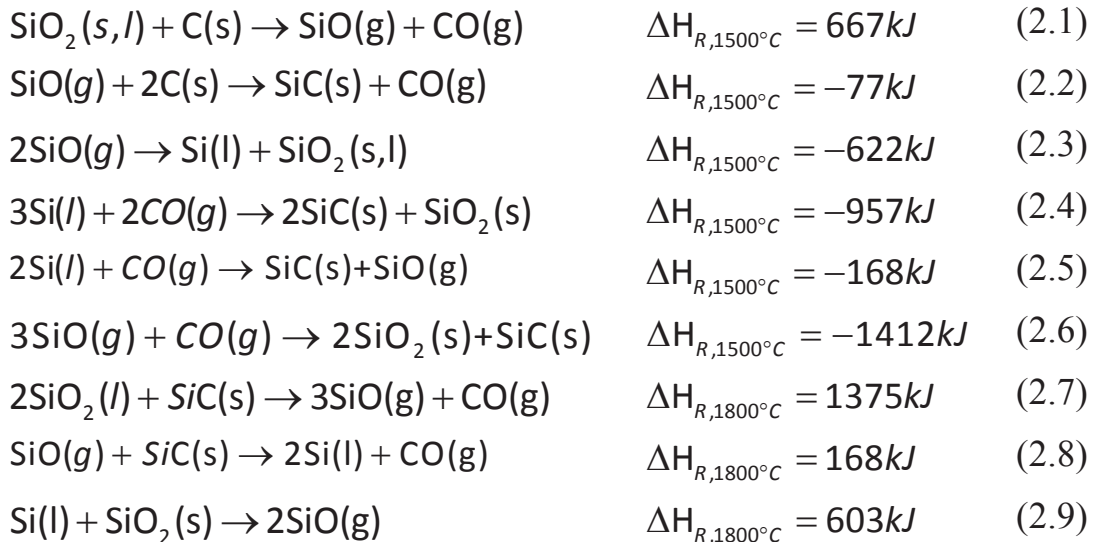


Fig. 2.3 shows the equilibrium SiO partial pressure P_{SiO} of the above reactions as a function of the temperature at atmospheric total pressure.

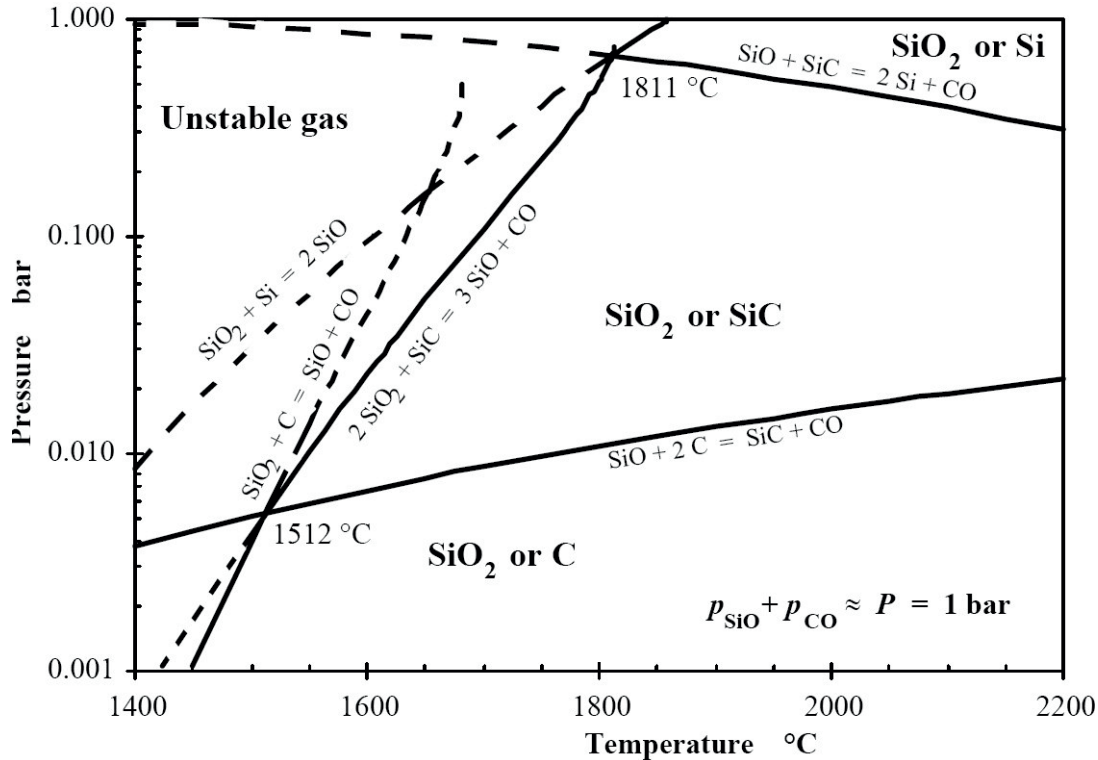


Fig.2.3 Equilibrium partial pressure of SiO as a function of the temperature (Schei *et al.* 1998). Equilibrium SiO pressure above the condensed phase combinations C-SiC, SiO₂-C, SiO₂-SiC, SiC-Si and SiO₂- Si at a total pressure 1 atm. The pressure is calculated from data in JANAF Thermochemical tables (Chase 1985).

2.1.3 High temperature zone: reactions involving SiO₂, SiC and Si

In the high temperature crater zone of the furnace (T ranging from 1800 °C to 2000 °C), SiC and molten SiO₂ react to form SiO(g), CO(g) and Si according to reactions (2.7), (2.8) and (2.9). Si forms on the SiC particle and at equilibrium Si is produced at 1811 °C.

Andersen (Andersen 2009) investigated the kinetics of reaction (2.7) and (2.9) in a DTA-TGA experimental setting. He observed that the reaction rate of (2.7) was higher for temperatures below 1900 °C. In particular the rate of conversion of the SiO₂-SiC mixture was two times and nine times higher than the SiO₂-Si mixture at 1650 °C and 1850 °C respectively.

Tada and Hirasawa (Tada *et al.* 2000) produced silicon in a two-stage reduction process using SiO₂ and SiC. They observed that more silicon was formed at 2000 °C than at 1950 °C, and that a larger amount of Si was

obtained for longer holding time. They found that the reduction of SiO_2 into SiO(g) as written in (2.7) was the reaction rate controlling step.

According to Wiik and Sahajwalla (Wiik 1990; Sahajwalla *et al.* 2003) reaction (2.7) was a combination of reactions (2.10) and (2.11) where SiO_2 reacted with CO(g) to form $\text{CO}_2(g)$ and SiC reacted with $\text{CO}_2(g)$ to form SiO(g) and CO(g) . Concurrently to reaction (2.10) and (2.11) Si formed on the SiC particles according to (2.8). Fig.2.4 shows schematically the production and absorption path of SiO , CO and CO_2 at the SiC-SiO_2 interface.

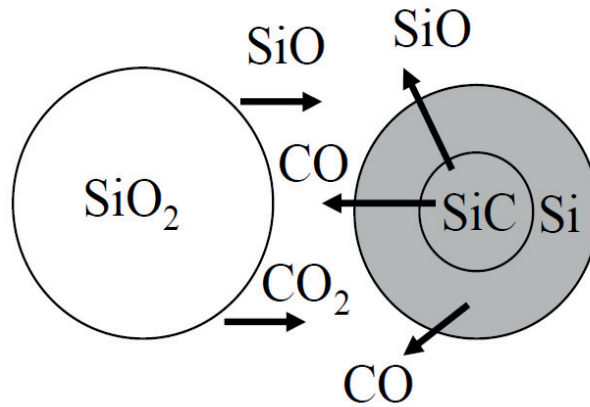
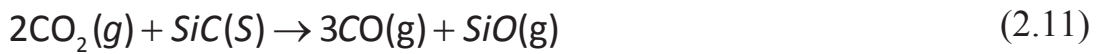
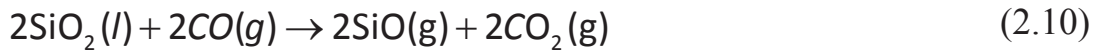
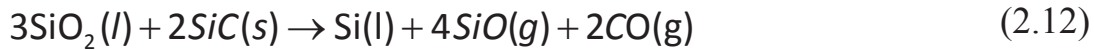


Fig.2.4 Production and absorption of CO , CO_2 and SiO at the $\text{SiO}_2\text{-SiC}$ interface.

The reaction (2.10) describes the formation of SiO(g) by reacting CO(g) with quartz. The reaction involves four steps: 1) adsorption of CO(g) in the SiO_2 surface; 2) production of SiO(g) ; 3) desorption of SiO(g) and $\text{CO}_2(g)$ from the quartz surface and 4) diffusion of $\text{CO}_2(g)$ and SiO(g) away from the quartz surface by bulk gas flow. According to Wiik (Wiik 1990) the rate controlling step is the chemical adsorption of CO in the SiO_2 (step 1).

If we assume equilibrium between the phases SiO_2 , SiC and Si at 1bar, the inner zone of the furnace can be explained by equation (2.12) (Schei 1967; J.K.Tuset 1976; Schei *et al.* 1998). If we assume non equilibrium conditions, $T = 1980^\circ\text{C}$ and $\frac{P_{\text{SiO}}}{(P_{\text{SiO}} + P_{\text{CO}})} = 0.5$ the inner zone reaction is expressed by equation (2.13) (Müller *et al.* 1972; Schei, Tuset *et al.* 1998).



2.1.4 Low temperature zone: reactions involving SiO₂ and C

In the upper part of the furnace SiO₂ and C react to form SiC according to (2.1) and (2.2). Reaction (2.1) is questionable: if C and SiO₂ are at their solid state, the reaction can occur only at phase contact, in addition the diffusion in the solid state is very low (Schei *et al.* 1998). Reaction (2.1) is therefore believed to occur through gaseous intermediate phases involving CO₂(g) as described by equation (2.14) and (2.10) (Schei 1967; Fruehan *et al.* 1985; Wiik 1990; Weimer *et al.* 1993) and shown in Fig. 2.5. Concurrent with reactions (2.14) and (2.15) a SiC layer grows thicker toward the inside of the C particles, therefore SiO(g) has to diffuse through the SiC into the C, and CO(g) has to diffuse out through the SiC layer. The density of the SiC depends on the density/porosity of the carbon: if the carbon is porous, SiC will be porous. If the SiC is very dense, the reaction (2.2) will be slower.

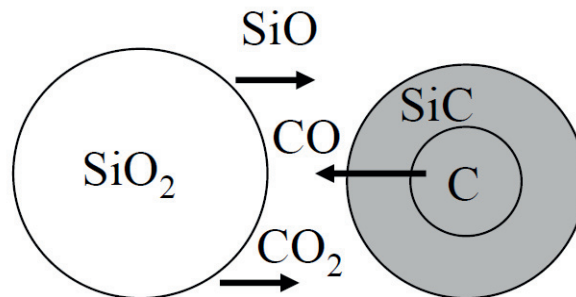


Fig. 2.5 Production and absorption of CO, CO₂ and SiO at the SiO₂-C interface. A SiC layer grows thicker towards the inside of the C particle, and the gaseous species have to diffuse through the SiC layer.

Carbon materials for the silicon production, are with the exception of woodchips, usually charged as small pieces (3-12 mm) and is selected to have high porosity and reactivity. High reactivity carbon materials, have

the ability to rapidly react with SiO(g) to form SiC. If the carbon has low reactivity, 1) the non reacted carbon will end up in the silicon melt creating problems during tapping; and 2) more SiO(g) will leave the furnace lowering the Si-yield. This happens because SiO(g) instead of reacting with carbon partly condenses and partly leaves the furnace. The condensate formation releases heat (negative ΔH), as a consequence the charge becomes too hot for further condensation to occur and more SiO(g) is lost. The reactivity of carbon materials can be determined by the SINTEF SiO reactivity test (Tuset *et al.* 1976; Lindstad *et al.* 2007). The SiO reactivity of coal based reductants depends on the ranks of the coal, on the petrographic properties (Tuset *et al.* 1976), on the carbon particle size (small particles, such in agglomerates, are converted faster than the large ones) (Gjermundsen *et al.* 1972) and on the porosity (higher porosity results in a easier access for reacting gases) (Raness *et al.* 1998; Myrvågnes 2008). Myrvågnes found that, given the same radius, charcoal particles are converted faster than coke particles and that the bio carbon has higher porosity than the fossil carbon (Myrvågnes 2008). Coal contains minerals such as clay minerals, carbonates, sulphides, oxides, quartz and phosphates. Among different coal samples, the samples including abundant quartz inclusions were the most reactive (Myrvågnes 2008). The quartz inclusions reacted with the carbon at the reaction temperature of 1650 °C to produce SiC and CO(g). This reaction increased the porosity and surface area of the carbon material contributing to an easier access for reacting gases which in turn resulted in an increased reactivity and degree of conversion.

2.1.5 Low temperature zone: condensation reactions

Four condensation reactions are thermodynamically possible: (2.3), (2.4), (2.5) and (2.6). The reaction described by equation (2.3) is believed to occur at the temperature range of 1600-1700 °C (Førland *et al.* 1966; Andersen *et al.* 2010). The reactions described by equations (2.4), (2.5) and (2.6) are believed to occur at temperatures lower than 1500 °C (Poch *et al.* 1962; Schei 1967; Schei *et al.* 1998). The reaction described by equation (2.3) produces a brownish condensate (Førland *et al.* 1966; Andersen *et al.* 2010; Vangskåsen 2011), the reaction (2.6) produces a white condensate, while the reaction (2.5) a green condensate (Schei 1967). Many authors (Førland *et al.* 1966; Andersen *et al.* 2010; Vangskåsen 2011) showed that the brown condensate consists of silicon spheres, ranging in size from 100

to 1000 nm, in a SiO₂ matrix. According to Schei (Schei 1967), the green condensate contains SiC particles in a SiO₂ matrix, where the SiC particles might have formed by the reaction of the Si phase contained in the brown condensate with CO(g).

While four condensation reactions are possible, however, the brown and the white condensates were mainly found in the excavation of a FeSi furnace (Tranell *et al.* 2012) and in small scale silicon production experiments (Tangstad *et al.* 2010). The picture and morphology of the brown and white condensates are shown in Fig. 2.6 and Fig. 2.7 respectively.

Andersen (Tangstad *et al.* 2010) and Ksiazek (Tangstad *et al.* 2009) investigated qualitatively the impurity content in the brown and white condensate. Fig 2.8 shows the elemental mapping of the brown condensate: Al and Mg (less visible) are preferentially located in the Si phase of the condensate (where the concentration of Al in the silicon phase is estimated to 0.7 wt%). Fig.2.9 shows the elemental mapping of the white condensate: Fe, Al, Ti, Ni Ca and K are present in the condensate.

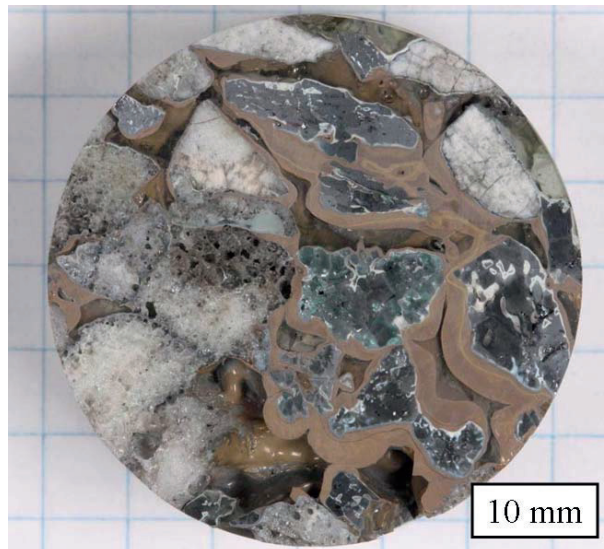


Fig. 2.6 White and brown condensate formed during small scale silicon producing experiments. The charge materials were quartz and silicon in lumps of 1-2 cm size. The condensates surround the quartz particles (white) and the silicon carbide particles (black) (Ksiazek *et al.* 2009).

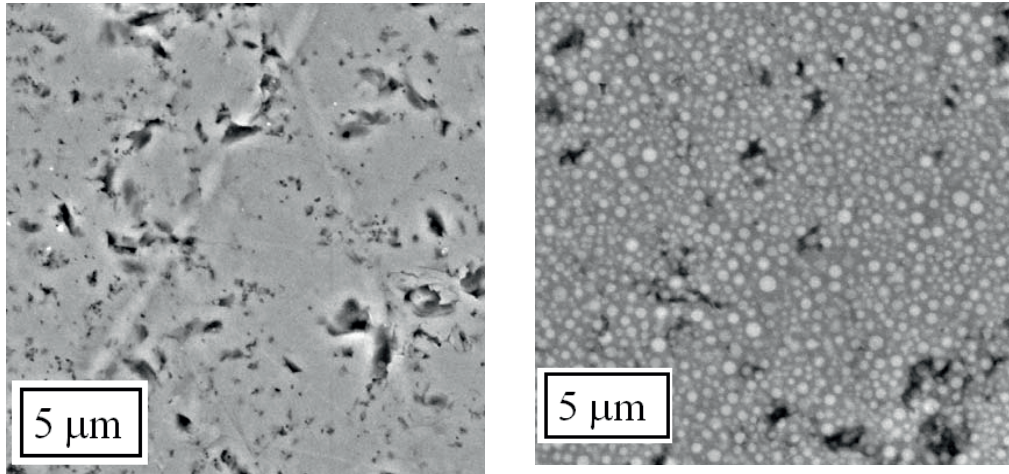


Fig. 2.7 Morphology of the white condensate (on the left) and the brown condensate (on the right). The white condensate is a mixture of Si, SiC and SiO₂ phases without any distinction among the different phases. The brown condensate is characterized by Si droplets in a SiO₂ matrix (Tangstad *et al.* 2010).

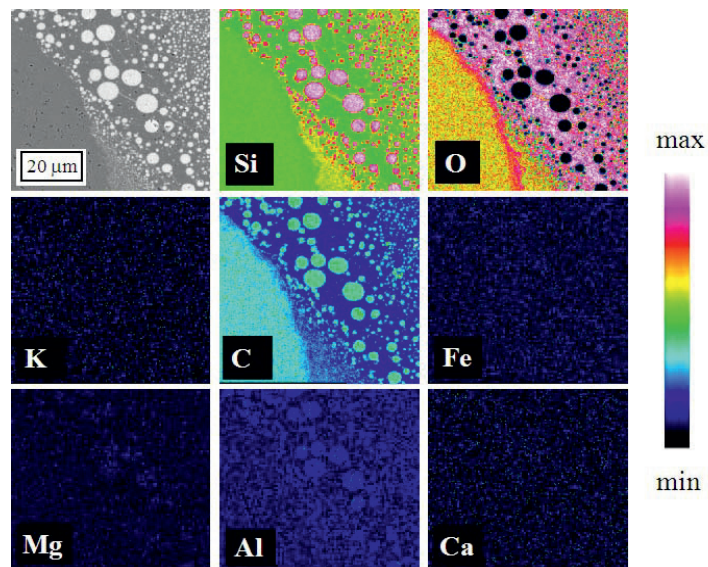


Fig. 2.8 Brown condensate on a quartz particle. The brown condensate (mixtures of spherical silicon particles in a silica matrix) is on the top right and the quartz particle on the bottom left (Tangstad *et al.* 2010).

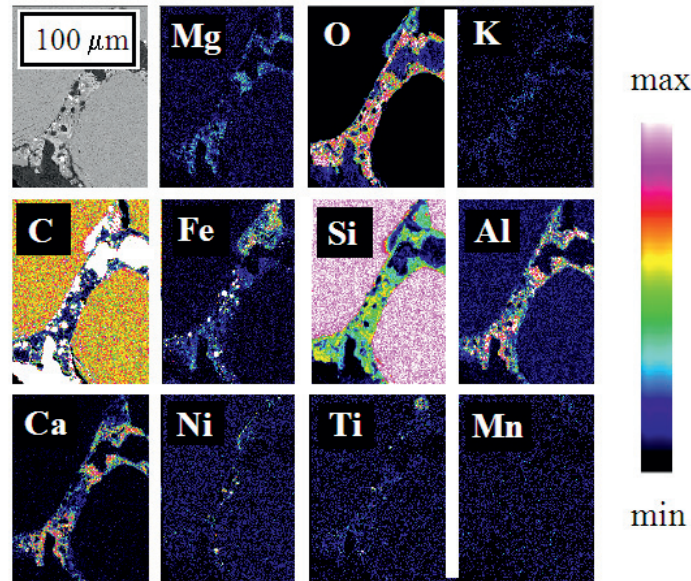


Fig. 2.9 White condensate between two SiC particles. The condensate is polluted in K, Fe, Al, Ca, Ni and Ti. The condensate was formed at a temperature range of 1540 °C - 1600 °C when heating quartz and silicon carbide to 2000 °C (Tangstad *et al.* 2009).

2.2 Impurity distribution in a silicon furnace

As mentioned in the introduction, the impurities in silicon affect the final efficiency of the silicon solar cells.

The carbothermic production of silicon is an important source of contamination: quartz, carbonaceous materials as well as electrode and refractories carry detrimental impurities which transfer to silicon. Table 2.1 shows the typical content of impurities in the raw materials for a ferro-silicon and silicon furnace (Myrhaug 2003).

Table 2.1 Typical contents of trace elements in the raw materials and proximate analysis of the reduction materials for ferrosilicon and silicon production (Myrhaug 2003).

	Unit	Quartz	Coal	Coke	Charcoal	Wood chips	Petrolcoke	Electrode
Fixed carbon	%	---	39-62	81-95	75-85	20-26	88-93	85-99
Volatiles	%	---	34-58	2-5	10-25	70-75	7-12	1-10
Ash	%	---	1-5	1-10	0.5-10	1-10	0.05-1	0.1-5
Si	%	46.1-46.6	0.3-2	0.6-4	0.05-9	0.2-1	---	---
C	%	~0	71-81	84-96	81-91	45-50	94-97	91-97
O	%	53.1-53.6	10-16	1-7	2-15	40-45	2-3	2-8
H	%	~0	5-8	0.5-4	1-8	5-6	1-1.5	0.2-1.3
N	%	~0	1.5-2.5	0.1-0.2	0.3-1.0	0.1	0.2-0.5	0.05-0.5
Hg	ppbw	<5-10	<5-60	<5-20	<5	<5	<5	<5-40
Ti	ppmw	20-200	50-600	60-4000	10-300	~1	<0.5-50	~100
Al	ppmw	300-3200	800-5700	1000-10000	100-6200	<50-100	70-110	<50-4000
As	ppmw	<1-3	<1-3	<1-14	<1	<1-5	<1-10	<1-10
B	ppmw	<10-45	<10-110	<10-100	<10-16	<10-23	<10	<10
Ba	ppmw	0.5-25	4-130	15-220	10-30	2-70	1-9	6-90
Be	ppmw	<0.5-0.6	<0.5-4	<0.5-3	<0.5	<0.5	<0.5	<0.5
Bi	ppmw	<0.5	<0.5	<0.5	<0.5	<0.5	<0.5	<0.5-2
Ca	ppmw	<75-160	150-2400	600-3400	1000-4000	600-1000	<75	200-1500
Cd	ppmw	<0.1-1.5	<0.1-1.1	<0.1-1.1	<0.1	<0.1-0.3	<0.1	0.6-1.2
Co	ppmw	<1-200	1-16	6-120	<1	<1	<1-13	<1-13
Cr	ppmw	3-25	<1-12	15-40	5-15	<1-13	1.5-12	<1-24
Cu	ppmw	1-3	1.5-22	4-40	2-7	1.8-4.3	<1-6	<1-20
Fe	ppmw	100-1500	700-5200	1400-9000	100-1700	<100-1400	<100-600	100-3500
K	ppmw	<75-1700	<75-1800	300-1800	100-1800	250-900	<75	<75-210
Mg	ppmw	20-140	80-1100	300-1400	200-1100	75-200	<15-100	<15-500
Mn	ppmw	3-600	4-110	<1-270	80-120	10-50	1-6	50-3500
Mo	ppmw	<2-8	<2-4	<2-7	<2	<2	<2-12	<2
Na	ppmw	50-170	<320	230-2100	170-230	<50-130	<50-110	<50-300
Ni	ppmw	<1-9	2-33	3-240	~30	<1-7	60-360	<1-50
P	ppmw	<5-50	<5-143	16-160	80-300	20-110	<5-13	<5-170
Pb	ppmw	<0.1-9	0.3-13	1-106	<0.1-2.3	<0.1-0.2	<0.1-3.5	<0.1-1.6
S	ppmw	<5-1400	1200-8300	3300-11000	200-1500	100-1300	20000-50000	55-3400
Sb	ppmw	<0.1-0.9	<0.1-0.7	0.3-3.9	<0.1	<0.1	<0.1	<0.1-1.4
Se	ppmw	<2-5.2	<2-6.6	<2-3.3	<2	<2	<2	<2
Sn	ppmw	<0.5-2.2	<0.5-2.7	<0.5-3	<0.5	<0.5-4.5	1.1-2.4	<0.5-2.4
Sr	ppmw	<0.5-12	3-90	11-80	14-80	1.6-9	<0.5-6.6	1.4-20
V	ppmw	<1-4	2-60	4-30	<1	<1	400-1200	<1-92
W	ppmw	<0.5-640	<0.5-3	<0.5	<0.5	<0.5	<0.5	<0.5-0.8
Zn	ppmw	<1-3	3-40	4-80	2-40	6-16	3-10	1-100
Zr	ppmw	<0.5-3.3	0.8-3.3	<0.5-1.5	<0.5	<0.5-1	<0.5	<0.5-1.7

SiO(g), CO(g), C (s) and SiC(s) are reducing agents for the impurity oxides present in the charge material. Oxides of Ni, Co, Fe, Pb, Cu, Cr, Mn, Zn, Na and K are easily reduced to metals, while oxides of Ca, Al, Ti, and Mg are stable at temperatures and conditions of quartz reduction. Impurities can be removed from quartz with a gas phase if the reduced species are volatile. The vapour pressure of the reduced species is also influenced by the activities of the species in the raw materials and reaction products and by the reaction temperature. If the activity coefficient is very low, an element tends to remain in the liquid (silicon or slag) phases (Tveit *et al.* 2000). Fig. 2.10 shows the Ellingham diagram for several oxides (Lynch 2009).

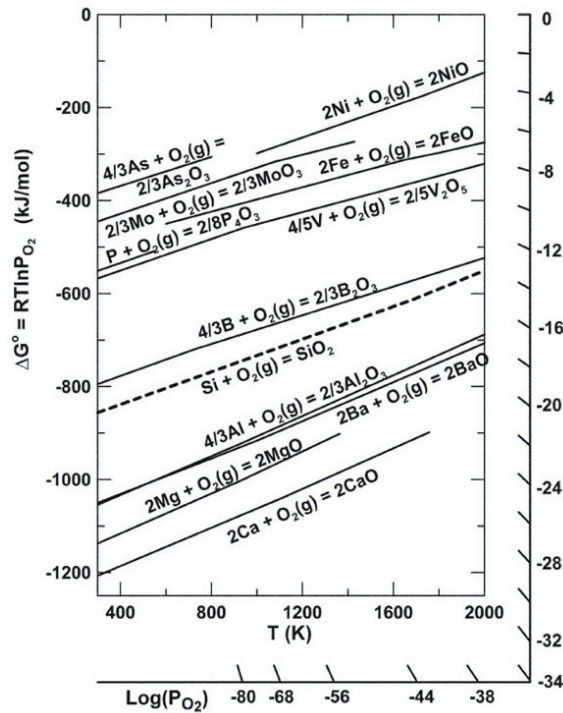


Fig. 2.10 Ellingham diagram for oxides: standard Gibbs energy versus temperature. The SiO_2 equilibrium line in the diagram delineates oxides above the lines that are reduced in the furnace and those below the line that are not reduced (Lynch 2009).

Impurities in carbon material are mainly oxides and sulphides present in the ash. Because the carbon is very porous, the impurities are easily exposed to the furnace reducing gases and the volatile compounds which form can be easily removed when the carbon charge is still at the furnace top (Yao *et al.* 2001; Wang *et al.* 2004; Garcia *et al.* 2007). The behaviour of the impurities in the quartz during the silicon production is still not well understood. The impurities present in the quartz do not have easy access to the reducing atmosphere because the quartz is not porous. The oxides embedded in the quartz are believed to be accessible for reduction once the quartz melts (at around 1700 °C), which occurs just above the cavity (Myrhaug *et al.* 2000). As a consequence, any volatile compound, which forms from reduction, may not leave the furnace because of the interaction with the upper charge layer. If cracks formed in the quartz through thermal expansion are invaded by reducing gases, the impurities can be exposed to reducing atmosphere before the quartz is molten, however this is a topic not yet investigated. Impurities are found in the metal-slag phase, in the microsilica or silica fume (Myrhaug *et al.* 2000) and in the condensate (Tangstad *et al.* 2010). The presence of impurities in micro-silica and in the

condensate provides evidence that the impurities enter the gas phase. Industrial studies of micro-silica show that all the detrimental impurities for solar cell purpose distribute, in different ratios, to micro-silica (Myrhaug *et al.* 2000). Myrhaug and Tveit studied the distribution of trace elements present in the metal, microsilica and off-gases for a Fe-Si furnace (Myrhaug *et al.* 2000) and Si furnace (Tveit *et al.* 2000; Garcia *et al.* 2007). The trace elements found in the microsilica were K, Zn, Na, Mg, and Pb, while the elements found in the silicon were primarily Cu, Cr, P, Mn, Al, Cr, Ni, Fe, B, and Ti. The behaviour of P was dependent on the Fe content in the charge: in the Si furnace 85% of the P input distributed to microsilica, while in the Fe-Si furnace only 25%. The distribution of trace elements between metal, microsilica and off-gases is shown in Fig. 2.11.

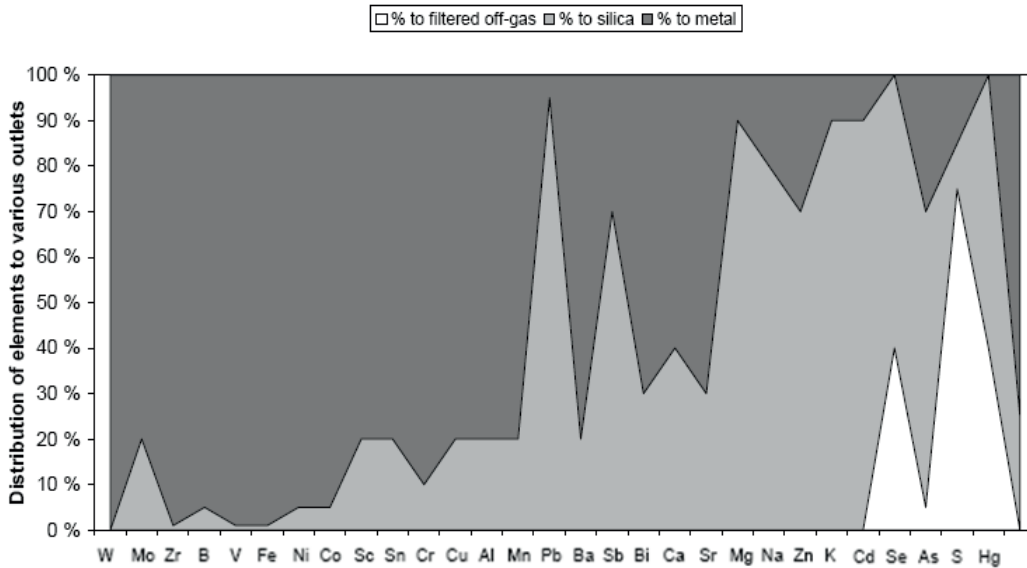


Fig. 2.11 Distribution of the elements to the Fe-silicon-slag phase, micro-silica and off-gases. Industrial measurements of a Fe-Si plant (Myrhaug *et al.* 2000).

Myrhaug (Myrhaug *et al.* 2000) described the behaviour of the trace elements in the silicon furnace with a model based on the boiling temperature of the pure elements. The model assumes that an element evaporates when its boiling point is lower than the process temperature. The boiling point model refers to the case of the partial pressure of the elements over the pure element p_{EL}^0 equals 1 atm, and the activity of the elements a_{EL} equals 1, which is not representative of the real case. Moreover the model does not take into account the fact that gaseous compounds other than pure elements may form. The boiling point model is shown schematically in Fig 2.12: if the boiling point of the pure element is lower

than 160 °C the element enters the off gas, if the boiling point is between 160 °C and 1300 °C the element enters the microsilica, if the boiling point is between 1300 °C and 2000 °C the element circulates in the furnace and end ups in the metal-slag phase. The circulation of the impurities in the furnace is a process known in the manganese production ($Zn(g)$ and $K(g)$ react with $CO(g)$ and $CO_2(g)$ forming $ZnO(s)$ and $K_2CO_3(l,s)$ respectively (Lee *et al.* 1993; Sterneland 1993; Ishak 2002)) but has not been well documented in the Si production. The biggest disagreement of the boiling point model and real observations involves P: the model predicts that all P should leave the furnace in the gas phase, but 75 % of P was found in the Fe-Silicon metal. According to Lynch (Lynch 2004; Lynch 2009) this is a phenomena characteristic of the Fe-Si production: in presence of Fe, P dissolves in the molten Fe forming the stable Fe-P alloy, while the gradual addition of Si destabilizes the P and much of it enters the gas phase under reducing conditions.

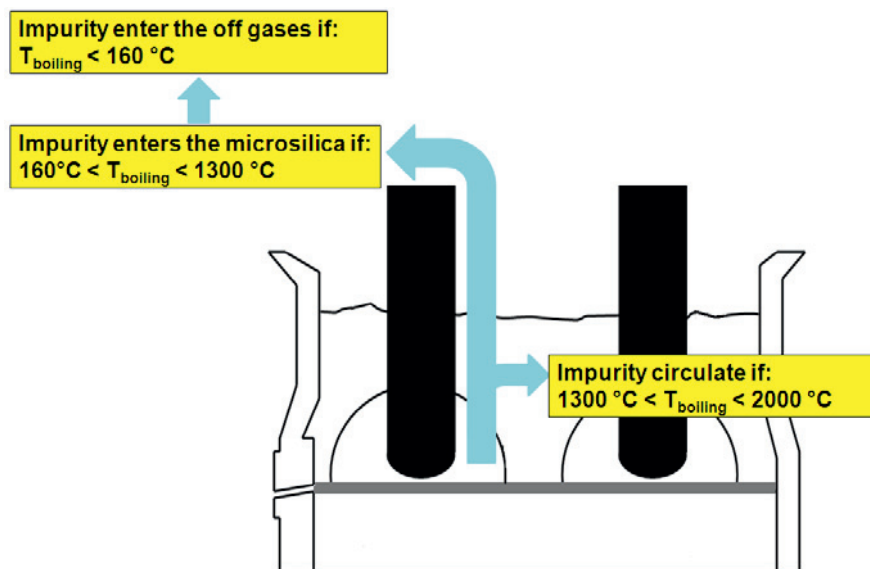


Fig. 2.12 Silicon furnace: distribution of the impurities to the gas phase according to their boiling point ($T_{boiling}$).

2.3 Requirements of quartz in the silicon production

The industry has defined a list of absolute requirements necessary in quartz feedstock for the silicon production (Schei et al., 1998). They are: 1) high mechanical strength, 2) high thermal strength and 3) low impurity content.

1) The *mechanical properties* of quartz affect the generation of fines during mining, transport and storage before charging. Fines (particles below 2 mm) represent a problem for the silicon process because they form a packed charge on the top of the furnace, lowering the permeability i.e. obstructing the gas flow from the lower parts of the furnace to the upper part. As a results unwanted gas channels form and SiO(g) is lost affecting the Si yield.

2) As for the mechanical properties, the *thermo-mechanical properties* are mainly related to the generation of fines, however, in this case, the fines generation occurs inside the furnace where quartz disintegrates as a result of the extreme heat in the furnace. Ideally, the lumpy quartz should keep its original size as it moves down through the charge, until the quartz starts softening and melting in the lower part of the furnace near the cavity wall (Aasly 2008). The thermo-mechanical properties of quartz are described in more detail in paragraph 2.5.

3) Quartz *chemistry*: quartz contains impurities which enter the silicon phase during the silicon production reaction in the electric arc furnace. Metallurgical quartz 99.95% pure (less than 500 ppmw impurities) is currently used to produce solar silicon. This quartz is geologically classified as “intermediate-purity quartz” (Harben 2002; Norwegian Geological Survey 2012). A classification of quartzes according to their impurity content is shown in Table 2.2. Most of the hydrothermal deposits are intermediate-purity quartz and are currently the main quartz feedstock in commercial production of metallurgical silicon and SoG-Si. Nevertheless, relative pure quartzite may be used in the silicon process as well, especially if mixed with other quartzes (Aasly 2008). Pegmatite quartz is potentially a very pure raw material. However, it is not frequently used today because of the characteristic small size of quartz rock and presence of impurity minerals such as feldspar and mica which require manual sorting and quality control (Aasly 2008). The impurity distribution and diffusion in quartz are described in detail in the paragraphs 2.4 and 2.6. Techniques for beneficiation of quartz are discussed in the paragraph 2.7.

Table 2.2 Classification of quartz depending on the impurity content (Harben 2002).

Purity	Total ppm	Sources
Low	>5000	Silica sand or quartz as flotation tailings.
Medium	300-500	Quartz after complete physical and chemical beneficiation.
Intermediary	300-50	Quartz with high-purity capability through further chemical beneficiation. Quartz double floated, magnetically treated.
High	2-50	Quartz where impurities are confined to the lattice structure. Natural quartz acid leached, magnetically separated, calcinated, or hot chlorinated.
Ultra-high	1-8	Exceptional natural quartz after complete physical and chemical beneficiation. Precipitated silica from high purity silica tetrachloride.
Hyper	<1	Excludes natural quartz crystal. Silicon compound glass derived from the oxidation of hyper pure silicon powder.

Pellets charge was introduced only recently in the silicon production as an alternative to the conventional lumpy charge. In a recent process developed for production of solar grade silicon from pure raw materials (Kvande *et al.* 2010), quartz is charged in the furnace in form of pellets of intermixed SiO₂ and SiC. Pellets contain micronized beneficiated quartz particles which are held together by a binder. In this case mechanical, thermo-mechanical and chemistry properties are not anymore an issue, and a wider range of quartz deposits can be considered. There are many alternatives to beneficiate quartz and they will be discussed in the paragraph 2.7.

2.4 Impurities in quartz

Quartz can carry impurities in three different forms: 1) structural impurities, 2) fluid inclusion and 3) minerals.

2.4.1 Structural impurities in quartz

Structural impurities are trace elements confined to the lattice structure. They can be substitutional or interstitial. Substitutional impurities replace Si⁴⁺ in the Si-O tetrahedra. Interstitial impurities are mostly small monovalent ions that fit into structural channels running parallel to the c-axis or in lattice vacancies and defects and act as charge compensators to

balance the substitutional impurities (Grimstvedt *et al.* 2002). Fig. 2.13 is an example of the crystalline structure of quartz: a continuous framework of tetrahedra where Si^{4+} is situated at the center and O^- at the corners of the tetrahedra. Impurities that substitute Si occupy the red positions, while interstitial impurities occupy the green position in Fig. 2.13.

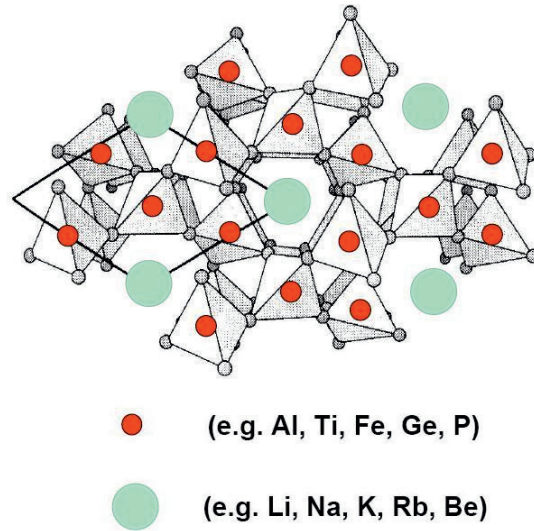


Fig. 2.13 Example of a crystalline quartz structure (α -quartz): continuous framework of SiO_4 : Si^{4+} is situated at the center and O^- at the corners of the tetrahedra. In red Si substitution sites, in green interstitial sites.

Al^{3+} , Fe^{3+} , Ti^{4+} , Ge^{4+} , P^{5+} , B^{3+} are generally substitutional impurities which replace Si^{4+} site in the Si-O tetrahedral and present strong ionic-covalent bonds (Grimstvedt *et al.* 2002). Li^+ , Na^+ , K^+ , Rb^{4+} , H^+ , Be^{4+} are interstitial impurities and present ionic bonds. Ti and Al form strong ionic-covalent bonds with the oxygen atoms (Larsen *et al.* 2004). The ferrous ion (Fe^{2+}) is believed to be too large to occupy the fourfold Si^{4+} position (Kawasaki *et al.* 2008). Iron has been observed to be mostly concentrated in the marginal parts of quartz grains and in the outer rim of the quartz crystals (Müller *et al.* 2002; Van der Kerkhof *et al.* 2004). The incorporation of Fe^{3+} and Al^{3+} in quartz can be non-uniform (Pankrath *et al.* 1994). Al, Fe can form micro-clusters incorporated along specific growth axes in α -quartz that also may contain structurally-bound water (Müller *et al.* 2003). Al^{3+} or Fe^{3+} can combine with OH^- and replace Si^{4+} - O^{2-} (Kawasaki *et al.* 2008).

Interstitial and substitutional impurities accommodate in the lattice and compensate electrically to reach charge neutrality. In quartz, three main substitution modes govern the incorporation of structural trace elements:

single substitution, double substitution and compensated substitution. The interstitial and substitutional atoms are located in neighboring Si-O tetrahedra to facilitate charge equilibrium. Fig. 2.14 is a schematic representation of the three cases.

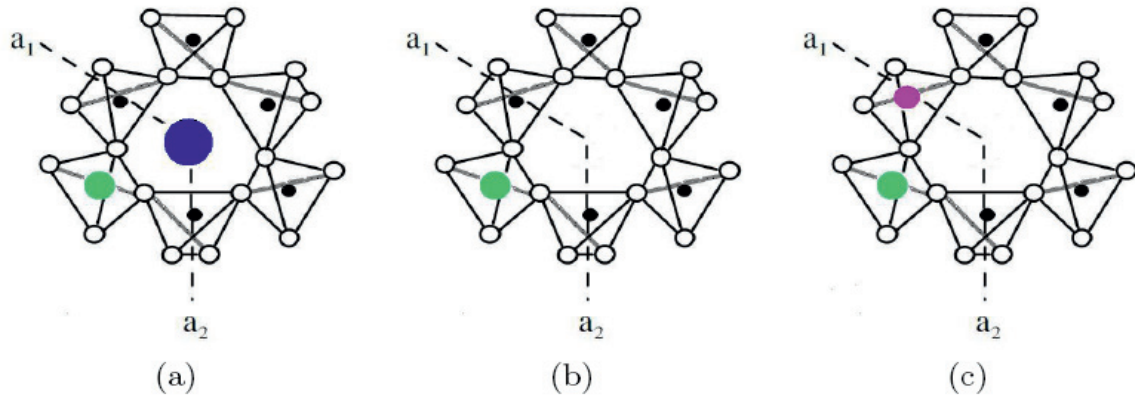


Fig. 2.14 Impurities distribution in the low temperature quartz (α -quartz): (a) compensated substitution: a ion among Al^{3+} , Fe^{3+} , B^{3+} replaces Si^{4+} with concomitant entry of a charge compensator ion such as K^+ , Li^+ , Na^+ or H^+ into an interstitial position; (b) single substitution: Si^{4+} is substituted by tetravalent ions Ti^{4+} or Ge^{4+} that balance the missing positive charge; (c) double substitution: two Si^{4+} are substituted by one trivalent ion among Al^{3+} , Fe^{3+} , B^{3+} and a pentavalent P^{5+} (Larsen *et al.* 2000; Penniston-Dorland 2001; Grimstvedt *et al.* 2002; Müller *et al.* 2003; Larsen *et al.* 2004).

2.4.2 Liquid inclusions in quartz

Liquid inclusions are common in *hydrothermal quartz*. Hydrothermal quartz formed from hot aqueous solutions percolating through fractures in the earth's crust. The hot aqueous solutions (p ranging from 1 to 3000 bar, T from 50 to 600 °C) contain primarily ortosilicic acid H_4SiO_4 with significant quantities of cationic species such as Na^+ , K^+ , Si^{4+} , Ca^{2+} , Mg^{2+} and Fe^{2+} and anionic species such as Cl^- , HS^- , HCO^{-3} , SO_2^{-4} . When the silica solubility decreases and the solution get saturated with respect to quartz, H_4SiO_4 decomposes and quartz is formed. Hydrothermal fluids are variable in composition depending on the solubility of the trace elements in the aqueous solutions, the different rocks through which the fluids have been circulating, the contamination from other types of fluid and the conditions for precipitation. Depending on all these factors, hydrothermal

quartz veins can be host to ore deposit or may be extremely pure, containing only a few ppm of impurity elements (Robb 2004).

Liquid inclusions are common in hydrothermal deposits, because the quartz crystals enclose drops of the surrounding watery solutions during growth. Fluids inclusions are typically 5-30 μm in diameter, an example is shown in Fig.2.15. Micro-thermometry and Laser-ablation inductively coupled plasma mass-spectrometry (LA-ICP-MS) is the technique that can be used to analyze a wide range of cationic species in the inclusions. Cl^- , OH^- , Na^+ , and K^+ , are the major constituents of fluid inclusions in natural quartz (Hosaka *et al.* 1981). Ca, Fe, Mg and Mn are also common in fluid inclusions together with a host of trace elements (Larsen *et al.* 2004). In the most complex cases both liquid, solid and liquid phase are present. Fig. 2.15 is a typical example of fluid inclusions in a hydrothermal quartz matrix.

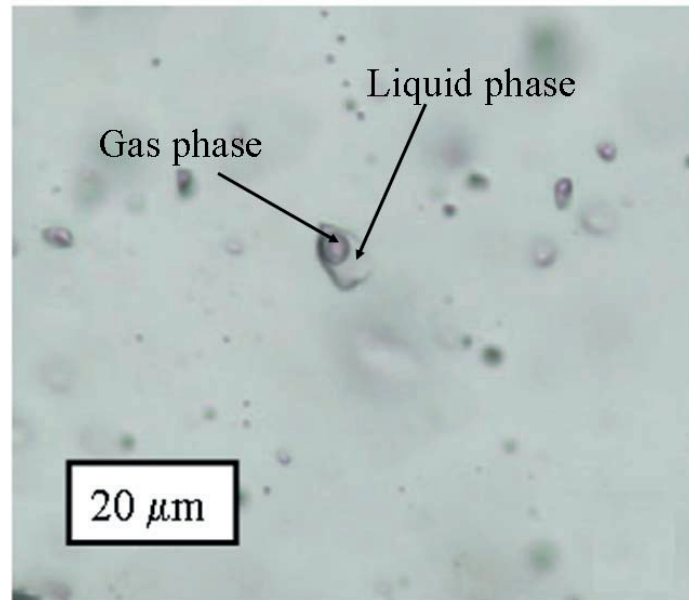


Fig. 2.15 Example of fluid inclusions in the quartz matrix. In particular a gas phase (bubble) is visible in the biggest fluid inclusion (Aasly 2008).

Fein (Fein *et al.* 1992) found that Fe combined with Cl^- or OH^- depending on the salinity of the solution. FeOH^+ , FeCl^+ and FeCl_2 were stable compounds and among them the most stable compound was FeCl_2 . The stability of FeCl_2 , for the range of temperature between 300 and 600 $^\circ\text{C}$ and the range of pressure between 0.5 kbar and 2 kbar, increased by increasing the temperature and decreasing the pressure in the solution.

The affinity of Cl^- with metallic cations such as Cu, Mn, Fe, Pb, Zn is described by the Lewis acid/basic principle (Robb 2004).

2.4.3 Mineral inclusions in quartz

Quartz can contain different typologies of mineral inclusions depending on its geological setting. Mineral inclusions are commonly situated in the quartz grain boundaries. A classification of the more common existing mineral groups is shown in Fig. 2.16.

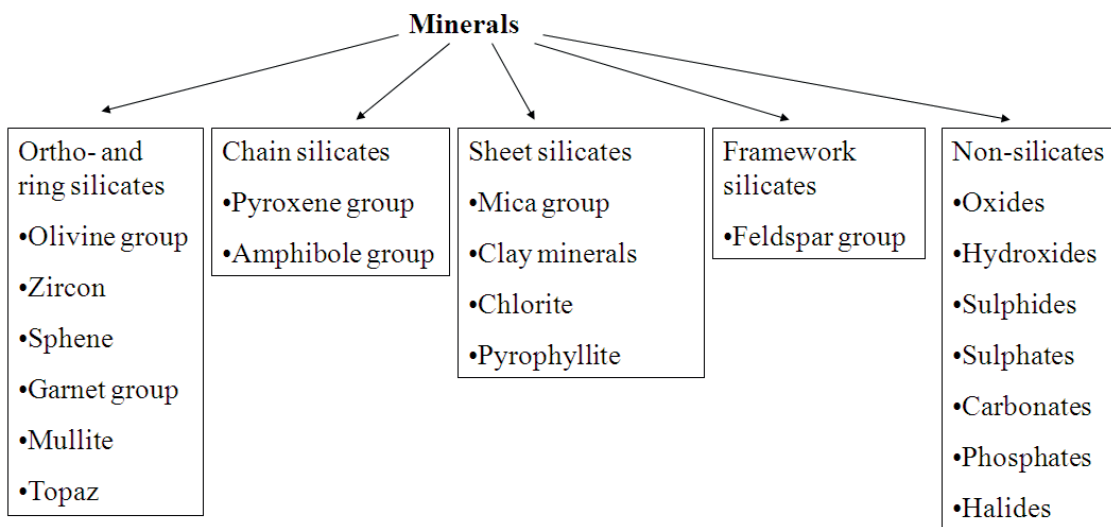


Fig. 2.16 Classification of the existing mineral groups (Deer *et al.* 1966).

Typical mineral inclusions in quartz are muscovite and feldspar. *Muscovite* $\text{KAl}_2(\text{Si}_3\text{Al})\text{O}_{10}(\text{OH},\text{F})_2$ is part of the mica group. Because it is a sheet mineral it has a strong cleavage in one particular plane. The layers are linked by K. The atomic structure of muscovite is shown schematically in Fig. 2.17. The repeat unit is formed by three octahedral, two of which have Al^{3+} at their center. One fourth of the tetrahedral cations are Al^{3+} rather than Si^{4+} . The principal isomorphous replacements which occur in muscovite are Na, Rb, Cs, Ca, Ba for K; Mg, Fe^{2+} , Fe^{3+} , Mn, Li, Cr, Ti, V for octahedral Al and, F or Cl for OH. In particular, the phengite substitution refers to the substitution of Mg or Fe^{2+} for Al in the octahedral sites (Deer *et al.* 1966). *Orthoclase* KAlSi_3O_8 , one of the most common mineral inclusion in quartz, is part of the feldspar group. The structure is formed by tetrahedra of $(\text{Si},\text{Al})\text{O}_4$ linked to one another (by shared oxygen) in all the directions (Deer *et al.* 1966). The atomic structure of orthoclase is shown in Fig. 2.17. Muscovite carries detrimental impurities for silicon

solar cells such as Al (20 wt%) and in case of isomorphous replacements, Fe, Mn and Ti. Orthoclase carries mainly Al (8 wt%).

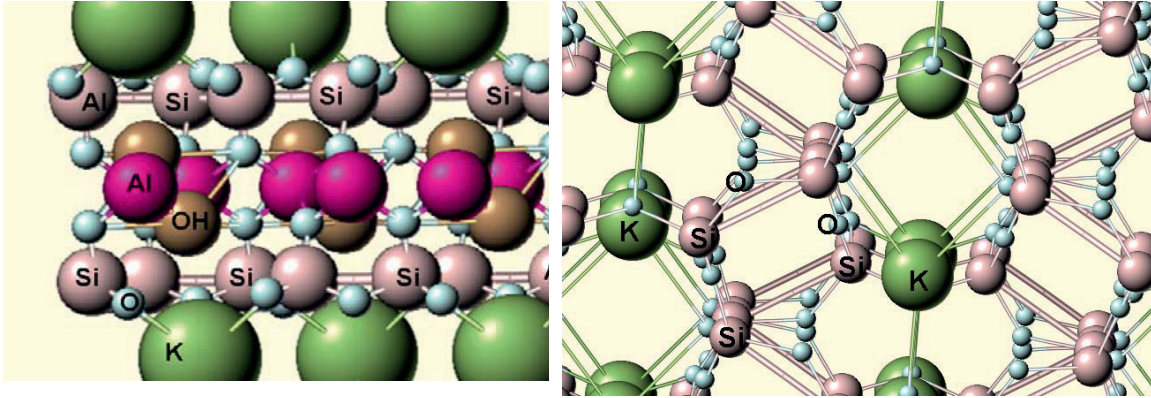


Fig. 2.17 Structure of the muscovite (left) and orthoclase (right) (Webmineral 2012).

2.5 High temperature properties of quartz

2.5.1 *Silica polymorphs*

Quartz assumes different crystalline structures or polymorphs during heating. By increasing the temperature at atmospheric pressure, quartz transforms to tridymite and to cristobalite. Quartz, tridymite and cristobalite are silica polymorphs.

There are two types of transformation among the silica polymorphs: reconstructive and displacive transformations. *Reconstructive* transformations involve the breaking of the Si-O bonds and the establishment of new bonds; as a result they are quite sluggish. The transformations from quartz to tridymite and to cristobalite are examples of reconstructive transformations. In the *displacive* transformations, the silica tetrahedra are slightly distorted (tilted) and the lattice assumes higher symmetry. The chemical bonds are not broken and each atom remains surrounded by the same neighbours. The transformation from the low temperature- α forms to the high temperature- β forms are examples of displacive transformations. Quartz, tridymite and cristobalite exist in both α (low temperature) and β (high temperature) forms. Displacive

transformations are faster than reconstructive transformations (Prewitt *et al.* 1994).

The different crystal structures which quartz assumes upon heating and cooling are summarized in Fig. 2.18. When α -quartz is heated without the addition of mineralisers or fluxes, it transforms to β -quartz, which, in turn, transforms to β -cristobalite, and by further heating β -cristobalite melts (Chaklader *et al.* 1961). The formation of tridymite during heating depends on the presence of mineralizers. Fenner studied the different phase transformation of quartz upon heating and used the flux $\text{Na}_2\text{WO}_4 \cdot 2\text{H}_2\text{O}$ to increase the reaction rates of the different phase transformations (Fenner 1913). He found that α -quartz transforms to β -quartz at 573 °C, β -quartz transforms to β -tridymite at 870 °C, β -tridymite transforms to β -cristobalite at 470 °C, and β -cristobalite melts at 1713 °C. He also found that without the flux (i.e. when pure quartz was heated), cristobalite was formed and the tridymite structure was totally absent. It is now generally accepted (Chaklader *et al.* 1961; Kucharski *et al.* 1981; Moroz *et al.* 1985; Waclawska *et al.* 1985; Sharp *et al.* 1997; Sharp *et al.* 1998), that the tridymite formation/stability depends on the presence of alkali and alkaline ions.

When cooled under non equilibrium conditions, β -cristobalite and β -tridymite are transformed to the metastable low temperature modification α -tridymite and α -cristobalite (Moroz *et al.* 1985). In particular, when β -quartz is cooled below 573 °C at 1 bar, α -quartz forms. The transition temperature between low- and high-temperature modifications in cristobalite differs on heating and cooling (Prewitt *et al.* 1994).

Excavations of silicon furnaces show that quartz transforms to cristobalite. The transformation from β -quartz to β -cristobalite was a subject of extensive studies. There is a controversy about whether the quartz-cristobalite transformation is a direct process or necessitates the presence of an intermediate amorphous/liquid phase. Kuellmer and Poe (Kuellmer *et al.* 1964) found no pronounced amorphous phase below 1550 °C and showed that the transformation occurred through highly fragmented quartz. Mackenzie (Mackenzie 1960) heated quartz up to 1900 °C, in some cases he found the transitional phase, in some other not. However, many authors (Chaklader *et al.* 1961; Scherer *et al.* 1970; Mitra 1977) showed from DTA and XRD-determinations that the quartz-cristobalite transformation was indirect and involved an intermediate non crystalline amorphous, highly fragmented transition phase. Under conditions where the rate of crystallization to cristobalite is the faster process, little or no amorphous phase may be observed and one might erroneously conclude that a direct

transformation from quartz to cristobalite was taking place (Scherer *et al.* 1970).

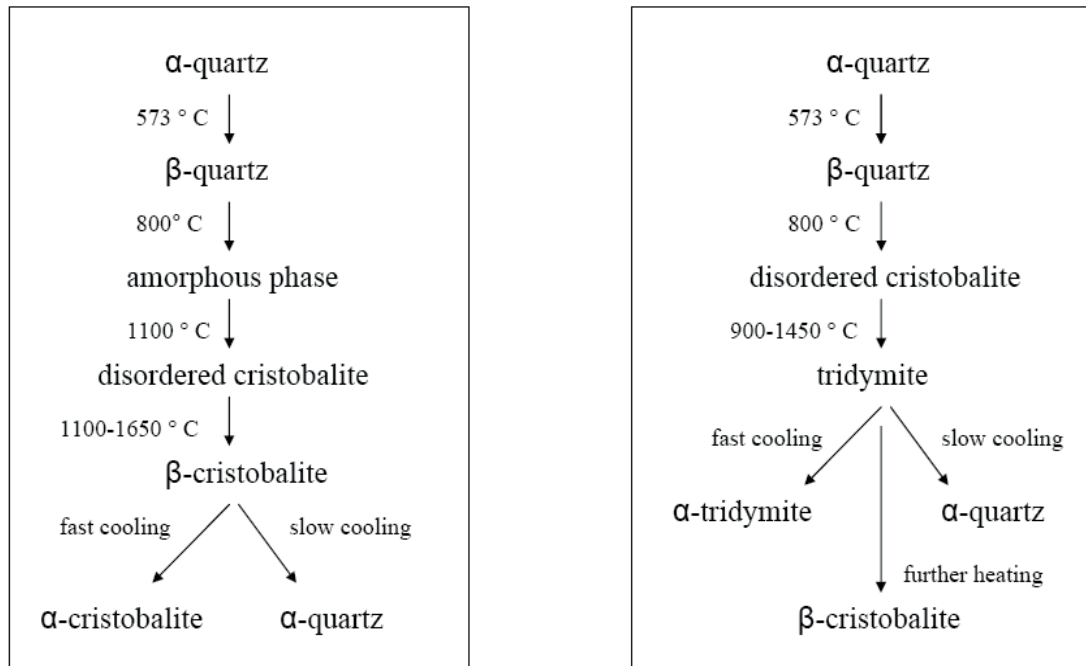


Fig. 2.18 Silica polymorphs during heating: (on the left) heating of quartz in absence of mineralisers (Chaklader *et al.* 1961); (on the right) heating of quartz in presence of mineralisers (Fenner 1913).

Grain boundaries, cracks, fissures (Waclawska *et al.* 1985), liquid inclusions (Gemeinert *et al.* 1992), impurities, inclusions (Chaklader 1961; Kucharski *et al.* 1981; Stoch *et al.* 1985; Waclawska *et al.* 1985), the atmosphere (Ainsle *et al.* 1962; Andersen 2009), the heating profile (Aasly 2008; Andersen 2009) and the quartz particle size (Chaklader *et al.* 1961; Hand *et al.* 1998) affect the transformation of quartz to the transitional phase and therefore to cristobalite.

Liquid inclusions decrepitate upon heating leaving porosities and promoting the formation of cristobalite (Gemeinert *et al.* 1992). *Cracks and grain boundaries* favour the transformation to the transitional phase and therefore to cristobalite. The transformation of quartz to transitional phase can proceed from the grain boundaries, which become molten during prolonged heating, or inside the grains, through cracks and fissures (Waclawska *et al.* 1985). According to Aasly (Aasly 2008) more cristobalite forms when quartz having *small grains* is used. According to Balek and Steinike (Balek *et al.* 1988; Steinike *et al.* 2000), *mechanically activated quartz* (low temperature form) transforms directly into

cristobalite at a lower temperature of 1200 °C. According to Chaklader (Chaklader *et al.* 1961) and Hand (Hand *et al.* 1998), when *fine quartz particles* are heated less cristobalite formed. The reason is that the amorphous intermediate phase is more readily formed and the fine particles sinter together. *Trace elements*, such as alkaline ions (Li, Na, K) and alkaline earths (like Ca and Mg) present in quartz promote the formation of the transitional phase and then its crystallization into cristobalite because they weaken the bonds in the silicon-oxygen network and lower the viscosity facilitating the migration of ions (Stoch *et al.* 1985). According to Chaklader (Chaklader 1961) Al³⁺ has a catalytic effect on the formation of cristobalite. *Minerals*, with melting temperature lower than that of pure silica promote the formation of melts at the grain boundaries and therefore of cristobalite (Stoch *et al.* 1985). Compared to other quartz rocks, *hydrothermal quartz* contains more alkalis, and forms more transitional phases and more cristobalite upon heating (Waclawska *et al.* 1985). More cristobalite forms in Ar *atmosphere* than in CO(g) atmosphere (Andersen 2009). The cristobalite growth rate is sharply decreased in a reducing atmosphere (Ainsle *et al.* 1962). Also the *heating profile* influences the cristobalite formation: more cristobalite forms if quartz is heated slowly rather than shock heated (Aasly 2008).

2.5.2 Crack formation

During heating quartz develops cracks. There are three main factors which contribute to the crack formation in quartz: 1) low density high temperature silica polymorphs; 2) presence of liquid inclusions and 3) mineral inclusions at the grain boundaries.

1) Quartz has a high thermal expansion coefficient and during heating transforms to low density polymorphs. For a single isolated crystal this does not matter much, but in a crystal group the individual grain expand differently in different directions, inducing considerable stress and therefore cracks (Aasly 2008). In addition, because the density of the transition phase is much lower than that of the quartz (Table 2.3), the transition phase occupies a greater volume than the parent phase and cracks form. Examples of expansion of quartz pieces during heating are reported by (Andersen 2009). Examples of fragmentation of quartz during heating are reported by Aasly (Aasly 2008). According to Aasly (Aasly 2008), the strongest quartz types are probably the quartzes having fine-grained and

lobate grain boundary textures. Cracks follow the mechanically weakest path through the rock which is along grain boundaries or healed cracks. This path requires a long propagation distance for fine grained and lobate grain boundaries, and therefore breaking this quartz is difficult. On the other hand, coarse-grained and polygonal grain boundary textured samples are the weakest because the fracture follows the shortest path straight through each single grain.

Table 2.3 Density of the silica phases during heating quartz at ambient pressure (Chaklader *et al.* 1961; Ford *et al.* 2004).

Silica	Density (g/cm ³)
α -quartz	2.65
β -quartz	2.53
Intermediate transition phase	2.3
β -tridymite	2.25
β -cristobalite	2.20

2) During heating of quartz, the internal partial pressure of the fluid inclusions increases and they decrepitate; i.e. cracks develop in the quartz enabling degassing of water and CO₂ from the inclusions (Gemeinert *et al.* 1992). Decrepitation occurs in the temperature range from 200 to 600 °C depending on the fluid composition and size. For example H₂O-CO₂ mixtures have a very steep P-T path, and decrepitate early during heating (Samson *et al.* 2003).

3) The presence of mineral inclusions, such as muscovite, can lead to cracks formation in quartz during heating. This is because the mineral inclusions have generally lower melting point than quartz and are mostly present at the grain boundaries.

2.5.3 Melted quartz

Quartz (β -cristobalite) melts at 1723 °C. The melting point increases by increasing the quartz particle size and decreasing the impurity content (Stoch *et al.* 1985). The preferred sites for nucleation of melting are the external surface of the crystal, the grain boundaries and the dislocations.

Silicate melt is a highly viscous liquid amorphous material that lacks long-range order (Henderson 2005). The structure of melted silica is a mixture of silica rings, tetrahedra, chains, sheets as well as polymerized SiO₂. In the silica melt the tetrahedral are randomly oriented, while the average (Si-O)

distance is still 1.61 Å (Vukceвич 1971) as in the crystalline forms. Scherer et al. (Scherer et al. 1970) calculated the entropy of fusion of quartz and cristobalite, the values were very small, which reflects the similarity of the coordination polyhedra and their arrangement in the liquid and crystal modification.

The most recognized model of silica melts is the continuous random-network model “CRN model” by Zacharian and described in (Henderson 2005). According to this model, bridging oxygen atoms (BO) are oxygen atoms, which are bonded to two silicon atoms, and non-bridging oxygen atoms (NBO) are oxygen atoms bonded to one silicon atom. NBO atoms have a negative charge, which can be balanced by a positively charged cation. Network formers, such as Fe, Al and Ti share BO atoms and make up the bulk of the structure through corner. Network modifiers, such as Na, Ca and K, modify the continuous silicate network by breaking the BOs.

2.5.4 Minerals behavior when heating quartz

Mineral inclusions generally melt at temperature below the quartz melting point. Hammouda (Hammouda *et al.* 1999) studied the kinetics of melting of fluorphlogopite, a model muscovite, in quartz. After heating the assemblage of the two minerals above 1300 °C, two immiscible melts containing crystals of chondrodite ($MgF_2 \cdot 2Mg_2SiO_4$) were found at the contact between the two reactants. Chondrodite was stable in both liquids. In particular, the two immiscible phases consisted of a SiO_2 rich phase in contact with quartz and a MgO, F, Al, K- rich phase in contact with the mica. Al, K, Mg partitioned between the two immiscible liquids.

Lynch (Lynch 2004) described the interaction between two minerals in quartz, apatite $Ca_3(PO_4)_2$ and iron-oxide Fe_3O_4 , when the quartz is heated in a silicon furnace. As quartz is heated to 1600 °C iron oxide fuses and dissolves in SiO_2 forming a slag. At higher temperatures quartz starts melting becoming viscous and the Fe-containing slag is exposed to the reducing atmosphere of the furnace. Iron oxide is reduced to Fe droplets. When P in apatite and Fe droplets enter in contact, they form a very stable compound, which has a low volatility and therefore will dissolve in the silicon metal.

2.6 Diffusion of impurities in quartz

2.6.1 *Diffusion of impurities in crystalline quartz*

In a crystalline solid diffusion can occur by volume diffusion through the crystal lattice, and by easier routes involving grain boundary diffusion and surface diffusion. Grain boundary diffusion and surface diffusion involve line or surface defects (grain boundaries, dislocation, free surfaces). Grain boundary diffusion is the dominant diffusion mechanism in fine grained polycrystalline material at low temperatures. Surface diffusion is important when free surfaces are exposed to fluids or when fluid-mineral exchange occurs. Volume diffusion is the dominant mechanism at high temperatures and requires the existence of lattice defects (usually vacant lattice sites or interstitial ions) (Freer 1981).

The diffusion of cations in quartz is influenced by 1) the typology of the impurity, and 2) the silica polymorph.

1) The *type of the impurity* affects the diffusion of cations in quartz. The effective ionic radius of various cations and diffusivity data are reported in Table 2.4. The diffusion coefficient varies with the cation radius, the charge and the lattice position (VDEh 1995). Alkaline ions (Li^+ , Na^+ , K^+) diffuse into structural channels parallel to the c-axis where the interstitial positions are placed (Grimstvedt *et al.* 2002; Larsen *et al.* 2004). Na^+ , Li^+ , K^+ , due to the relative weakness of purer ionic bonds (Larsen *et al.* 2009), are easily mobilized along the c-axis (Kronenberg *et al.* 1987) and their diffusivity is high in comparison to other substitutional elements such Al^{3+} , Ti^{4+} and P^{5+} (Verhoogen 1952; Pankrath *et al.* 1994; Cherniak *et al.* 2007). The mobilization of Al depends on the alkali compensator. If the alkali cation is large, the polarization and attraction of the surrounding oxygen atoms is weaker, more lattice distortion results and hence the Al mobilization becomes easier (Cherniak 2010). Ti has a larger charge than Al (+4 vs. +3), which may contribute to its lower diffusivity with respect to Al. Fe^{3+} diffuses together with a O^- vacancy or H^+ (Penniston-Dorland 2001). The diffusion coefficient of O isotopes in quartz in “wet” hydrothermal experiments are four to seven orders of magnitude larger than in “dry” experiments (Joesten 1991), hence, demonstrates that the presence of water increases the diffusion of Fe by affecting either the rate of the diffusion of O^- vacancies or H^+ cations.

Table 2.4 shows the calculated diffusivity values D (m^2/s) for various impurities in quartz for a narrow range of temperatures. Only a limited

range of temperature is available because the Arrhenius plots are not always linear outside the range of temperature experimentally measured as temperature-dependence of diffusion data exhibit extrinsic and intrinsic regimes changing the slope of the lines. Intrinsic diffusion regimes operate when volume diffusion is controlled, extrinsic regime when surface grain boundary diffusion is the dominant one.

The data relative to quartz have been calculated under the condition $P_{O_2} = \text{air}$. Quartz in the furnace experiences a reducing atmosphere. The data in the table have therefore not to be taken as absolute, but relative comparison among diffusivities of different cations is possible.

2) The *silica polymorphs* influence the diffusion properties of cations. Voids, cracks and open structures accommodate foreign ions easily. Tridymite and cristobalite have more open structures than quartz (Table 2.3) and their voids in the structure are large enough to accommodate atoms such as Na^+ , K^+ or Ca^{2+} (Presser *et al.* 2008). Consequently the solubility of these elements in tridymite and cristobalite is higher than in quartz. Kawasaki *et al.* (Kawasaki *et al.* 2008), found that the solubility of Fe^{3+} in cristobalite increases with the temperature. According to Frischat (Frischat 1970), the change in silica crystal structure from lower to higher symmetry would permit “easier” transport of Na. There is a wide scatter among the data for Na diffusion (Table 2.4).

Impurities diffuse also during hydrothermal alteration when primary quartz re-crystallizes to secondary quartz which is generally of higher purity. Armington and Balascio (Armington *et al.* 1984) experimentally recrystallized quartz under hydrothermal conditions and found that Fe, Al, K, Li are easily mobilized with Fe the most mobile. According to Larsen *et al.* (Larsen *et al.* 2004) Li, K and B are easily mobilized during hydrothermal alteration of pegmatitic quartz. In particular the content of B and Li decreases in the quartz. Müller (Müller *et al.* 2005) observed that the iron content of quartz adjacent to the Fe-bearing minerals increased exponentially indicating a diffusion profile for Fe.

Table 2.4 Effective ionic radius (Å), diffusivity D (m²s⁻¹) of elements in quartz under certain temperatures, and estimated diffusion distance after 1h at the indicated temperatures. The diffusion distance was calculated by using the approximate relation $x^2 \cong Dt$, where x is the diffusion distance (m), D the diffusion coefficient (m²s⁻¹) and t the time (s).

Ion	D (m ² /s)	T (C°)	Matrix and direction of diffusion	Effective ionic radius, (Å) (Whittaker <i>et al.</i> 1970)	Diffusion distance (µm/h)	Measurement method	Ref.
Ca ²⁺	1.3x10 ⁻¹⁴	600	to c-axis	1.08-1.43	6.84	Istantaneous plane source	(Frischat 1970)
Na ⁺	2.1x10 ⁻¹⁴	500	to c-axis	1.46-1.68	8.69	Electrical conductivity	(Verhooogen 1952)
	1.3x10 ⁻¹³				21.6	Diffusion couple	(Verhooogen 1952; Frischat 1970)
Li ⁺	4.2x10 ⁻¹³	500	to c-axis	0.68-0.82	39	Electrical conductivity	(Verhooogen 1952)
K ⁺	4.4x10 ⁻¹⁵	500	to c-axis	1.46-1.68	3.98	Electrical conductivity	(Verhooogen 1952)
Al ³⁺	10 ⁻²⁴	500	and ⊥ to c-axis	0.47-0.61	10 ⁻⁴	Electrochemical	(Pankrath <i>et al.</i> 1994)
Fe ³⁺	10 ⁻¹⁶		Geological measurements	0.57-0.73	0.6	Electron probe point analysis	(Stock <i>et al.</i> 1976; Penniston-Dorland 2001)
Ti ⁴⁺	10 ⁻²²	700	and ⊥ to c-axis	0.94-0.69	10 ⁻⁴	Electrical conductivity	(Cherniak <i>et al.</i> 2007)

2.6.2 Diffusion of impurities in molten quartz

Scherer *et al.* (Scherer *et al.* 1970) calculated the entropy of fusion of quartz and cristobalite, the values were very small, reflecting the similarity of the coordination polyhedra and their arrangement in the liquid and crystal. Moreover, both amorphous silica and β-cristobalite have almost equal densities. These two factors lead to the assumption of potentially

similar transportation-diffusion processes through both crystalline and molten silica (Presser et al. 2008).

Na⁺, Li⁺, K have the property to form percolation channels in melted silica (Greaves 1985). In particular Na⁺ and K⁺ adopt a non uniform distribution: they exist as clusters around NBOs and with increasing content, form percolation channels (Greaves 1985; Huang *et al.* 1991). Fowkes et al. (Fowkes *et al.* 1970) found that Na accumulates at the silica surface: 2 ppm Na as bulk concentration in silica resulted in 2 wt% Na at the SiO₂ surface after annealing the sample at 1000 °C.

The diffusion of species in ionic molten silicate base is higher than in crystalline silica. Table 2.5 shows the diffusivity values for various silicate slags (VDEh 1995). The diffusion coefficient increases by increasing the temperature, by decreasing the SiO₂ content and the cation radius. Molten minerals, as well as regions of contact between melted minerals and quartz are examples of silicate slag.

Table 2.5 Impurity diffusion in silicate slags (VDEh 1995). RA= residual activity; DC= diffusion couple; CR= capillary method; CHRP= chrono-potentiometry. Diffusivity D (m²s⁻¹) of elements in quartz under certain temperatures and slag composition, and estimated diffusion distance after 1h at the indicated temperatures. The diffusion distance was calculated by using the approximate relation $x^2 \cong Dt$, where x is the diffusion distance (m), D the diffusion coefficient (m²s⁻¹) and t the time (s).

Ion	D [m ² /s]	T [C°]	Composition, slag is in mol fraction	x [mm]	Method
Ca ⁴⁶	1.5 · 10 ⁻⁵	1150	Slag: Na ₂ O(0.25) - SiO ₂ (0.75)	180	RA
Mg	3.2 · 10 ⁻⁶	1450	Slag: Al ₂ O ₃ (0.12)-SiO ₂ (0.43)-CaO(0.43)	11.5	DC
	2.1 · 10 ⁻⁶	1450	Slag: CaO(0.37)-Fe ₂ O ₃ (0.1)-SiO ₂ (0.52)	7.6	DC
K	3.1 · 10 ⁻⁷	1050	Slag: Na ₂ O(0.25) - SiO ₂ (0.75)	1.1	CR
P	2.9 · 10 ⁻³	1450	Slag: CaO(0.37)-Fe ₂ O ₃ (0.1)-SiO ₂ (0.52)	6 · 10 ³	DC
Ti	2.3 · 10 ⁻⁷	1450	Slag: Al ₂ O ₃ (0.12)-SiO ₂ (0.43)-CaO(0.43)	0.8	DC
Mn	1.6 · 10 ⁻²	1450	Slag: Al ₂ O ₃ (0.12)-SiO ₂ (0.43)-CaO(0.43)	6 · 10 ⁴	DC
Fe ²⁺	0.7	1450	Slag: Al ₂ O ₃ (0.12)-SiO ₂ (0.43)-CaO(0.43)	2 · 10 ⁶	DC
Ni ²⁺	4.3 · 10 ⁻⁷	1150	Slag: Na ₂ O(0.33)-SiO ₂ (0.67)	1.6	CHRP
Ni	2.8 · 10 ⁻³	1450	Slag: CaO(0.37)-Fe ₂ O ₃ (0.1)-SiO ₂ (0.52)	1 · 10 ⁴	DC

2.7 Quartz beneficiation

As mentioned in paragraph 2.3, a high purity quartz is an important requirement in the silicon production. When high purity quartz is too expensive or not easily available, beneficiation of less pure quartz is the suggested solution.

As described in paragraph 2.4 natural quartz carries many impurities in the form of structural impurities, fluid inclusions, and solid inclusions. Structural impurities are difficult to remove, therefore the quartz quality largely depends on their amount. Fluid inclusions can be removed by heating the quartz but may leave stable elements in solution. According to Gemeinert (Gemeinert *et al.* 1992) fluid inclusions decrepitate during heating of quartz enabling degassing of water and CO₂ and possibly other contaminants included in the gas phase. However it is not clear to which extent the contaminants present in the liquid inclusions leave in form of gaseous compounds. Solid inclusions, which are most commonly located at the grain boundaries, can be removed by means of mineral processing beneficiation techniques.

Mineral processing techniques adopt a combination of comminution and separation techniques in order to remove mineral inclusions from the rock matrix. Comminution is the liberation of individual mineral particles, while separation is the physical separation of the liberated mineral particles.

The size of the contaminating mineral defines the size reduction to be accomplished with the comminution techniques. Since separation techniques can be performed only on specific range size particles, the size of the contaminating mineral defines also the separation technique to be used.

Liberation techniques, such as crushing, grinding, milling and electric fragmentation reduce the raw quartz to the required product size and liberate to some extent the mineral impurities from the matrix. Among these techniques, electric fragmentation has the advantage to liberate selectively the mineral inclusions from the rock matrix and producing the lowest amount of undesirable fines (Andres *et al.* 1999; Cho *et al.* 2006; Selfrag 2011). Example of separation techniques are sieving, magnetic separation, flotation and optical sorting. In order to achieve physical separation, the minerals to be separated must exhibit differences from quartz with respect to one or more physical or chemical properties: sieving is a suitable separation method for particles having different size; magnetic separation is effective for particles having different magnetic susceptibility; classification, gravity separation, flotation, electrostatic separation and

optical sorting are effective when particles show different settling velocity, density, surface chemistry, electrical conductivity and appearance respectively (Sandvik *et al.* 1999). Leaching is a chemical separation technique that allows the dissolution of liberated minerals or of minerals still attached to the quartz surface.

The most effective way to partially remove structural impurities from quartz is by leaching the quartz surface. The traditional acid is hydrogen fluoride (HF) mixed with different fractions of strong acids such as HCl, HNO₃ or H₂SO₄. Examples of beneficiated quartz of total impurity content below 1 ppmw can be found in (Aulich *et al.* 1982) and (Yoshiyagawa *et al.* 1985). However the disadvantage of using acids is that they are not environment-friendly, moreover HF containing acids react with the quartz itself leading to unnecessary losses (c. 25%) and is rather expensive.

2.7.1 Electric fragmentation

Electric fragmentation is an interesting alternative to the conventional crushing. Crushing does not liberate selectively the mineral from the rock matrix and produces a high amount of fines, which are lost since they cannot be introduced in the furnace. Electric fragmentation, on the other hand, selectively disintegrates rock minerals along the grain interfaces and between mineral constituents and ore matrices. The selective fracture pattern of rocks depends on the electric properties, material properties and geometries, and dynamic fracture processes of the rock.

The equipment for the electrical disintegration consists of a pulse generator and a disintegration chamber, where the material is submitted to the action of high voltage electrical pulses. The rock is immersed in a dielectric liquid, usually water and short pulses of high-voltage electrical field (pulse rise times less than 500 ns) are applied. In a response a local electrical field and streamers form at the interfaces between minerals and matrix of different permittivity (Schon 2004; Andres 2010). When the local field in the rock specimen exceeds its dielectrical strength, an electrical breakdown occurs: intramolecular bonds break, converting the solid directly to gas, and generating a pattern of thin ($\sim 1\mu\text{m}$) capillaries (Andres 1995). The preferential tunneling of the tree like current paths occurs at interfaces of mineral inclusions with different electrical properties (Andres 1995; Andres *et al.* 1999). The plasma channels, i.e. vaporization of extremely small amounts of material, cause an instantaneous thermal expansion (10^{-6} - 10^{-4} sec (Burkin *et al.* 2010)) and produce an acoustic shock wave (Bluhm

2000). The shock wave propagates spherically throughout the material. The oscillation of the shock waves, causes repeated compression/expansion in the matrix (Andres and Bialecki 1986). The fragmentation takes place as a result of the weakening of cohesion by repeated compressive-expansive loading of a lump during oscillations of the shock waves. Phase contacts act as a discontinuity where cracks may initiate and propagate. Micro-cracks can nucleate and propagate where two mineral phases have different rheological properties and local stress accumulates. The principles of electrical fragmentation are shown schematically in Fig. 2.19.

De Elio de Bengy (De Elio de Bengy *et al.* 2010) compared the effect of conventional crushing and electric fragmentation in hydrothermal quartz. Mineral inclusions were mostly iron oxides and feldspars. Quartz was fragmented to 4 mm size and magnetic separation, acid leaching, flotation were performed after fragmentation. The degree of liberation was higher for the quartz electrical fragmented when magnetic separation and flotation were applied.

Andres (Andres *et al.* 1986) studied the liberation of Mg from the S.African willimite ore both by conventional mechanical crushing and by electrical fragmentation. Microscopic observations of the liberation products showed a system of fissures in the area of joints of different materials with different electrical parameters. He also observed an increased efficiency of leaching in the electrically fragmented rock.

Cho *et al.* (Cho *et al.* 2006) fractured by electric pulses circular rock samples of three different types: granite, tuff and sandstone of 3 cm diameter. They studied the microstructure and fracture pattern of the test samples. Radial tensile cracks developed from the current flow path between two electrodes regardless of the rock constituents or minerals. The number of cracks decreases by increasing the sample size. The number of fragments, and the fragment pattern varied with different rock types and applied voltages. In the granite samples, radial cracks propagated quickly regardless of rock constituents. In the tuff sample, major cracks propagate along the boundaries of minerals. The sandstone sample was a relatively homogeneous material and therefore the radial cracks propagated with a more tortuous path. These results are in agreement with Andres (Andres *et al.* 1999).

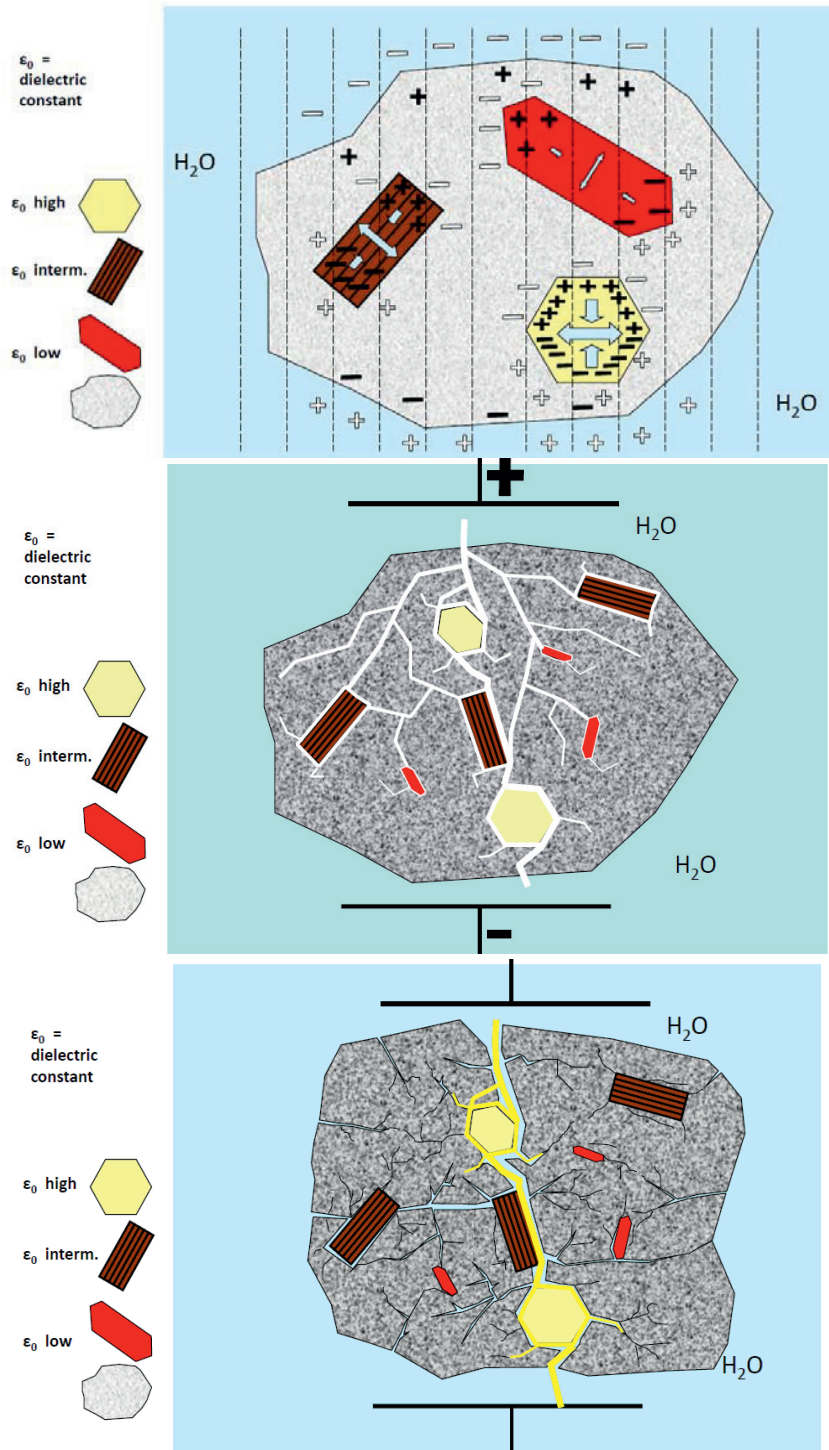


Fig 2.19 Electric fragmentation On a rock sample. From the top to the bottom: local electrical field at the interfaces between minerals and matrix of different permittivity; formation of streamers directed to the mineral inclusions, electrical breakdown and shock wave cause rock disintegrations. Drawings by Alexander Weh (Selfrag).

2.7.2 Beneficiated quartz needs to be milled: mechanical activation of quartz and agglomeration

Fines should be avoided in the furnace because they lower the permeability of the charge. Beneficiation of quartz produces a fine-grained material which requires agglomeration and subsequent charging of the quartz in form of pellets. In order to be agglomerated, the particles need to be milled to micrometer size.

During milling the quartz is mechanically activated: Si-O bonds are broken and highly disordered silica layers form on the surface of the quartz grains, the disorder decreases moving from the surface towards the middle of the quartz particle, still in crystalline form. The thickness of the distorted zone varies from 20 to 500 nm (Balek 1988). The distorted zone is a deviation from the ideal lattice and the metastable defects lead to storage of energy and increase the solid reactivity of the quartz (Balek *et al.* 1988; Benezet *et al.* 1988; Steinike *et al.* 2000; Damn *et al.* 2009). According to Steinike and Tkáčová (Steinike *et al.* 2000), mechanically activated quartz shows an increase in the extent of adsorption and gas diffusion into the disturbed near surface layers. Quartz seems more reactive with CO₂(g) than O₂(g). They also observed that mechanically activated quartz (low temperature form) transforms directly into cristobalite at a temperature of 1200 °C, which is lower than the 1400 °C high-temperature quartz-cristobalite transformation. This was confirmed by (Balek *et al.* 1988).

High purity silicon can be produced with pellets made of beneficiated quartz and high purity carbon black (Fabris *et al.* 1984; Amick *et al.* 1985; Yoshiyagawa *et al.* 1985; Strake *et al.* 1988; Kvande *et al.* 2010). Fesil has developed the Solsilc process, where high purity quartz and reducing agents are processed. Natural gas is cracked to produce high-purity carbon black that is combined with quartz and SiC fines using a high purity binder. No wood chips or coal, which are significant sources of impurities, are used in the reduction process.

Agarwal and Pal (Agarwal *et al.* 1998) studied the kinetics of reactions in pellets made of carbon black and quartz. The reaction rate increased by reducing both the carbon and quartz particle size, but no significant improvement occurred below a critical particle size of 20 µm. When pellets made of carbon and silica mixture were heated, they reacted quickly to SiO(g) and CO(g). The pellets porosity led to higher rates of diffusions of CO(g) and SiO(g) from pellets and therefore an increase in reaction rate for the reduction of SiO₂ to SiO(g) (equation 2.7).

3 EXPERIMENTAL SETTING AND ANALYTICAL TECHNIQUES

The aim of this research work is to develop the strategies for impurity removal in the quartz feedstock prior to charging into the silicon furnace, and to understand the properties of the impurities during the carbothermic reduction of quartz. Particularly we wish to study the removal of mineral impurities from quartz prior to carbothermic reduction by means of selective fragmentation, the reaction mechanisms when producing silicon from mixtures of quartz and silicon carbide in form of lumps or pellets, and the distribution of impurities between the quartz and the process gases during the quartz carbothermic reduction.

The experimental methods are summarized in Table 3.1 and described in detail in the following paragraphs. The different characterization methods are summarized in paragraph 3.2. Thermodynamic calculations were done using the software package FactSage. The purpose was to test and verify, alternatively to falsify the experimental results in the settings 2 and 4.

The considered variables include charge type, reaction time and temperature, charge mixture and atmosphere. These variables have a continuous range of values in the real production process, however only selected values were used in the experimental work. Experimental conditions are compared to full scale production in Table 3.2.

Table 3.1. Summary of the experimental methods and analysis techniques used.

Experiments	Purpose	Analysis technique used
<p>1- A novel beneficiation route for hydrothermal quartz based on electrical fragmentation, sieving and magnetic separation has been tested in laboratory scale equipments. This novel route has been compared to the conventional method based on mechanical crushing.</p>	<p>The purpose was to investigate the advantages of using electric fragmentation in terms of cracks distribution, mineral liberation, fragment morphology.</p>	<p>The morphology of the fragmented quartz particles was studied by EPMA and OPTICAL MICROSCOPY, the impurity content in quartz after beneficiation was estimated with ICP-MS.</p>
<p>2- Mixtures of SiO₂+SiC were charged in graphite crucibles and heated to 2000 °C for 10 min in an inductive furnace. The variables tested were: pellets and lumpy charge, two different hydrothermal quartzes and two initial SiO₂:SiC molar ratios (1:1; 1:2).</p>	<p>The purpose was to compare the properties of pellets and lumps during the silicon production reactions.</p>	<p>The morphology of the reacted charge was studied by EPMA. XRD and XRF analyses were used to quantify the output phases of the experiments.</p>
<p>3- Quartz pieces were heated in a reducing CO(g) atmosphere in a sessile drop furnace. SiO(g) was produced. Two hydrothermal quartz types were studied.</p>	<p>The purpose was to study the ability of different quartz types to produce SiO(g).</p>	<p>The production of SiO(g) was calculated from the weight losses after heating quartz at different temperatures.</p>
<p>4- Mixtures of SiO₂+Si and SiO₂+SiC were heated in graphite crucibles to 1650 °C and 1850 °C. A graphite tube furnace was used. The charges were either pellets or lumps and either hydrothermal quartz or quartzite. The elements studied were B, P, Al, Fe, Mn, Pb, Zn and K. SiO(g), CO(g) and other gaseous compounds formed and were collected as a condensate.</p>	<p>The purpose was to investigate which gas compounds form other than SiO(g), during quartz reduction, and to which extent.</p>	<p>The morphology of the reacted quartz was investigated by EPMA, the nature of the reacted charge and the condensate was analyzed by XRD. The chemical composition of the condensate was analyzed by ICP-MS.</p>

Table 3.2. Experimental results compared to full scale production

Experimental work: selected values for each variable	Full scale production: each variable may have a range of values
Charge type investigated: <ul style="list-style-type: none"> • Pellets ($\phi=1-3$ mm) • Lumps (3-5 mm) 	Quartz can be charged in the silicon furnace in form of lumps or pellets. Lumps are usually charged in 5-8 cm size. However when lumps in the furnace experience thermal shock they disintegrate to fragments of any size down to mm depending on the type of quartz, charging strategy and on the high temperature properties of the quartz. Pellets are far smaller than lumps: they are aggregate of particles of μm size pelletized to a diameter of $\phi=1-3$ mm.
Beneficiation route investigated: Electrical fragmentation → sieving → magnetic separation	Pellets only recently applied in full scale silicon production and are made from beneficiated quartz. However, standard processing routes for quartz pellets are unavailable.
Quartz reaction time investigated: <ul style="list-style-type: none"> • min 10 min • max 5h 	The charge in the furnace experiences different retention times. A charge close to the electrode will experience a lower retention time (minutes) than the one near the lining (days).
Reaction temperatures investigated: <ul style="list-style-type: none"> • Heating to 1650°C • Heating to 1850°C • Heating to 2000°C 	The process temperature varies from 1500 °C on the top of the furnace to 2000 °C in the crater zone. As the charge moves down to the crater zone, it features higher temperatures. If the charge moves slowly down to the crater zone, it experiences a slow heating profile. However, the charge may experience unpredicted quick variation in temperature when it cascades from the top to the crater zone, or if it encounters gas channels, which develop from the crater zone toward the upper zone.
Phase mixtures and molar ratios investigated: <ul style="list-style-type: none"> • $\text{SiO}_2:\text{SiC} = 1:1; 1:2$ • $\text{SiO}_2:\text{Si} = 1:1$ 	Quartz, once charged in the furnace, interacts with various reacting phases: carbon, silicon carbide and silicon and is reduced. The reacting phases form complex aggregates without a defined molar ratio and phase mixture composition. Examples of mixture which can be found in the furnace are: $\text{SiO}_2+\text{C}+\text{SiC}+\text{condensate}$; SiO_2+C ; $\text{SiO}_2+\text{SiC}+\text{C}$; SiO_2+SiC ; $\text{SiC}+\text{Si}$; SiO_2+Si ; SiC ; Si . Charge mixture SiO_2+SiC is representative of the inner, high temperature zone of the silicon furnace.
Atmosphere investigated: <ul style="list-style-type: none"> • P_{CO} and P_{SiO} created while heating the charge mix. • $P_{\text{CO}}=1$ 	The charge mixtures do not necessarily face a gas partial pressure formed by the local mixtures composition: gas channels develop from the crater zone toward the upper zone allowing unpredictably quick variations in $\text{SiO}(\text{g})$, $\text{CO}(\text{g})$ concentrations; in addition the charge at the top may collapse in to the crater zone and experience sudden high P_{SiO} and temperature.

Type of contamination investigated: <ul style="list-style-type: none"> • Diffusion • Condensation 	Quartz containing impurities is a source of contamination for the silicon. The mechanisms of silicon contamination are not clear: contamination can happen through diffusion from the quartz matrix to the silicon phase, or through the silicon production reactions, which occur in the reduction of silicon carbide or during condensation.
---	--

3.1 Materials

Three quartz-types have been investigated in this thesis work:

1. Hydrothermal quartzA
2. Hydrothermal quartzB (batch1)
3. Hydrothermal quartzB (batch2)
4. Quartzite

Nordic Mining provided the hydrothermal quartzB from the Nesodden deposit, which is located in the Hardanger fjord (Norway). The quartz was chosen because of the promising low trace element content, and the availability of min. 2.7 million ton which provides an interesting raw feedstock for SoG-Si production with a purity of more than 99,95% (Ihlen *et al.* 2009; NordicMining 2011). QuartzB (batch1) and quartzB (batch2) are samples collected from two different locations of the same hydrothermal deposit. Hydrothermal quartzA and quartzite have been used industrially for the production of Si and Fe-Si respectively.

The quartzes were used as lumps or pellets. Lumps were obtained by crushing quartz to 3-5 mm size. Pellets consisted of a mixture of quartz and silicon carbide milled to powder (quartz particles below 20 μm and SiC particles below 10 μm size). Particle size was chosen according to the work done by Agarwal and Pal (Agarwal *et al.* 1998). Water was used as binder during the pelletizing process. The two components of the mixture, SiC and SiO₂, were dry blended together and subsequently fed into a pelletizing plate (22 cm diameter and 24 cm rim on its outer circumference). Simultaneously with the feeding of the two components mixture into the pelletizing plate, demineralised water was supplied to enable the formation of micro pellets (1-2 mm diameter). Since pellets contain water, the charge was dried in a graphite crucible at 80 °C for 10 h prior to the experiments. Saccharine C₁₂H₂₂O₁₂ supplied by Danisco AS was used as a binder.

Table 3.3. Chemical analyses (ppmw) of hydrothermal quartz and quartzite (ICP-MS) after mechanical crushing and jet milling but before charging. Each value comprises a single analysis.

Trace element	B	P	K	Al	Fe	Mn	Zn	Pb	Cr	Ni	Cu
QuartzB(batch1) after crushing	2	-	96	400	54	3.6	-	0.5	<1	<1	<1
QuartzB(batch1) after milling	9	-	118	129	233	-	-	0.7	\	\	\
QuartzB(batch2) after crushing	1.4	<3.4	<43	44	21	0.3	-	0.2	<1	<1	<1
QuartzB(batch2) after milling	3.7	-	142	199	182	1.9	1.5	0.3	<1	<1	<1
Quartzite after crushing	2.9	6.4	60	453	207	2.8	6.7	1.8	<1	<1	<1
Quartzite after milling	6.4	20.3	195	927	571	6.3	25.3	3.9	<1	<1	<1

Table 3.4. Chemical analysis (in ppmw) of other material used in the experiments. Graphite was analyzed by ICP-AES, SiC by GDMS while Si by ICP-MS.

Trace element	B	P	K	Al	Fe	Mn
Isotropic graphite type IG-110	0.15	-	0.04	0.012	0.06	<0.001
Ultra pure SiC	0.45	0.02	-	6.1	0.37	-
Electronic grade silicon	<0.001	<0.001	-	<0.001	<0.001	<0.001

After milling and crushing, the quartz was analyzed by the ICP-MS method for elements that typically are detrimental for the efficiency of solar cell silicon. They are shown in Table 3.3. K is not particularly detrimental, but is a very common element in mineral inclusions in quartz. The analysis shows the effect of all the contamination sources of quartz such as trace elements, mineral inclusions, fluid inclusion, as well as any contamination from the crushing equipment. The jet milling contaminates the samples with Fe. Hydrothermal quartz is purer than quartzite and generally has lower contents of B, Al, Fe, Mn, Pb. Analyses of other materials used in the experiments are shown in Table 3.4.

3.2 Analytical techniques

This chapter provides a description of the operation of the characterization techniques used. The applicability of the analytical technique for each of the experiments is described in the “Experimental methods” paragraphs.

3.2.1 Electron Probe Micro Analyzer (EPMA)

EPMA, JEOL JXA 8500F was used to identify the morphology of quartz and mineral inclusions embedded in it, to analyze the chemical composition of the mineral inclusions and to study the morphology of phase mixtures such as SiO_2+Si and SiO_2+SiC .

EPMA is a non-destructive technique that requires mechanical polishing of the sample. It provides precise, qualitative and quantitative analysis and mapping of elements in the sample at a resolution of 2 μm or higher. The smallest inclusions that can be analyzed are in the order of 2-3 μm . Elements that can be analyzed go from 4^{Be} to 92^{U} . Quantitative analysis requires extensive use of internationally recognized standards and, depending on the detection limit, mass of the element, counting time, background noise and instrumental settings may be as low as 10 ppmw for optimal elements and conditions.

3.2.2 X-ray diffraction (XRD)

D8 Advance XRD, BRUKER-EVA was used to identify minerals, quartz and silicon carbide polymorphs and to determine the chemical composition of crystalline phase mixtures. BRUKER-TOPAS quantitative Rietveld was used for the phase quantification. The sample preparation consists of milling the solid sample below 50 μm size and pressing it into pellets. XRD has the advantage of quantifying different polytypes of the same phase. This technique becomes challenging when the sample contains an amorphous phase, because the analysis can only be semi-quantitative. However, in the presence of a mixture of crystalline and amorphous phases the relative proportions of the crystalline phases are considered accurate.

3.2.3 X-ray fluorescence spectroscopy (XRF)

X-ray fluorescence (XRF) Bruker AXS S8 Tiger WDXRF, 4 kW generator 60 kV (max.) and 170mA (max.) was used for certain analyses. The instrument provides highly accurate quantitative analysis of the elemental Si composition. The sample preparation consists of milling the solid sample below 50 μm size and pressing it into pellets.

3.2.4 Inductively Coupled Plasma –Mass Spectrometry (ICP-MS)

Element 2* Inductively Coupled Plasma –Mass Spectrometry (ICP-MS) by Thermo Scientific has been used to measure the trace element concentration in bulk samples of quartz, silicon carbide and silicon. Only liquid sample material can be analyzed and, therefore, solid samples must be completely dissolved in various solutions. It is very important to use standard samples with certificated values for the elements and in the concentration range of interest and that the standard sample is derived using at least two independent techniques from two independent laboratories. The major challenge in using ICP-MS is associated with the dissolution of silicon carbide. The dissolution process of SiC is extremely slow because it is only a thin layer (around 100 nm (Presser et al. 2008)) of cristobalite formed on the SiC surface that is dissolved. During SiC digestion, after the first silica layer had dissolved, a new layer forms by thermal oxidation. The digestion time of SiC depends on both particle size and the SiC modification. Finer SiC particles are more prone to digestion than larger particles. Different methods for digestion of SiC are reported in literature include: 1) SiC particles smaller than 5 μm with an average of 0.5 μm can be dissolved in $\text{HNO}_3+\text{H}_2\text{SO}_4+\text{HF}$ solution in a PTFE digestion bomb at 240°C for 8h (Docekal et al. 1992) or at 250 °C for 5 h (Graule et al. 1991); 2) a quantity of 250 mg SiC in a mixture of 3ml HNO_3+ 3ml HF + 6ml H_2SO_4 can be digested in DAB-2 by Berghof for a time varying from 12 to 72 hours depending on the SiC source (GmbH 2012). The complete dissolution of SiC could not be acquired with the crushing and digestion facilities available at NTNU: there is not a crushing machine which reduces SiC down to 5 μm size without contaminating the sample; DAB-2 vessels are not available, and a clean room for the sample dissolution is also unavailable.

3.3 Quartz beneficiation by electrical fragmentation (Experimental set 1)

A novel beneficiation route for hydrothermal quartz based on electrical fragmentation, sieving and magnetic separation was tested with laboratory scale equipment. This novel route was compared to the conventional method which is based on mechanical crushing. Mineralogy beneficiation makes use of comminution and separation techniques. The comminution technique aims at liberating the individual mineral particles. The conventional comminution techniques are crushing and grinding (Sandvik *et al.* 1999).

The jaw crushing and electrical fragmentation unit are shown schematically in Fig 3.1. Electrical fragmentation was performed on a Selfrag Lab utility. The batch equipment handles samples from 1 to 10 kg, and consists of a HV power supply, HV pulse generator, portable process vessels and a lifting table. Samples are loaded into a portable water loaded processing vessel which subsequently is placed onto the lifting table in the loading section. Subsequently, short pulses (pulse rise time less than 500 ns) of high voltage electrical fields are applied. Once the predetermined voltage is reached, the energy of the pulse generator is discharged from the electrode through the solid sample to the bottom of the processing vessel. A shock wave propagates spherically throughout the quartz material and electrical fragmentation occurs. A sieve is inserted in the bottom of the process vessel to collect the fragmented particles.

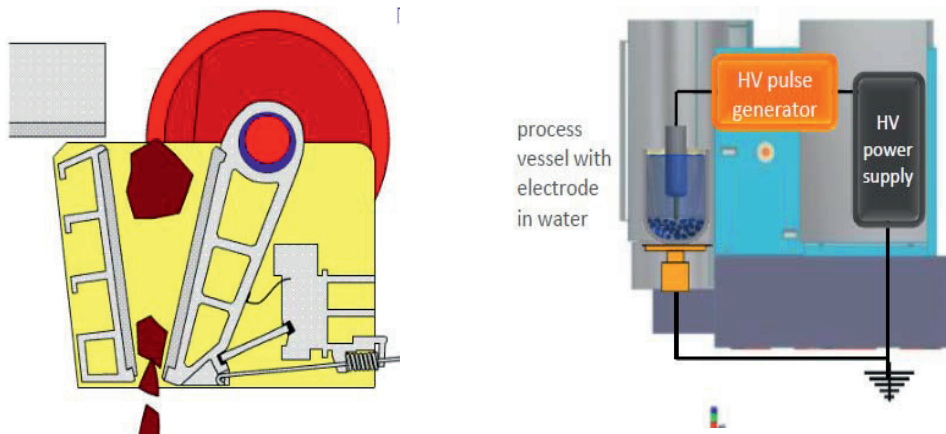


Fig. 3.1 Equipment for quartz crushing: jaw crusher on the left, and electrical fragmentation unit on the right.

One source of quartz was used: quartzB (batch2). Two 8 kg bulk samples were crushed to 5 cm lump sizes and split into three batches of 1 kg each. The first kg was mechanically crushed in a laboratory Retsch steel jaw crusher at NTNU. The remaining 2 kg (Test 1 and Test 2) were fragmented by SELFRAG AG (Kerzers, Switzerland) in a laboratory electrical fragmentation chamber. The experimental flow chart is represented in Fig.3.2. The process parameters used for the electrical fragmentation are provided in Table 3.5. It was decided to apply low voltage, in order to maintain the shock wave strength low and to direct preferentially the streamlets towards the inclusions. The magnetic field intensity of the magnetic separator is 2 T.

Subsequently, two size ranges were sampled for detailed studies: [0.3-0.5 mm] and [0.5-4mm]. The 4 mm upper boundary represents the largest grains produced during fragmentation. The fraction [0.5-4mm] was chosen with the aim of studying fracture distribution associated with partially liberated contaminant trace minerals. The [0.3-0.5 mm] fraction was chosen for the study of successfully liberated foreign minerals. The lower boundary 0.3 represents the average size of the minerals detected in the sample. If electrical fragmentation selectively fragments the minerals, a sieve size of 0.3 mm can successfully separate the liberated minerals from the quartz particles.

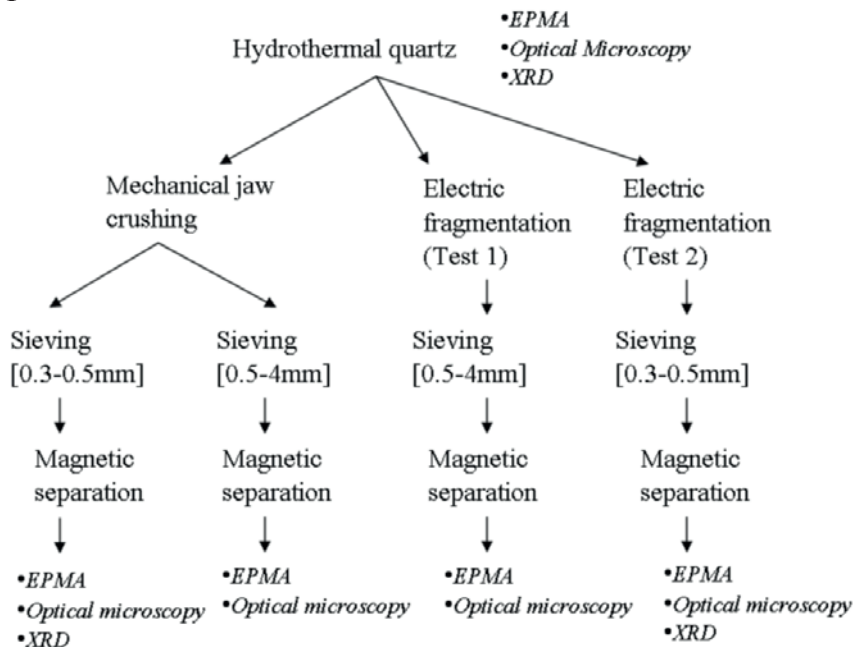


Fig. 3.2 Experimental flow chart: hydrothermal quartz beneficiation by electric fragmentation compared to beneficiation by mechanical crushing.

Table 3.5 Process parameters used for the electrical fragmentation tests.

Experiments	Process parameters		
	Voltage pulses [kV]	Pulses	Vessel sieve [mm]
1st	121	424	4
2nd	125	2660	0.5

3.3.1 *Method of analysis*

The sieved fractions were embedded in standard polished petrographic 30 μm sections and analyzed by *optical microscopy* and *EPMA*.

XRD, and *XRF* were used for mineral identification and to determine the quartz polymorphs present after fragmentation.

Approximately 1500 mineral fragments were studied in each size fraction. The structure of the fragments, in terms of size, shape, texture, structure, fracture distribution, and the degree of liberation/separation were studied by point counting. The degree of liberation is defined as the fraction of minerals still present in the quartz fragments, while the degree of separation as the fraction of free minerals separated by sieving and magnetic separation. It was not the purpose of this work to study the fines generated with the two techniques.

3.4 Production of silicon from pellets and lumps (Experimental set 2)

The conventional way of charging the quartz from the top of the furnace does not allow the use of fines, as they may block the gas passages up through the furnace. For this reason, beneficiated mm- μm particles of quartz cannot be charged to the furnace but need to be milled and agglomerated. Reduction mechanisms and material behavior are expected to be different if pellets instead of lumps are charged into the furnace. The experimental setting described in this paragraph was used to study and compare the reaction mechanisms when using pellets and lumps, respectively.

Mixtures of SiC and SiO₂ in the form of pellets and lumps were heated to 2000 °C to produce silicon, and to study the reaction mechanisms in pellets and lumps. This mixture was chosen because representative of the high

temperature zone of the furnace where silicon is produced. It was decided to start the experiment without liquid Si bath on the bottom, in order to focus on the reactions between SiC and SiO₂. The carbothermic reduction experiments were carried out in a small scale 6 kW induction furnace setting. The furnace is shown in Fig 3.3.

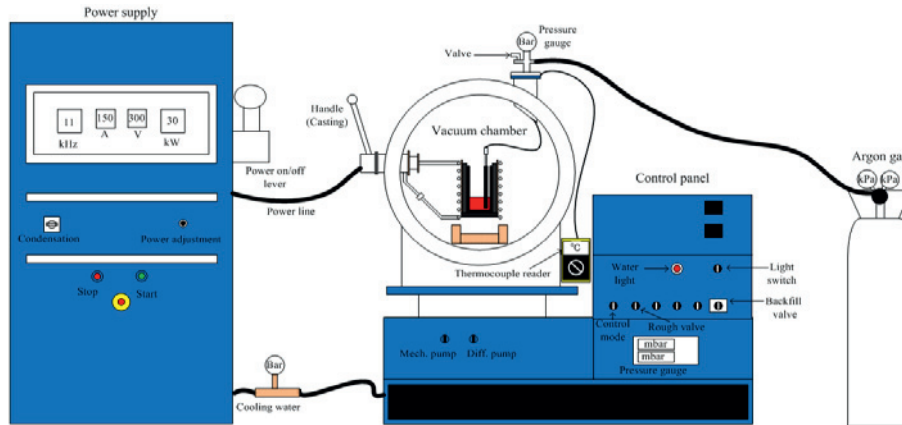


Fig. 3.3 Furnace apparatus. Drawing of furnace by Buhle Xakalashé.

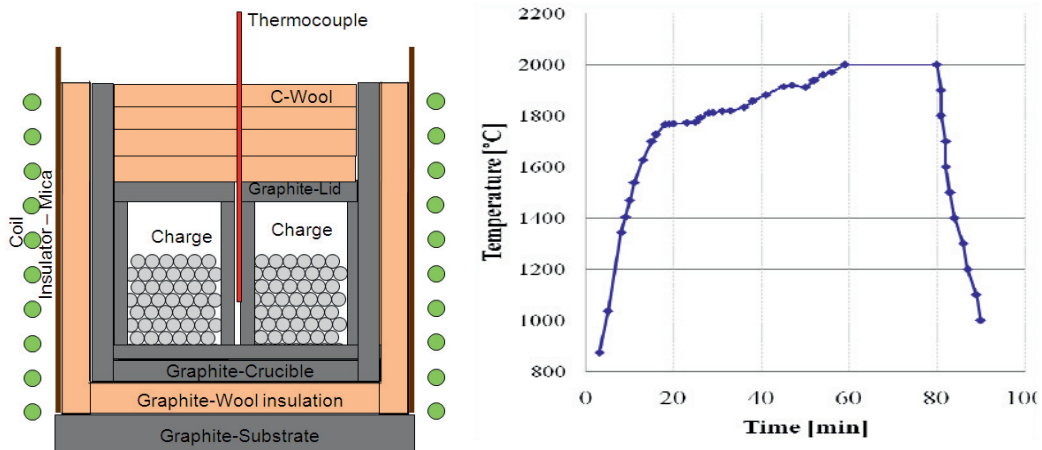


Fig. 3.4 On the left: experimental set-up of carbothermic reduction experiments in an induction furnace, two crucibles are contained in a bigger one in order to carry out parallel experiments. On the right: a temperature profile measured by thermocouple type C placed in between the two crucibles.

The experimental set-up is shown in Fig. 3.4. Two high purity graphite crucibles (7 cm in diameter and 15 cm in height) were filled with the charge (lumps or pellets). The crucibles were then fitted in a bigger graphite crucible. This configuration allowed running two experiments at the same time under the same conditions. It was decided to run the two

different quartz sources at the same time. Similar to the experiments by Filsinger, Bourrie and Wiik (Filsinger *et al.* 1990; Wiik 1990), the crucibles were closed with a loose-fit vented lid in order to create a SiO-CO atmosphere necessary for the silicon production reaction.

The experiments prevailed for 80 min. The heating profile is shown in Fig. 3.4. The charge was first heated to 1800 °C at a heating rate of 90 °C/min, then from 1800 °C to 2000 °C at 5 °C/min, and subsequently the temperature was held at 2000 °C for 20 min. Subsequently, the sample was rapidly cooled at a rate of 100 °C/min. Type C Tungsten-Rhenium thermocouples were placed in the holding crucible between the two reaction crucibles. The temperature outside the crucibles was assumed to be the same as inside the crucible. New thermocouples were used for each experiment, since they degraded fast in the high temperature and SiO/CO atmosphere.

A reducing atmosphere was maintained during the whole experiment. The furnace was first evacuated: the calculated oxygen content after evacuation was $\sim 1.2 \cdot 10^{-6}$ moles O₂. The furnace was subsequently filled with argon of 5.0 purity at 580 Pa ($5 \cdot 10^{-3}$ atm): the oxygen content carried by the argon filling was $\sim 4 \cdot 10^{-5}$ moles O₂. Oxygen coming from the crucible was assumed negligible since the crucible was preheated to 100 °C in Argon overnight. Leakages were measured in a time interval of 10 h, and were found to be negligible for the time needed by the experiment: 0.3 Pa ($3 \cdot 10^{-6}$ atm) during the argon filling, and 0.25 Pa ($0.25 \cdot 10^{-6}$ atm) during the experiment. At the beginning of each experiment, the chamber was filled to approximately 75000 Pa (0.75 atm) with argon. During heating the pressure inside the chamber increased. The total pressure in the chamber reached approximately 10^5 Pa (1 atm) at 2000 °C.

Two high-purity hydrothermal quartzes, quartzB (batch1) and quartzA, one source of high-purity SiC, and two SiO₂:SiC molar ratios were used. The experiments were designed to study 3 factors in eight runs. The eight runs design was constructed with a full factor standard table of signs (as summarized in Table 3.6) for two quartz types, SiO₂:SiC molar ratios and charge type. Each run was repeated three times when lumps were used and two times when pellets were used. The experiments with pellets were repeated only twice, because they showed little variability in the weight loss. The molar ratio 1:2 refers to the stoichiometry of the Si production reactions as described in (Schei *et al.* 1998). The molar ratio SiO₂:SiC = 1:1 refers to the stoichiometric overall reaction taking place in the inner zone as proposed by Schei and Müller (Müller *et al.* 1972; Schei *et al.* 1998).

Table 3.6 Experimental variables: quartz source, charge size and SiO₂:SiC molar ratio. QzB is quartzB (batch1).

quartz	qzA	qzB	qzA	qzB	qzA	qzB	qzA	qzB
charge size	lumps	lumps	lumps	lumps	pellets	pellets	pellets	pellets
Molar ratio	1:2	1:2	1:1	1:1	1:2	1:2	1:1	1:1

3.4.1 *Method of analysis*

The reacted crucibles were cut and the charge morphology studied by EPMA. Because of kinetics and carbon reactivity (Tuset *et al.* 1976; Chen *et al.* 2000) the reactions did not go to completion, and non-reacted carbon, quartz and silicon carbide were found together with the reaction products. Solid phases remaining after the experiments were solid reaction products and solid non-reacted charge. In particular the solid phases consisted of Si, C, amorphous SiO₂, and different SiC polytypes.

In order to investigate the reaction mechanisms, the silicon yield and the reaction kinetics when using pellets and lumps, a quantification of the phases in the crucibles after the experiments was required. This quantification is not trivial, and a new method, which combines the results from XRD and XRF with an elemental Si, C, O balance, was developed for this purpose. XRD and XRF were not able, when used individually, to quantify the phases. XRF provides highly accurate information about the elemental composition of a sample. The instrument can be used to estimate the weight percentage of the total elemental Si, but does not detect light elements such as C and O and does not give direct phase information. XRD is the most direct and accurate analytical method to identify and determine the amounts of phases in a sample. However, only polymorphs of crystalline phases can be quantified. In order to confirm the reproducibility of the sampled material, two parallels of each sample were analyzed by XRD. XRD analysis requires a few grams of specimen, while XRF needs about 9 g. Both methods require powder with particle size below 50 μm. XRD and XRF were used to quantify a phase mixture as described in *Article I*.

3.5 Quartz behaviour during heating (Experimental set 3)

In situ melting experiments on small silica pieces were run in a sessile drop set-up to study the high-temperature properties of lumpy quartz. The experimental set-up, shown in Fig 3.5, allowed the observation of the high temperature properties of samples placed on a substrate when both the atmosphere and the heating rates were controlled. A camera placed in one end outside the furnace recorded the sample during heating by taking a picture every second. From this image the melting temperature and the volume expansion were estimated. Silica cylindrical samples ($\varnothing = 3 \text{ mm}$; $h = 3 \text{ mm}$) were investigated. Cylindrical samples, drill cores from a 3 mm thick plate cut out of the original quartz sample with a diamond saw, were used for these experiments. Two hydrothermal quartzes, quartzB (batch1) and quartz A; seven samples of quartzB (batch1) and eleven samples of quartzA were investigated.

The quartz samples were placed on a non-reactive glassy carbon substrate and heated to $900 \text{ }^\circ\text{C}$ in about 3 minutes. From $900 \text{ }^\circ\text{C}$ to $1200 \text{ }^\circ\text{C}$ the heating rate was set to $100 \text{ }^\circ\text{C}/\text{min}$, and from $1200 \text{ }^\circ\text{C}$ to $2000 \text{ }^\circ\text{C}$ was set to $20 \text{ }^\circ\text{C}/\text{min}$. The experiments were run in CO atmosphere. The temperature was measured by a pyrometer calibrated against the melting point of iron. Similar experiments, with other quartz types, have been performed by Andersen (Andersen 2009) in CO and Ar atmosphere using a similar heating rate.

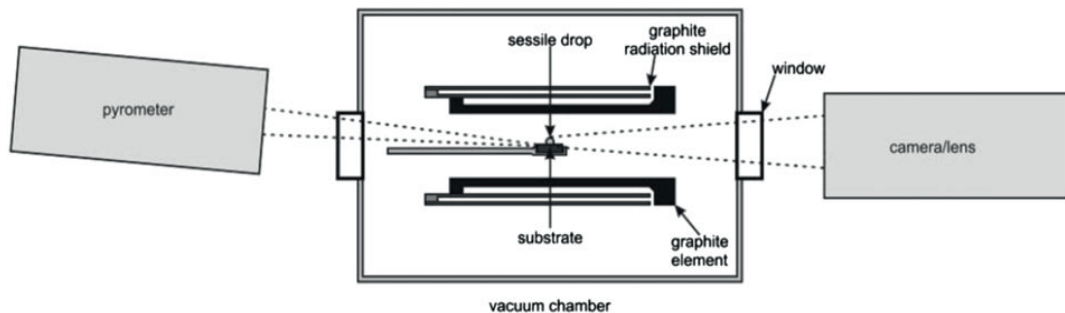


Fig. 3.5 Sessile drop setting in a wettability furnace. The sample is placed in a sample holder of 1cm diameter. The furnace is sealed and heated with a controlled atmosphere. A pyrometer measures the sample temperature while a camera records the sample appearance during heating.

3.5.1 Method of analysis

Experiments in the sessile drop furnace aimed at measuring the temperature of melting and the quartz weight losses (as SiO(g) losses) in CO atmosphere following reaction 2.10. Both the melting point and the reaction rate of the different quartzes with CO, were measured. It was possible to calculate the weight losses by *weighing* the silica sample before and after the experiments. The reaction rate was determined in terms of SiO losses. The temperature of melting was determined by the moment the quartz became glassy: when the quartz starts melting, voids are sealed, there is no more light refraction and the sample turns transparent and glassy. Fig 3.6 is an example of the quartz microstructure during heating. The method here described, is valid to compare the melting properties of different quartzes, but the melting temperature is not regarded as an absolute value, since it is influenced by the sample size and by the heating rate.

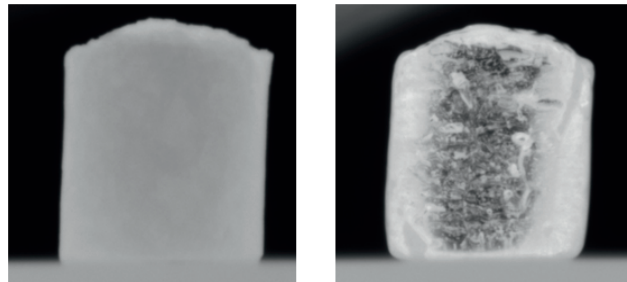


Fig. 3.6 Pictures of quartz cubic samples during heating: crystalline quartz on the left, glassy quartz on the right.

3.6 Production of SiO(g) and CO(g) from quartz, silicon carbide and silicon (Experimental set 4)

This set of experiments was carried out at the University of New South Wales UNSW. Mixtures of SiO₂+Si and SiO₂+SiC in the shape of pellets or lumps were heated to 1650 °C and to 1850 °C. The main aim was to produce SiO(g) and other gaseous compounds and to investigate the volatility of the impurities in quartz. Different quartz types, together with Si or SiC in different charge types (pellets or lumps) were studied. Hydrothermal quartzA (batch2), quartzite, ultra pure SiC and ultra pure saccharine binder were used.

The reduction experiments were carried out in a 23 kW graphite tube furnace (model 1000-3560-FP20). The furnace chamber is 76 mm in diameter, and 153 mm in height. The experimental set-up is schematically presented in Fig 3.7.

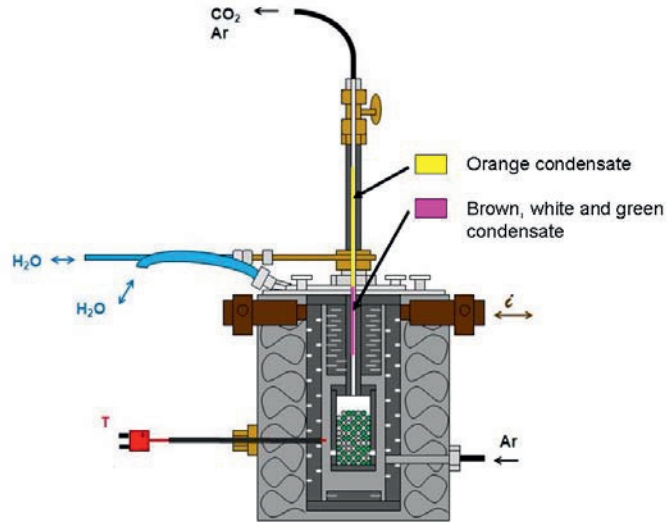


Fig. 3.7 On the left: graphite tube furnace and electrical panel control. On the right: graphite tube containing the charge material connected to a graphite tube.

A high purity graphite crucible containing the charge material was connected to a gas ducting tube 500 mm long and 10 mm in inner diameter. The tube end outside the furnace was connected to a two-way valve. A type C thermocouple with hafnium oxide insulator was inserted from the side of the furnace to measure the temperature close to the crucible wall. The charge was directly heated to the targeted temperature at 60 °C/min when lumps were used. For pellets, the charge was first heated to 1000 °C and kept steady for 10 minutes, in order to ensure the complete decomposition of the binder and then heated at 60°C/min to the targeted temperature. The furnace was cleaned prior to the experiments by heating to 1900 °C for 3 hours while purging argon at 1 l/min. Argon passed through a tube furnace containing steel wool at 400°C before entering the graphite furnace in order to flush out any oxygen impurity. The furnace was evacuated to 4×10^{-2} mbar before purging argon to remove any adsorbed moisture and CO₂ from the graphite parts comprising the furnace. Since the graphite tube was porous (density 1.7 mg/m³), the outer surface of the graphite tube was coated with superglue, in order to ensure good hermetic condition. The furnace leakage was measured by keeping the furnace at vacuum

conditions for 1 day and was estimated to be 1.1mbar/h. The CO(g) and SiO(g) formed during reduction were purged by argon outside the crucible. The temperature along the ducting tube decreased sharply outside the chamber, and a condensate deposited on the inner surface of the tube. The tube experienced a strong reduction in temperature and a condensate deposited on the inner surface shown in the pink and yellow region in Fig 3.7. The condensate eventually blocked the tube. The experiment was stopped when the overpressure in the chamber reached approximately 50 kPa.

Table 3.7 Experimental matrix. #Exp= number of experiments run under the conditions in the corresponding row. C represents the carbon contained in the binder and is associated with the pellets charge type. The quartz “hydro” is hydrothermal quartzB (batch2).

# Exp	Charge mixture	Temperature	Charge type	Quartz Type	SiO ₂	SiC	Si	C
2	SiO ₂ +SiC	1650°C 1923K	lumps	Hydro	1mol	1mol	-	-
2				Quartzite				
2			pellets	Hydro	0.9mol	0.9mol	-	0.3mol
2				Quartzite				
1		1850°C 1923K	lumps	Hydro	1mol	1mol	-	-
1				Quartzite				
1			Pellets	Hydro	0.9mol	0.9mol	-	0.3mol
1				Quartzite				
2	SiO ₂ +Si	1650°C 1923K	lumps	Hydro	1mol	-	1mol	-
2				Quartzite				
2			Pellets of SiO ₂	Hydro	0.9mol	-	1mol	0.5mol
2				Quartzite				
1		1850°C 2123K	lumps	Hydro	1mol	-	1mol	-
1				Quartzite				
1			Pellets of SiO ₂	Hydro	0.9mol	-	1mol	0.5mol
1				Quartzite				

The experimental matrix is given in Table 3.7. The experimental condition “pellet Si+SiC” refers to pellets of silica and silicon carbide intermixed. The experimental condition “pellet Si+SiO₂” refers to pellets of quartz mixed with pieces of silicon. The temperature 1650 °C and 1850 °C are below and above the silica melting point, respectively. The melting point of the hydrothermal quartz was estimated in a reducing atmosphere for a 3

mm particle size to be 1819 °C. Since quartzite contains more contaminants than hydrothermal quartz (Table 3.3) and the impurities in quartz lower the melting point of quartz (as described in paragraph 2.5), quartzite is expected to have a lower melting point than hydrothermal quartz. Therefore a temperature of 1650 °C was chosen in order to study the behaviour of both quartz-types in their solid state.

3.6.1 Method of analysis

Different methods were used to analyze the reacted charge and the condensate: XRD, EPMA and ICP-MS. In addition the experimental conditions were simulated by Fact-Sage software package.

EPMA was used to identify the trace minerals as inclusions in the original quartz and to investigate the nature of the reacted minerals and the morphology of the reacted quartz and condensate. The chemical composition of the reacted minerals was analyzed qualitatively by elemental mapping and quantitatively by point analysis. Standard microanalysis reference materials Astimex 53 Minerals Mount MINM25-53 were used for standardization and calibration of the instrument (Astimex 2011).

XRD was used for chemical and mineralogical analysis of the reacted quartz and the condensate. For phase quantification, the Rietveld method was used (Albinati *et al.* 1982). For the quantification of the amorphous silica 10 wt% Al₂O₃ was added as an internal standard to measure the quantity of glassy phases present in the samples. First of all, the crystalline phase proportions were calculated; then the standard weight percentage of alumina was entered in order to recalculate the proportions of the crystalline phases. The glassy phase content was calculated as the difference between 100 wt% and the percentage of the crystalline phases (including alumina). This is a useful method to quantify an amorphous phase with XRD; the disadvantage is that is reliable only if the amorphous (glassy) phase content is greater than 10 wt%.

ICP-MS was used to quantify the bulk impurity concentrations in the reacted charge and the condensate. The reacted charge, Si, SiO₂ and SiC phases were mixed. In addition, single phases of reacted charge were sampled, where possible, from the reacted charge mix and analyzed by ICP-MS. The condensate was collected in the graphite ducting tube and removed using a tungsten carbide tool. The different types of condensate

were collected together in one sample. The sample was crushed with an agate mortar of 99.91% purity SiO₂. Standard materials DIABASE W-2, BCS-CRM 313/1, NIST 57b (Si) and JCRM R 021 were used for the calibration. 3 scans were run for each sample with an average error of 4%. The errors refer to the instrumental precision, and not the uncertainty imposed by partial digestion. Each value, which will be shown in the results section, is related to a single analysis. Although each sample has been analyzed only once, the conclusions are based on similar trends under the eight different experimental variations. SiC only partially dissolved due to limitation of the sample digestion facilities used in this study.

Two procedures of digestion were applied in this work. If a sample contained SiC, the procedure of digestion was: 20-40 mg sample in a mixture 0.5ml concentrated HNO₃ + 0.5ml concentrated H₂SO₄ + 0.5ml concentrated HF at 255 °C (518 K) for 1 hour. It should be mentioned that complete digestion of SiC was not achieved. A sample which did not contain SiC, was digested in a mixture 0.5ml HF + 1.5ml HNO₃ at 250 °C for 1 h. The solution was digested in PTFE containers in a digestion bomb.

4 DISCUSSION OF RESULTS

The purpose of this chapter is not to summarize the single investigations, which are available in the articles at the end of this thesis, but rather to discuss the results.

The aim of this research work was to investigate the impurity distribution throughout the processing of quartz feedstock to solar silicon via the metallurgical route. In particular three areas were investigated.

- 1) Removal of mineral impurities from quartz prior to carbothermic reduction by means of selective fragmentation.
- 2) Beneficiation of quartz produces a fine grained material which requires agglomeration and subsequent charging the quartz in form of pellets, which is different from the conventional lumpy charge. The second aim was therefore to investigate the effect of pellets and lumps on the silicon production reactions.
- 3) High temperature proprieties of quartz under reducing condition.
- 4) Distribution of contaminants from quartz to the gas phase during quartz reduction. Pellets and lumpy charge, hydrothermal quartz and quartzite were studied.

4.1 Removal of mineral inclusions from quartz

4.1.1 Impurities in mineral inclusions in quartz diffuse out from the mineral to the surrounding quartz matrix when heating quartz

The investigations described in this section refer to *Article IV*. The *Experimental set 4* was used to investigate the high temperature properties of the minerals in quartz. Minerals in quartz generally melt at temperatures below the melting point of silica.

Fig. 4.1 shows a representative section of the investigated quartz before heating. The coarse grains (up to 4mm) and the presence of deformation lamellae denote that the quartz was subjected to deformation. Only muscovite minerals are found in the quartz batch. The minerals are below 0.3 mm size and situated mostly at the quartz grain boundaries.

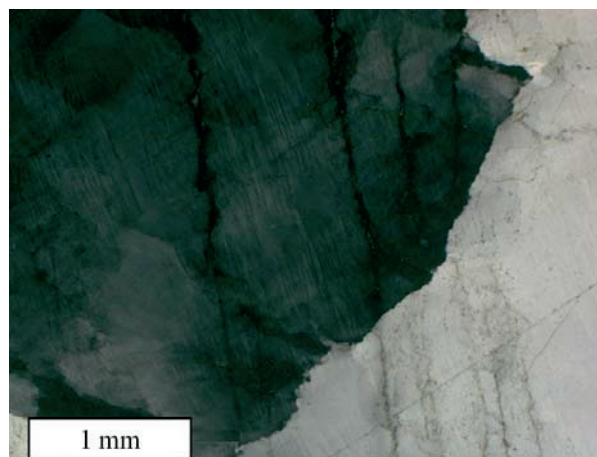


Fig. 4.1 Representative cross polarized light image of the quartz investigated. Trails of fluid inclusions (visible as dotted lines) and cracks are present.

The major contaminants present in muscovite are Al, K and Fe. High temperature experiments reveal that at temperatures above the melting point of muscovite, Al, Fe and K present in the muscovite partially diffuse into the surrounding SiO₂-matrix leaving behind a more SiO₂-rich phase. Fig. 4.2 shows the melted mineral at 1650 °C (below the silica melting point) and at 1850 °C (above the silica melting point). While K shows a constant distribution in the melted mineral region, Al occurs in two different concentrations in the melted region (visible from the color gradient in the maps). The low concentration of Fe in the muscovite (4 at% Fe compared to 7 at% K and 15 at% Al) does not allow seeing if Fe features two distinct melt regions. Two distinct liquids formed when muscovite melted: a Al-rich melt at the core of the mineral, and a SiO₂-rich melt at the mineral boundaries confirming the findings of Hammouda (Hammouda *et al.* 1999). Melted muscovite is associated with a cavity, which was previously filled by H₂O formed by dehydration of muscovite, a phenomena referring to a process where hydrous silicates re-crystallize to an assemblage with fewer or no volatile components (Deer *et al.* 1992). The dehydration reaction of mica minerals taking place at calcinations temperatures lower than the melting point of silica was also reported by Zhu (Zhu B.-z *et al.* 2008). In the muscovite object of this study, Fe³⁺ partly substitutes for Al according to the phengite substitution (Fe is linked to 2OH and an O). Fe is found concentrated at the cavity showing to have a strong affinity with the OH group. The affinity properties of Fe with OH are reported by Fein (Fein *et al.* 1992).

XRD analyses show that when heated to 1650 °C, quartz transforms to cristobalite which has a more open structure than β -quartz (2.6 g/cm³ and 2.3g/cm³ (Ford *et al.* 2004) respectively) and can incorporate a higher concentration of contaminant cations. Fig. 4.2 on the left, shows that Al and K diffuse from the molten muscovite to the cristobalite surface.

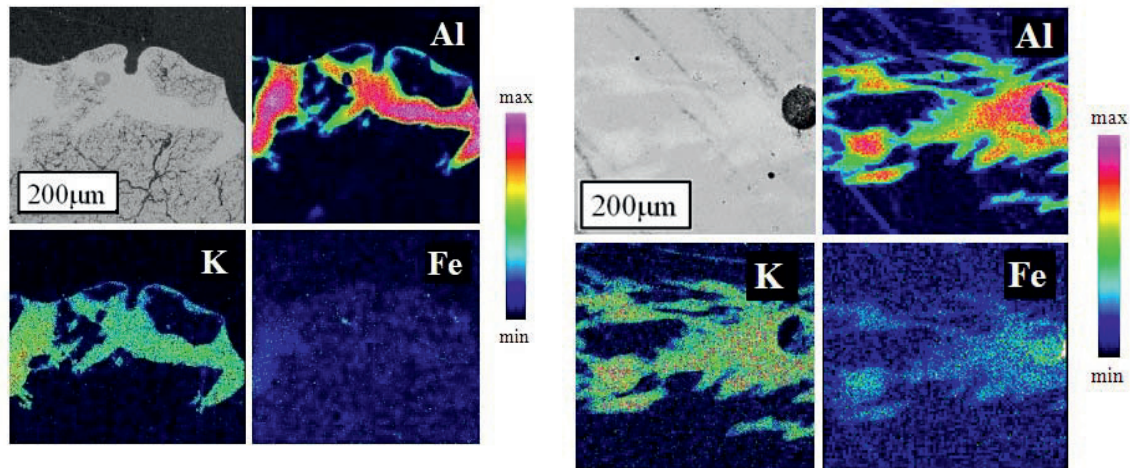


Fig. 4.2 Quartz microstructure and elemental mapping after heating of quartz in reducing atmosphere: on the left solid quartz (cristobalite) heated to 1650 °C; on the right molten quartz heated to 1850 °C. Muscovite is molten in both cases, and its major constituents, Al, K and Fe, diffuse from the muscovite to the quartz matrix.

4.1.2 Mineral inclusions in quartz can be efficiently removed by means of electric fragmentation, sieving and magnetic separation

The experimental results reported in this section refer to *Article III*. It has just been shown that minerals inclusions dissolve into the silica matrix. This should be avoided because when the elements dissolve they feature a lower driving force to vaporization. It is therefore necessary to selectively remove the minerals in quartz prior to charging.

Electrical fragmentation is a high-voltage pulsed generator, which fragments selectively rocks, electrical breakdown and subsequent shock wave propagation. More information on this topic can be found in the literature review chapter. Electrical fragmentation, was used in the *Experimental set 1* to selectively remove the fine-grained minerals present in hydrothermal quartz. The experimental results, agree with previous work and show that electrical fragmentation is effective in removing mineral

inclusions, and its large scale use for hydrothermal quartz should be investigated further.

Electrical fragmentation was compared to conventional crushing and showed to generate more liberated minerals. Fig. 4.3 compares the cracks distribution in mm size quartz particles after mechanical crushing (on the left) and electrical fragmentation (on the right). In the mechanically crushed quartz, the population of fractures does not show any preferential concentration in close proximity to muscovite. In the electrically fragmented quartz, fractures are polarised at the muscovite grain boundaries where they also feature the highest concentrations. Trails of fluid inclusions (visible as dotted lined in Fig. 4.3) are still present in both samples after fragmentation.

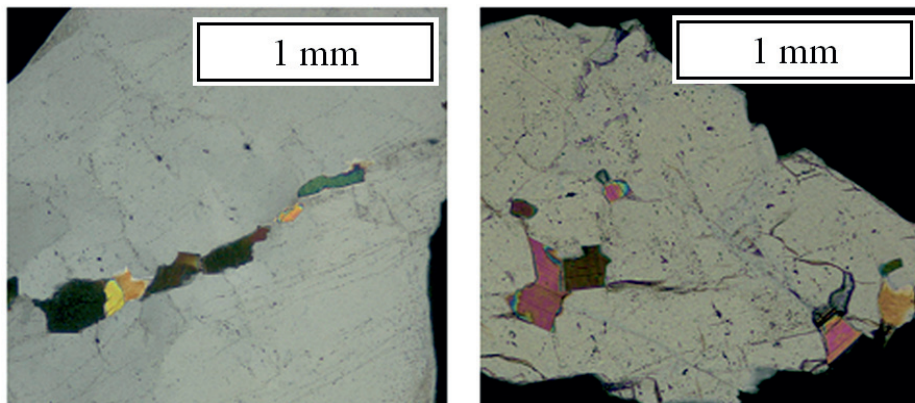


Fig. 4.3 Cross polarized light images of hydrothermal quartz particles after fragmentation: quartz after conventional crushing (on the left) and after electrical fragmentation (on the right). In grey the quartz matrix, in black the epoxy, in colours the muscovite mineral inclusions embedded in the quartz.

Electrical fragmentation selectively directs cracks to the minerals. Selectivity of cracks leads to selectivity of mineral breakage at the grain boundaries. As a consequence electrical fragmentation generates quartz particles that are larger than the liberated mineral inclusions, and sieving was effective to separate the liberated mineral inclusions from the quartz particles. The efficiency of beneficiation, after fragmentation, sieving and magnetic separation, is shown in Table 4.1. Four types of fragments are distinguished: i) quartz particle, ii) mineral on the surface of a quartz particle, iii) mineral embedded in a quartz particle, and iv) liberated mineral. The highest percentage of liberated quartz particles (99.1 %) occurs when electrical fragmentation is applied. The advantage of using

electrical fragmentation is more evident for the bigger size range where liberation is 10 % better than for the same size range in mechanically crushed material.

















		SIEVED SIZE	
		0.3-0.5mm	0.5-4mm
FRAGMENTATION	MECHANICAL	 = 94.9%	 = 85.9%
		 = 2.9% (2.6% muscovite + 0.3% orthoclase)	 = 7.86% (7.37% muscovite+0.5% orthoclase)
		 = 0.3% (muscovite)	 = 4.3% (4.1% muscovite+0.2% orthoclase)
		 = 1.95% (0.2% muscovite +1.8% orthoclase)	 = 1.9% (1 muscovite+1.9 orthoclase)
	ELECTRICAL	 = 99.1%	 = 95.8%
		 = 0.3% (muscovite)	 = 3.1% (3% muscovite+0.05% orthoclase)
		 = 0.5% (muscovite)	 = 1.1%
		 = 0.1% (muscovite)	 = 0.1% (orthoclase)

Table 4.1 Quantitative analysis of the fragmented-sieved and magnetically separated quartz particles. The meaning of the four symbols from the top to the bottom is: refined quartz particle, mineral attached to the surface of a quartz particle, mineral embedded in a quartz particle, and liberated mineral.

The fragmented pieces were analyzed by ICP-MS to investigate quantitatively the beneficiation effect of electrical fragmentation. Fig. 4.4 shows a chemical analysis of the quartz particles after fragmentation, sieving and magnetic separation. Two sieve sizes are considered. Electrical fragmentation and mechanical crushing are compared for the two fraction sizes. K, Al, Fe, the major contaminants in muscovite, and B and P, detrimental elements very difficult to remove from silicon, are the impurities analyzed. Because of the high concentration of P in the blank used as reference, P analyses are not shown. The electrically fragmented quartz particles contain fewer impurities (particularly evident for K, Al, Fe) than the mechanically fragmented ones. Mechanically fragmented particles have approximately the same impurity content for both fraction sizes, this

agrees well with the observations that conventional crushing is not a selective technique.

However, the comparison of the chemical composition of the electrically fragmented-sieved fragments and the original quartz, indicates that both techniques are intrinsically polluting the quartz with B, K, Al and Fe. The steel jaws and the steel electrode are probably the source of contamination during the jaw crushing and the electric fragmentation respectively. In particular, the contamination of B and P should be avoided since these impurities are very difficult to remove from silicon.

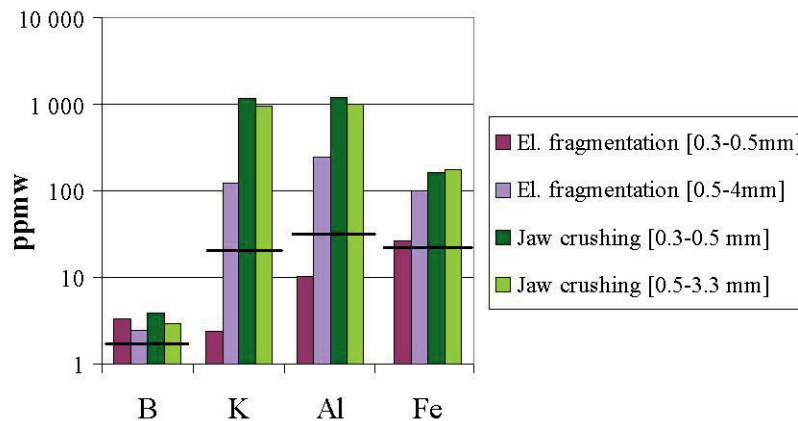


Fig. 4.4 Chemical analysis of the original quartz (black lines) and of the beneficiated quartz fragments for different crushing methods and sieving sizes (coloured bars).

4.2 Effect of pellets and lumps on the silicon producing reactions

The experimental results reported in this section refer to *Experimental Set 2, Article I* and *Article II*.

Mixtures of quartz and silicon carbide were heated to 2000 °C for 10 min in graphite crucibles. A quantitative analytical method for the estimation of the output phases was proposed. The output phases consisted of a mixture of non-reacted charge material (amorphous SiO₂, crystalline 6H:SiC, 15R:SiC and graphite C) and reaction products (crystalline 3C:SiC and Si). The technique combines XRD and XRF analyses with elemental mass balances. Mineralogy and geological applications often use a combination

of XRD and XRF analysis techniques to identify phase and elemental composition of rocks (Verryn 2008). Fig. 4.5 is the total phase mass balance of the set of experiments: moles of single phases in input (left side) and output (right side). The first four columns of each graph refer to the experiments with lumps, the last four to pellets.

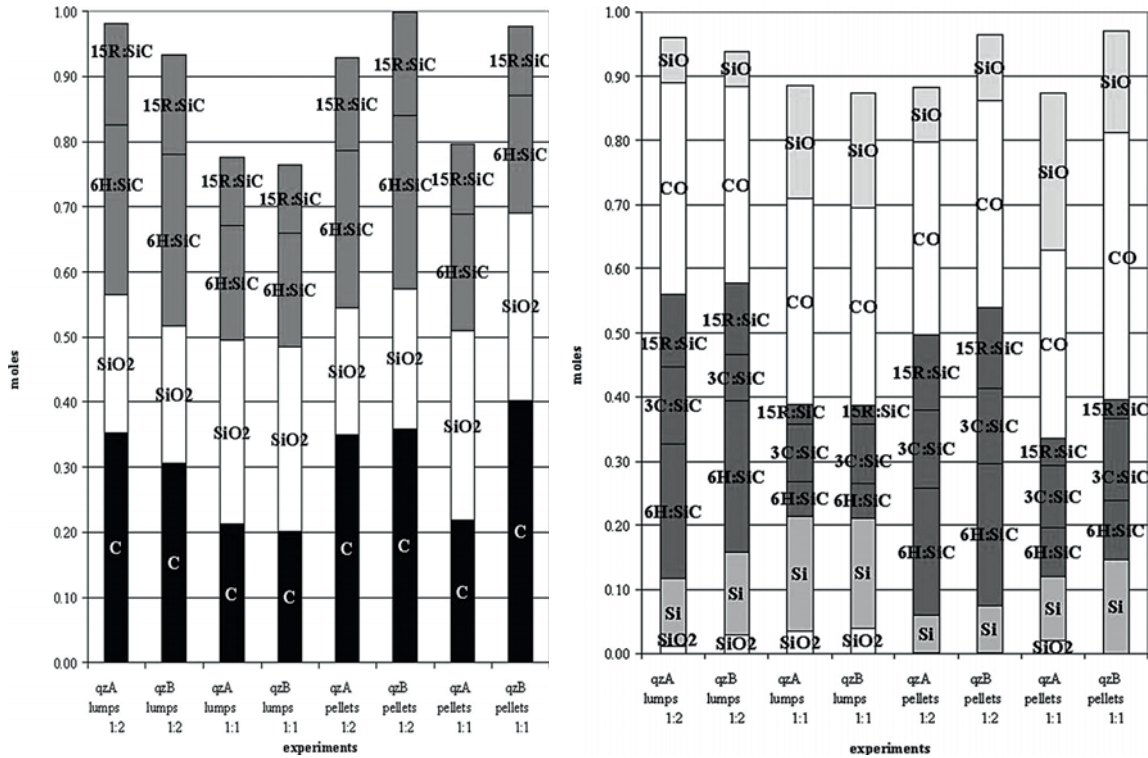


Fig. 4.5 Mixture of SiO₂+SiC in form of lumps and pellets are heated to 2000°C and silicon is produced. Total mass balance of the experiments: input phases on the left, output phases (non reacted input phases and reaction product) on the right figure. Only the amount of graphite C which reacted with quartz is shown.

Non-reacted silica (on average 2 wt%) is always found after the experiments with lumps, opposite case for pellets (on average 0.18 wt%). Not only mass balance calculations, but also the study of the morphology of the reacted charge confirmed this statement. In addition more silicon is formed when lumpy charge is used. More SiO(g) is produced and lost with pellets charge resulting in a higher Si yield for lumpy charge. The reaction between SiO₂ and SiC is faster for the case of pellets, because of the larger surface area available and closer contact between reactants in the charge mixture. As a consequence more SiO₂ reacts with SiC when pellets charge is used.

The silicon production reaction when pellets are used takes place inside the pellets and mostly in the rim zone (Fig. 4.6). The more favorable Si formation at pellets rim may be pressure related. Larger zones of silicon occur with lumpy charge. This is probably due to several Si forming reactions occurring simultaneously in the lumpy charge.

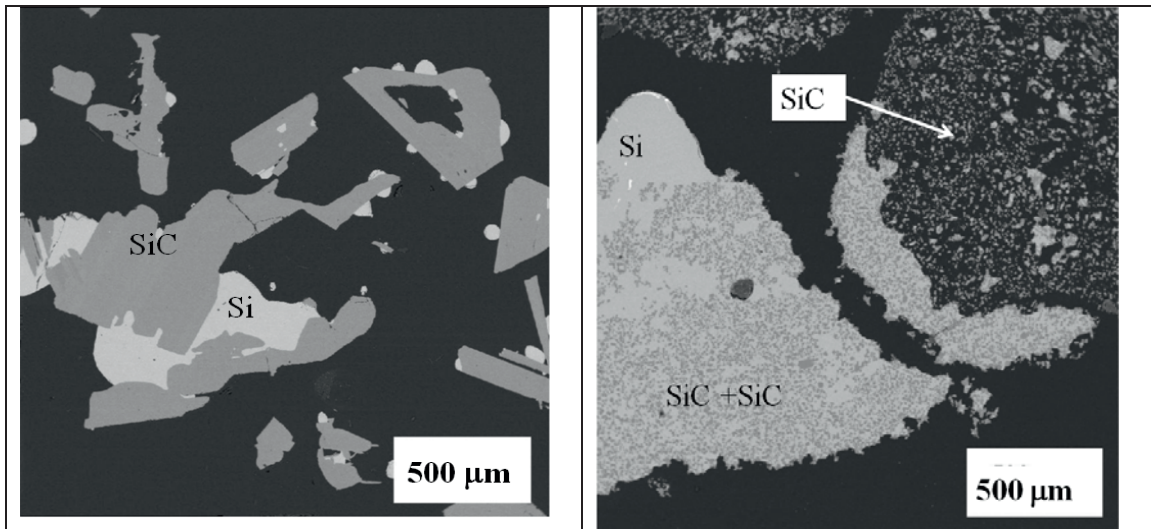


Fig. 4.6 Morphology of the reacted charge (backscattering images): lumps on the left, pellets charge on the right.

The differences which exist between pellets and lumpy charge, when heated under reducing conditions, are summarized in Table 4.2 and Table 4.3. Major focus is on the quartz charge. The results reported in the tables refer to *Article II*, *Article III*, *Article IV* and *Article V*.

Table 4.2 Description of the impurity behavior and distribution in quartz when lumpy quartz is heated in a reducing atmosphere in a silicon furnace. Mixtures of quartz and silicon carbide are considered for the silicon production reactions.

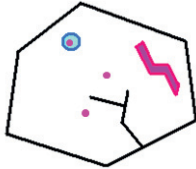
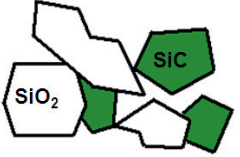




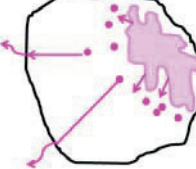

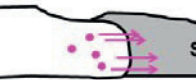

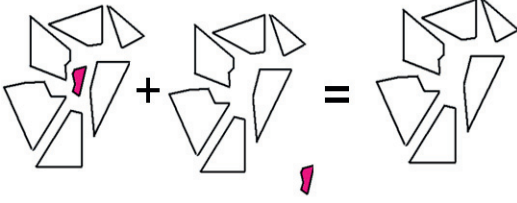
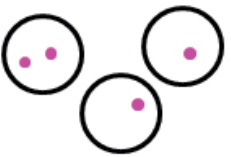
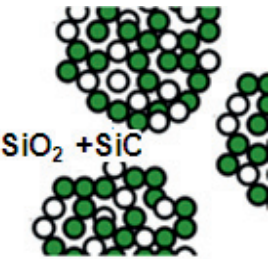
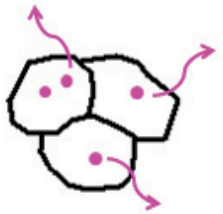
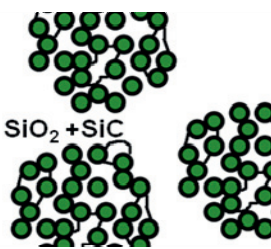
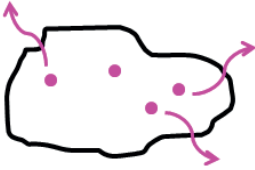
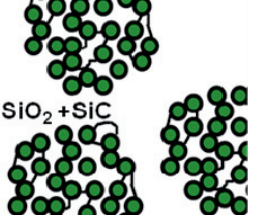
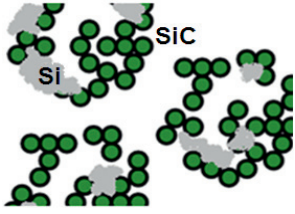
Comments	Micropicture (SiO ₂)	Macropicture (SiO ₂ +SiC)
Quartz lumps containing mineral inclusions (pink area), trace elements (pink dots) and fluid inclusions (blue bubble) are charged into the furnace.	 A schematic diagram of a quartz crystal lattice. It contains a blue circular bubble representing a fluid inclusion, a pink irregular area representing mineral inclusions, and several small pink dots representing trace elements.	 A collection of white angular particles labeled SiO ₂ and green angular particles labeled SiC.
<u>T<800 °C</u> Trace elements combine with Cl present in the fluid inclusions and form gaseous compounds which leave the quartz during fluid inclusions decrepitation.	 The quartz crystal lattice diagram from the previous row, but with a pink arrow pointing away from the blue bubble, indicating the release of gaseous compounds.	 The same collection of SiO ₂ and SiC particles as in the previous row.
<u>T=1650 °C</u> Quartz is still solid and is transformed to cristobalite. SiO(g) is produced. The formation of SiO(g) is dependent on the amount of cracks present in the quartz matrix. Trace elements diffuse to the cracks and to the quartz surface, where they can be reduced to gaseous compounds and leave the quartz. Minerals melt at temperature below the quartz melting point. The impurities diffuse from the melted mineral into the quartz matrix.	 The quartz crystal lattice diagram with several cracks. Pink arrows show trace elements (dots) moving from the pink mineral inclusions towards the cracks and the outer surface of the quartz.	 The same collection of SiO ₂ and SiC particles as in the previous rows.
<u>T=1850 °C</u> Quartz is melted, there are no more cracks and the diffusion distance to the nearest available reducing atmosphere increases. The cations, which diffuse to the quartz surface, and are reduced to gaseous compounds leave the quartz. Because of diffusion of contaminants out from the mineral, the mineral has become SiO ₂ rich.	 The quartz crystal lattice is now a smooth, rounded shape representing molten quartz. Pink arrows show trace elements (dots) diffusing from the interior towards the surface.	 The same collection of SiO ₂ and SiC particles as in the previous rows.
<u>T=2000 °C</u> When silicon is produced, non-reacted silica is still present. Areas of contact between silicon and quartz are frequent, and trace elements diffuse from the quartz to the silicon.	 A diagram showing a grey area labeled 'Si' in contact with the molten quartz. Pink arrows point from the quartz towards the silicon, indicating the diffusion of trace elements.	 The collection of SiO ₂ and SiC particles, now with a grey area labeled 'Si' (silicon) at the bottom, representing the final product mixture.

Table 4.3 Impurity behavior and distribution in quartz when agglomerates of quartz and silicon carbide are heated in reducing atmosphere.

Comments	Micropicture (SiO ₂)	Macropicture (SiO ₂ +SiC)
<p>Quartz lumps contain mineral inclusions, fluid inclusions and trace elements. Electrical fragmentation is an efficient method to liberate the minerals from the quartz matrix. Sieving and magnetic separation can be used to separate the liberated minerals. Quartz particles mineral free are obtained.</p>		
<p>Quartz particles and silicon carbide are milled and pellets are formed. Fluid inclusions, still present in quartz after electrical fragmentation, partially or fully disappear during milling. Mineral inclusions were removed from previous beneficiation. Trace elements remain in quartz (pink dots).</p>		
<p><u>T=1650 °C</u> Quartz particles sinter together; cristobalite is formed. SiO(g) is produced. More SiO(g) is produced than for the case of lumps. The trace elements which diffuse to the quartz surface, and are reduced to gaseous compounds leave the quartz.</p>		
<p><u>T=1850 °C</u> Quartz is molten. SiO(g) is produced. The trace elements which diffuse to the quartz surface, and are reduced to gaseous compounds leave the quartz.</p>		
<p><u>T=2000 °C</u> Silica reacts readily with silicon carbide, and contact areas between quartz and silicon are therefore not expected. However, in case of contact, for example pellets falling from the top of the furnace to the silicon bath, the trace elements diffuse out from the quartz to the silicon phase.</p>	<p style="text-align: center;">-</p>	

4.3 High temperature properties of quartz in reducing atmosphere

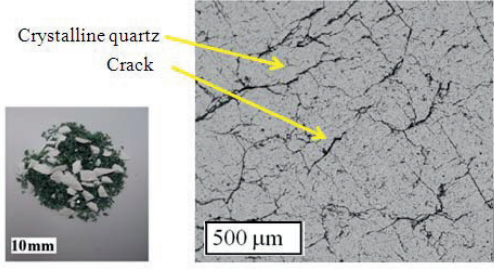
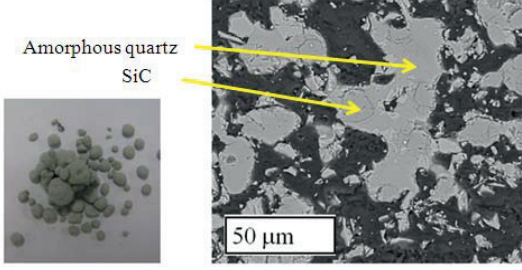
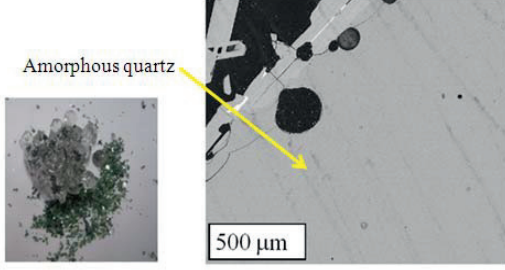
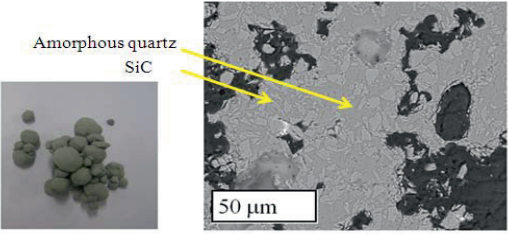
This paragraph refers to investigations described in *Article II* and *Article IV*. It is well known that in presence of a reducing atmosphere and CO(g), quartz is reduced and forms SiO(g). SiO(g) is produced on the quartz surface according to equation (2.10). Investigations, which are described in the following paragraphs, show that pellets rather than lumps of quartz and the presence of cracks in quartz enhance the production of SiO(g). Pellets and cracks increase the quartz surface available per unit mass, and therefore more SiO(g) is produced when quartz is heated in reducing atmosphere. From these results, it follows that SiO(g) and CO(g) molecules are not able to permeate inside the quartz matrix but that they are able to diffuse inside the μm wide cracks in crystalline quartz. The experimental results are discussed below.

4.3.1 Effect of pellets and lumps

Table 4.4 compares the morphology of pellets and lumps and of solid quartz with cracks and molten quartz without cracks. The pictures refer to studies carried out in *Experimental set 4* and show that pellets and cracks in quartz increase the surface available to reduction.

At 1650 °C quartz particles in pellet sinter in clusters of 50 μm size while lumpy quartz develops a thick network of cracks with an average distance between two cracks comparable to 50 μm . Crack are created during heating because of the thermal expansion of quartz and the reconstructive transformation from β -quartz to β -cristobalite. Cracks are also generated by the decrepitation of fluid inclusions which are typical in hydrothermal quartz (Gemeinert *et al.* 1992). Clusters of sintered quartz particles in pellets charge are separated by open spaces greater than 25 μm , while the fractures in lumps are of the order of several micrometers.

Table 4.4 Visual observations and backscattering of reacted SiO_2+SiC for the different experimental conditions. Focus on the quartz microstructure.

Lumps - SiO_2+SiC - 5h at 1650°C	Pellets - SiO_2+SiC - 40 min at 1650°C
 <p>Crystalline quartz Crack</p> <p>10mm 500 µm</p>	 <p>Amorphous quartz SiC</p> <p>50 µm 50 µm</p>
Lumps- SiO_2+SiC - 20 min at 1850°C	Pellets - SiO_2+SiC - 10min at 1850°C
 <p>Amorphous quartz</p> <p>500 µm</p>	 <p>Amorphous quartz SiC</p> <p>50 µm 50 µm</p>

The property of pellets to produce more $\text{SiO}(\text{g})$ than lumpy charge was shown in Fig. 4.5 which refers to *Experimental set 2*. Fig. 4.5 represents the total mass balance of the experiments carried out. The first 4 columns refer to experiments with lumps, the last four to pellets charge. Although pellets and lumps have the same initial $\text{SiO}_2:\text{SiC}$ molar ratio, quartz is almost completely reacted after the experiments with pellets. This indicates that more $\text{SiO}(\text{g})$ forms with pellets.

The property of pellets to produce more $\text{SiO}(\text{g})$ than lumpy charge is shown by another set of experiments carried out in *Experimental set 4*. Mixtures of SiO_2+SiC and SiO_2+Si were heated to 1650 °C and 1850 °C and $\text{SiO}(\text{g})$ and $\text{CO}(\text{g})$ were produced. Pellets and lumps were investigated. For the case of pellets, a C-containing binder was added. The mixtures were charged in open graphite crucibles, which were connected to a tube. The experiments stopped when the condensate derived from $\text{SiO}(\text{g})$ and $\text{CO}(\text{g})$ blocked the tube. It was found that when pellets were used, less time was required to block the tube than lumps. The condensates were analyzed

by XRD and there is not a significant difference in phase composition between experiments with lumps and pellets, confirming that more SiO(g) is formed per unit time when using pellets charge. The condensate composition and the time required to block the tube are shown in Fig. 4.7.

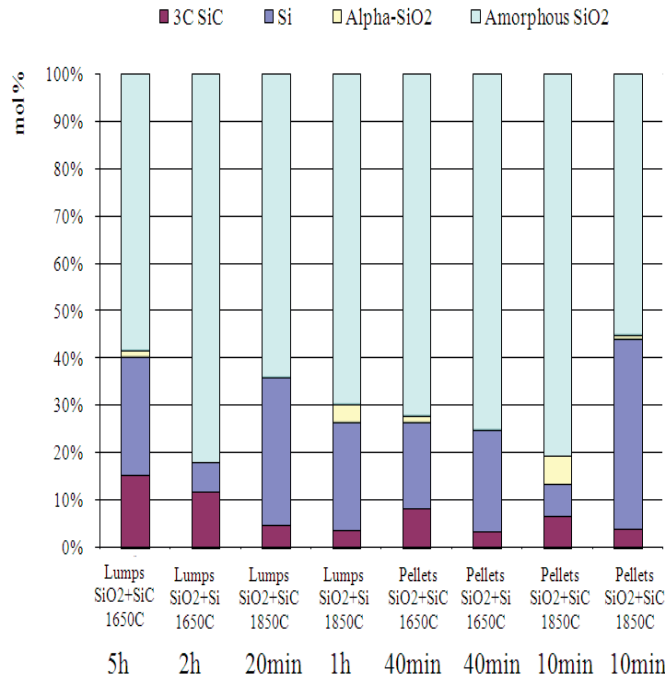


Fig. 4.7 Condensate composition in mol fractions. Eight different experimental conditions are considered. The first four columns refer to the experiments with lumps, the last ones to the experiments with pellets. The time required for the condensate to block the tube is shown below the graphs.

4.3.2 Effect of the quartz morphology

The ability of the cracks in quartz to enhance the formation of SiO(g) is shown in Fig 4.8 and Fig. 4.9 which show the results of the experiments carried out in *Experimental set 2* and *Experimental set 3* respectively.

Two hydrothermal quartzes (qzA and qzB) with same sieved size and different initial cracks and fluid inclusions amount (fluid inclusions generate cracks in quartz upon heating) were studied. In particular qzA contains significantly more fluid inclusions than qzB. The quartz containing more cracks and fluid inclusions was more reactive, producing

more SiO(g) (as shown in Fig. 4.8) and presenting higher weight losses (as shown in Fig. 4.9).



Fig. 4.8 Silicon carbide and two hydrothermal quartzes (qzA and qzB) are respectively heated to 2000 °C in graphite crucibles. Two molar ratios SiO₂:SiC are considered. The graph plots the total production of SiO(g) with the experimental conditions. Total SiO(g) is due to the contribution of three components: 1) SiO(g) which has reacted with the SiC charge to form Si, 2) SiO(g) which has reacted with the graphite crucible to form SiO(g), 3) SiO(g) which was lost out of the crucible.

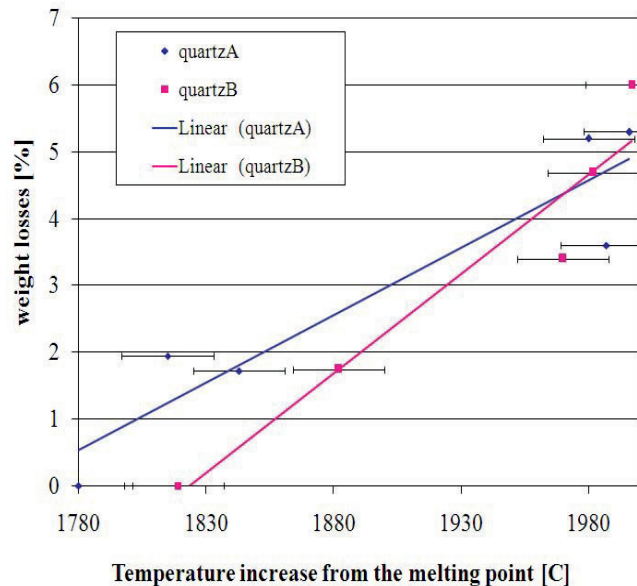


Fig. 4.9 Quartz weight losses (wt%) vs temperature (°C). QuartzA (qzA) presents higher weight losses than quartzB (qzB).

Cracks in quartz influence also the melting point of quartz. The quartz containing more cracks and fluid inclusions (qzA) showed to have the highest melting point. The melting point was measured to $1780\text{ }^{\circ}\text{C} \pm 18\text{ }^{\circ}\text{C}$ and $1819\text{ }^{\circ}\text{C} \pm 19\text{ }^{\circ}\text{C}$ for qzA and qzB respectively. The quartz melting point was measured in a sessile drop set-up (*Experimental Set 3*), and was defined as the temperature when the silica surface becomes glassy.

4.4 Distribution of contaminants from quartz to the gas phase during quartz reduction

4.4.1 Gaseous compounds other than SiO(g) form during quartz reduction

The results reported in this paragraph refer to *Article IV* and *Article V*. Andersen (Tangstad *et al.* 2010) and Ksiazek (Tangstad *et al.* 2009) investigated qualitatively the impurity content in the white and brown condensate formed from small scale silicon producing experiments. Mapping of the condensate shows that Al and Mg concentrate in the Si phase of the brown condensate (Fig 2.8) and that Fe, Al, Ti, Ni, Ca and K are present in the white condensate (Fig. 2.9). However also maps where contaminants were not visible in condensate were observed. Industrial studies of micro-silica show that all the detrimental impurities for solar cell purpose distribute, in different ratios, to micro-silica (Fig. 2.11) (Myrhaug *et al.* 2000). The presence of impurities in the condensate and in the micro-silica provides evidence that the impurities enter the gas phase when quartz and carbonaceous materials are heated under reducing atmosphere.

The ability of an impurity element situated in quartz to form gaseous compounds depends on the thermodynamic conditions (ability to be reduced to a volatile compound), on the diffusion distance to the quartz surface (which depends on cracks in quartz and quartz particle size) and on the impurity types (fast diffuser or slow diffuser depending on the cation size). In general, oxides more stable than SiO₂ remain in the molten mixed oxide/carbide/Si phase, while oxides less stable than SiO₂ are expected to reduce to pure elements or sub-oxides during the reduction of quartz. If these reduced compounds have a high partial pressure they will leave the quartz in form of gaseous compounds.

The aim of *Article IV* and *Article V* was to quantify the impurities, which enter the gas phase during quartz reduction. *Experimental set 4* was used: charge mixtures of quartz and silicon and quartz and silicon carbide were heated above $1650\text{ }^{\circ}\text{C}$ and the produced gaseous compounds condensed to

room temperature. High purity SiC and Si were used, the only source of contamination derived from the quartz used. The condensate mixture collected in the tube was removed with a tungsten carbide tool, and analyzed chemically and showed to contain, in different percentage, all the impurities, which were present in the quartz charge. Table 4.5 shows the average impurity content in ppmw of the collected condensates.

Table 4.5 Impurity contents (ppmw) of the condensate mixtures formed in the Experimental setting 4.

The only source of contamination in the charge mix is the quartz. Two quartzes are considered: quartzite and hydrothermal quartz.

Impurity content in ppmw	B	P	K	Fe	Al	Mn	Zn	Pb
If hydrothermal quartz charged	9.3	8.8	644.1	73.8	23.0	18.6	4.8	2.6
If quartzite charged	61.1	65.5	396.4	128.9	53.8	32.2	33.2	21.2

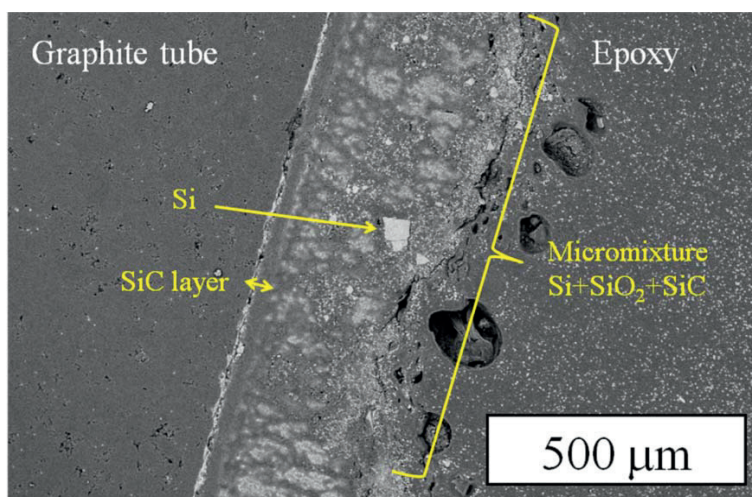


Fig. 4.10 Backscattering image of a mixture of white and brown condensate collected in a graphite tube. The condensate has reacted actively with the graphite tube forming a thin SiC layer which is the region containing the two white lines.

Four different types of condensate (based on colors) were produced: white, green, brown and orange. The orange condensate has probably a temperature of formation lower than the brown and white condensate. The morphology of the brown and white condensate is shown in Fig. 4.10.

Three main structures are found: single Si particles (as indicated in Fig. 4.10); amorphous SiO₂ and random mixtures of SiC, Si and SiO₂.

4.4.2 *Effect of pellets and lumps*

The results reported in this paragraph refer to *Article V*. Gaseous compounds were formed by heating charge mixtures of SiO₂+Si and SiO₂+SiC above 1650 °C as described in *Experimental set 4*. The major source of contamination was quartz and the aim was to study the behaviour of the impurities included in quartz. The elements studied were B, P, Al, Fe, Mn, Pb and Zn because of their detrimental effect on the silicon solar cell. In addition K was studied because of its abundance in the quartz impurity minerals. The gaseous species were collected in form of condensate and analyzed chemically. Both quartzite and hydrothermal quartz were investigated.

The degree of volatilization is here defined as the ability of the impurity, present in the quartz to report to the gas phase. The volatilization of detrimental impurities in quartz is summarized in Fig.4.11. Each value is the average of 4 experiments.

In general Fe and Al show the lowest volatility. Fe is not a stable oxide and is easily reduced to Fe(l), however Fe has a high boiling point and therefore only a few percent of it enters the gas phase. Al is a very stable oxide, as a consequence it remains primarily in the slag phase. Mn, Pb, Zn, K, B and P are less stable oxides than quartz and enter significantly in the gas phase during quartz reduction.

The rate of silica reduction is faster in pellets than in lump quartz; as a consequence, the reduction of impurity oxides is expected to be faster in pellets (it is however not yet known the rate controlling stage: the rate of impurity oxides reduction can be controlled by diffusion in quartz). However, investigations do not show this trend: Fig 4.7 shows that impurities have a lower volatility when pellets instead than lumps are used. The different behaviour of pellets may be explained by the fact that SiO₂ micron particles in pellets react readily to SiO(g), giving a locally higher P_{SiO}, which may result in a lower volatility of the impurities. Phenomena of local pressure in pellets were also found in previous publications where Si formed preferentially in the rim region of pellets (Dal Martello *et al.* October 2011).

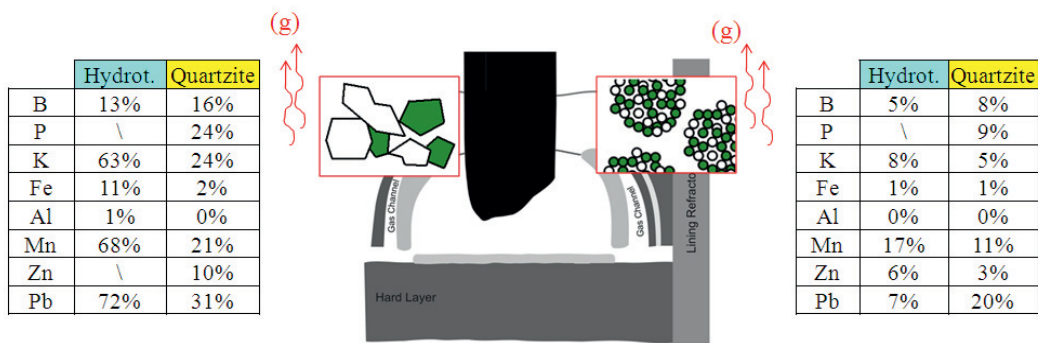


Fig. 4.11 Volatilization of gaseous compounds when heating quartz in a reducing atmosphere. Table on the left refers to lumpy charge, table on the right to pellets charge; the blue columns refer to hydrothermal quartz, the yellow ones to quartzite.

As discussed in *Article IV*, in presence of liquid silicon, trace elements dissolved in quartz can diffuse from the quartz into the neighbouring silicon. Chemical analyses on the reacted charge reveal that B, Fe, Mn, Pb and Al diffuse easily into the silicon. Any contact between quartz and silicon will therefore transfer impurities. The contamination of silicon through diffusion of impurities from quartz is less likely to occur when pellets are used: investigations on the reaction mechanisms between pellets and lumps (*Experimental set 2, Article II*), summarized in Fig. 4.5, showed that quartz in pellets of $\text{SiC}+\text{SiO}_2$ is very reactive and completely reacts when the formation of silicon takes place.

4.4.3 Effect of the quartz type

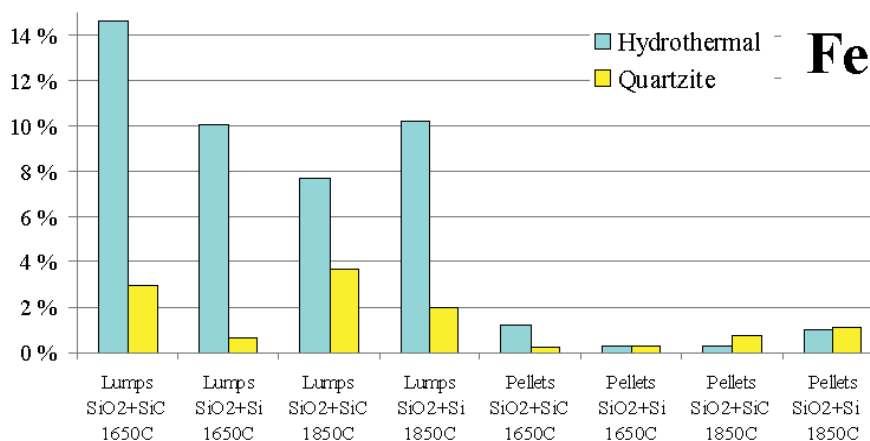
The results reported in this paragraph refer to *Article IV*, *Article V* and *Experimental Set 4*. As shown in Fig. 4.11, hydrothermal quartz features higher volatilization than quartzite for Mn, Fe, K and Pb. Fig. 4.12 shows the degree of volatilization of Fe, Pb, K and Mn for the eight experimental conditions described in Experimental Set 4.

The specific activity of the elements in the charged quartz material seems not to be the reason since the concentration of Pb, Fe, Mn and K is lower in hydrothermal quartz than in quartzite. Liquid inclusions present in hydrothermal quartz may be the reason for the higher volatility presented. Liquid inclusions are only present in lumps of hydrothermal quartz (since the micrometer sized inclusions open and disappear during quartz milling, as in the preparation of pellets).

Fluid inclusions may have enhanced the volatilization by increasing the surface available to reduction of the quartz or by enhancing the formation of volatile Cl-based compounds. During heating of quartz, the internal pressure of the fluid inclusions increases and they decrepitate; i.e. fissures run through the gas-liquid inclusions enabling degassing of water and CO₂ from the inclusions. Decrepitation occurs from 200 to 600 °C depending on the fluid composition. Fluid inclusion decrepitation leaves cracks in quartz (Gemeinert *et al.* 1992). The cracks increase the surface available to reduction, reduce the diffusion distance to the surface and therefore increase the volatilization of the impurities.

Fluid inclusions contain H₂O as well as Cl⁻ ions in solution. Fe, K, Pb and Mn present in the quartz lattice or mineral impurities may have reacted with the species in the fluid inclusions to form volatile compounds, subsequently liberated during reduction of the quartz. Alternatively, these contaminants were already present in the fluid inclusions. According to Larsen (Larsen *et al.* 2004) elements like Ca, Fe, Mg and Mn are likely to be concentrated in sub microscopic fluid inclusions. The affinity of Fe with Cl⁻ was studied by Fein (Fein *et al.* 1992) and the affinity of Fe³⁺, Mn²⁺, Pb²⁺ with Cl⁻ was reported by Deer (Deer *et al.* 1992). Additional FactSage equilibrium calculations, which are shown in *Article IV*, also indicate that addition of Cl in quartz improves the evaporation of the impurities.

Study of the concentrations of impurities before and after reaction in hydrothermal quartz and quartzite show that quartzite was more polluted than hydrothermal quartz both before reduction and after reduction, However the difference in concentration decreased after reduction.



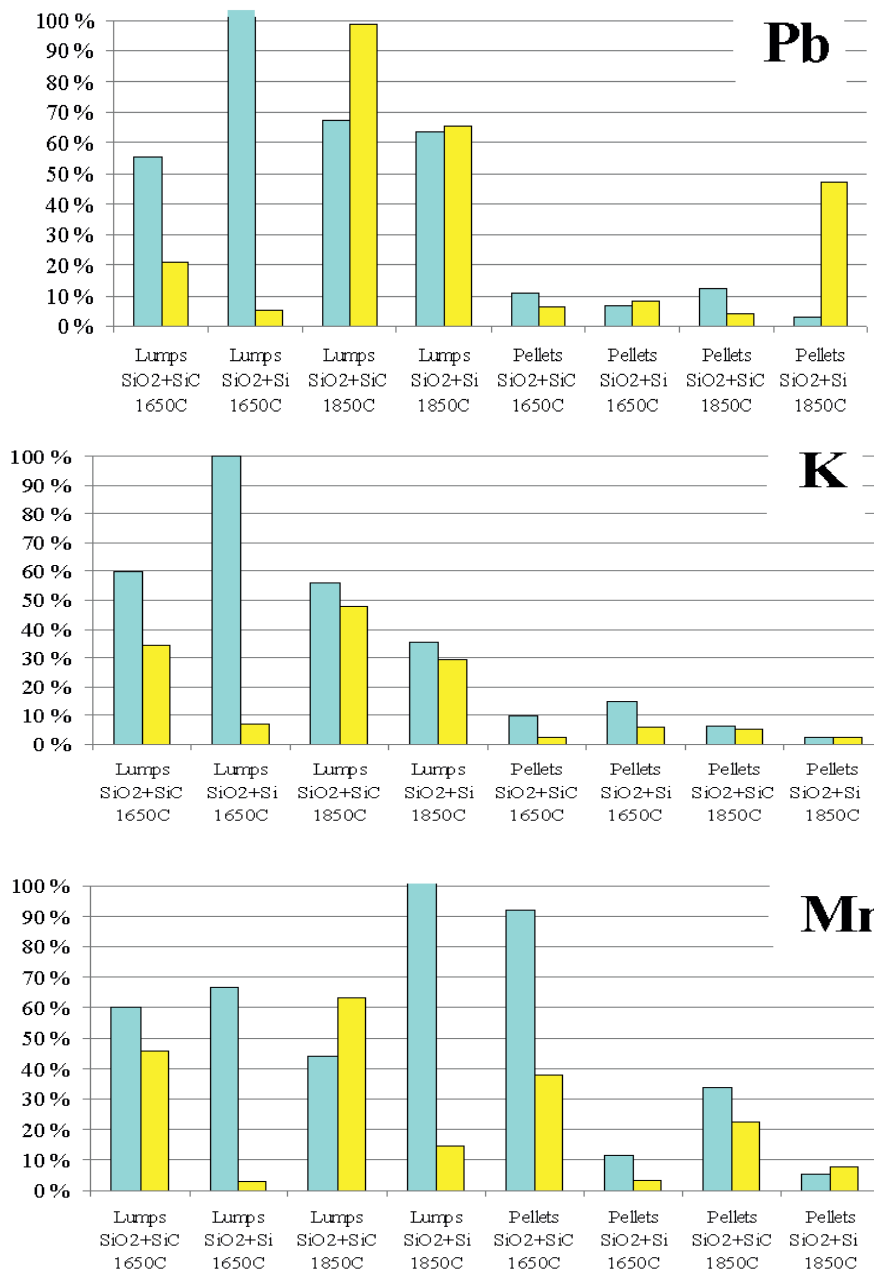


Fig. 4.12 Degree of volatilization for different experimental conditions (hydrothermal quartz rather than quartzite, pellets rather than lumps, SiO₂+SiC mixture instead of SiO₂+Si, 1650 °C instead that 1850 °C).

5 SUGGESTIONS FOR FUTURE WORK

This chapter proposes conceptual approaches to production and refining that have the potential to improve the quality of the silicon produced by the metallurgical route. The approaches refer to the conventional lumpy route, to the pellets route and to an innovative route.

5.1.1 *Further investigations*

The knowledge achieved from the investigations on the silicon feedstock and on the carbothermic reduction of quartz, illustrates the necessity to further study the effect of the condensation reactions on the silicon purity. Here, some investigations to be performed in laboratory equipments are suggested:

- It has been shown that impurities in the quartz contaminate the silicon by *diffusion* (impurities diffuse from quartz to the neighboring silicon phase) and by *condensation* reactions (the condensate contains impurities and the silicon phase is present in the condensate). There may be another way of contaminating the silicon that was not studied here: contamination through the *gas phase*. In the direct way of producing silicon, SiO(g) reacts with SiC and Si forms on the SiC particle (equation 2.8). It is necessary to investigate if the gaseous contaminants carried by SiO(g) enter the SiC structure during this reaction.
- It has been shown that the impurities enter the condensate phase. However there are four types of condensate: white, brown, green, orange. It is necessary to investigate if the impurities distribute preferentially in one type of condensate rather than another one.
- During stoking the condensate in the furnace features higher temperatures. It is necessary to investigate if, during heating of the condensate, the impurities entrapped in the condensate have the chance to leave by forming new compounds. Heating of specific type of condensate is recommended.
- In addition it is necessary to understand how the condensation temperature affects the distribution of the impurities in the condensate rather than in the micro-silica. This knowledge would help understanding the effect of the heat recovery systems or pre-heat

charge systems (one example is described in paragraph 5.1.2) on the final purity of the silicon.

- Paragraph 5.1.4 suggests a new carbon free approach to produce silicon and it is necessary to test the feasibility of this process.
- The experimental setting 4 collects gaseous compounds formed during the carbothermic reduction of silica in form of condensate. The condensate is found distributed inside the gas ducting tube. The experiment stopped when the condensate blocked the ducting tube and an overpressure appeared in the furnace. However, for the purpose of mastering the reduction time, the measurement of overpressure in the furnace is not suitable, due to the fact that the condensate collected in a large area inside the tube without forming a repeatable distribution. A measurement on situ of the crucible weight losses, or the addition of a controlled cooling system on the gas ducting tube are suggested alternatives for future improvement of the experimental setting.

5.1.2 New method for charging lumpy quartz

The conceptual approach here described finds application in the conventional lumpy route.

It has been shown that the impurities enter the gas phase when quartz is still solid, and that the presence of cracks and fluid inclusions enhance this property. The current way of charging the quartz presents some disadvantages. The temperature at the top of the furnace (charge surface) is in the range 1100-1700 °C (Schei *et al.* 1998) and the quartz is charged in batches from the top (Aasly 2008). As a consequence the quartz is heated rapidly to this temperature, the fluid inclusions decrepitate without efficiently removing harmful trace impurities in the host quartz. Furthermore, quartz is shock heated and may disintegrate into mm size fines that lower the permeability of the charge. Finally, when quartz is charged in batches, a part of the charge experiences higher temperatures and a high temperature gradient compared to other charged material (Aasly 2008). As an alternative, it is suggested here that lumpy quartz is preheated by the exhaust gases from the furnace before being charged in to the furnace. The average time (~ 1h) that was used in the *Experimental setting 4* can be suggested for a normal process since it was shown that cracks in solid quartz are permeated by reducing gases, and this phenomena occurs in mm lumps size as well as cm size. The experiments used 0.5 mm size

quartz particles, while lumps of 5-8 cm size are usually charged into the furnace. In the experiment quartz was heated to 1650 °C and 1850 °C, respectively, however the maximum temperature for the fluid inclusion decrepitation is 800 °C. It is therefore here suggested that the charge is heated to 800 °C for 1 h. The preheated charge is then gently and homogeneously conveyed into the furnace. Elements with high affinity to Cl are expected to leave the quartz in the form of gaseous compounds.

5.1.3 New quartz refining route to be used in the pellets route

The conceptual approach here described finds application in the pellets route.

There is not an established beneficiation route for the metallurgical quartz currently used to produce solar grade silicon. Here an innovative route is proposed. At first a tungsten carbide jaw crusher is applied to the quartz to reduce its size to ~2 cm. Secondly electrical fragmentation is applied up to a size comparable with the average quartz grain size. Mineral inclusions, which appear mostly at the grain boundaries, are likely to be liberated during this process. As a third step the liberated minerals are removed by sieving and magnetic separation. Then the quartz particles are heated in a reducing atmosphere in order to permit volatilization of trace elements through the highly fragmented quartz generated by electrical fragmentation. It should be noted that fluid inclusions are still conserved after electrical fragmentation, and can contribute to facilitate the gasification of compounds that are not easily reduced to gaseous compounds like Fe. Finally, liberated quartz particles are ground mechanically to 10 µm size, mixed with the recovered-beneficiated fines (i.e. fraction <10 µm) and agglomerated to pellets meeting the requirements for electrical arc furnaces. Fines formed by mechanical crushing would also need to be recovered since they are required in the agglomeration process.

5.1.4 Production of silicon via a carbon-free metallurgical route

The conceptual approach described in this section refers to an innovative route.

It has been shown that impurities enter the gas phase and the condensate. Because of the recovery of SiO(g) through condensation and stoking,

volatile compounds circulate in the furnace and may end up in the silicon. The temperature of the top charge influences the partitioning of the gas compounds between the condensate phase and the microsilica. Aitcin (Aitcin *et al.* 1984) compared the micro-silica impurity content of a FeSi furnace in the presence and absence of a heat recovery system (charge top at 800 °C and at 1100 °C respectively). Measurements revealed that the micro-silica was purer when the charge top was at a lower temperature, meaning that the elements distributed preferentially to the condensate phase. The condensation process contributes to increase the Si-yield but intrinsically pollutes the silicon. To separate the production of the condensate from the production of silicon seems a possible solution to improve the quality of the Si produced without affecting the Si yield.

The condensate reaction is a way to separate the impurities from SiO(g) when the condensation temperature of the volatile compounds is below the temperature of condensation of SiO(g). It has been shown that the presence of Cl enhance the volatilization of impurities in silica. Among the different condensates, the brown condensate (“SiO₂+Si” composition) has the advantage to decompose into Si and SiO₂ by heating to 1400 °C in argon atmosphere (Vangskåsen 2011). It seems that there is a way to produce clean silicon by means of the condensation reaction (2.3).

Here two “ideal” processes to produce pure silicon are proposed and illustrated schematically in Fig. 5.1 and Fig. 5.2.

The two processes are based on the same principles: quartz, metallurgical grade-Si, fluxes containing Cl and other compounds, which easily can form gaseous compounds with the most detrimental contaminants for silicon, are heated to 1600 °C while purging argon. The flux compositions should be chosen to form volatile compounds, which condensate at temperatures lower than the condensation reaction of SiO(g). The condensation temperature should be kept at the highest in order to avoid other impurities to condensate together with SiO(g). Pure SiO(g) will therefore condense first and the volatile species, which should have higher boiling point, leave the reactor. The condensate is subsequently heated in an argon atmosphere and Si separates from the silica matrix. Upgraded silicon is produced. The silica, which is of high purity can be re-used in the process or be used for other purposes. The argon atmosphere is necessary to assure a reducing atmosphere; in presence of oxygen all the volatile compounds would oxidize indiscriminately. The process might be sealed to prevent corrosion and other emission problems related to Cl.

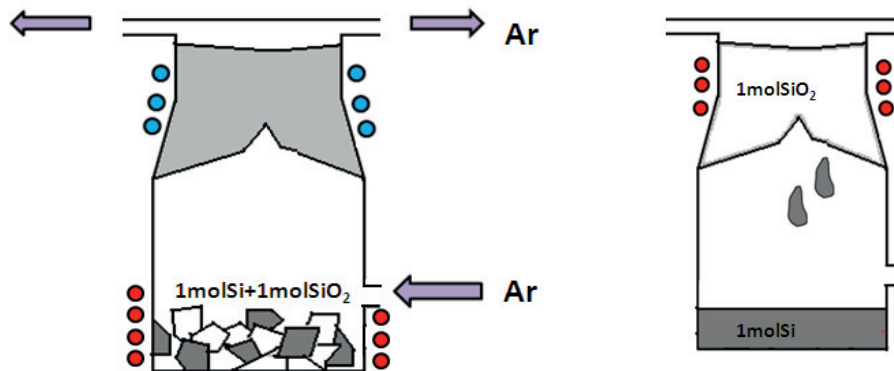


Fig. 5.1 Production of clean condensate (on the left) and clean silicon (on the right) while continuously purging argon. Production in batches. Image on the left: quartz and metallurgical grade silicon are heated to around 1600 °C and SiO(g) is formed. SiO(g) together with other detrimental gaseous compounds leave the charge and reach the top of the reactor which is at a lower temperature. SiO(g) condenses while the other compounds, carried by argon, leave the reactor at the top openings. When the charge at the bottom has completely reacted, the process stops and the bottom of the reactor is cleaned. Image on the right: the condensate is then heated to 1400°C and silicon separates from quartz. Pure silicon droplets migrate to the floor of the reactor.

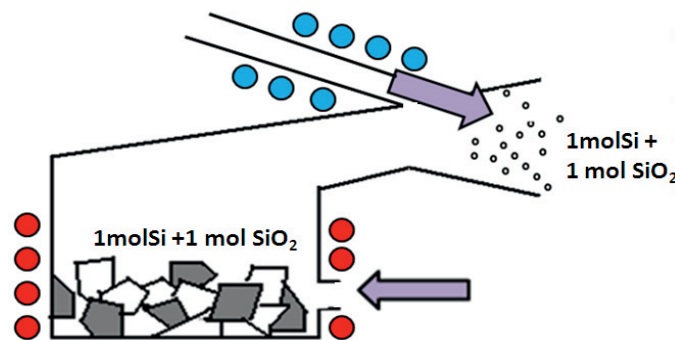


Fig. 5.2 Production of clean SiO(g) and clean Si in series. Silicon and silica react together at the bottom of the reactor. SiO(g) is produced. Argon is continuously purged. Condensation occurs when cold argon is purged directly to the hot gases from the top of the reactor. Micron particles of condensate form and are collected in another reactor where the heating process takes place. The gaseous compounds, which do not condensate leave the furnace. The condensate particles, mixture of silicon and silica matrix, are collected and heated in an argon atmosphere. The separation of the two phases may be done by draining since the density of the two phases is close.

Many advantages are associated with this proposal:

- the process requires to heat twice to 1500 °C but heat recovery systems can be easily integrated, for example running two process lines at the same time
- there is no contamination from the electrode
- detrimental volatile compounds separate naturally from the condensate and leave the furnace thanks to a low condensation temperature
- Si separates naturally from the condensate during heating of the condensate
- it is possible to use quartz of any size and any mechanical properties, since it is charged from the bottom of the reactor and is not affecting the permeability of the process
- it is possible to use silicon and silica of any quality.

6 CONCLUSIONS

The main findings of this PhD work may be summarised in the following points:

1. The beneficiation of hydrothermal quartz by means of fragmentation, sieving and magnetic separation was studied. Two fragmentation techniques were compared: electrical fragmentation and mechanical crushing. Electrical fragmentation, compared to mechanical crushing, liberates more efficiently the minerals from the quartz matrix, resulting in better beneficiated quartz particles.
2. The Si reaction behaviour of lumps and pellets was studied at 2000 °C in reducing atmosphere in small scale reduction furnace. SiO₂ and SiC were the charged materials. More SiO(g) is produced and lost with pellets charge resulting in a higher Si yield. Si is formed in pellets mostly in the rim zone, while larger volumes of single phase Si were found when a lumpy charge is used.

A quantitative analytical method for the estimation of solid phases co-present in a mixture of amorphous SiO₂, SiC, Si and C was proposed in order to study the reaction mechanism of pellets and lumps. The method can be used to calculate total phase mass balance in silicon production experiments and to study the kinetics of reactions. The technique is not based on thermodynamic assumptions and combines XRD and XRF analyses with elemental mass balance.

3. The factors affecting the reaction rate of different types of hydrothermal quartz when heated under reducing conditions were studied using a sessile drop set-up. The quartz containing more fluid inclusions and more micro-cracks has a lower melting point and produces more SiO(g).
4. The factors affecting the distribution of impurity from quartz to the gas phase during quartz reduction were studied in reducing atmosphere in a graphite tube furnace under reducing conditions. All the impurities which were present in the quartz charge entered, to various extents, the gas phase during quartz reduction. The average measured volatility of B, P, K, Fe, Al, Mn, Zn, Pb, as given by the ratio of the impurity which entered the gaseous phase over the impurity content in the charged

quartz, was respectively 11%, 25%, 26%, 4%, 1%, 38%, 10%, 36%. Quartzite and hydrothermal quartz have different initial compositions and approach similar chemistry upon silica reduction. Liquid inclusions, common in lumps of hydrothermal quartz, enhance the distribution of the contaminants to the gas phase.

REFERENCES

- Aasly K. , *Properties and behavior of quartz for the silicon process*, NTNU Department of Geology and Mineral Resources Engineering. Ph.D thesis, 2008.
- Agarwal A. and Pal U., "Influence of pellet composition and structure on carbothermic reduction of silica." *Metallurgical and materials transactions B* **30B**: 295-305, 1998.
- Ainsle N.G., Morelock C.R. and Turnbull D., "Devitrification kinetics of fused silica." *Symposium on Nucleation and Crystallization in Glasses and Melts* 97-107, 1962.
- Aitcin P.C., Pinsonneault P. and Roy D.M., "Physical and chemical characterization of condensed silica fumes." *Ceramic bulletin* **63**(12): 1487-1491, 1984.
- Albinati A. and Willis B.T.M., "The Rietveld method in neutron and X-ray powder diffraction." *J. Appl. Cryst.* **15**: 361-374, 1982.
- Amick J.A. and Dismukes J.P., "Improved High-Purity Arc-Furnace Silicon for Solar Cells." *J Electrochem Soc* **132**(2): 339-345, 1985.
- Andersen V., *Investigation of thermal properties of quartz for the silicon industry under reducing atmosphere*. Department of materials science and engineering. Trondheim, NTNU. Master thesis, 2009.
- Andersen V., Ringdalen E., Tangstad E. and Ksiazek M., Small scale laboratory experiments simulating an industrial silicon furnace. *Infacon XII*, Helsinki, Finland, 2010.
- Andres U., "Development and prospects of mineral liberation by electrical pulses." *International Journal of Mineral Processing* **97**(1-4): 31-38, 2010.
- Andres U. and Bialecki R., "Liberation of Minerals Constituents by High-Voltage Pulses." *Powder Tehcnol* **48**: 269-277, 1986.
- Andres U., Jirestig J. and Timoshkin I., "Liberation of minerals by high-voltage electrical pulses." *Powder Tehcnol* **104**: 37-49, 1999.
- Andres, U. "Electrical disintegration of rock." *Mineral Processing and Extractive Metallurgy Review* **14**: 87-110, 1995.
- Armington A.F. and Balascio JF., "The growth of high purity low dislocation quartz." *Proceedings of the 38th Annual Frequency Control Symposium, USAI*. pp. 3-7, 1984.

- Astimex "<http://astimex.com/com/catalog/min.html>." Retrieved 26th June 2011.
- Aulich H.A., Eisenrith K.H., Urbach H.P and Schulze F.W., "Preparation of high purity starting materials for the production of solar grade silicon." *Siemens Forsch Entw* **11**(6): 327-331, 1982.
- Balek V., Fusek J., Križ J. and Murat M., "Differences in the thermal behaviour of natural quartz before and after mechanical grinding as observed by emanation thermal analysis." *Thermochim Acta* **262**: 209-214, 1988.
- Benezet J.C. and Benhassaine A., "Grinding and pozzolanic reactivity of quartz powders " *Erzmetall* **41**: 126-131, 1988.
- Bluhm, H., W. Frey, Giese, H.. *Application of pulsed HV discharges to material fragmentation and recycling*, IEEE T Dielec El Insul. **7**: 625-636, 2000.
- Burkin V.V., Kuznetsova N.S. and Lopatin V.V., "Formation of a spall cavity in a dielectric during electrical explosion." *Journal of Applied Mechanics and Technical Physics* **51**(1): 137-144, 2010.
- Chaklader A.C.D., "Effect of trace Al₂O₃ on transformation of quartz to cristobalite." *J. Am. Ceram. Soc.* **44**(4): 175-180, 1961.
- Chaklader A.C.D. and Roberts A.L., "Transformation of Quartz to Cristobalite." *J Am Cer Soc* **44**(1): 35-41, 1961.
- Chase M. V. Jr., Ed. *JANAF Thermochemical Tables*. Midland, Michigan 48674, U.S.A, C. A. Davies, J. R. Downey Jr., D.J.Frurip, R. A. Macdonald and A. Syverud, 1985.
- Chen C.Y. , Lin C.I. and Chen S.H., "Kinetics of synthesis of silicon carbide by carbothermal reduction of silicon dioxide." *British Ceramic Transaction* **99**(2): 57-61, 2000.
- Cherniak D.J, "Diffusion in Quartz, Melilite, Silicate Perovskite, and Mullite." *Rev Mineral Geoc* **72**: 735-756, 2010.
- Cherniak D.J, Watson E.B. and Wark D.A., "Ti diffusion in quartz." *Chem Geol* **236**: 65-74, 2007.
- Cho S.H., Mohanty B., Ito M., Nakamiya Y., S.Owada, S.Kubota, Y. Ogata, A.Tsubayama, M.Yokota and K.Kaneko, Dynamic fragmentation of rock by high-voltage pulses. *41th Symposium on rock mechanics (USRMS) "50 Years of rock Mechanics - Landmarks and Futur Challenges*, Golden, Colorado, 2006.
- Coletti G., *Impurities in silicon and their impact on solar cell performance*. Petten, Utrecht University. Ph.D. Thesis, 2011.
- Dal Martello E., Tranell G., Gaal S., Raaness O., Tang K. and Arnberg L., "Study of pellets and lumps as raw materials in silicon production

- from quartz and silicon carbide." *Met. Trans. B* **42B**: 939-950, October 2011.
- Damn C. and Peukert W., "Kinetics of Radical Formation during the Mechanical Activation of Quartz." *Langmuir* **25**: 2264-2270, 2009.
- De Elio de Bengy S., Rodriguez-Avello A.S., Bonilla A.B. and Rosaldo I.A., New fragmentation system using high voltage. *I National Congress of Industrial Minerals*, Zaragoza, 2010.
- Deer, Howie and Zussman, Eds. *An introduction to the rock-forming minerals*, Longman scientific and technical, 1992.
- Fabris P., Pirazzi R., Margadonna D. and Rstioni M., *Method of producing metallic silicon particularly for use in the photovoltaic industry*, Patent 85112506.2, Italy, 1984.
- Fein J.B., Hemly J.J, D'Angelo W.M., Komninou A. and Sverjensky D.A., "Experimental study of iron-chloride complexing in hydrothermal fluids." *Geochim Cosmochim Acta* **56**: 3179-3190, 1992.
- Fenner C.N., "The Stability Relations of the Silica Minerals " *Am. Jour. Sci.* **XXXVI**: **36** (4): 331-384, 1913.
- Filsinger D.H. and Bourrie D.B., "Silica to Silicon : Key Carbothermic Reactions and Kinetics." *J.Am.Ceram. Soc.*, **73**: 1726-1732, 1990.
- Ford H.M., Auerbach S.M. and Monson P.A., "On the mechanical properties and phase behavior of silica: A simple model based on low coordination and strong association." *J. Chem. Phys.* **121**(17): 8415-8422, 2004.
- Førland T. and Flood H., Eds. *Selected topics in high temperature chemistry. A collection of papers dedicated to professore Hakon Flood on his 60th birthday, 25 September 1965*. Oslo, Universitetforlaget, 1996.
- Fowkes F.M. and Burgess T.E., Eds. *Clean Surfaces: Their preparation and Characterization for Interfacial Studies*. New York, Marcel Dekker, 1970.
- Freer R., "Diffusion in silicate minerals and glasses: a data digest and guide to the literature." *Contrib. Mineral. Petrol.* **76**: 440-454, 1981.
- Frischat G.H., "Cation transport in quartz crystals. VI. Connection between electrical conductivity and sodium diffusion." *Ber Deut Keram Ges* **47**: 364-368, 1970.
- Frischat G.H., "Sodium diffusion in natural quartz crystals." *J Am Ceram Soc* **53**: 357-360, 1970.
- Fruehan R.J. and Ozturk B., "The Rate of Formation of SiO by the Reaction of CO and H₂ with Silica and Silicate Slags." *Met. Trans. B* **16B**: 801-806, 1985.

- Garcia, M. and E. H. Myrhaug, *Revisjon av materialbalanse for sporelementer i Si-ovn basert på målekampanje på Elkem Thamshavn april 2007*. Oslo, Elkem Silicon, 2007.
- Gemeinert M. , Gaber M. , Hager I. , Willfahrt M. and Bortschuloun D. , "On correlation of Gas-Liquid inclusion's Properties and Melting Behaviour of Different Genetic Quartzes for Production of Transparent fused Silica." *Neues Jahrbuch Miner. Abh.* **165**(1): 19-27, 1992.
- Gjermundsen, K., Raaness O. and Tuset J.Kr.. *Reaktivitet av reduksjonsmaterialer*, SINTEF Selskapet for industriell og teknisk forskning ved Norges tekniske høgskole Trondheim, 1972.
- GmbH,B.P.I., "http://www.berghof.com/multimedia/Downloads/BPI/Dokumente/Haendlerbereich/MWS_DAB_BSB/Berghof_Applications/DAB/AR_DAB_Technology.pdf." Retrieved 10th January 2012.
- Greaves G.N., "EXAFS and structure of glass." *J. Non-Cryst. Solids* **71**: 203-217, 1985.
- Green M.A., Emery K., Hishikawa Y. and Warta W., "Solar cell efficiency tables (version 37)." *Prog. Photovolt: Res. Appl.* **19**: 84-92, 2011.
- Gribov B.G. and Zinov'ev K.V., "Preparation of high-purity silicon for solar cells." *Inorg Mater*, **39**: 653-662, 2003.
- Grimstvedt A, Mansfeld J., Flem B. and Larsen R.B., "In situ analysis of trace elements in quartz by using laser ablation inductively coupled plasma mass spectrometry." *Chem Geol* **182**: 237-247, 2002.
- Bluhm H. Frey W., Giese H., Hoppe P., Schultheib C., Strabner R., "Application of pulsed HV discharges to material fragmentation and recycling." *IEEE Transaction on Dielectrics and Electrical Insulation* **7**(5): 625-636, 2000.
- Hammouda T. and Pichavant M., "Kinetics of melting of fluorophlogopite-quartz pairs at 1 atmosphere." *Eur. J. Mineral.* **11**: 637-653, 1999.
- Hand R.J., Stevens S.J. and Sharp J.H., "Characterisation of fired silicas." *Thermochim. Acta* **318**: 115-123, 1998.
- Harben P.W, Ed. *The Industrial Minerals HandyBook*, 2002.
- Henderson G.S., "The structure of silicate melts: a glass perspective." *The canadian mineralogist* **43**: 1921-1958, 2005.
- Hosaka M. and Taki S., "Hydrothermal growth of quartz crystals in NaCl solution." *J Crystal Growth* **52**: 837-842, 1981.
- Huang L. and Cormack A.N., "Structural differences and phase separation in alkali silicate glasses." *J. Chem. Phys.* **95**: 3634-3642, 1991.
- Ishak R.J., *Reaction kinetics for reduction of manganese ore with carbon monoxide in the presence of carbon*, NTNU. PhD Thesis, 2002.

- Jensen R., *Gass-stabilisert AC og DC lysbue i Si-metallovn*. Elkem A/S, Forskningssettret Kristiansand. Master Thesis, 1986.
- Joesten R., Ed. *Grain-boundary diffusion kinetics in silicate and oxide minerals*. Diffusion, Atomic Ordering, and Mass Transport: Selected Topics in Geochemistry. New York, Springer-Verlag, 1991.
- Kawasaki T. and Ishizuka H., "Experimental study of Fe³⁺ solubility in cristobalite and its application to a metamorphosed quartz-magnetite rock from Mt. Riiser-Larsen area, Napier Complex, East Antarctica." *J. Miner. Petr. Sci.* **103**: 255-265, 2008.
- Kronenberg A.K. and Kirby S.H. , "Ionic conductivity of quartz: DC time dependance and transition in charge carriers." *Am mineral* **72**: 739-747, 1987.
- Kucharski J., Stoch L. and Laczka M., "The role of impurities in the high temperature transformation to cristobalite." *Min. Polonica* **12**: 57-65, 1981.
- Kueller F.J. and Poe T.I., "The quartz-cristobalite transformation." *J.Am.Ceram. Soc.* **47**: 311-312, 1964.
- Kvande R., Nygaard L., Stute S. and Bronsveld P.C.P., Solar cells manufactured from Silicon made by the Solsilc process. *25th European Photovoltaic Solar Energy Conference and Exhibition / Conference on Photovoltaic Energy Conversion*, Valencia, Spain, 9th Septmeber 2010.
- Ksiazek, M. and V. Andersen, *Simulation of the silicon process in a laboratory scale inductive furnace - preliminary version*. Trondheim, Norway, Report SINTEF, 2009.
- Larsen, R. B., Flem B., Dundas S., Lahaye Y. and Mansfeld J., *LA-HR-ICP-MS analysis of quartz and principles governing the distribution and speciation of structural impurities in igneous quartz*. Trondheim, Report NGU, North Cape Minerals: 43, 2000.
- Larsen R.B and Jacamon F, "Trace elements evolution of quartz in the charnockitic kleivan granite, sw-norway: the ge-ti ratio as an index of igneous differentiation." *Lithos* **107**: 281-291, 2009.
- Larsen R.B. , Henderson H. , Ihlen P.M. and Jacamon F. , "Distribution and petrogenic behaviour of trace elements in granitic pegmatite quartz from granite from South Norway." *Contrib Mineral Petr* **147**: 615-628, 2004.
- Lee Y.E. and Kozak D.S., "The Role of Zinc in the Eruption of High Carbon FeMn Smelting Furnace." *Electric Furnace Conference Proceedings*: 145-150, 1993.

- Lindstad T., Gaal S. and Hansen S., Improved Sintef Si-reactivity test. *Infacon XI*, New Dehli, India, 18-21TH Febraury 2007.
- Lynch D., The physical chemistry of silicon production: Phosporous in the arc furnace and catalytic elements in the rochow process. *Silicon for the Chemical Industry VII*, 2004.
- Lynch D., "Winning the gobal race for solar silicon." *JOM* **61**(11): 41-48, 2009.
- Mackenzie J.D., "Fusion of quartz and cristobalite." *J. Am.Ceram. Soc.* **43**(12615-620), 1960.
- Mitra S., "Kinetics of quartz-cristobalite transformation." *Trans. J. Brit. Ceram. Soc.* **76**(4): 71-74, 1977.
- Moroz I.Kh. and Maslennikova G.N., "Thermal transformations of silica." *Steklo i Keramika* **12**: 21-23, 1985.
- Müller A. , Lennox P. and Trzebski R. , "Cathodoluminescence and microstructural evidence for cristallisation and deformation processes of granites in the Eastern Lachlan Fold Belt (SE Australia)." *Contrib Mineral Petr* **143**: 510-524, 2002.
- Müller A., B.J. Williamson and Smith M., "Origin of quartz cores in tourmaline from Roche Rock, SW England." *Mineralogical Magazine* **69**(4): 381-401, 2005.
- Müller A., Wiedenbeck M., M.Van Den Kerkhof A. and Kronz A., "Trace elements in quartz - a combined electron microprobe, secondary ion mass spectrometry, laser ablation ICP-MS,and cathodoluminescence study." *Eur J Mineral* **15**: 747-763, 2003.
- Müller M.B., Olsen S.E. and Tuset J.Kr., "Heat and mass transfer in the ferrosilicon process." *Scand. J. Metall.* **1**: 145-155, 1972.
- Myrhaug E. H., *Non-fossil reduction materials in the silicon process-properties and behavior*. PhD thesis, Department of Materials technology Norwegian University of Science and Technology, 2003. Trondheim, 2003.
- Myrhaug E.H. and Tveit H., "Material Balance of trace elements in the Ferrosilicon and Silicon Processes." *Electric furnace conference proceedings* **58**, 2000.
- Myrvågnes V., *Analyses and characterization of fossil carbonaceous materials for silicon production*. NTNU. Trondheim, NTNU. PhD Thesis, 2008.
- Nichol S., Method for purifying silicon, *PatentUS 7, 727, 503 B2*, 6N Silicon Inc. Vaughan, Ontario(CA),2009.
- NordicMining"<http://www.nordicmining.com/kvinnherad/category276.html> ." Retrieved 16th June 2011.

- Norwegian Geological Survey NGU "<http://www.ngu.no/en-gb/hm/Resources/industrimineraler/Kvarts-og-kvartsitt/High-purity-quartz/>." Retrieved 29-01-2012.
- Panel discussion, Arriving at well-founded SoG-Silicon feedstock specifications. *Crystal Clear in the 6th framework of program of EU*, Amsterdam, 2008.
- Pankrath R. and Florke O.W., "Kinetics of Al-Si exchange in low and high quartz: calculation of Al diffusion coefficient." *Eur J Mineral* **6**: 435-457, 1994.
- Penniston-Dorland S., "Illumination of vein quartz textures in a porphyry copper ore deposit using scanned cathodoluminescence: Grasberg Igneous complex, Irian Jaya, Indonesia." *Am Mineral* **86**(5-6): 652-666, 2001.
- Poch W. and Dietzel A., *Ber. Dtsch. Keram. Ges.* **39**: 413-426, 1962.
- Presser V. and Nickel K.G., "Silica on silicon carbide." *Crit. Rev. Solid State Mater. Sci* **33**: 1-99, 2008.
- Prewitt C.T., Heaney J.P. and Gibbs G.V., Eds. *SILICA Physical Behavior, geochemistry and materials applications*, 1994.
- Raaness O., Kolbeinsen L. and Byberg A., Statistical Analysis for Coals Used in the Production of Silicon Rich Alloys. *8th International Ferroalloys Congress (INFACON8) Proceedings Beijing China 7th-10th June 1998*.
- Robb L., Ed. *Introduction to ore forming processes*, John Wiley & Sons, 2004.
- Sahajwalla V., Khanna C., Wu R., Chaudhury N.S. and Spink J., "Kinetic Study of Factors Affecting in Situ Reduction of Silica in Carbon-Silica Mixtures for Refractories." *ISIJ International* **43**: 1309-1315, 2003.
- Samson I., Anderson A. and Marshall D., Eds. *Fluid Inclusions: Analysis and Interpretation*, 2003.
- Sandberg B., High performance solar cells based on low cost solar silicon with low carbon footprint. *PHOTON's 10th Solar Silicon Conference*, Berlin, Germany, 2012.
- Sandvik K.L., Digre M. and Malvik T., *Oppredning av primære og sekundære råstoffer*. Tapir forlag, Trondheim, 1999.
- Schei A., "On the chemistry of ferrosilicon production." *Tidsskr. Kjemi Bergv* **27**: 152-158, 1967.
- Schei A., Tuset J.Kr. and Tveit H., Eds. *Production of High Silicon Alloys*, Tapir forlag, N-7005 Trondheim, 1998.

- Scherer G., Vergano P.J. and Uhlmann D.R., "A study of quartz melting" *Phys. Chem. Glasses* **11**(3): 53-58, 1970.
- Schon J.H., Ed. *Physical Properties of Rocks*. Bergakademie Freiberg, Germany, Elsevier, 2004.
- Selfrag, www.selfrag.com, Retrieved 12th March 2012.
- SEMI "<http://ams.semi.org/ebusiness/standards/SEMISTandardDetail.aspx?ProductID=211&DownloadID=2084>." Retrieved 14th April 2012.
- Sharp J.H., Hand R.J. and Stevens S.J., "Characterization of fired silicas." *Thermochimica Acta* **318**: 115-123, 1998.
- Sharp J.H., Stevens S.J. and Hand R.J., "Polymorphism of silica." *J Mat Science* **32**: 2929-2935, 1997.
- Steinike U. and Tkáčová K., "Mechanochemistry of Solids-Real Structure and Reactivity." *J Mater Synth Proces* **8**: 197-203, 2000.
- Sterneland J., *Alkalis in the HCFeMn-Furnace, a mass balance of potassium oxide on the furnace no 12 at Elkem Mangan a.s. PEA*. Department of Metallurgy. Stockholm, Sweden, Royal Institute of Technology, KTH. Diploma Thesis, 1993.
- Stoch L. , Laczka M. and Waclawska I. , "The role of impurities in the high-temperature transformations of SiO₂." *Mineralogia Polonica* **16**(2): 43-54, 1985.
- Stock H.D. and Lehmann G., "Phenomena associated with diffusion of trivalent iron in amethyst quartz." *J. Phys. Chem. Solids* **38**: 243-246, 1976.
- Strake B. and Aulich H.A., "Carbothermische Herstellung von Solarsilizium." *Erzmetall* **41**: 126-131, 1988.
- Swanson R.M. (SunPower Corporation), Approaching the 29% limit efficiency of silicon solar cells. *Proceedings of the 31st IEEE Photovoltaic Specialists Conference*, 2005.
- Tada M. and Hirasawa M., "A Two-Stage Reduction Process for Silicon Production." *High Temp Mat Pr-Isr* **19**: 281-297, 2000.
- Tangstad M., Ksiazek M. and Andersen V., *FeSi/Si process understanding* Trondheim, NTN, 2009.
- Tangstad, M. and M. Ksiazek, *Investigation of white and brown condensate*. Trondheim, SINTEF Materials and Chemistry, 2010.
- Tranell G., Ciftja A. and Ringdalen E., "Reaction Zones in a FeSi75 Furnace, Part I: Results from an Industrial Excavation." *to be published at Met Mat Trans B*, 2012.
- Tranell G., di Sabatino M. and Tronstad R., Silicon feedstock for solar cells - availability, quality criteria and future production routes. *CSSC4*, Taipei, Taiwan, 2010.

- Tsuo Y.S, Gee J.M. , Menna P., Strebkov D.S. and A. Pinov and V. Zadde. *2nd World Conference and Exhibition on Photovoltaic Solar Energy Conversion* Vienna, Austria, 1998.
- Tuset J.K. and Raaness O., Reactivity of reduction materials for the production of silicon, silicon-rich ferroalloys and silicon carbide. *Electr Furn Proc Metall Soc AIME Iron Steel Div* **34**: 101-107, 1976.
- Tveit H. and Myrhaug E., Important sub-processes in the silicon process. The behavior of trace elements. *Silicon for the chemical industry V*, Tromsø, 2000.
- Van der Kerkhof A.M. , Kronz A. , Simon K. and Scherer T. , "Fluid controlled quartz recovery in granulite as revealed by cathodoluminescence and trace elements analysis " *Contrib Mineral Petr* **146**: 637-652, 2004.
- Vangskåsen J., *Condensate formation in the silicon process* Unpublished work Trondheim -Internal report, NTNU, Department of Materials Science and Engineering, 2011.
- VDEh, Ed. *Slag Atlas, 2nd ed.*, Verlag Stahleisen GmbH, Düsseldorf, 1995.
- Verhoogen J., "Ionic diffusion and electrical conductivity in quartz." *Am Mineral* **37**: 637-655, 1952.
- Verryn Maggi Loubser and Sabine, "Combining XRF and XRD analyses and sample preparation to solve mineralogical problems." *S Afr J Geol*, **111**:229-238, 2008.
- Vukceovich M.R., "A new interpretation of the anomalous properties of vitreous silica " *J. Non-Cryst. Solids* **11**: 25-63, 1971.
- Waclawska I., Stoch L. and Laczka M., "The role of impurities in the high temperature transformations of SiO₂." *Min. Polonica* **16**: 43-53, 1985.
- Wang Q., Qiu Jianrong., Liu Y. and Zheng C., "Effect of atmosphere and temperature on the speciation of mineral in coal combustion." *Fuel Process. Technol.* **85**: 1431-1441, 2004.
- Webmineral "www.webmineral.com." Retrieved 28th February 2012.
- Weimer A.W., Nilsen K.J., Cochran G.A and Roach R.P, *AICHE Journal* **39**: 409, 1993.
- Whittaker E.J.W. and Muntus R., "Ionic radii for use in geochemistry." *Geochim Cosmochim Ac* **34**: 945-956, 1970.
- Wiik K., *Kinetics of reactions between silica and carbon*. NTH Universitet i Trondheim, PhD Thesis, 1990.

- Yao H., Minato H., Mkilaha I.S.N. and Naruse I., "Fundamentals on vaporization behavior of trace metal compounds at different atmospheres and temperatures." *J.Jpn. I. Met.* **81**(4): 256-262, 2002.
- Yoshiyagawa M. and Tamenori H., Preparation of high purity silica for solar grade silicon. *Proceedings of the 20th Intersociety Energy Conversion Engineering Conference, Energy for the Twenty-First Century*, Miami Beach, FL, 1985.
- Zhu B.-z., Sun Y.l. and Xie C.-w., "Spectroscopy research on the Guizhou Xingyi gangue of different calcined temperatures." *Journal of china coal society*: 1049-1052, 2008.

ARTICLES

Article I

Combined XRD and XRF Technique for the Quantification of the Mass Balance in a Si Carbothermic Production Experiment

Elena Dal MARTELLO,^{1)*} Gabriella TRANELL,¹⁾ Ola RAANESS²⁾ and Lars ARNBERG¹⁾

1) NTNU Department of Materials Science and Engineering, Trondheim, 7491 Norway. E-mail: dalmarte@material.ntnu.no

2) SINTEF Materials and Chemistry, Trondheim, 7465 Norway.

(Received on April 20, 2011; accepted on May 26, 2011)

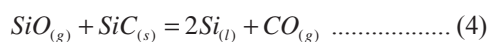
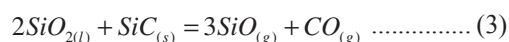
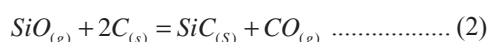
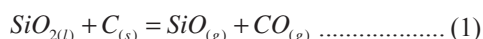
The production of metallurgical grade silicon is based on carbothermic reduction of silica in the submerged arc-furnace. Small scale silicon production experiments have been performed aiming at investigating the kinetics and the reaction mechanisms occurring in the furnace. This paper describes a new combined quantitative technique for the analysis of reaction products from silicon experiments. The method is based on a combination of XRD and XRF techniques and can be used to estimate the total phase mass balance in silicon experiments.

KEY WORDS: silicon; XRD; XRF; phase mass balance.

1. Introduction

Metallurgical grade silicon is produced conventionally by the reduction of silicon dioxide with carbon in a submerged electric arc furnace. In this process, the charge materials, consisting of quartz rock and carbonaceous reducing agents, are charged into the furnace from the top and molten silicon is tapped from the bottom. The system includes many compounds: solid (C, SiC and SiO₂), liquid (Si and SiO₂) and gaseous phases (CO, SiO) are copresent. The reactions take place under atmospheric pressure in a temperature interval of 1 500–2 000°C.

The main reactions are:¹⁾



In the upper low temperature zone of the furnace, carbon and silica react to SiO and CO according to Eq. (1), and the ascending SiO reacts with C to form SiC according to Eq. (2) or condenses to Si and SiO₂. SiO is produced mainly from the reaction of Si with molten SiO₂ (Eq. (5)) that takes place in the lower and hottest part of the furnace. In the hottest part of the furnace SiO₂ reacts with SiC to form Si, SiO and CO according to Eqs. (3) and (4).

Small scale silicon producing experiments have been performed to simulate an industrial furnace. Because of kinetics and carbon reactivity^{2,3)} the reactions do not go to completion, and nonreacted carbon, quartz and silicon carbide are found together with the reaction products.

A quantification of the reaction products involved in the

silicon production experiments allows a study of the reaction mechanisms, the silicon yield and the reaction kinetics. Agarwal and Pal⁴⁾ have calculated a phase mass balance to study the reduction kinetics of pellets made of C carbon black and SiO₂. Combustion analysis of the reacted pellets gives the C and O content of the samples. Oxygen content corresponds to retained silica, while carbon content corresponds to the SiC and retained carbon in the system. Total weight loss measured is attributed to the CO and SiO evolution. The calculated CO amount has been verified against the total CO evolution measured by a gas analyzer. Errors below 10% have been reported. Nagamori *et al.*⁵⁾ have studied the thermodynamics of the whole Si–C–O system theoretically. A mass balance is established before and after the reactions. The number of moles before and after the reaction are interrelated by the Si–O–C element balance and one equilibrium reaction. Nagamori based his quantification on thermodynamic assumptions. Agarwal and Pal based their quantification on measured values, but the analysis method presents several disadvantages: it requires a CO analyzer, it does not distinguish between different SiC polytypes and does not distinguish between C in SiC and elemental C. Mineralogy and geological applications often use a combination of XRD and XRF analysis techniques to identify phase and elemental composition of rocks.⁶⁾ This method alone is not able to quantify the output phases of a silicon production experiment. The reacted charge contains amorphous silica that can not be quantified by XRD and graphite that can not be quantified by XRF.

The aim of this study is to quantify, without thermodynamic assumptions, the products of different reactions occurring simultaneously in a silicon production experiment. The method combines XRD, XRF with elemental Si, C, O mass balances. The reaction products of a series of small scale silicon producing experiments have been stud-

ied. The method can be used to quantify different SiC polytypes, C, Si, amorphous SiO₂ reaction products as well as SiO and CO lost.

2. Materials and Methods

2.1. Materials and Experimental Procedures

The charged material was in the form of lumps or pellets. Two high-purity hydrothermal quartzes, denoted quartzA and quartzB, one source of high-purity SiC and high purity graphite crucibles have been used. The experimental set-up is shown in Fig. 1. The SiC was a mixture of hexagonal (6H:SiC) and tetragonal (15R:SiC) polytypes, no crystallographic cubic SiC (3C:SiC) was present. The number indicates the number of layers in the stacking sequence, and the letter the class: H, R, C stands for hexagonal, rhombohedral and cubic respectively. According to another designation, hexagonal and rhombohedral polytypes are denoted as α -type, while cubic polytype as β -type.⁷⁾ The total weight of the charge was 25 g when pellets were used and 18 g for the case of lumpy charge. The lumps size was 3–5 mm and the pellets had a diameter of 1–2 mm. Pellets consisted of a mixture of quartz and silicon carbide milled to powder (quartz up to 20 μ m and SiC up to 10 μ m size). Particle size was chosen according to the work done by Agarwal and Pal.⁴⁾ Water was used as binder during the pelletizing process. The charge was dried in a graphite crucible at 80°C for 600 min.

The experiments lasted 80 min. The charge was first heated to 1800°C at a heating rate of 90°C/min, then from 1800°C to 2000°C at 5°C/min, and then the temperature was maintained at 2000°C for 20 min. The sample was subsequently rapidly cooled at a rate of 100°C/min.

Two SiO₂:SiC molar ratios have been considered. A molar ratio 1:2 refers to the stoichiometry of reactions (3)

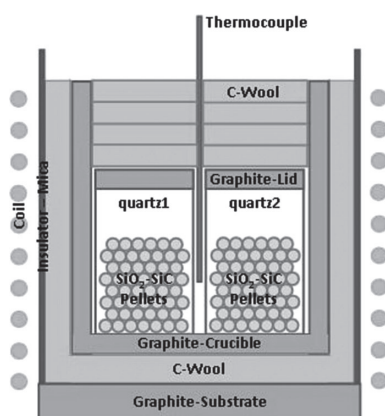


Fig. 1. Experimental set-up of small scale silicon production experiments in induction furnace. Example for the case of pellets.

Table 1. Experimental variables: quartz source, charge size and SiO₂:SiC molar ratio.

	quartz	qzA	qzB	qzA	qzB	qzA	qzB	qzA	qzB
Charge size	lumps	lumps	lumps	lumps	pellets	pellets	pellets	pellets	pellets
Molar ratio	1:2	1:2	1:1	1:1	1:2	1:2	1:1	1:1	1:1

and (4). The molar ratio SiO₂:SiC = 1:1 refers to the stoichiometric overall reaction taking place in the inner zone as proposed by Schei and Müller.^{8,9)}

The experiments were designed to study 3 factors in eight runs. The eight run design was constructed with a full factor standard table of signs (see Table 1) for two quartz types, SiO₂:SiC molar ratios and charge type. Each run was repeated three times when lumps were used and two times when pellets were used. The experiments with pellets were repeated only twice, because they showed little variability in the weight loss. Representative samples that showed weight losses closer to the average value for each experimental condition were analyzed quantitatively. Solid phases remaining after the experiments were solid reaction products and solid unreacted charge. In particular the solid phases consisted of Si, C, amorphous SiO₂, and different SiC polytypes.

2.2. Method for Analysis

XRD and XRF quantitative analysis X-ray powder diffraction (XRD) and X-ray fluorescence spectroscopy (XRF) are highly complementary materials analysis methods which, when combined, allow phase identification and quantitative analysis. XRF provides highly accurate information about the elemental composition of a sample. The instrument used in the present investigation can be used to estimate the weight percentage of the total elemental Si, but does not to detect light elements such as C and O and not give direct phase information. In contrast to XRF, XRD is the most direct and accurate analytical method to identify and determine the amounts of phases in a sample. However, only polymorphs of crystalline phases can be quantified. A qualitative comparison between the two techniques is shown in Table 2. D8 Advance XRD, BRUKER-EVA qualitative, BRUKER-TOPAS quantitative Rietveld and XRF BRUKER S8 Tiger 4 kW X-ray spectrometer have been used for the analysis. XRD analysis requires a few grams of specimen, while XRF needs about 9 g. In order to confirm the representativity of the sampled material, two parallels of each sample were analyzed by XRD.

Sample preparation The crucible and reacted charge were crushed to a fine powder by means of a tungsten carbide vibratory disc mill. The particle range size was 200 nm–50 μ m, which is consistent with XRD and XRF requirements. Particles larger than 50 μ m lead to poor statistics and preferred orientation effects. Overcrushed material has highly distorted structure and limited number of crystal planes which lead to a broadening and eventually disappearance of the XRD peaks. Different crushing times combined with particle size analyses have been tested. The optimum crushing procedure consisted of crushing the sample for 5 minutes, sieving the powder obtained at 50 μ m, and crushing the

Table 2. Qualitative comparison between XRD and XRF technique.

phase	XRD	XRF
SiC	Quantification of different SiC polytypes	Quantification of the elemental Si contained in Si, SiC and SiO ₂
SiO ₂	Only quantification of crystalline SiO ₂	
Si	Quantification of silicon phase	
C	Quantification of carbon phase	Not possible to quantify

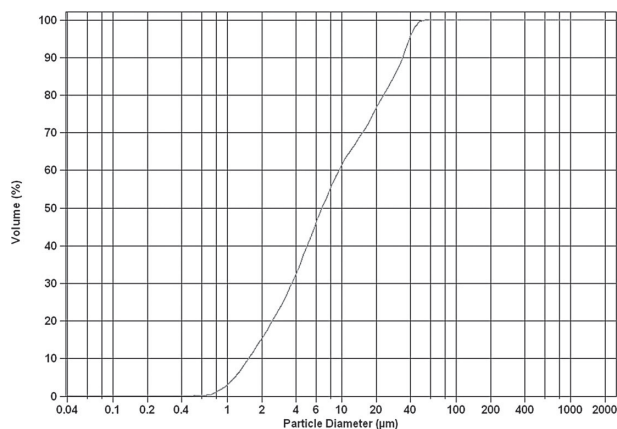
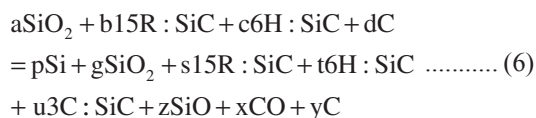


Fig. 2. Particle size analysis for the sample: lumps qzA SiO₂:SiC = 1:2. Cumulative distribution curve. D₅₀ = 8 μm.

powder above 50 μm for 10 more minutes. Particle size was measured by Laser Scattering (LS) Particle Size Analyzer. The cumulative distribution curve is shown in Fig. 2. Since the sample is a mixture of different solid phases (SiC, SiO₂, Si and C) and each phase has different specific weight, the volume distribution curve does not coincide with the weight distribution curve.

Calculation of total mass balance The purpose is to identify and quantify the reaction products and unreacted charge of silicon carbothermic production experiments. The unreacted charge consists of SiO₂, SiC and C phase. The reaction products consist of Si, SiC, CO(g), SiO(g). Input components are SiO₂, SiC charge materials and C from the graphite crucible. The graphite is included in the mass balance, because the crucible reacts with SiO(g) and a thin layer of SiC is formed according to reactions (1), (2). In particular since the experiments are carried out between 1 400°C and 2 000°C cubic SiC (3C:SiC) is formed.^{8,10,11} The absence of cubic silicon carbide in the input charge represents a great help for the solution of the mass balance. In this way it is possible to distinguish the SiC consumed in the charge from the SiC formed during the reaction between the crucible and the SiO(g). The amount of reactants is known, while the amount of unreacted charge and reactants products is unknown. The overall input-output phase mass balance is written in Eq. (6). The coefficients in Eq. (6) represent the moles of phases. Values in input refer to the dried charge.



Total weight losses, total weight content of elemental Si, ratio in weight between Si and SiC, Si–O–C element mass balances are all necessary information to solve the phase mass balance. Total weight losses are in grams and are attributed to the CO(g) and SiO(g) evolution. Total weight content of elemental Si and the ratio in weight between Si and SiC are measured by XRF and XRD respectively. Element mass balances for respectively Si, O and C species are written in Eqs. (7), (8) and (9). The element mass balances are solved in moles of elements.

$$a + b + c = g + s + t + u + z + p \dots\dots\dots (7)$$

$$2a = z + 2g + x \dots\dots\dots (8)$$

$$b + c + d = y + s + t + u + x \dots\dots\dots (9)$$

By knowing the total amount of elemental silicon present in the reacted charge, it is possible to solve the silicon mass balance and to estimate the parameter z (Eq. (10)). The symbol totSi stands for the total amount of elemental silicon present in Si, SiC and SiO₂ phases. This value is in grams, and is calculated from the mass% of elemental silicon, the silicon atomic number and from the total weight of the reacted crucible. From this information, and from the additional information of total weight losses, the amount of CO(g) can be estimated (Eq. (11)). Now the oxygen mass balance can be written and the amount of nonreacted quartz can be estimated (Eq. (12)). With the additional information of the ratio Si/SiC, it is possible to calculate the amount of Si (Eq. (13)) and the three SiC polytypes (Eq. (14)). As last, a carbon mass balance is written and the amount of nonreacted carbon is estimated.

Weighing of the nonreacted silica, quantification of the graphite by Carbon Leco and observations of backscattering images of the reacted charge, have been used to estimate the error of the method.

$$z = a + b + c - \frac{\text{totSi}}{28.086} \dots\dots\dots (10)$$

$$x = \frac{\text{weightlosses} - z \cdot 44.085}{28.01} \dots\dots\dots (11)$$

$$g = \frac{a - (x + 2)}{2} \dots\dots\dots (12)$$

$$p = \frac{40 \cdot (a + b + c - z - g)}{\frac{\text{SiC}}{\text{Si}} \cdot 28.086 + 40.097} \dots\dots\dots (13)$$

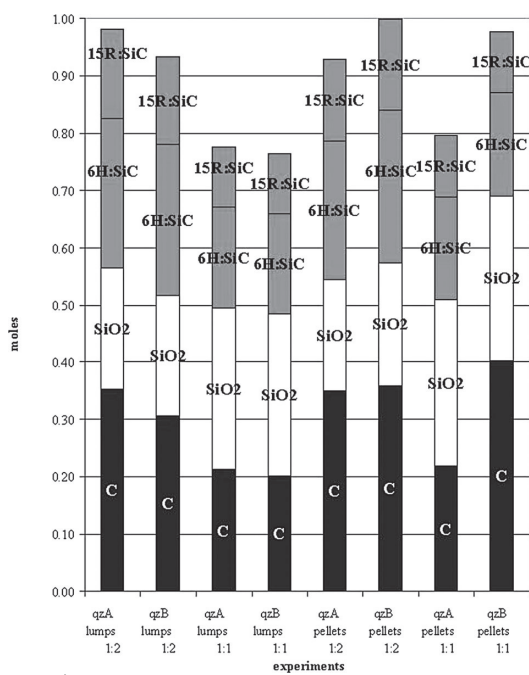
$$s + t + u = a + b + c - (g + z + p) \dots\dots\dots (14)$$

3. Results and Discussion

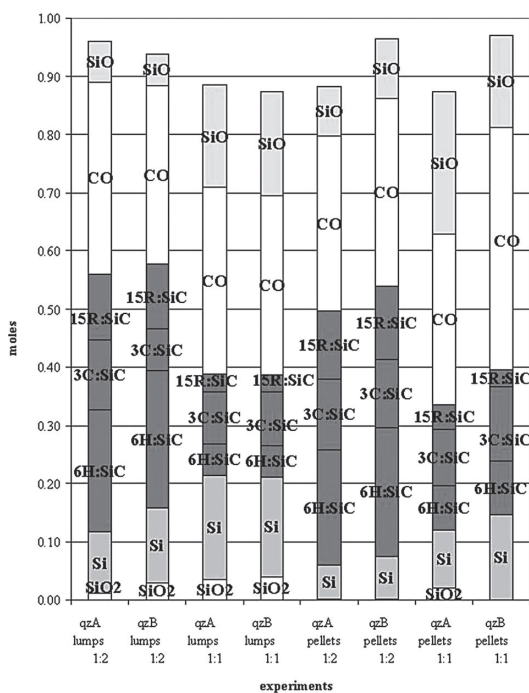
The total mass fraction for the eight experiments is shown in Fig. 3. Only the fraction of graphite that has reacted to form SiC is shown as carbon input.

Figure 4 is an example of a XRD spectrum of the reacted charge. The green curve represents the spectrum, the blue curve represents the phase theoretical peaks. The two curves are almost overlapping, and the deviation between them is the error represented by the red curve. Negative and positive deviation peaks represent respectively over and under quantitative estimation for that phase. The quantification of Si and SiC phases shows small errors. On the other hand, the graphite phase shows large asymmetric error peaks. In addition graphite has high X-ray absorption because of its low atomic number and the analysis is probably affected by the matrix effect. Other sources of errors are the presence of a tungsten phase due to the tungsten carbide crusher used for the sample preparation and the presence of amorphous silica that cannot be quantified. Since the error for the Si and SiC phase is low, their ratio is used for the calculation of the mass balance.

The errors in the quantification of the total C and SiO₂



a)



b)

Fig. 3. a) Reactants (in moles) for each experimental run; b) Reaction products and unreacted reactants (in moles) for each experimental run.

phases for the samples “qzA lumps 1:2”, “qzB lumps 1:2”, “qzB pellets 1:2” and “qzA pellets 1:1” have been calculated. The errors have been calculated on the total weight of the reacted crucible, and are nearly the same for the different phases considered.

In the samples “qzA lumps 1:2” and “qzB lumps 1:2”, nonreacted silica was present as small spheres and it was hence easy to detach the silica from the charge and weigh it. The silica was then mixed again into the charge, crushed to μm size particle and the total mass balance calculated. The calculated amount of silica is compared to the weighed value: 0.62 g SiO_2 and 1.81 g SiO_2 have been calculated

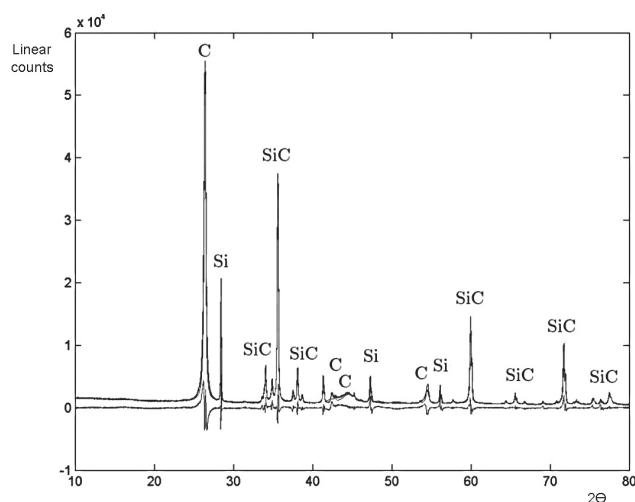


Fig. 4. XRD spectrum of the reacted charge. The main Si, SiC and C peaks are shown. The green curve represents the spectrum of the sample, the blue curve represents the phase theoretical peaks. The red curve is the deviation curve.

Table 3. Errors between calculated and estimated values for the phases SiO_2 and C. All the values are mass% of the overall amount of the reacted crucible.

sample	qzA lumps 1:2	qzB lumps 1:2	qzB pellets 1:2	qzB pellets 1:2	qzA pellets 1:1
Phase	SiO_2	SiO_2	C	C	SiO_2
Calcul. value	1.1%	2.8%	72%	74.7%	2.3%
Meas. value	1.6%	4.1%	74.5%	73.9%	0
Technique	weighing	weighing	Leco C&S	Leco frac. C	epma
Error	0.57%	1.2%	2.8%	0.8%	1.7%

respectively for “qzA lumps 1:2” and “qzB lumps 1:2” while 1 g SiO_2 and 2.6 g SiO_2 have been measured respectively for “qzA lumps 1:2” and “qzB lumps 1:2”. The error calculated on the total weight of the reacted crucible is +0.57% for the sample “qzA lumps 1:2” and +1.23% for “qzB lumps 1:2”.

In the third case, “qzB pellets 1:2”, the total elemental carbon content in mass% has been measured by the Leco technique and compared with the value estimated from the phase mass balance. The total elemental carbon includes both C and SiC phase. Both Leco Carbon run on RC-412 and Leco Carbon & Sulphur run on a CS-444 have been used. The measurements were performed by Leco Sweden. The errors are +2.79% and -0.81% for Leco C&S and Leco Carbon respectively.

Two experiments “qzA pellets 1:1” with similar weight loss have been made. The first sample was analyzed in EPMA and no silica has been found. The second sample was analyzed quantitatively. The calculated silica content was 1.24 g corresponding to 1.71 mass%.

Calculated and estimated values as well as the errors between them are shown in **Table 3**. The method is intended to give a realistic quantification of the phases present in a mixture of SiO_2 , SiC, Si and C with absolute errors below 3%. The accuracy of the measurement for each phase depends on its relative amount in the mixture, since the error is calculated on the overall weight of the sample.

4. Conclusion

Conclusions that can be drawn from the work are:

- A quantitative analytical method for the estimation of solid phases co-present in a mixture of SiO₂, SiC, Si and C has been proposed.
- The method combines XRD and XRF analyses with elemental mass balances.
- Absolute errors below 3 mass% are reported.
- The method is not based on thermodynamic assumptions.
- The method allows calculation of a total phase mass balance in silicon producing experiments. The method can be used to study the kinetics of reactions.
- The method requires crushing of the sample to μm size.
- The present quantitative analytical technique appears to be a valid method for the comparison of samples made of mixture of phases and a good tool for the study of kinetics and reacted products.

Acknowledgments

The authors acknowledge Bjørn Eske Sørensen, Kjell Kvam, Morten Raaness, Torill Sørlokke and Mikael Lund for the analyses and interesting discussions.

REFERENCES

- 1) M. W. Jr. Chase, C. A. Davies, J. R. Downey, D. J. Frurip, R. A. McDonald and A. N. Syverud: JANAF Thermochemical Tables (Third Edition), *J. Phys. Chem. Ref. Data*, **14**, Suppl. 1, (1985), 1.
- 2) J. Kr. Tuset and O. Raaness: Electric Furnace Proc., Electric Furnace Division of the Iron and Steel Society (AIME), Warrendale, PA, (1976), 101.
- 3) C. Y. Chen, C. I. Lin and S. H. Chen: *Br. Ceram. Trans.*, **99** (2000), 57.
- 4) A. Agarwal and U. Pa: *Metall. Trans. B*, **30B** (1998), 295.
- 5) M. Nagamori, I. Malinsky and A. Claveau: *Metall. Trans. B*, **17B** (1986), 503.
- 6) M. Loubser and S. Verryn: *SAJG*, **111** (2008), 229.
- 7) Kirk-Othmer Encyclopedia of Chemical Technology. vol. 22, Wiley-Interscience, (2007), 525.
- 8) M. B. Müller, S. E. Olsen and J. Kr. Tuset: *Scand. J. Metall.*, **1** (1972), 145.
- 9) A. Schei, J. K. Tuset and H. Tveit: Production of High Silicon Alloys, Tapir forlag, Trondheim, (1998), 65.
- 10) Dijen FKv: *J. Eur. Ceram. Soc.*, **7** (1991), 177.
- 11) S.-H. Chen and C.-I. Lin: *J. Mater. Sci. Lett.*, **17** (1998), 657.

Article II

Study of Pellets and Lumps as Raw Materials in Silicon Production from Quartz and Silicon Carbide

E. DAL MARTELLO, G. TRANELL, S. GAAL, O.S. RAANESS, K. TANG,
and L. ARNBERG

The use of high-purity carbon and quartz raw materials reduces the need for comprehensive refining steps after the silicon has been produced carbothermally in the electric reduction furnace. The current work aims at comparing the reaction mechanisms and kinetics occurring in the inner part of the reduction furnace when pellets or lumpy charge is used, as well as the effect of the raw material mix. Laboratory-scale carbothermic reduction experiments have been carried out in an induction furnace. High-purity silicon carbide and two different high-purity hydrothermal quartzes were charged as raw materials at different molar ratios. The charge was in the form of lumps (size, 2–5 mm) or as powder (size, 10–20 μm), mixed and agglomerated as pellets (size, 1–3 mm) and reacted at 2273 K (2000 °C). The thermal properties of the quartzes were measured also by heating a small piece of quartz in CO atmosphere. The investigated quartzes have different reactivity in reducing atmosphere. The carbothermal reduction experiments show differences in the reacted charge between pellets and lumps as charge material. Solid–gas reactions take place from the inside of the pellets porosity, whereas reactions in lumps occur topochemically. Silicon in pellets is produced mainly in the rim zone. Larger volumes of silicon have been found when using lumpy charge. More SiO is produced when using pellets than for lumpy SiO₂ for the same molar ratio and heating conditions. The two SiC polytypes used in the carbothermal reduction experiments as carbon reductants presented different reactivity.

DOI: 10.1007/s11663-011-9529-y

© The Author(s) 2011. This article is published with open access at Springerlink.com

I. INTRODUCTION

METALLURGICAL silicon is produced by the reduction of silica in an electric arc furnace by means of carbonaceous materials. As alternatives to the dominating Siemens chemical route, two main direct metallurgical routes have been established for the production of low-cost solar grade silicon in Norway: the Elkem route (developed by Elkem Solar^[1]) and the Solsilc route (developed by Fesil Sunergy^[2]). The Solsilc route uses high-purity raw materials in form of pellets. It aims at “direct” high-purity silicon production, avoiding several downstream refining steps. Elkem produces a high-grade MG-Si, which is subsequently refined using pyrometallurgical and hydrometallurgical processes.

For both routes, the raw materials play an important role for the optimization of the process. The main quartz specifications are the purity chemistry, lump size, lump mechanical and thermal strength, and softening properties. The absence of fines (particles less than 2 mm in size) and a softening temperature close to the quartz melting point are desirable to maintain a high gas

permeability in the furnace burden.^[3] Common impurities in quartz, like Na, K, Al, and Fe, come from minerals like mica and feldspar. Hydrothermal quartz and pegmatite core are the purest among the silica sources.

These can be purified even more by means of mineral liberation, separations, and acid treatments.^[4,5] The purification processes must be carried out with fine particles (in the range of micrometers). To charge these materials in an electric arc furnace, agglomeration (pellets or briquettes) is necessary.

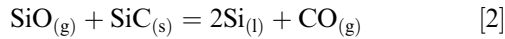
SiO reactivity^[6] and chemistry are the most important distinguishing properties of carbon. High-reactivity carbon materials are desirable as reductants, because they preserve matter and energy in the process by rapidly reacting with energy-rich SiO(g). The SiO reactivity of coal based reductants depends mainly on the ranks of the coals, on its petrographic properties,^[7] on the carbon particle size and on the SiO diffusion in pores.^[8] Coal and charcoal contain both B, P, and ash minerals mainly consisting of SiO₂, Fe₂O₃, Al₂O₃, TiO₂, CaO, and MgO. B and P originate from the plants, whereas ash containing oxides derive from clay minerals deposited onto the plant material precursors.^[9] High-purity carbon black is a synthetic carbonaceous powder material produced from pure liquefied natural gas or methane. Low B and P content in the metal produced is necessary because these elements are difficult to remove by directional solidification in the subsequent ingot production of silicon for photovoltaic purposes.

E. DAL MARTELLO, Ph.D. Student, G. TRANELL, Professor, and L. ARNBERG, Research Scientist, are with the NTNU Department of Materials Science and Engineering, 7491 Trondheim, Norway. Contact e-mail: dalmarte@material.ntnu.no S. GAAL, O.S. RAANESS, and K. TANG, Research Scientists, are with the SINTEF Materials and Chemistry, 7465 Trondheim, Norway.

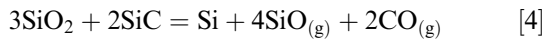
Manuscript submitted February 26, 2011.

Article published online May 20, 2011.

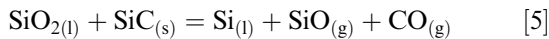
In the submerged arc furnace, silicon and carbon raw materials react under atmospheric pressure over a range temperature of 1573 K to 2273 K (1300 °C to 2000 °C). The upper low temperature part of the furnace is called the outer zone, whereas the hottest part of the furnace the inner zone. There is general agreement about the reactions taking place in the inner zone of the furnace.^[6,10–13] The main reactions in the inner zone are as follows:



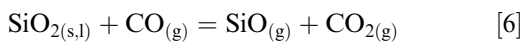
The prevailing gaseous species in the furnace are SiO(g) and CO(g). In the inner crater zone silicon carbide and molten silica react with each other and form SiO(g), CO(g), and Si according to Eqs. [1] and [3]. In the outer zone of the furnace, carbon reacts with the ascending SiO and CO.^[14,15] SiO(g) produced in the inner zone is recovered in the outer zone through condensation to Si and SiO₂ and through the reaction with C to form SiC. Equation [4] is the overall reaction for the inner zone under equilibrium condition at 1 atm (10⁵ Pa).^[6,14,15]



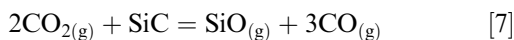
Equation [5] represents the overall reaction for the inner zone under nonequilibrium conditions when $P_{\text{SiO}} = 0.5$ and the temperature is about 2253 K (1980 °C).^[14,16]



SiO is formed at lower temperatures at the silica-gas interface by the reaction^[12,15,17–19]



According to Wiik^[12] and Sahajwalla *et al.*,^[18] SiO can also be generated at the SiC–gas interface at higher temperatures. In absence of free carbon, SiC may take over the role of carbon and react with CO₂(g) to form SiO(g) and CO(g).



Danes *et al.*^[13] carried out a thermodynamic study of the Si-C-O system in an isobaric reactor. The reactor was first filled with inert gas at 1 atm and the pressure was held constant by means of a regulating valve which allowed gas evacuation. When an initial complex of SiC + SiO₂ is heated, SiO + CO pressure increases until it reaches 1 atm (10⁵ Pa). This condition represents the invariant points where three condensed phases (Si, SiC, and SiO₂) are in equilibrium at the specific temperature 2104 K (1811 °C) and gas composition. The reaction [1] runs at constant temperature until either SiC or SiO₂ is consumed. Above 2104 K (1811 °C) depending on the progress of the reactions [2] and [3], Si, SiC + Si, or Si + SiO₂ will not be consumed completely.

Hirasawa^[11] produced silicon in a two-stage reduction process. It was observed that more silicon was formed at 2273 K (2000 °C) than at 2223 K (1950 °C), and that a larger amount of Si was obtained for longer holding time at 2273 K (2000 °C). They found that the reduction of SiO₂ into SiO(g) (reaction [1]) is the reaction rate-controlling step.

Fruehan and Ozturk^[17] and Wiik^[12] studied the rate of formation of SiO(g) by reacting CO(g) with silica (reaction [6]). Experimental observations strongly indicated that the rate of formation of SiO(g) is controlled by chemical kinetics on the silica surface.

SiC occurs in different polytypes. According to the JANAF Thermochemical Tables,^[20] the cubic polytype (β-SiC) is more stable than the hexagonal (α-SiC) at all temperatures, but the difference is so small that is not important in the equilibrium evaluation of the system. Filsinger and Bourrie^[10] and Presser and Nickel^[21] stated that the reactivity of silica with SiC does not depend on the crystal structure of the SiC.

The solid-state reactivity and the surface structure of quartz changes when the surface is activated mechanically.^[22–25] During the mechanical treatment of quartz (grinding or milling), Si-O bonds are broken and highly disordered silica layers (thickness from 20 to 500 nm) are formed on the surface of the quartz grains.^[24] These deviations from ideal lattice are metastable defects that lead to the storage of energy and increase the reactivity of the material. According to Steinike and Tkáčová,^[23] mechanically activated quartz shows an increase in the extent of adsorption and gas diffusion into the disturbed near surface layers. Quartz seems more reactive with CO₂(g) than O₂(g). They also observed that mechanically activated quartz (low temperature form) transforms directly into cristobalite at a temperature of 1473 K (1200 °C), which is lower than the high-temperature quartz-cristobalite transformation at approximately 1673 K (1400 °C). This was confirmed by Balek *et al.*^[24]

Agarwal and Pad^[26] used thermogravimetry to study the kinetics of reactions in pellets, which were made of carbon black and silica. The reaction rate increases by reducing both carbon and silica particle size, but no significant improvement occurs below a critical size of 20 μm. In general, in a powder compact, where the reaction occurs between solids through gaseous intermediates, the possible reaction controlling steps can be surface reactions or diffusion of the gases through the pores or a combination of these. When pellets made of carbon and silica mixture are heated, they react quickly to SiO(g) and CO(g). When ($P_{\text{CO}}/(P_{\text{CO}} + P_{\text{SiO}})$) reaches the chemical equilibrium value, the reaction retards quickly. CO(g) has to diffuse out of the pellet for subsequent reaction taking place. Agarwal and Pad state that pellets porosity leads to higher rates of diffusions of CO(g) and SiO(g) from pellets and, therefore, an increase in reaction rate for the reduction of SiO₂ to SiO(g).

Jensen^[27] recorded the reactions taking place in the crater zone of a 50-kW single electrode pilot scale furnace when lumpy charge was used. From the images, the crater appears complex and dynamic. SiO₂ reacts with SiC and forms Si(l), SiO(g), and CO. The cavity

expands as the reaction proceeds. The expansion of the cavity is balanced by SiO_2 and SiC entering slowly the crater. Melted viscous quartz enters in the crater zone slowly. SiC is still a solid phase and is covered by a thin Si layer. A Si bath is present on the bottom; SiC pieces and melted quartz float into it. When quartz enters in contact with SiC , it reacts violently starting bubbling and SiO(g) is produced according to reaction [1]. When SiC enters in the crater zone it disappears fast according to reaction [2]. When Si and SiO_2 enter in contact, SiO_2 starts bubbling and the reactants quickly disappear according to reaction [3].

Although there have been some theoretical suggestions^[13,15] and experimental attempts^[11,12,17,28] to produce silicon on small scale, no experiment has successfully reproduced the inner zone environment of the industrial furnace. There have also been investigations on the reactivity of lumpy silica^[12,17,28] and pellets.^[26] However, these studies were not performed under the conditions of silicon production and did not attempt to compare the reaction mechanisms and kinetics of the same raw materials used either as lumpy or pellet charge.

The aim of the present investigation was therefore:

- To develop a small-scale experimental setup that can adequately simulate the hot zone of the industrial silicon production furnace
- To study the mechanisms and kinetics of the reactions between quartz and SiC when the two compounds are present as fine powder in pellets or as lumps in different charge mixes

II. MATERIALS AND METHODS

A. Materials

The charge materials were in the form of lumps or pellets. Two high-purity hydrothermal quartzes, denoted quartz A and quartz B, and one source of high-purity SiC have been used as charge materials. Quartz A has been used previously for production of SoG-Si,

whereas the second quartz type, quartz B, comes from another deposit showing promise as raw material for SoG-Si production. The quartz structures were investigated by optical microscopy. Micrographs of the samples are shown in Figure 1. Quartz A, Figure 1(a), has big grains of 3–4 mm size and plenty of fluid inclusions. The square shape and the size of the grains indicate that the quartz has a geological history of metamorphism without strain. The grain boundaries have been investigated under fluorescent microscopy and appear to be relatively dense. Quartz B, Figure 1(b), is characterized by smaller grains and less fluid inclusions. The size of the grains and the interlocked grain boundaries indicate that this quartz has been subjected to recrystallization, strain, and distortion processes. The grain boundaries are open and interconnected. The SiC used as charge is a mixture of hexagonal (6H: SiC) and rhombohedral (15R: SiC) polytypes; no cubic SiC (3C: SiC) is present. The number indicates the number of layers in the stacking sequence, the letter the class: H, R, C stands for hexagonal, rhombohedral, and cubic, respectively. According to another designation, hexagonal and rhombohedral polytypes can be denoted as α type, whereas cubic polytype as β type.^[29]

Lumps of size 3–5 mm and pellets of 1–2 mm diameter were used. The total weight of the charge was 25 g when pellets were used and 18 g for the case of lumpy charge. Pellets consist of a mixture of quartz and silicon carbide powder. The powder was produced by milling the quartz up to 20 μm and the SiC up to 10 μm size (the values represent the median). The size was chosen following the study by Agarwal and Pal.^[26] The two components of the mixture, SiC and SiO_2 , were first dry blended together and then delivered into a pelletizing plate (22 cm diameter and 24 cm rim on its outer circumference). Simultaneously with the feeding of the two-component mixture into the pelletizing plate, demineralized water was supplied to enable the formation of micro pellets (1–2 mm diameter). No binding agents have been used. Because pellets contain water, the charge was dried in a graphite crucible at 353 K (80 °C) for 10 hours prior to the experiments.

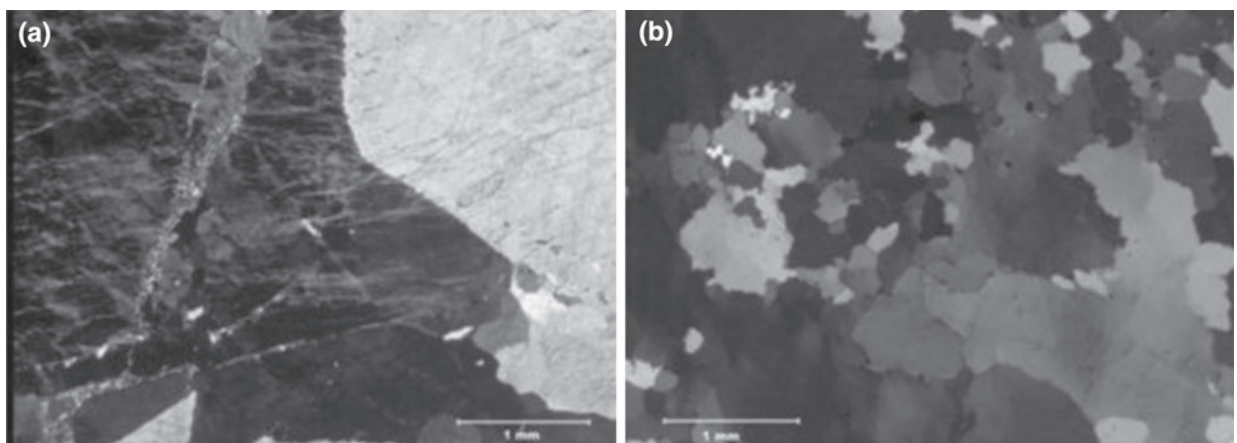


Fig. 1—Micrographs of quartz A (a) and quartz B (b) in cross-polarized light.

B. Experimental Setup and Procedure

The following two types of experiments were carried out:

- Carbothermic reduction experiments, where mixtures of SiC and SiO₂ in the form of pellets or lumps were used as charge materials, for the purpose of studying and comparing reaction mechanisms
- *In situ* melting experiments on small silica pieces, to study their thermal properties

The carbothermic reduction experiments were carried out in a small-scale 6-kW induction furnace setup. Two high-purity graphite crucibles (7 cm in diameter and 15 cm in height) were filled with charge (lumps or pellets). They were then fitted in a bigger graphite crucible as depicted in Figure 2. This configuration allowed running two experiments at the same time under the same conditions. Next, two different quartz sources were run at the same time. Similar to the experiments by Filsinger and Bourrie^[10] and Wiik,^[12] the crucibles were closed with a loose-fit vented lid to create a SiO-CO atmosphere necessary for the silicon production reaction. The graphite crucible has the advantage to withstand high temperatures, to be available in high purity even if it reacts with SiO(g), and to form SiC and Si; the amount of SiC and Si formed can be quantified.^[30]

In an industrial electric furnace, the charge follows different paths in its decent through the furnace, each of the paths with a different retention time. The shortest time from when the raw material is charged until it reaches the crater in an industrial furnace is typically 1–2 hours.^[3] A heating profile 80 minutes long was chosen to be representative to the shortest retention time^[3] and to reproduce previous silicon production experiments.^[11] The heating profile is shown in Figure 3. The charge was heated to 2073 K (1800 °C) at 90 K/min, then from 2073 K to 2273 K (1800 °C to 2000 °C) at 5 K/min, and then the temperature was kept constant at 2273 K (2000 °C) for 20 min. After the

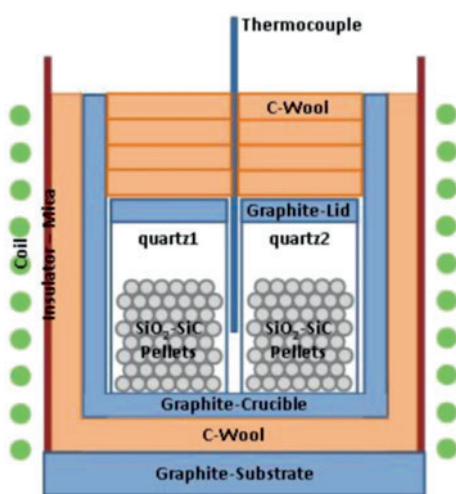


Fig. 2—Experimental setup of carbothermic reduction experiments in an induction furnace. In the figure: pellets as charge material.

experiments, the crucible was cooled rapidly (approximately 100 K/min). Type C tungsten-rhenium thermocouples were placed in the holding crucible between the two reaction crucibles. The temperature outside the crucibles was assumed to be the same as inside the crucible. New thermocouples were used for each experiment because they degraded fast in the high-temperature and SiO/CO atmosphere.

A reducing atmosphere was maintained during the whole experiment. The furnace was first evacuated: The calculated oxygen content after evacuation was $\sim 1.2 \times 10^{-6}$ moles O₂. The furnace was subsequently filled with argon 5.0 purity at 5.8 mbar (580 Pa): The oxygen content carried by the argon filling is $\sim 4 \times 10^{-5}$ moles O₂. The oxygen coming from the crucible is assumed negligible because the crucible was preheated to 373 K (100 °C) overnight. Leakages were measured in a time interval of 10 hours and were found to be negligible for the time needed by the experiment: 0.003 mbar (0.3 Pa) during the argon filling and 0.0025 mbar (0.25 Pa) during the experiment. At the beginning of each experiment, the chamber was filled to approximately 0.75 atm (75000 Pa) with argon. During heating the pressure inside the chamber increased. The total pressure in the chamber reached approximately 1 atm (10⁵ Pa) at 2273 K (2000 °C).

The experiments were designed to study three factors during eight runs. The eight-run design was constructed with a full factor standard table of signs (Table I) for varying quartz type, SiO₂ to SiC molar ratio, and charge type.

The total weight of the charge mix was maintained constant for all the experiments; 25 g and 18 g have been used for pellets and lumpy charge, respectively. The weight difference is caused by the pelletizing procedure. The pellets were weighed once in the crucible and once dried, and it was not possible to predict the amount of water adsorbed during the pelletizing procedure. Two molar ratios have been investigated. The molar ratio of SiO₂/SiC = 1/2 refers to the stoichiometry of reactions [1] and [2]. A molar ratio of 1:1 refers to the stoichiometric overall reaction taking place in the inner zone proposed by Schei *et al.*^[14] and Müller.^[16] It was decided to start the experiment without liquid Si bath on the bottom to focus on the reactions between SiC and SiO₂.

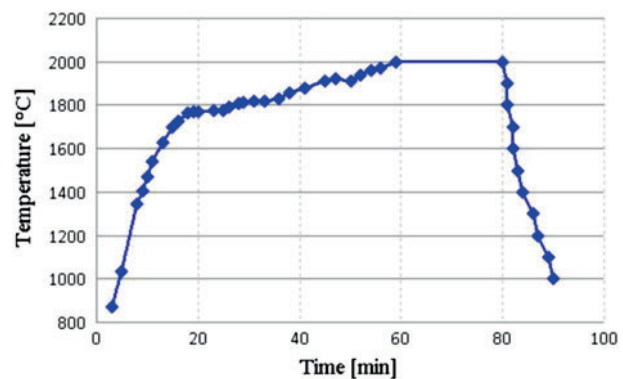


Fig. 3—Heating profile for the carbothermic reduction experiments.

Table I. Experimental Variables in the Carbothermic Reduction Experiments: Quartz Source, Charge Size, and SiO₂:SiC Molar Ratio

Quartz	A	B	A	B	A	B	A	B
Charge size	Lumps	Lumps	Lumps	Lumps	Pellets	Pellets	Pellets	Pellets
Molar ratio	1:2	1:2	1:1	1:1	1:2	1:2	1:1	1:1

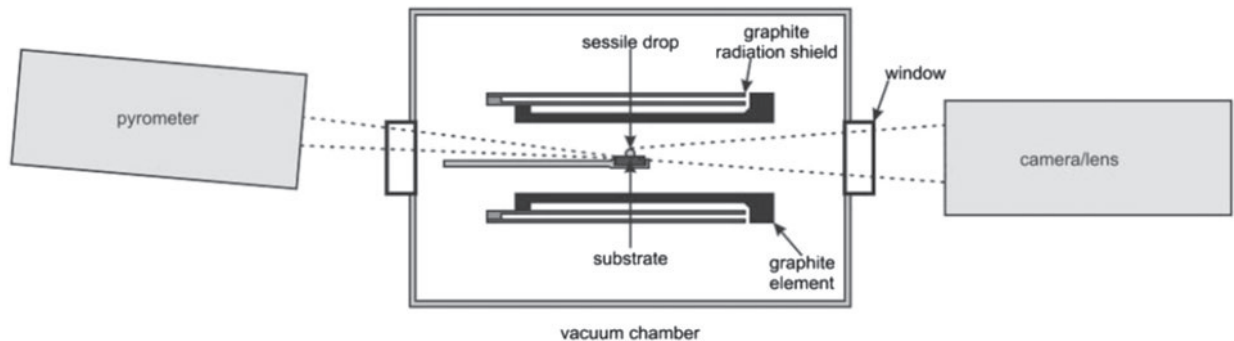


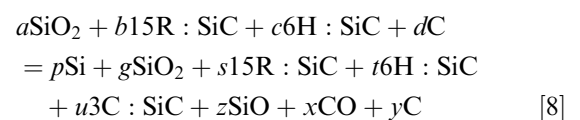
Fig. 4—Experiment in a sessile drop furnace: The furnace records high-temperature properties of quartz. The sample is placed on a substrate and heated. A camera records the sample and a pyrometer measures the temperature of the sample surface during heating.

The second type of experiments aimed at studying the high-temperature properties of lumpy silica. The experiments were run in a sessile drop setup shown in Figure 4. This setup allows us to record high-temperature properties of samples placed on substrate when both atmosphere and heating rates are controlled. The silica samples were placed on a substrate and heated. A camera placed in one end outside the furnace records the sample during heating by taking a picture every second. From this image, the melting temperature and the volume expansion can be estimated. Silica cylindrical samples ($\phi = 3$ mm; $h = 3$ mm) have been investigated. Cylindrical samples and drill cores from a 3-mm-thick plate cut out of the original quartz sample with a diamond saw were used for these experiments. Seven samples of quartz A and 11 samples of quartz B have been studied. The experiments were run in CO atmosphere and reaction [6] is expected to take place. Both the melting point and the reactivity, *i.e.*, the SiO production, of the quartz with CO(g) have been measured. The samples were placed on a nonreactive glassy carbon substrate and heated to 1173 K (900 °C) in approximately 3 minutes. From 1173 K to 1473 K (900 °C to 1200 °C), the heating rate was set to 100 K/min, and from 1473 K to 2273 K (1200 °C to 2000 °C) was set to 20 K/min. The temperature was measured by a pyrometer calibrated against the melting point of iron. Previously, similar experiments have been performed by Andersen^[28] in CO and Ar atmosphere using a similar heating rate.

C. Method for Analysis

The reaction products of the carbothermic Si production experiments were analyzed both qualitatively and quantitatively. The samples were embedded in epoxy and their microstructure studied in JEOL JXA-8500F electron probe microanalyzer (EPMA) (JEOL Ltd.,

Peabody, CA). Each experiment was repeated three times when lumps were used and two times when pellets were used. The experiments with pellets were repeated only twice because they showed little variability in the weight losses. The representative samples that showed weight losses close to the average value for each experimental condition were analyzed quantitatively. The crucibles and reacted charges were crushed together to a fine powder with 50- μ m upper size by means of a tungsten carbide vibratory disk mill and analyzed by X-ray diffraction (XRD) and X-ray fluorescent (XRF). D8 Advance XRD (Bruker, Bruker AXS Nordic AB, Solna, Sweden) generator, BRUKER-EVA qualitative, BRUKER-TOPAS quantitative interpreter program, and XRF BRUKER S8 Tiger 4kW X-ray spectrometer have been used.^[31] XRF uses a semiquantitative method to estimate the weight percentage of Si, and it does not detect elements such as C and O. XRD quantifies crystalline phases and all their polymorphs. The combination of XRF and XRD techniques make them a valuable tool for quantitative phase analysis.^[30] The overall mass balance is presented in Eq. [8]. The phases to the left are input charge material and their amount has been analyzed. The phases to the right are output products and their amount is unknown. C represents the graphite in the crucible; it has to be included in the mass balance because it participates in the reaction with SiO(g).



Experiments in the sessile drop furnace aimed at measuring the temperature of melting and the quartz weight losses (as SiO) in CO atmosphere. It was possible to calculate the weight losses by weighing the silica sample before and after the experiments. The reaction

rate was determined in terms of SiO losses. The temperature of melting was determined by the moment the quartz became glassy. When the quartz starts melting, voids are sealed; there is no more light diffraction and the sample turns transparent and glassy. This valid method is used to compare the melting properties of different quartzes, but the melting temperature must not be considered an absolute value because it is influenced by the sample size and by the heating rate. In an industrial furnace, the large quartz lumps subjected to the highest possible heating rate do not usually soften before reaching the hot inner crater zone of the furnace.^[28]

III. RESULTS

A. Silicon Production Experiments

The carbothermic reduction experiments simulate a complicated system involving reactions between solid,

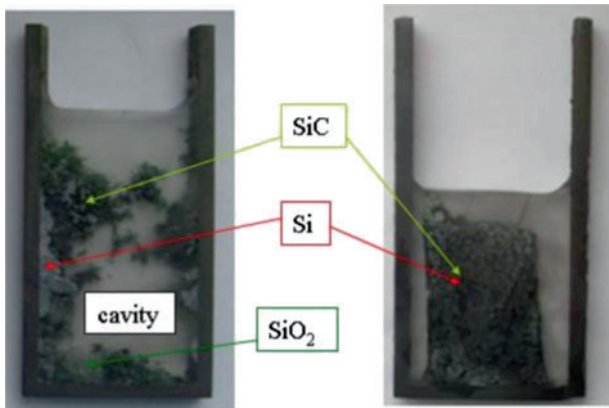


Fig. 5—Reacted charge for different charge size and molar ratio $\text{SiO}_2:\text{SiC} = 1:1$. On the left is lumps, and on the right is reacted pellets.

liquid, and gaseous phases. Because the duration of the experiment is short, these reactions might not reach equilibrium but the experiments are instead intended to represent the relative rates of the predominant reactions.

Non-reacted quartz, silicon carbide and silicon phases have been found in the crucible after experiments. Figure 5 shows the product morphology of the reacted crucible for the case of lumps (on the left side) and pellets (on the right side). The cross sections of the reacted crucibles looked similar regardless of the type of quartz and molar ratio used. Reacted lumpy charge is shown in Figure 5 on the left side: the structure is loose, a cavity is present, melted quartz and droplets of silicon are found mainly on the bottom of the crucible. Microscope and XRD investigations showed that non-reacted silica was present only as an amorphous (melted) phase. A cavity and large area of single phase silicon metal were also found. Pellets have a different reaction pattern than lumps. The reacted pellet charge is compacted, porous and has low interaction with the crucible. The pellets have shrunk and Si is found mainly in the bottom of the crucible. It is difficult to recognize the spherical original shape of pellets for the experiments with molar ratio $\text{SiO}_2:\text{SiC} = 1:1$. SiC particles decrease in size from a mean diameter of $9.26 \mu\text{m}$ to approximately $5 \mu\text{m}$.

Figure 6 shows the microstructure of the reacted lumps and reacted pellets for molar ratio $\text{SiO}_2:\text{SiC} = 1:2$. Figure 6(a) is a SEM backscatter image of reacted SiC lumps. Silicon, in light grey, has nucleated on the carbide surface. Figure 6(b) shows the microstructure of the reacted pellets where SiC particles have dark grey and silicon light grey contrast. The original acicular shape of the SiC particles has become round indicating that carbide has reacted to Si, $\text{SiO}(\text{g})$ and $\text{CO}(\text{g})$. In both cases silicon nucleates on the SiC surface without any direct contact with silica, indicating that a solid-solid reaction has not taken place. Almost all of the silica has reacted when pellets have been used. Figure 7 shows a cross-section of the crucible as seen by

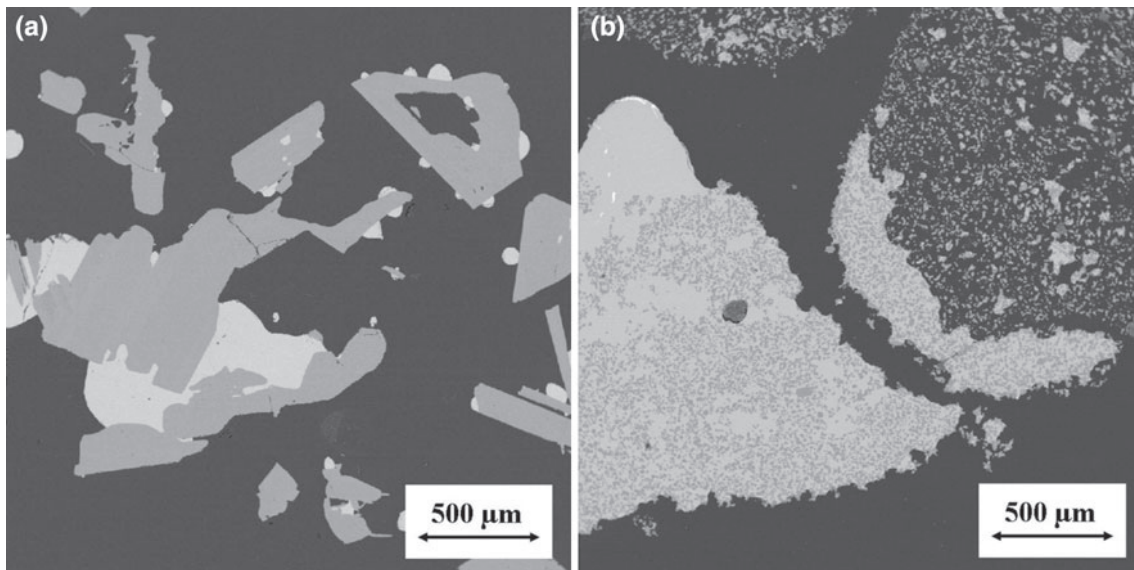


Fig. 6—Backscattering images of reacted charge. (a) Lumps, molar ratio $\text{SiO}_2:\text{SiC} = 1:2$. (b) Pellets, molar ratio $\text{SiO}_2:\text{SiC} = 1:2$.

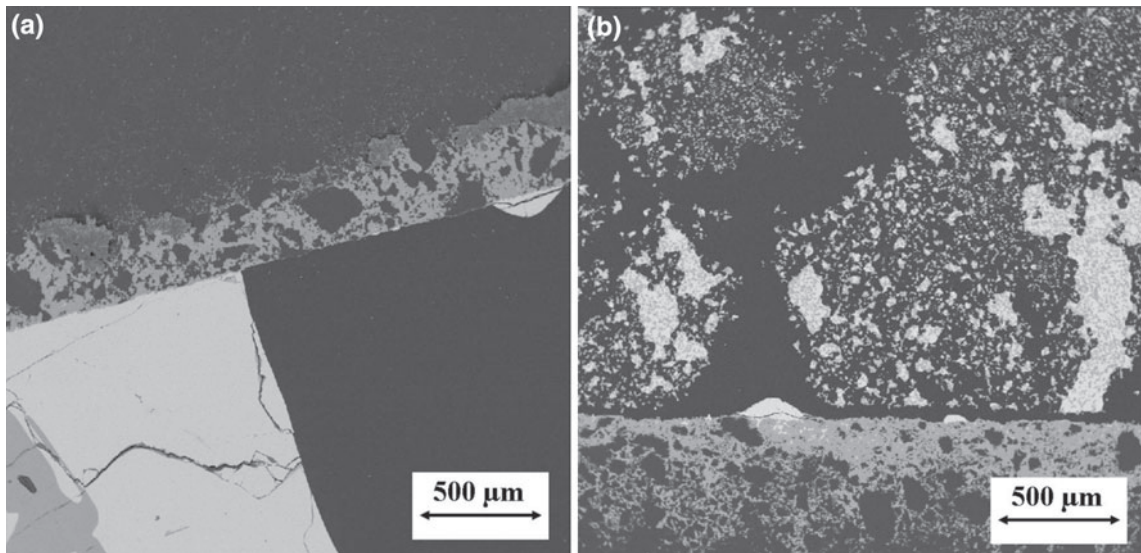


Fig. 7—Backscattering of the reacted crucible: (a) lumps and (b) pellets. The gray rim on the crucible surface is 3C:SiC. Small droplets of silicon on the silicon carbide surface are present in light grey tone. The pictures are at the same magnification.

Table II. Average Total Weight Losses for Different SiO₂:SiC Molar Ratio and Type Charge*

Type	Lumps	Lumps	Pellets	Pellets
Ratio	1:2	1:1	1:2	1:1
Losses	42.1 pct	58.0 pct	44.8 pct	65.8 pct

*The variance in the process is 2.5 pct. It has been calculated over all the experimental results, assuming them to have the same variance.

EPMA. The graphite surface is coated by a thin layer of cubic silicon carbide (3C:SiC), and some tiny droplets of silicon (50 μm size) are also found.

The total weight losses, as total CO(g) and SiO(g), are shown in Table II. The table does not distinguish between the two quartz types because they have almost the same weight losses. High weight losses are caused by the absence of an outer zone for the SiO recovery.^[32] Weight losses are dependent on the raw material ratio according to the stoichiometry, and higher weight losses are found with pellets.

A total phase mass balance between phases in input and output has been calculated and described in Reference 30. The phase mass balance is shown in Figure 8. The mass balance is written in moles of single phases. Graphite from the crucible participates in the reactions, but only the fraction that has actually reacted with the charge is shown in the balance. The graphite reacts to form 3C:SiC. Approximately the same amount of 3C:SiC is formed in all the experiments. More SiO(g) is formed and more SiC has reacted for molar ratio SiO₂:SiC = 1:2. Almost no quartz was left in the experiments with pellets.

An equilibrium phase diagram for different initial molar ratios SiC:SiO₂ and under the condition of total pressure 0.1 atm (10⁴ Pa) is shown in Figure 9. The diagram shows the stable equilibrium phases during heating of a charge mixture for different initial molar

ratios SiC:SiO₂. The equilibrium simulation describes an experimental situation where a mixture of SiO₂-SiC is brought to a certain temperature in a crucible surrounded by inert gas. The system reacts and diffusion in the crucible makes the gas composition equal at the top and in the pores between the particles. Because the equilibrium pressure of the system is higher than the gas outside the crucible, the gas flows out through the lid. The equilibrium calculations refer to a total pressure equal to 0.1 atm (10⁴ Pa) (where P_{CO} + P_{SiO} = 0.1 atm and P_{CO} + P_{SiO} + P_{Ar} = 1 atm). Because argon is inert, only P_{CO} and P_{SiO} influenced the chemical equilibrium. When a mixture of silica and silicon carbide of molar ratio SiO₂:SiC = 1:1 is heated up to 2273 K (2000 °C), the stable solid phase is Si according to the equilibrium phase diagram. If the amount of SiC in the charge mix is increased, both SiC and Si become stable phases. These conditions are represented by the two points marked in Figure 9. Although the experiments are not run at equilibrium conditions, more SiC was left in a charge mix richer in SiC, in agreement with the stable phases predicted by the phase diagram.

Figure 10 shows the total SiO(g) production. The total SiO(g) has three components: SiO(g) lost out from the crucible, denoted SiO_{lost}; SiO(g) that has reacted with the graphite crucible to form 3C:SiC, denoted SiO_{3C:SiC}; and SiO(g) that has reacted with SiC to form Si, denoted SiO_{Si}. These values have been calculated from Eqs. [9] through [11], respectively, and are normalized on the initial amount of silica and silicon carbide. Note that the normalized fraction of SiO(g) that has reacted to produce Si is the silicon yield. Figure 10 shows that more SiO(g) is produced and lost and less silicon is produced when pellets are used as charge material. The parameters *z*, *a*, *b*, *c*, *u*, and *p* are the coefficients in Eq. [8].

$$\text{SiO}_{\text{lost}} = \frac{z}{a + b + c} \quad [9]$$

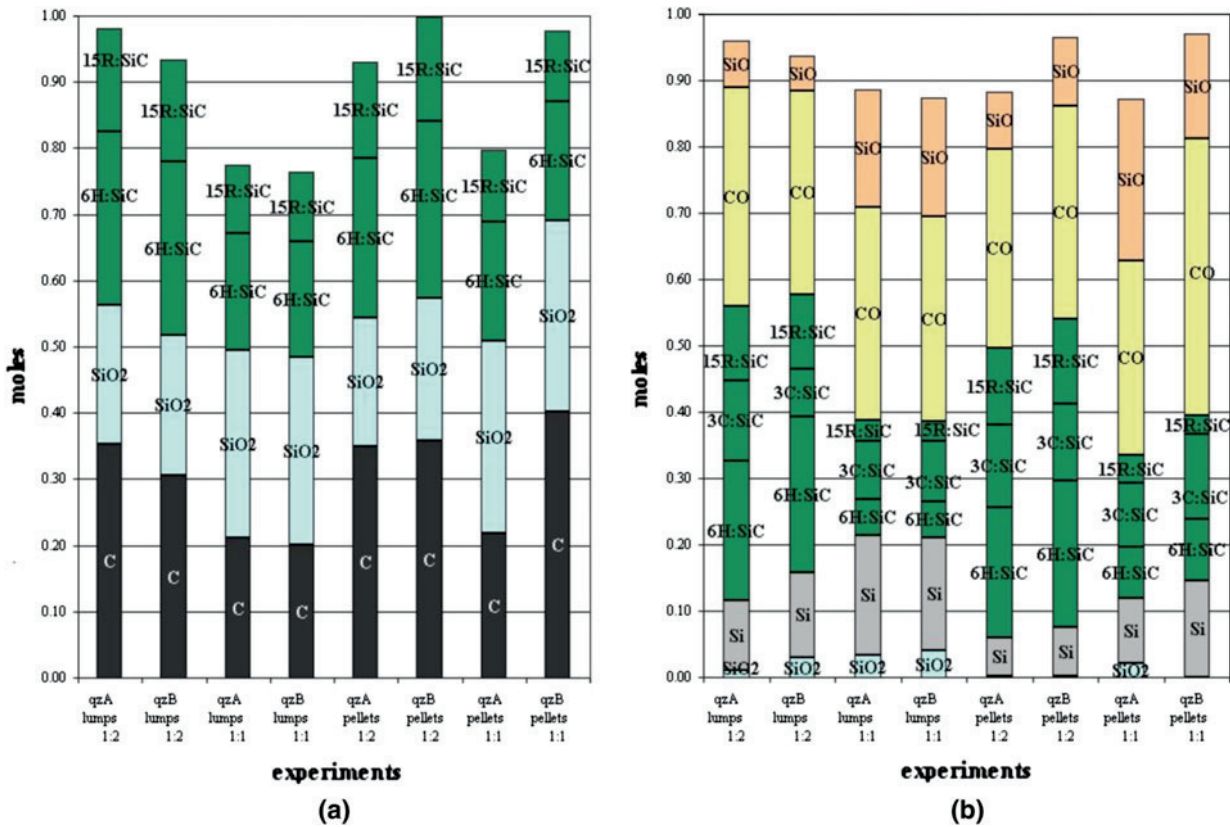


Fig. 8—(a) Reactants (in moles) for each experimental run; (b) Reaction products and nonreacted charge (in moles) for each experimental run.

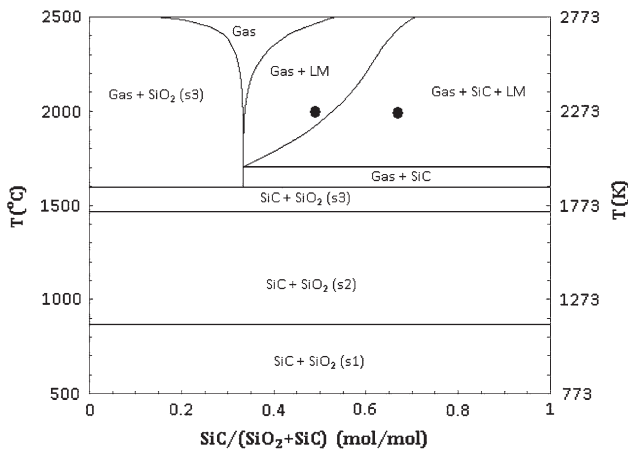


Fig. 9—Equilibrium phase diagram: temperature [°C] vs charge molar ratio. “Gas_{ideal}” refers to the gaseous phase and is mainly composed by SiO and CO, “LM” stands for liquid silicon, and “SiO₂” stands for the four different silica polymorphs occurring during heating.

$$SiO_{3C:SiC} = \frac{u}{a + b + c} \quad [10]$$

$$SiO_{Si} = \frac{p}{a + b + c} \quad [11]$$

The silicon yield is plotted in Figure 11. It has been calculated as the fraction between the number of moles

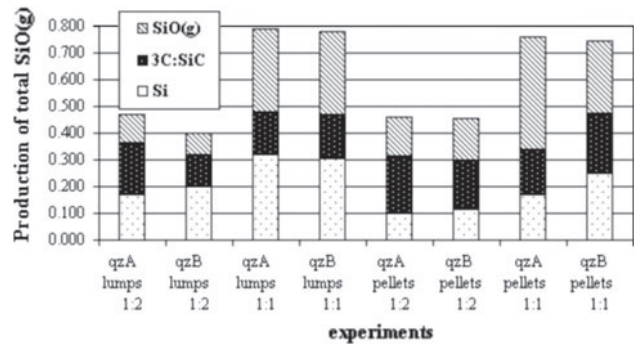


Fig. 10—Three components of the total SiO(g) produced in the experiments: SiO lost out of the crucible, SiO reacted with the graphite crucible to form 3C:SiC, and SiO reacted with SiC to form Si. The values are normalized on the initial amount (in moles) of the SiC and SiO₂ charge.

of Si produced and the number of moles of SiC and SiO₂ in the charge (Eq. [11]). Higher silicon yield is obtained when lumpy charge is used. Low silicon yield is a consequence of the high SiO(g) losses during the experiment.

Figure 12 shows the amount of reacted 6H:SiC and 15R:SiC polymorphs with silica. The values are normalized on the total amount of SiC charge material according to Eqs. [12] and [13]. Generally, 6H:SiC shows higher reactivity to SiO(g) than 15R:SiC with the exception of experiment “qzB lumps 1:2.”

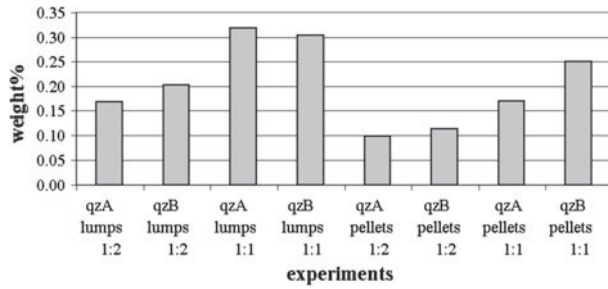


Fig. 11—Si yield for each experimental condition.

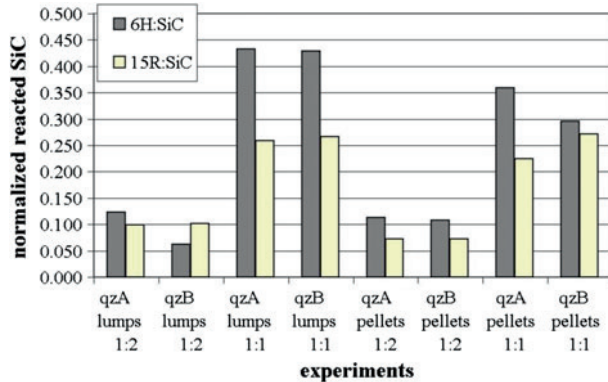


Fig. 12—Moles of reacted 6H:SiC and 15R:SiC polytypes normalized on the moles of SiC input.

$$6\text{H} : \text{SiC}_{\text{reacted}} = \frac{c - t}{b + c} \quad [12]$$

$$15\text{R} : \text{SiC}_{\text{reacted}} = \frac{b - s}{b + c} \quad [13]$$

B. Thermal Properties of Silica

The melting point was defined as the temperature when the silica surface becomes glassy. Quartz A has a melting point of $2053 \text{ K} \pm 18 \text{ K}$ ($1780 \text{ }^\circ\text{C} \pm 18 \text{ }^\circ\text{C}$), whereas quartz B melted at $2092 \text{ K} \pm 19 \text{ K}$ ($1819 \text{ }^\circ\text{C} \pm 19 \text{ }^\circ\text{C}$). It was a challenge to measure the melting temperature for some of the quartz A samples because they did not turn transparent during heating but presented only a whitish appearance. The samples were examined by optical microscopy after the experiment, and it was found that the whitish samples contained larger amount of bubbles. The diffraction of light through these bubbles can explain the whitish appearance of the samples. The experiments were stopped at temperatures between the silica melting temperature and 2273 K ($2000 \text{ }^\circ\text{C}$), and the weight losses were measured. Figure 13 shows weight losses vs time. The weight losses depend on the reactivity of silica in CO atmosphere. According to reaction [6], SiO_2 reacts with $\text{CO}(\text{g})$ and $\text{SiO}(\text{g})$, $\text{CO}_2(\text{g})$ are produced at high P_{CO} . The more $\text{SiO}(\text{g})$ is produced, the larger the weight losses.

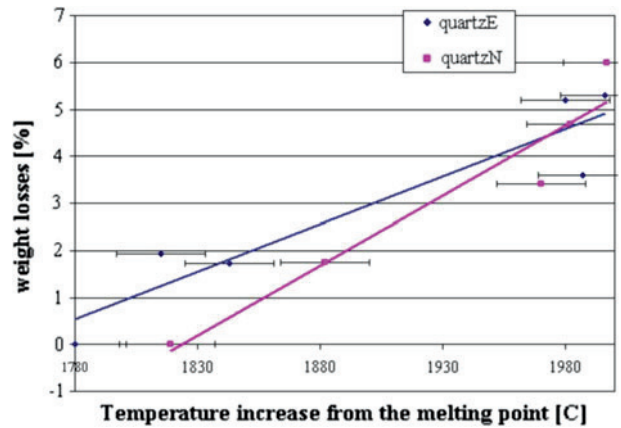


Fig. 13—Silica weight losses [pct] vs temperature $^\circ\text{C}$.

IV. DISCUSSION

A. Difference Between Pellets and Lumps: Reaction Mechanisms

The images of the reacted charge and the calculated $\text{SiO}(\text{g})$ total production (Figures 6, 7, and 10) make it possible to suggest the predominant reactions when pellets or lumps of SiO_2 and SiC are heated up to 2273 K ($2000 \text{ }^\circ\text{C}$).

At the beginning, $\text{SiO}(\text{g})$ is produced and reacts with the graphite crucible to form $3\text{C}:\text{SiC}$. As the SiC layer on the inner surface of the crucible builds up, the reaction slows down and the SiC forming reaction stops. A slightly greater amount of $3\text{C}:\text{SiC}$ has been formed with pellet charge probably because of the larger production of $\text{SiO}(\text{g})$. Three reactions involving silica and silicon carbide take place: reaction [1] between $\text{SiO}_2(\text{l},\text{s})$ and $\text{SiC}(\text{s})$, reaction [2] between $\text{SiO}(\text{g})$ and $\text{SiC}(\text{s})$, and reaction [3] between $\text{SiO}_2(\text{l})$ and $\text{Si}(\text{l})$.

1. Reaction(1) between SiO_2 and SiC

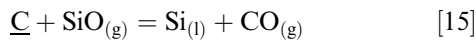
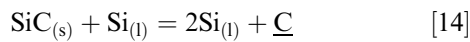
The reaction is expected to be faster in presence of molten SiO_2 ^[28,33] and for the case of pellets because of the larger surface area available and closer contact between the reactants in the charge mixture. More SiO_2 is expected to react with SiC in pellets for the same reason. This was confirmed by the calculated mass balance. The estimated nonreacted silica was on average 2 wt pct for the case of lumpy charge and on average only 0.18 wt pct for the case of pellets.

2. Reaction (2) between SiO and SiC

As the P_{SiO} increases, the reaction between $\text{SiO}(\text{g})$ and SiC takes place and Si is produced. The pellets and the SiC particles inside the pellets decreased in size as the reduction proceeds. The silicon production reaction when pellets are used takes place inside the pellets and mostly in the rim zone (Figure 6(b)). The more favorable Si formation at pellets rim might be pressure related. Larger zones of silicon occur with lumpy charge. This is probably because of several Si -forming reactions that occur simultaneously in the lumpy charge. Si forms on the SiC surface in SiC pores and concave surfaces according to reaction [2]. Once the silicon has covered

the available SiC surface, instead of reaction [2], a coupled reaction between SiC and Si(l) and between dissolved carbon in Si(l) and SiO may take place. SiC grows inward both the SiC particle and the molten silica. SiC at higher temperatures may dissolve in Si. Dissolved carbon diffuses to the surface of the Si droplets, reacts with SiO(g), and forms Si. The carbon solubility in liquid silicon at 2073 K and 2273 K (1800 °C and 2000 °C) is 500 ppmw and 2100 ppmw, respectively.^[34] The proposed reactions are described by Eqs. [14] and [15].

When the Si droplets become coarser, the Si-SiC surface tension can no longer sustain the liquid Si droplets, and the Si starts dripping toward the bottom of the crucible. Free SiC surface is available for further reactions, SiC particles are consumed and decrease in size as the reduction proceeds. Another explanation for the larger amount of silicon formed with lumps may be that in lumps more non-reacted silica is available to react to Si before reaching the chemical equilibrium.



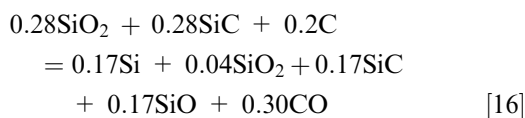
3. Reaction (3) between SiO₂ and Si

When lumpy charge was used, melted quartz and silicon were found on the bottom of the crucibles. The reaction between SiO₂(l) and Si(l) is expected to take place at high temperatures after some silicon has been produced. Because for the case of pellets, no quartz was left after the experiments and, as mentioned previously, SiO₂ seems to react quickly to SiO(g) before any Si(l) is produced, the reaction between SiO₂ and Si(l) seems to be negligible in the pellet charge.

B. Difference Between Pellets and Lumps: SiO Production

More SiO(g) has been produced with pellets. The particles in the pellets are in close contact so that the diffusion of CO₂ from the SiO₂ particle to the SiC particle and the diffusion of CO from the SiC particle to the SiO₂ particles are enhanced. Moreover, because the quartz powder has been milled, the silica surface is mechanically activated, which leads to an increase in the extent of adsorption and gas diffusion into the disturbed near surface layers.^[22–25]

The experiments aim at reproducing the hot inner zone of a furnace. From the total mass balance, it is possible to write the overall reaction representative of the inner crater zone. The overall reaction for the experimental condition “lumps qzN 1:1” is given in Eq. [16]. The overall reaction for the eight representative experiments differ from reaction [4]; the calculated equilibrium reaction of the inner zone at 1 atm (10⁵ Pa) and at 2273 K (2000 °C).



The reactions depart from equilibrium and the SiO(g) content of the gas in the crucible is determined by the reaction kinetics. The parameter *s* is defined in Eq. [17] as the equilibrium fraction of SiO(g) that leaves the silicon-producing zone. The parameter *s* is variable but is here assumed constant for certain combination of raw materials and operation conditions.^[14,35] The lower the *s* value, the less SiO(g) leaves the silicon-producing zone and the slower the reaction rate.

$$s = \frac{P_{\text{SiO}}}{P_{\text{SiO}} + P_{\text{CO}}} \quad [17]$$

The *s* value can be estimated from the CO and SiO coefficients in the overall reaction in Eq. [8]. During the initial heating, low-temperature reactions occur and the partial pressure of CO(g) and SiO(g) are different from the ones occurring at higher temperatures. For this reason, the amount of CO(g) and SiO(g) calculated from the mass balance are not representative of the inner zone and should not be used to estimate the *s* value. Two tentative *s* values have been calculated and are shown in Figure 14. The figure refers to the experiments run with quartz B. The first calculation uses the total moles of CO(g) and SiO(g) calculated from the mass balance. This value is expected to be low because it includes the fraction of SiO(g) and CO(g) produced during the initial heating at low P_{SiO} atmosphere. The second calculation uses the same value of SiO(g) but decreases CO(g) of an amount corresponding to the production of 3C:SiC in the crucible. The two *s* values have the same trend: *s* is dependent on the mix ratio and charge size, and *s* increases by increasing the amount of SiO₂ in the charge mix. The dependence on the reactant ratio is even stronger for the case of lumps. A possible reason might be that Si reacts with the remaining SiO₂ to form SiO(g) when lumpy charge is used.

With pellets materials, there is a bigger amount of SiO(g) leaving the high-temperature zone. In industrial practice, the SiO(g) is recovered in the upper part of the furnace by reaction with carbon that is a strongly heat-consuming reaction. Then, the gas is cooled and the

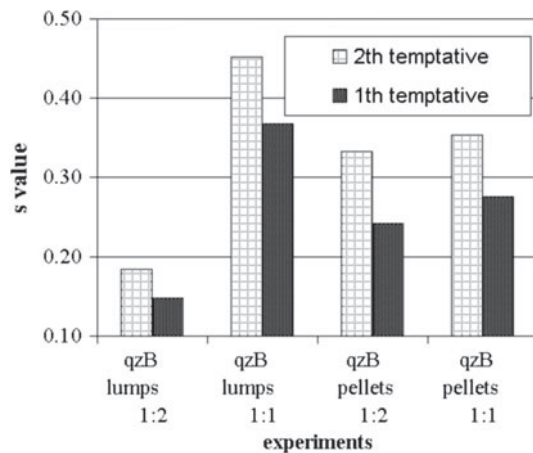


Fig. 14—Calculated *s* value for the same quartz type and different charge mix and size.

heat-producing condensation reaction takes place. The produced heat will raise the temperature of the charge, and again, the strongly heat consuming reaction takes place. However, the price of the increased silicon recovery is a high load of condensed SiO that may obstruct the gas flow and make stoking difficult and inefficient.^[15]

C. Effect of Raw Material Mixtures

The reactivity of different quartz and silicon carbide sources has been studied. The SiC charge material is a mixture of hexagonal and rhombohedral polytypes. In contrast with Filsinger and Bourrie^[10] and Presser and Nickel,^[21] the two polytypes show different reactivity with silica (Figure 12). Hexagonal silicon carbide 6H:SiC is more reactive than the rhombohedral 15R:SiC for all the experiments. All polytypes have the same distance between neighboring Si or C atoms, and same distance of the C atom to each of the Si atoms. The only difference between them is the degree of hexagonality, which is defined as the ratio of number of atoms at hexagonal sites to the total number of atoms per unit cell.^[36] 6H:SiC has degree of hexagonality 0.33, whereas 15R:SiC has a 0.4 degree of hexagonality. The degree of hexagonality seems to influence the SiC reactivity: The lower the degree of hexagonality, the better the reactivity.

The reactivity of different hydrothermal vein quartzes has been studied in two experimental setups: the sessile drop furnace and induction furnace. The reactivity of SiO₂ is measured as the amount of SiO(g) produced. Silica reacts with CO(g) and it forms SiO(g) and CO₂(g), both in presence of high and low P_{SiO}. In particular, on the one hand, the experiments in the sessile drop furnace were run in CO(g) atmosphere and were significant for reaction [6] occurring at high P_{CO} pressure. On the other hand, the reactions in the induction furnace take place both at high and low P_{CO} and the total amount of SiO(g) formed is also caused by the reaction of SiC with CO₂(g). Because the same SiC has been used for all the experiments, we can assume SiO₂ as the only source for difference in the amount of SiO(g) produced. The experiments in the sessile drop furnace show higher reactivity for quartz A (Figure 13), which has been confirmed by the carbothermic reduction experiments (Figure 10). This study shows that the reactivity of quartz depends on the silica source used. The higher reaction rate in quartz A might be caused by the larger amount of fluid inclusions. Fluid inclusions contain gaseous and liquid compounds. When the quartz is heated, the fluid inclusions are opened and might induce cracks. The cracks increase the surface available for further reactions.

The two quartz types present different melting points. Quartz A has slightly lower melting point than quartz B. A higher melting point quartz is preferable because softened and melted silica on the upper part of the furnace obstruct the gas flow. Melted quartz A presents larger amount of bubbles than melted quartz B. Quartz A may also be more reactive because of the presence of bubbles that increase the available surface. The

formation of bubbles can be correlated to the presence of fluid inclusions or to the dehydration reaction of mica minerals taking place at calcination temperatures lower than the melting point of silica,^[37] or it may be a result of the production of SiO(g). Microscopy investigation prior to melting revealed a larger amount of microcracks and fluid inclusions in quartz A. Mica was found in both quartz sources.

V. CONCLUSIONS

Experiments reproducing the inner zone of a furnace have been performed in an induction furnace. Silica and silicon carbide have been charged as lumps and pellets for different molar ratio. The reaction behavior of lumps and pellets was studied in terms of qualitative and quantitative analysis of the reacted phases.

The main conclusions that can be drawn from the present work are as follows:

1. The reactions in pellets take place inside the pellets mostly in the rim zone, whereas the reactions in lumps occur on the outside. Larger zones of single-phase silicon have been found when a lumpy charge is used. A cavity is present when lumpy charge is used, whereas for the case of pellets, the reacted charge is porous and compacted.
2. More SiO(g) is produced and almost no quartz is left when pellets are used as charge material for the same molar ratio. Lumps are characterized by a higher silicon yield because of less loss of SiO(g).
3. Different SiC polytypes have been used as charge materials. The polytype with lower degree of hexagonal SiC content has a higher reactivity in terms of reaction rate.
4. Two different hydrothermal vein quartzes have been used as charge materials. The quartz containing more fluid inclusions and more microcracks has lower melting point and better reactivity in terms of reaction rate with SiO(g).
5. The thermal properties and reactivities of the two quartzes have also been investigated in a sessile drop furnace, and the results from investigation done in the silicon production experiments were confirmed.

OPEN ACCESS

This article is distributed under the terms of the Creative Commons Attribution Noncommercial License which permits any noncommercial use, distribution, and reproduction in any medium, provided the original author(s) and source are credited.

REFERENCES

1. M.J. de Wild-Scholten, R. Glockner, J.-O. Odden, G. Halvorsen, and R. Tronstad: *23rd European Photovoltaic Solar Energy Conf.*, Valencia, Spain, 2008.

2. R. Kvande, L. Nygaard, S. Stute, and P.C.P. Bronsveld: *25th European Photovoltaic Solar Energy Conference and Exhibition/Conference on Photovoltaic Energy Conversion*, Valencia, Spain, 2010.
3. K. Aasly: Ph.D. Dissertation, Norwegian University, Trondheim, Norway, 2008.
4. B. Strake, F.W. Schulze, and H.A. Aulich: *Erzmetall*, 1988, vol. 41, p. 126.
5. H.A. Aulich, H.-P. Urbach, F.W. Schulze, and J.G. Grabmaier: *Siemens Forsch.-u. Entwickl.-Ber. Bd.*, 1982, vol. 11, p. 327.
6. J.K. Tuset and O. Raaness: *Electric Furnace Proceedings*, 1976, p. 101.
7. O. Raaness, L. Kolbeinsen, and A. Byberg: *8th International Ferroalloys Congress (INFACON8) Proceedings*, Beijing, China, 1998, p. 116.
8. K. Gjermundsen, O. Raaness, and J. Kr. Tuset: *SINTEF Selskapet for Industriell Og Teknisk Forskning Ved Norges Tekniske Høgskole*, Trondheim, Norway, 1972.
9. P. Motavalli, T. Marler, F. Cruz, and J. McConnell: *Essential Plant Nutrients*, College of Agriculture and Life Sciences, University of Guam, <http://www.cartage.org.lb/en/themes/Sciences/BotanicalSciences/PlantHormones/EssentialPlant/EssentialPlant.htm>.
10. D.H. Filsinger and D.B. Bourrie: *J. Am. Ceram. Soc.*, 1990, vol. 73, p. 1726.
11. M. Hirasawa: *High Temp. Mater. Process*, 2000, vol. 19, p. 281.
12. K. Wiik: *Kinetics of Reactions Between Silica and Carbon*, NTH Universiteti, Trondheim Norway, 1990.
13. F. Danes, E. Saint-Aman, and L. Coudurier: *J. Mater. Sci.*, 1993, vol. 28, pp. 489–95.
14. A. Schei, J.K. Tuset, and H. Tvei: *Production of High Silicon Alloys*, Tapir Forlag, Trondheim Norway, 1998.
15. A. Schei: *Tidsskr. Kjemi Bergv.*, 1967, vol. 27, pp. 152–58.
16. M.B. Müller: *Scand. J. Metall.*, 1972, vol. 1, p. 145.
17. R.J. Fruehan and B. Ozturk: *Metall. Trans. B*, 1985, vol. 16B, p. 801.
18. V. Sahajwalla, C. Wu, R. Khanna, N.S. Chaudhury, and J. Spink: *ISIJ Int.*, 2003, vol. 43, p. 1309.
19. A.W. Weimer, K.J. Nilsen, G.A. Cochran, and R.P. Roach: *AIChE Journal*, 1993, vol. 39, p. 409.
20. M.V. Chase, Jr: *JANAF Thermochemical Tables*, C.A. Davies, J.R. Downey, Jr., D.J. Frurip, R.A. Macdonald, and A. Syverud, eds., Bureau of Standards, Midland, MI, 1985.
21. V. Presser and K.G. Nickel: *Crit. Rev. Solid State Mater. Sci.*, 2008, vol. 33, p. 1.
22. W. Peukert and C. Damn: *Langmuir*, 2009, vol. 25, p. 2264.
23. U. Steinike and K. Tkačová: *J. Mater. Synth. Process.*, 2000, vol. 8, p. 197.
24. V. Balek, J. Fusek, J. Križ, and M. Murat: *Thermochim. Acta*, 1988, vol. 262, p. 209.
25. J.C. Benezet and A. Benhassaine: *Erzmetall*, 1988, vol. 41, p. 126.
26. A. Agarwal and U. Pad: *Metall. Mater. Trans. B*, 1998, vol. 30B, pp. 295–306.
27. R. Jensen: *Gass-stabilisert AG og DL lysbue i Si-metallovn*, NTH Norges Tekniske Høgskole, 1986.
28. V. Andersen: Investigation of Thermal Properties of Quartz for the Silicon Industry Under Reducing Atmosphere, Department of Materials Science and Engineering, NTNU, 2009.
29. N.G. Wright: *Kirk-Othmer Encyclopedia of Chemical Technology*, University of New Castle Upon Tyme, p. 525.
30. E.D. Martello, G. Tranell, O. Raaness, and L. Arnberg: *Combined XRD and XRF Technique for Quantitative Mass Balance of Si Production Experiments*, Norwegian University of Science and Technology, Trondheim, Norway, 2011.
31. Bruker AXS homepage, <http://www.bruker-axs.com>.
32. Y. Sakaguchi, M. Ishizaki, T. Kawahara, M. Fukai, M. Yoshiyagawa, and F. Aratani: *ISIJ Int.*, 1992, vol. 32, p. 643.
33. V. Andersen: Master Thesis, NTNU, Trondheim, Norway, 2010.
34. R.I. Scace and G.A. Slack: *J. Chem. Phys.*, 1958, vol. 30, p. 1551.
35. A. Schei and K. Larsen: *39th Electric Furnace Conference of AIME*. Houston, TX, 1981.
36. A.A. Lebedev: *Am. Inst. Phys.*, 1999, vol. 33, p. 707.
37. B.-Z. Zhu, Y.-L. Sun, and C.-W. Xie: *J. China Coal Soc.*, 2008, p. 1049.

Article III



Electrical fragmentation as a novel route for the refinement of quartz raw materials for trace mineral impurities

E. Dal Martello ^{a,*}, S. Bernardis ^b, R.B. Larsen ^c, G. Tranell ^a, M. Di Sabatino ^a, L. Arnberg ^a

^a NTNU Department of Materials Science and Engineering, 7491 Trondheim, Norway

^b MIT Department of Materials Science and Engineering, Cambridge, MA 02139, United States

^c NTNU Department of Geology and Mineral Resources Engineering, 7491 Trondheim, Norway

ARTICLE INFO

Article history:

Received 4 October 2011

Received in revised form 31 January 2012

Accepted 25 February 2012

Available online 3 March 2012

Keywords:

Comminution

Crushing

Electric fragmentation

Liberation

Magnetic separation

Industrial minerals

ABSTRACT

The availability of a selective liberation method to eliminate contaminating minerals in quartz is crucial to achieve high purity silicon feedstock for solar cell Si-production. In this study we evaluate and compare the effects of electrical fragmentation to conventional mechanical crushing; particularly to remove fine-grained trace-minerals that often jeopardize otherwise promising high purity quartz commodities. The possibility to combine both comminution techniques upstream in the solar silicon value chain is also discussed. A bulk hydrothermal vein quartz sample containing trace impurities of muscovite and orthoclase is fragmented. After fragmentation the particles are sieved in two fraction sizes [0.3–0.5 mm] and [0.5–4 mm] and are magnetically separated. The morphology of the particles, the crack distribution, and the degree of mineral liberation are studied by optical microscopy, electron probe micro-analyzer (EPMA), and X-ray diffraction (XRD).

Electrical fragmentation generates particles with spherical geometries and deep cracks that selectively are pointing towards contaminant mineral inclusions, and produce a higher percentage of liberated minerals. Mechanical crushing, on the contrary, produces elongated fragments with fewer cracks that predominantly run parallel to the fragment surfaces.

Muscovite fractures both along its cleavage planes and along its grain boundaries whereas orthoclase fractures along its grain boundaries, only. Muscovite containing 5.8 wt.% Fe was easily removed by magnetic separation.

© 2012 Elsevier B.V. All rights reserved.

1. Introduction

The concentration of impurities strongly inhibits the performance of solar grade silicon (SoG-Si) for photovoltaic applications [1]. Industrially, silicon is extracted from quartz via carbothermic reduction in an electric arc furnace. Thermodynamic and experimental studies of the distribution of trace elements in silicon show the influence of the impurities in raw material to the final purity of silicon [2]. Metallurgical quartz 99.95% pure (less than 500 ppmw impurities) is currently used to produce solar silicon. This quartz is geologically classified as “intermediate-purity quartz” [3]. Most of the hydrothermal deposits are intermediate-purity quartz and will in the future be one of the most important raw feedstock sources to satisfy the explosive growth of the photovoltaic industry. Lumps of hydrothermal quartz conventionally crushed are currently the main feedstock in commercial production of metallurgical silicon and SoG-Si. However most of the contaminant, embedded in quartz as minute trace minerals, cannot be

removed with conventional crushing techniques, and contaminates the silicon.

Evonik is scaling up the innovative Solsilc route by Fesil [4] which uses pellets of high purity metallurgical quartz to produce SoG-Si. The advantage of using quartz pellets is that it is possible to refine the quartz prior to the furnace process. However fine grained quartz need to be micronized and agglomerated to cm-sized pellets in order to be charged into the electric arc furnace.

Our study aims at investigating the potential of electric fragmentation for the refinement of hydrothermal quartz. This is the first documentation of the efficiency of electrical fragmentation upon the removal of trace minerals comprising <1% of a mono-mineralogical rock type that does not benefit from the contrasting conductive properties that characterizes a mineralogically complex rock type such as, for example, a granite. In this work we investigate a novel route for the refinement of hydrothermal quartz under the removal of trace minerals. We performed electrical and mechanical fragmentation tests on the same quartz batch. After fragmentation, the particles are sieved and magnetically separated. Fraction sizes of [0.3–0.5 mm] and [0.5–4 mm] were studied. We analyzed the degree of liberation, the fragment morphology, the crack distribution, and interpret our

* Corresponding author. Tel.: +47 73 59 49 03.

E-mail address: dalmarte@material.ntnu.no (E. Dal Martello).

observations. Muscovite and orthoclase are the only contaminant inclusions present in the quartz batch; a discussion of their properties is also included in this paper.

1.1. Previous work

Quartz purification involves the removal of structural impurities, fluid inclusions, and solid inclusions [5]. While structural impurities are not easily removed [6], fluid inclusions can be removed upon heating [7,8].

Solid undesired inclusions may be partially or fully embedded in the quartz grains or occur at the interface between two grains.

Before removal the inclusion must be exposed for either acid leach [9], flotation techniques, magnetic separation or various other physical techniques [10]. Crushing to various grain sizes (typically 150 μm or larger) of the quartz commodity is required before removal of foreign minerals may be accomplished. Aulich [6] suggested an acid leach route on low purity quartzite to upgrade the quartz commodity to solar grade quartz. Some studied the mechanical and electrical fragmentation on multi-mineral aggregates [11]. Other authors [12–16] studied the dynamics and effects of electrical fragmentation on different ore types where the goal was to liberate the ore-minerals from the host rock (including hydrothermal quartz [10]). But neither of these studies documented the mechanisms of electric fragmentation upon minute foreign minerals in hydrothermal quartz as we do in the present study.

2. Materials, analytical methods, and experimental procedure

2.1. Materials

The company, Nordic Mining provided the hydrothermal quartz, from the Nesodden deposit, which is located in the Hardanger fjord (Norway). The promising low trace element content, and the availability of min. 2.7 million ton provides an interesting raw feedstock for SoG-Si production with a purity of more than 99.95% [17,18]. Two lumps (around 8 kg each) were collected from the sample locality of the deposit at a place where future mining is thought to commence.

2.2. HV pulse pulsed power equipment

Electrical fragmentation was done with a Selfrag Lab utility [19]. The batch equipment handles samples from 1 to 10 kg, and consists of a HV power supply, HV pulse generator, portable process vessels and a lifting table. Samples are loaded into a portable water loaded processing vessel which subsequently is placed onto the lifting table in the loading section. Subsequently, short pulses (pulse rise time less than 500 ns) of high-voltage electrical fields are applied.

Once the predetermined voltage is reached, the energy of the pulse generator is discharged from the electrode through the solid sample to the bottom of the processing vessel. Electrical fragmentation is the result when a shock wave propagates spherically throughout the material. A sieve is inserted in the bottom of the process vessel to collect the fragmented particles.

2.3. Analytical methods

Standard polished petrographic 30 μm sections were prepared and investigated by reflected and transmitted cross-polarized light (xpl) microscopy using a Nikon Eclipse E600 microscope with LJP at maximum 50 \times total magnification. A 2 megapixel SPOT Insight IN320 digital camera in combination with a SPOT software by Diagnostic Instruments Inc (Sterling Heights, MI, USA) allowed the recording of images in real time.

A JEOL JXA-8500F was used to collect primarily chemical maps of the samples. This instrument is a thermal field electron probe micro-

analyzer (EPMA) with submicron SEM capability integrated with X-ray analysis.

Standard microanalysis reference materials Astimex 53 Minerals Mount MINM25-53 were used for the standardization and calibration of the instrument [20].

D8 Advance XRD, BRUKER-EVA qualitative, and X-ray fluorescence (XRF) BRUKER S8 Tiger 4 kW X-ray spectrometer (Bruker AXS Nordic AB, Solna, Sweden) were used to confirm mineral identification and to determine silica phases present after fragmentation.

ICP-MS analyses were carried out to identify the purity of the original and the fragmented quartz. About 20–40 mg of quartz was dissolved in 0.5 ml conc. HNO_3 + 0.5 ml conc. HF and digested in autoclave at 255 $^\circ\text{C}$ for 1 h. Standard silica DIABASE W-2 and BCS-CRM 313/1 have been used as reference material.

2.4. Experimental procedure

The experiments were designed to perform electrical fragmentation and conventional mechanical jaw crushing followed by sieving and magnetic separation. The experimental flowchart is shown in Fig. 1.

The two 8 kg bulk samples were crushed to 5 cm lump sizes and split in three batches of 1 kg each. The first kg was mechanically crushed in a laboratory Retsch steel jaw crusher. The remaining 2 kg (Test 1 and Test 2) were fragmented by SELFRAG AG (Kerzers, Switzerland) in a laboratory electrical fragmentation chamber. Process parameters used for the electrical fragmentation are provided in Table 1. Low voltage was applied. Under these conditions, the shock wave strength is low and the streamlets selectively direct the fragmentation towards the inclusions.

Subsequently, two size ranges were sampled for detailed studies: [0.3–0.5 mm] and [0.5–4 mm]. The 4 mm upper boundary represents the largest grains produced during fragmentation. The fraction [0.5–4 mm] was chosen with the aim of studying fracture distribution associated with partially liberated contaminant trace minerals. Trace minerals are <0.3 mm hence the [0.3–0.5 mm] fraction was chosen for the study of successfully liberated foreign minerals.

The sieved fractions were analyzed by quantitative petrographic microscopy. Approximately 1500 mineral fragments were studied in each size fraction. The structure of the fragments, in terms of size, shape, texture, structure, fracture distribution, and the degree of liberation/separation were studied by point counting. The degree of liberation is defined as the fraction of minerals still locked in the quartz fragments, while the degree of separation as the fraction of free minerals separated by sieving and magnetic separation. It was not the purpose of this work to study the fines generated with the two techniques. Polished thin sections of mineral fragments were also studied by SEM and optical microscopy. Fragmented particles in the [0.3–0.5 mm] range were additionally studied by XRD for qualitative identification of the phases.

3. Results

3.1. Quartz before fragmentation

Fig. 2 is a representative micrograph of the un-processed quartz. Both intra- and trans-granular cracks are present. Trails of inter-granular fluid inclusions often intersect several grains. The shape of the grain is seriate interlobate. It is not possible to define an average grain size, rather the grain size distribution is bi-modal the most coarse-grained population falling around 4 mm in diameter and the other population clustering around 1 mm. The quartz rock experienced deformation and recrystallization. Bulging (BLG) recrystallization, sub-grain rotation (SGR) recrystallization and grain boundary migration (GBM) recrystallization are common features.

Two types of foreign trace-mineral inclusions are identified. These are orthoclase KAl_3SiO_8 , and Fe-rich muscovite, $(\text{Fe,Mg})\text{KAlSi}_4\text{O}_{10}(\text{OH})_2$,

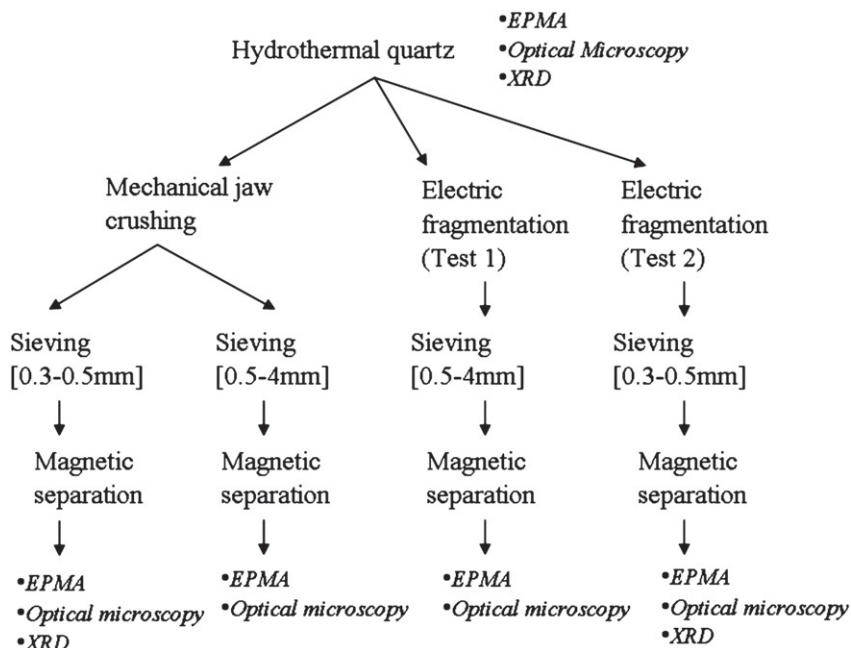


Fig. 1. Experimental flow chart.

Table 1

Process parameters used for the electrical fragmentation tests.

Experiments	Process parameters		
	Voltage pulses [kV]	Pulses	Vessel sieve [mm]
1st	121	424	4
2nd	125	2660	0.5

Table 2

Foreign mineral composition as detected by EPMA. Only the most significant oxides are included; compositions are in wt.%.

Minerals	SiO ₂	MgO	Al ₂ O ₃	FeO	K ₂ O
Muscovite	46.8	1.43	27.8	5.8	10.13
Orthoclase	64.5	0	28.7	0	15.4

Table 3

ICP-MS bulk chemical analysis of hydrothermal quartz prior to fragmentation.

B	P	K	Al	Fe
1.4	<3.5	120	44.4	20.74

respectively. Their composition in terms of oxides is shown in Table 2. Only a few grains of orthoclase of 400 μm size were found. Muscovite occurs both single crystals and as complex aggregates wrapping around individual quartz grains. The average grain size is below 300 μm. Fig. 2 features muscovite grains located at a quartz/quartz grain boundary.

The batch of the original quartz was analyzed with solutions ICP-MS. The elements considered were K, Al, Fe, and Mg. Also B and P, which are very difficult to remove from silicon, were analyzed. Table 3 shows the results. Mg is not reported because the analysis didn't give a reliable measurement.

3.2. Quartz after fragmentation, sieving and magnetic separation

Fig. 3 depicts representative micrographs of fragmented quartz. Particles fragmented with the jaw crusher (second column) form elongated

irregular fragments. Electrically fragmented particles (third column) have relatively even spherical geometries.

The fracture distribution for both mechanically and electrically fragmented quartz is shown in the third row of Fig. 3. Mechanically crushed quartz features minor fractures that predominantly are running parallel to the surface of the fragments. It is difficult to distinguish the new micro-fractures from the original fractures and fluid inclusion trails. The density of fractures is higher in regions affected by undulatory extinction i.e. areas in the quartz that are storing more stress than neighbouring areas. Electrically fragmented quartz contains dense networks of fractures throughout the grain.

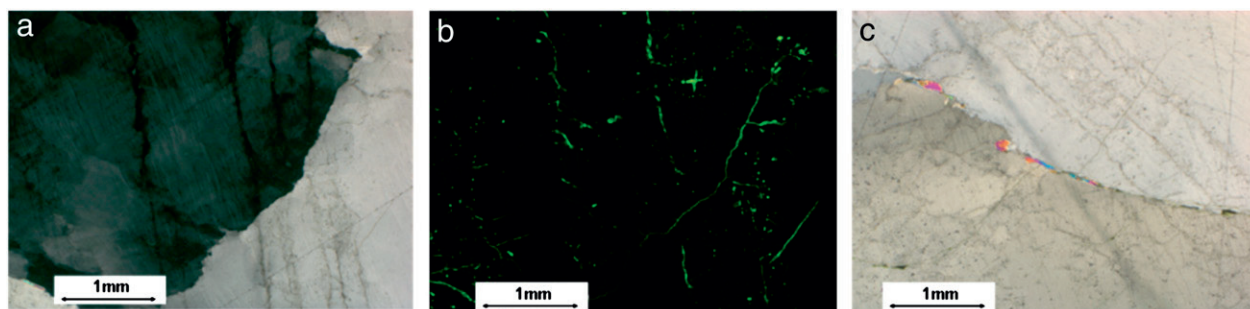


Fig. 2. Optical micrographs of the initial hydrothermal quartz: a) cross polarized light (xpl); and b) fluorescent microscopy of the same area depicted in a). Two quartz grains are distinguishable; several generations of cracks and trails of fluid inclusions intersecting the grain boundary are also visible. A xpl micrograph of a quartz grain boundary decorated with muscovite grains is shown in c).

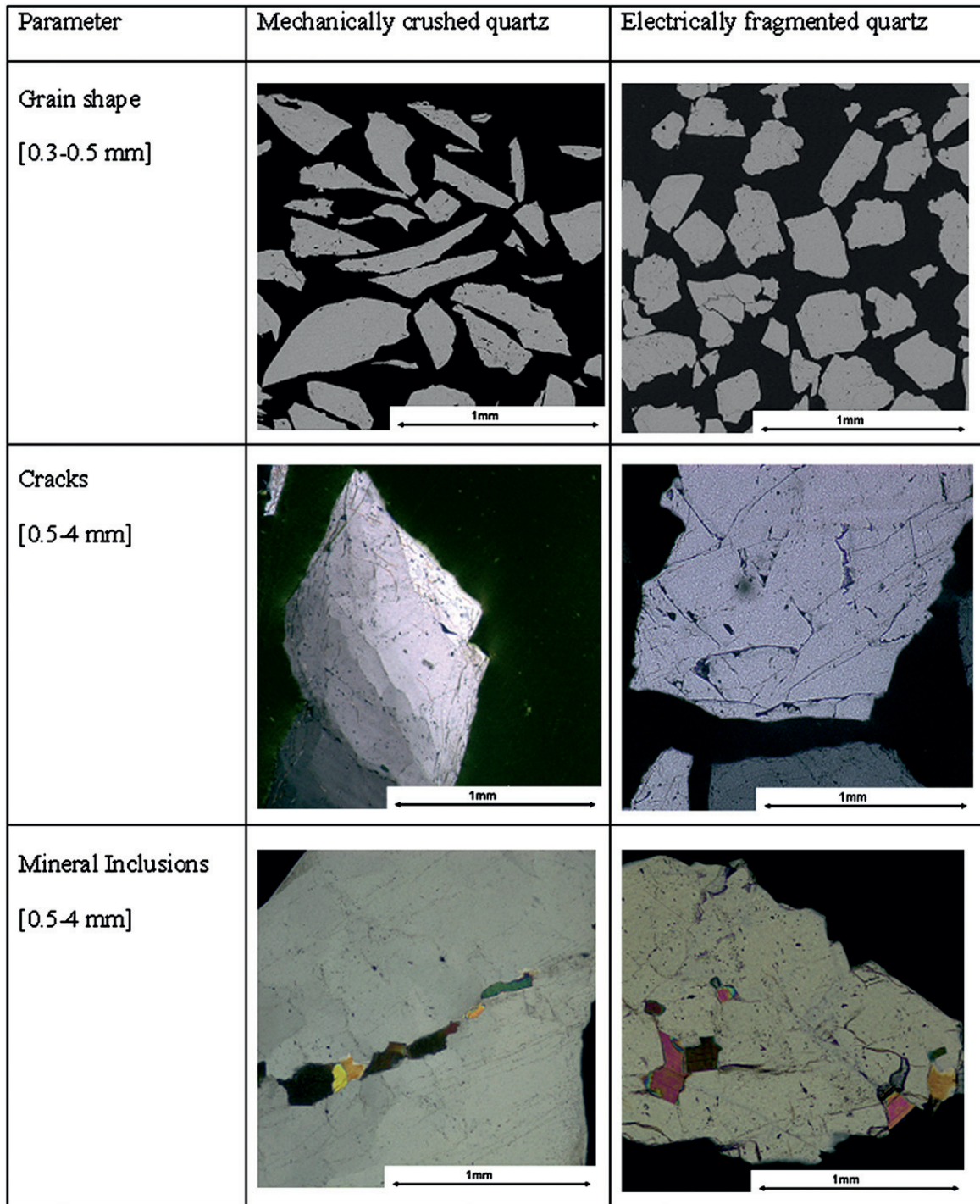


Fig. 3. Qualitative description of the quartz fragments. Grey: quartz, black: epoxy. Mechanical crushing (second column) generated fewer cracks mostly oriented parallel to the particle surface. Electrical fragmentation (third column) generated round shaped particles, uniform distribution of cracks, with cracks preferentially directed towards mineral inclusions embedded in the matrix.

The most recurrent crack spacing (for the size [0.5–4 mm]) is 200 μm . However extreme cases of pieces with 50 μm and 1 mm crack spacing are also observed. In both methods, most of the fluid inclusions in quartz survived the electric fragmentation.

The distribution of fractures relative to mineral inclusions is shown in the fourth row of Fig. 3. The analysis predominantly concentrates on muscovite, since orthoclase was effectively liberated. In *mechanically* crushed quartz the population of fractures does not show any preferential concentration in close proximity to muscovite. In the *electrically* fragmented quartz, fractures are polarized at the muscovite grain boundaries where they also feature the highest concentrations.

Muscovite grains that remain attached to the surface of the quartz grains are observed after both mechanical crushing and electrical fragmentation.

Quantitative analysis describing the mineral behavior after crushing, magnetic separation and sieving is summarized in Fig. 4. Four types of fragments are distinguished: i) quartz grain, ii) mineral on the surface of a quartz grain, iii) mineral embedded in quartz grain, and iv) liberated mineral.

- i) The highest percentage of liberated quartz particles occurs when HV-pulse and higher energy are applied. The advantage

















		SIEVED SIZE	
		0.3-0.5mm	0.5-4mm
FRAGMENTATION	MECHANICAL	 = 94.9%  = 2.9% (2.6% muscovite + 0.3% orthoclase)  = 0.3% (muscovite)  = 1.95% (0.2% muscovite + 1.8% orthoclase)	 = 85.9%  = 7.86% (7.37% muscovite + 0.5% orthoclase)  = 4.3% (4.1% muscovite + 0.2% orthoclase)  = 1.9% (1 muscovite + 0.9 orthoclase)
	ELECTRICAL	 = 99.1%  = 0.3% (muscovite)  = 0.5% (muscovite)  = 0.1% (muscovite)	 = 95.8%  = 3.1% (3% muscovite + 0.05% orthoclase)  = 1.1%  = 0.1% (orthoclase)

Fig. 4. Quantitative analysis of fragmented quartz particles after liberation and separation techniques. The meaning of the four symbols from the top to the bottom is: quartz fragment, mineral attached to the surface of a quartz fragment, mineral embedded in quartz fragment, and liberated mineral.

of using electrical fragmentation is more evident for the bigger size range where liberation is 10% better than for the same size range in mechanically crushed material;

- ii) regardless of the technique used, muscovite is only partially liberated whereas orthoclase is always liberated. In electrically crushed samples using HV-pulses, muscovite is mostly liberated along its grain boundaries rather than along its cleavage plane. In mechanically crushed quartz, there is a much higher percentage of quartz fragments with muscovite.
- iii) embedded muscovite always occurs in quartz pieces affected by ondulatory extinction.
- iv) liberated muscovite is completely removed after magnetic separation and sieving whereas it was not possible to separate orthoclase by magnetic separation and sieving.

4. Discussion

4.1. Mineral liberation

Table 4 summarizes the physical parameters involved in the two fragmentation techniques. In electrical fragmentation not only mechanical, but also the conductive contrasts amongst different minerals contribute to the fracture mechanism, hence resulting in a better mineral liberation.

The mechanical properties of a mineral deposit depend on its tensile strength and typology of defects. It is not possible to define numerically a tensile strength for the quartz investigated. The measured tensile strength is usually 10–20% of the theoretically calculated strength, due to the fact that stress is not applied homogeneously on grain boundaries, and to the presence of small defects in the material i.e. sites of high stress accumulations [21,22]. Defects in the crystal structure may be twinning planes, dislocations and other lattice defects, strain

Table 4

List of parameters that causes fracture formation during mechanical and electrical fragmentation.

	Physical phenomena	Parameters influencing crack formation
Mechanical crushing	Abrasion Splintering	• Tensile strength • Defects present
Electric fragmentation	Electrostriction Electrical breakdown Shock wave	• Permittivity • Conductivity • Mechanical integrity of the rock • Tensile strength • Defects present

accumulation (i.e. ondulatory extinction in quartz), cleavage planes, healed fractures, grain boundaries and cavities (i.e. fluid inclusions).

The electrical properties involved in the process are conductivity and permittivity (which influence the polarization effect of a material in response to an electric field). Experimental electrical values of rock-forming minerals are available in the literature [23]. These values are summarized in Table 5, which will be discussed in the section electrical fragmentation.

4.1.1. Mechanical crushing

Conventional crushing applies compressive stress, shearing and abrasion forces upon the material [21]. Although the rock is put directly under compression, it is the tensile forces that provoke most of the fracturing [24].

Shearing causes polarization of fracture to clusters running parallel to the fragment surfaces and the formation of elongated needle shaped fragments. Some fragments deviate from this general pattern in having fractures with a more random orientation. The fraction [0.3–0.5] showed a higher proportion of such particles. Since the two investigated sieved fractions come from the same mechanical crushing test, we suggest

Table 5

Summary of the electrical properties of quartz, orthoclase, muscovite, air and saline solutions. Reported values are in ranges according to the experimental measurements performed by [23,31,32].

	Relative permittivity ϵ_r [–] at 1 MHz	Electrical resistivity ρ [Ωm]	Source
Quartz	4.2–5.9	10^{11} – 10^{12}	Olhoeft
Muscovite	7.3	10^{13}	Olhoeft
Orthoclase	5.1–5.7	10^{12} – 10^{13}	Olhoeft
Air	1	10^{16}	Hearst
Pure water	80	2.8×10^5	Hearst
KCl	n.a.	0.1–800	Hearst
NaCl	>40	0.1–800	Peymann

that random fractures originated from quartz lumps which were not in contact with the jaws i.e. they were crushed by other quartz lumps and, therefore, were less affected by shearing. Phase contacts act as a discontinuity where local stress builds up and initiate failure [25]. Fractures located at the corner of mica boundaries are observed, but their occurrence is not as high as with electrically fragmented quartz. Mica is fracturing along its cleavage plane and along its grain boundaries.

Fine-grained particles are more easily liberated and feature a lower density of fractures. This is a result of a higher energy/surface ratio leading to a higher concentration of stress points and more easy fragmentation.

Orthoclase is easily detached from the quartz matrix and no cracks are found in the mineral itself. This is probably due to the fact that the toughness of quartz is lower than orthoclase, hence shear stress will accumulate along the orthoclase/quartz contacts rather than dissipating into the orthoclase crystals.

4.1.2. Electrical fragmentation

Electrostriction, electrical breakdown and subsequent shock wave interaction contribute to fracture formation and fragmentation.

Strictional tension is maximized where the electric field is higher. Local electrical fields accumulate at interfaces with deviating conductive properties [25] usually at grain boundaries and at matrix interfaces with different permittivity [16,26]. Strictional tension is not responsible for the mineral liberation, but generates weakness zones in the solid material [14] that ultimately leads to catastrophic failure [13,14,16]. The field distortion is proportional to the permittivity contrast between two minerals. The field distortion is also proportional to the particle size and the applied voltage. Many fractures are likely to form when a high stress field is present. The effect of electrostriction and correlated fractures can be studied for the sample *Test1*. According to the values in Table 5, the quartz–muscovite interface is expected to have a higher field distortion than the quartz–orthoclase interface, and micro-fractures at the quartz–muscovite interface are expected. Also, a field distortion is expected to occur at the fluid inclusion–quartz interface. Since the fluid inclusions are very small and are filled with saline aqueous fluids expected to be highly conductive, a high voltage needs to be applied in order to direct the cracks towards them and open them. Fluid inclusions remain intact after electrical fragmentation. Hence the applied voltage (121 kV) was probably too low. Fractures formed during electrical breakdown depend on the distribution of the plasma channels. The plasma channels prefer to run inside the quartz matrix avoiding cracks since quartz and air respectively have the lowest and highest resistivity (see Table 5). The plasma channels might also have developed inside the muscovite grains, since muscovite in our samples has relatively high Fe-concentrations, and the higher the iron concentration (Fe^{3+} or Fe^{2+}) in muscovite, the higher its electrical conductivity [27].

The vaporization of extremely small amounts of material during plasma channel formation, causes an instantaneous (10^{-6} – 10^{-4} s) thermal expansion [28] that produces an acoustic shock wave with

local pressures up to 10^{10} Pa [15]. The shock wave propagates spherically throughout the material. The reflection and refraction of the wave along physical boundaries like grain boundaries concentrate the stress at these interfaces and weaken them [29]. When enough pulses are applied, the interface experiences catastrophic failure and detachments of the mineral fragments. Electrical fragmentation ultimately produces a thick network of fractures and the formation of spherical particles. Also contrary to mechanical crushing, the spherical shock wave affects the material in all directions. Ideally, the thick network of fractures developed by the acoustic wave should also deprecipitate fluid inclusions and allow the contaminating fluids to escape. However, as previously mentioned, in our study the fluid inclusions were relatively unharmed.

Muscovite fractures preferentially along its grain boundaries rather than along its cleavage planes. The mechanism of micro-crack formation by electrostriction and plasma channels weakens the mica grain boundaries, such that the muscovite cleavage planes are no longer the weakest point as it was in mechanical crushing. Accordingly, the optimal condition for mineral liberation is obtained: the mechanical strength of the muscovite–quartz interface is lower than the mechanical strength of muscovite and of quartz, and fractures developed through the mineral–matrix interface. Orthoclase is completely liberated. Liberated orthoclase does not show fracture development and maintains its original crystal shape.

The degree of liberation is higher for electrical crushing. These results are in agreement with the work performed by [10,11] although these authors did not study a near mono-mineralogical material such as we did in our study. Quartz particles in the smaller fraction size show better liberation and present a lower density of intra-granular fracture networks. Compared to more coarse-grained material, this is an effect of more stress concentration points being activated in fine-grained particles.

During electrical fragmentation the quartz is subjected to high temperatures for a very short time, probably only a few milliseconds. Neither optical microscopy nor EPMA and XRD analyses of our sample material showed any traces of cristobalite or amorphous SiO_2 .

4.2. Mineral separation

Having the goal of developing a low cost route to a high purity quartz commodity for SoG-Si, we only applied sieving and magnetic separation to remove the liberated trace-mineral contaminants. Muscovite containing 5.8 wt.% Fe (Table 2) was effectively removed by magnetic separation (Fig. 4). However, orthoclase did not respond positively to magnetic separation but some of the more fine-grained specimens were removed by sieving.

4.3. Bulk chemical analysis

A bulk chemical analysis of the fragmented samples confirms our findings. Fig. 5 shows the impurity content in the 4 types of fragmented particles studied. Electrical fragmented quartz is of superior quality to the mechanically fragmented samples with the particle range size being the second most important factor. Accordingly, the fragmented particles in the range size [0.3–0.5 mm] show the lowest content in K, Al, Fe. Mechanically fragmented particles have approximately the same impurity content for both fraction sizes, this agrees well with the observations that conventional fragmentation does not selectively produce fractures that are directed towards contaminant inclusions.

However comparing these results with the original composition of the quartz, indicates that both techniques are intrinsically polluting the quartz. The major concern is B: its value is almost doubled. P is not shown because of uncertainty of the chemical analysis. The major contamination during electrically fragmentation is the electrode in steel. Selfrag is currently developing a laboratory scale equipment with a WC (tungsten-carbide) electrode.

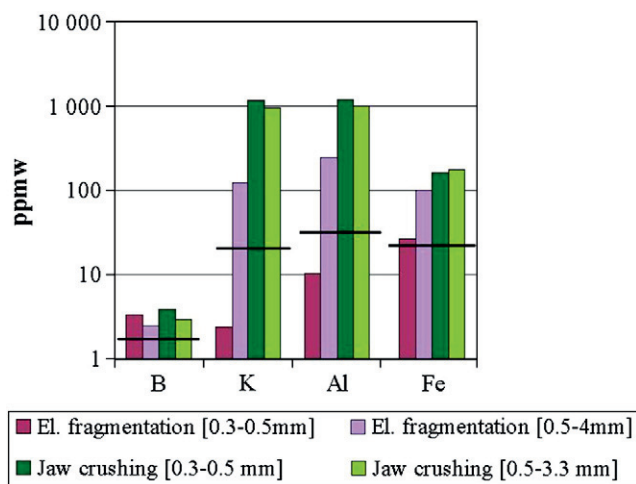


Fig. 5. Bulk chemical analysis of the fragmented particles (in columns) and the original quartz composition (black lines).

4.4. Application of electrical fragmentation for SoG-Si production

We have for the first time investigated the effects of electrical fragmentation on near mono-mineralogical commodity; a hydrothermal quartz deposit, with the goal of removing contaminant trace minerals comprising less than 1% of the commodity and to produce a novel source of SoG-Si raw material. Compared to mechanical crushing, electrical fragmentation is superior in liberating contaminant trace-minerals (Fig. 4).

Our results only applies to the investigated parts of the deposit, but since the diversity and total concentration of trace-minerals rarely exceeds 1%, we do not expect hugely different results from other parts of the deposit. However, future studies are required to elucidate this notion.

Al and Fe contained in muscovite are detrimental elements for the efficiency of SoG-Si [30]. In the batch we studied most of the Fe is in muscovite whereas Al comprises both orthoclase and muscovite. Electrical fragmentation is more efficient than mechanical crushing in liberating the contaminant minerals. Its potential could be even more exploited if a WC electrode was used.

The mechanical stability of quartz is an important issue. Quartz that is disintegrating in the furnace may cloak up the furnace and, therefore, should be avoided. Cracked lump quartz is undesired because quartz is charged in the top of the furnace. For the same reason, mm size particles cannot be charged to the furnace but need to be micronized and agglomerated. The use of milling is therefore a necessary step after electrical fragmentation. Here, the high density of cracks reduces the costs of micronization. In the end, micron fragments of fracture free quartz will be produced and ensure that the final agglomerated quartz is thermally stable during the furnace process.

In a scenario to produce SoG-Si raw materials we imagine the following processing steps. At first, electrical fragmentation is applied to fragments of quartz under the liberation of muscovite and orthoclase inclusion and perhaps other trace contaminants polluting the deposit. Secondly, liberated minerals are removed by sieving and magnetic separation, eventually assisted by acid leaching. Finally, liberated quartz particles are grinded mechanically to 10 μm size, mixed with the recovered fines (i.e. fraction < 10 μm) and agglomerated to pellets meeting the requirements for electrical arc furnaces.

After jaw crushing, quartz is electrically fragmented to a specific “target size”, followed by sieving and micronization. The “optimal grain size” is defined as the size required for optimal mineral liberation. When the contaminant minerals are situated at grain boundaries, the foreign minerals are easily liberated. However, in cases where the

mineral inclusions are embedded in the grain, the “target size” becomes smaller than the quartz grain.

Fines formed by mechanical crushing would also need to be recovered since they are required in the agglomeration process. The fine recovery process may be very costly particularly if special separation techniques are called for to remove foreign mineral inclusions. At a certain point of the size reduction process, the cost of mechanical crushing, recovery of fines and rinsing of the fines for contaminant minerals is higher than the costs of electrical fragmentation and, naturally, electrical fragmentation becomes more attractive.

5. Conclusions

- This is the first comparative study of the effects of electrical fragmentation and mechanical crushing, respectively, of a near mono-mineralogical quartz commodity where the goal is to remove minute trace minerals comprising less than 1% of the raw material.
- Electrical fragmentation technology generates more fractures that are selectively directed towards the mineral inclusions. Mechanical crushing produces fewer fractures, and a strong polarization of the fractures parallel to the grain boundaries.
- Electrical fragmentation increases the liberation of foreign trace-minerals and reduces the occurrence of embedded particles included in quartz.
- Muscovite containing 5.8 wt.% Fe can be easily removed by magnetic separation.
- Muscovite fractures both along its cleavage planes and along the grain boundaries, however, in electrical fragmentation it predominantly fractures along the grain boundary and is more efficiently liberated.
- Orthoclase always fractures along its grain boundaries.
- Electrical fragmentation is more advantageous in producing both larger liberated particles and quartz with a dense random network of fractures. This type of quartz is more brittle than mechanically crushed quartz and, therefore, less energy is required to micronize it.
- A possible route for quartz refining combining electrical fragmentation with conventional micronization was suggested.

Acknowledgments

The authors thank NORDIC MINING (Oslo, Norway) for providing the quartz and are grateful to Dr. A. Weh at SELFRAG AG (Kerzers, Switzerland) for experimental support and scientific discussions. The authors acknowledge also Professor Rolf Arne Kleiv for many interesting discussions. S.B. acknowledges the support of the Leiv Eiriksson mobility program through the Norwegian Research Council and the BASIC Project, Norwegian Research Council, under contract number 191285/V30.

References

- [1] Panel discussion. Arriving at well-founded SoG-Silicon feedstock specifications, Crystal Clear in the 6th Framework of Program of EU, 2008, Amsterdam.
- [2] E.H. Myrhaug, H. Tveit, Material balance of trace elements in the ferrosilicon and silicon processes, Electric Furnace Conference Proceedings, 58, 2000.
- [3] Norwegian Geological Survey, N, <http://www.ngu.no/en-gb/hm/Resources/industrimineraler/Kvarts-og-kvartsitt/High-purity-quartz/> 29-01-2012.
- [4] R. Kvande, et al., Solar cells manufactured from silicon made by the Solsilc process, 25th European Photovoltaic Solar Energy Conference and Exhibition/ Conference on Photovoltaic Energy Conversion, 2010, Valencia, Spain.
- [5] Deer, Howie, Zussman (Eds.), An Introduction to the Rock-forming Minerals, Longman scientific and technical, 1992.
- [6] H.A. Aulich, et al., Preparation of high-purity starting materials for the production of solar-grade silicon, Siemens Forschungs- und Entwicklungsberichte Bd 11 (6) (1982) 327–331.
- [7] K. Aasly, Properties and Behavior of Quartz for the Silicon Process, NTNU Department of Geology and Mineral Resources Engineering, 2008.
- [8] M. Gemeinert, et al., On correlation of gas-liquid inclusion's properties and melting behaviour of different genetic quartzes for production of transparent fused silica, Neues Jahrbuch für Mineralogie 165 (1) (1992) 19–27.

- [9] B. Strake, H.A. Aulich, Carbothermische Herstellung von Solarsilizium, *Erzmetall* 41 (1988) 126–131.
- [10] S.d.E.d. Bengy, New fragmentation system using high voltage, National Congress of Industrial Minerals, 2010, Zaragoza.
- [11] U. Andres, Liberation study of apatite–nepheline ore comminuted by penetrating electrical discharges, *International Journal of Mineral Processing* 4 (33–38) (1977).
- [12] U. Andres, Parameters of disintegration of rock by electrical pulses, *Powder Technology* 58 (1989) 265–269.
- [13] U. Andres, Electrical disintegration of rock, *Minerals and Metallurgical Processing* 14 (1995) 87–110.
- [14] U. Andres, J. Jirestig, I. Timoshkin, Liberation of minerals by high-voltage electrical pulses, *Powder Technology* 104 (1999) 37–49.
- [15] H. Bluhm, et al., Application of pulsed HV discharges to material fragmentation and recycling, *IEEE Transactions on Dielectrics and Electrical Insulation* 7 (5) (2000) 625–636.
- [16] U. Andres, Development and prospects of mineral liberation by electrical pulses, *International Journal of Mineral Processing* 97 (1–4) (2010) 31–38.
- [17] NordicMining, <http://www.nordicmining.com/kvinnherad/category276.html> 2011 16th June 2011.
- [18] P.I. Ihlen, A. Mueller, Forekomster av høyren kvarts langs Hardangefjorden, NGU, Trondheim, 2009.
- [19] www.selfrag.com 201124th February 2011.
- [20] Astimex, <http://astimex.com/com/catalog/min.html> 201126th June 2011.
- [21] K.L. Sandvik, M. Digre, T. Malvik (Eds.), *Oppredning av primære og sekundære råstoffer*. ed. T. forlag. 1999: 7005 Trondheim.
- [22] W.D. Callister (Ed.), *Material Science and Engineering: An Introduction*, 6th ed., John Wiley & Sons, 2003.
- [23] G.R. Olhoeft (Ed.), *Electrical properties of rocks. Physical properties of rocks and minerals*, ed. McGraw-Hill, 1981.
- [24] B.A. Wills, K. Atkinson, Some observations on the fracture and liberation of mineral assemblies, *Minerals Engineering* 6 (7) (1993) 669–706.
- [25] C.W. Passchier, R.A.J. Trow (Eds.), *Microtectonics*, Springer, 2005.
- [26] J.H. Schon (Ed.), *Physical Properties of Rocks*, Elsevier, Bergakademie Freiberg, Germany, 2004.
- [27] J.P. Crine, et al., The relationship between chemical composition and electrical conductivity of some North America micas, *Canadian Journal of Physics* 55 (1977).
- [28] V.V. Burkin, N.S. Kuznetsova, V.V. Lopatin, Formation of a spall cavity in a dielectric during electrical explosion, *Journal of Applied Mechanics and Technical Physics* 51 (2010) 137–144.
- [29] U. Andres, R. Bialecki, Liberation of mineral constituents by high-voltage pulses, *Powder Technology* 48 (1986) 269–277.
- [30] J.R. Davis, et al., Characterization of the effect of metallic impurities on silicon solar cell performance, Conference Record, 13th IEEE Photovoltaic Specialists Conference, 1978, Washington.
- [31] J.R. Hearst, P.H. Nelson (Eds.), *Well Logging for Physical Properties: A Handbook for Geophysicists, Geologists, and Engineers*, Wiley, 1985.
- [32] A. Peyman, C. Gabriel, E.H. Grant, Complex permittivity of sodium chloride solutions at microwave frequencies, *Bioelectromagnetics* 28 (2007) 264–274.

Article IV

TRACE ELEMENTS IN THE SI FURNACE

Part 1: Behaviour of impurities in quartz during reduction

Elena Dal Martello ^a (dalmarte@material.ntnu.no),
Gabriella Tranell^a (Gabriella.Tranell@ntnu.no),
Oleg Ostrovski ^b (o.ostrovski@unsw.edu.au),
Guangqing Zhang ^d (gzhang@uow.edu.au),
Ola Raaness ^c (Ola.S.Raaness@sintef.no)
Rune Berg Larsen^a (Rune.Larsen@ntnu.no),
Kai Tang ^c (Kai.Tang@sintef.no),
Pramod Koshy ^b (koshy@unsw.edu.au)

^aNTNU

^bUNSW

^cSINTEF

^dUOW

Quartz and carbonaceous materials, which are used in the production of silicon, as well as electrodes and refractories in the silicon furnace, contain trace elements mostly in the form of oxides. These oxides can be reduced to gaseous compounds and leave the furnace or stay in the reaction products - metal and slag. This paper examines the behavior of trace elements in hydrothermal quartz and quartzite in the reaction of SiO₂ with Si or SiC. Mixtures of SiO₂ (quartz or quartzite), SiC and Si in forms of lumps or pellets were heated to 1650°C (1923 K) and 1850°C (2123 K) in high purity graphite crucibles under Argon gas flow. The gaseous compounds condensed in the inner lining of the tube attached to the crucible. The phases present in the reacted charge and the collected condensates were studied quantitatively by X-ray diffraction (XRD) and qualitatively by Electron Probe Micro Analyzer (EPMA). Contaminants in the charge materials, reacted charge and condensate were analyzed by Inductively Coupled Plasma – Mass Spectroscopy (ICP-MS).

Muscovite in the mineral phase of quartz melted and formed two immiscible liquid phases: a Al-rich melt at the core of the mineral, and a SiO₂-rich melt at the mineral boundaries. B, Mn, and Pb in quartz were removed during heating in reducing atmosphere at temperature above 1650°C (1923K). Mn, Fe, Al and B diffused from quartz into silicon. P concentration was under the detection limit. Quartzite and hydrothermal quartz had different initial impurity levels; quartzite remained more impure after reduction experiment but approached purity of hydrothermal quartz upon silica reduction.

1 Introduction

Impurities in silicon affect the final efficiency of silicon solar cells. The required purity of solar grade silicon was brought forward by Coletti and co-workers[1]. The carbothermic production of silicon is an important source of contamination: quartz, carbonaceous materials as well as electrode and refractories carry detrimental impurities which transfer to silicon. Impurities in carbon material are mainly oxides and sulphides present in the ash. Because carbon is very porous, the impurities are easily exposed to the furnace gases up in the furnace and the volatile compounds which form can be easily removed when the charge is still at the top [2-4]. The behaviour of the impurities in quartz during the carbothermic reduction is still not well understood. The impurities present in the quartz do not have easy access to the reducing atmosphere as with carbon because the quartz is not porous. The quartz melts at around 1700°C (1973 K) and may not be melted in the production furnace until just above the cavity around the cavity, created by the electric arc. Consequently the oxides of the additional elements embedded in the quartz are believed to be accessible for reduction once the quartz reach the cavity [5] and any volatile compound which may form might not leave the furnace because of the interaction with the upper charge layer. If cracks formed by quartz thermal expansion are invaded by reducing gases, the impurities can be exposed earlier, however this is a topic not yet investigated.

SiO(g), CO(g), C (s) and SiC(s) are reducing agents for the impurity oxides present in the charge material. Oxides of Ni, Co, Fe, Pb, Cu, Cr, Mn, Zn, Na and K are easily reduced to metals, while oxides of Ca, Al, Ti, and Mg are stable at temperatures and conditions of quartz reduction. Impurities can be removed from quartz with a gas phase if the reduced or oxidic species are volatile. The vapour pressure of the reduced species is also influenced by the activities of the species in the raw materials and reaction products and by the reaction temperature.

Lumpy quartz contains impurities in form of a) mineral inclusions, b) liquid inclusions and c) trace elements in the quartz lattice. In a recent process developed for production of solar grade silicon from pure raw materials [6], quartz is charged in the furnace in form of pellets of intermixed SiO₂ and SiC. Quartz in these pellets is usually refined from mineral inclusions, and does not contain fluid inclusions because most of them are opened during the quartz milling process. An example of a refining route for hydrothermal quartz was studied by the present author [7]. Fig.1 describes the different paths and interactions of impurities (mineral inclusions, liquid inclusions and trace elements) while heating lumpy quartz in a reducing atmosphere. The case of pellets is a simplified version of Fig.1.

Mineral inclusions generally occur at the quartz grain boundaries and often have a melting point below that of quartz. How the mineral interacts with the silica matrix during heating is not clear. The elements can diffuse from the mineral into the silica matrix already at lower temperature or melt and diffuse/react with the matrix at higher temperatures. Alternatively, minerals with high melting points may maintain their initial composition until the silica melts with limited diffusion to the silica matrix. The high temperature properties of mica and quartz were studied by Hammouda and Pechavant [8]. The authors performed partial melting of an assemblage of synthetic quartz and millimetre-sized single crystal synthetic fluorine mica fluorophlogopite (KMg₃(AlSi₃O₁₀)F₂). The experiments were run under atmospheric pressure conditions. After 1 h at 1250°C (1523 K) a µm thick melt formed between the two reactants. Above 1300°C (1573 K) and within 2 hours run duration, two immiscible melt phases form: a SiO₂- rich melt in contact with the quartz, and a MgO- and F-rich melt in contact with the mica. However

muscovite is the common mica mineral found in quartz, and its high temperature properties are not yet understood.

Liquid inclusions may contain several phases: liquid, solid and gas. The most common composition comprises water in solution with Na^+ , K^+ , F^- , Cl^- , CO_2 , CH_4 [9]. However Ca, Cr, Cu, Mg, Mn, Pb and U are also likely to be concentrated in sub microscopic fluid inclusions [10]. Fluid inclusions are common in hydrothermal quartz and vary in size from 5 to 20 μm . It is not known how the trace elements in the quartz lattice interact with fluid inclusions during the heating of quartz. The gaseous phase may form and be released from quartz during fluid inclusions decrepitation at temperatures below 600 °C (873 K) [11].

Trace elements are impurities locked in the quartz lattice and accommodated at lattice specific sites. Interstitial cations, such as K^+ , are situated into vacancies or structural channels running parallel to the c-axis and present ionic bonds [10, 12]. Substitutional impurities such as Ti^{4+} , Al^{3+} , Fe^{3+} , B^{3+} , P^{5+} replace Si^{4+} site in the Si-O tetrahedral and present strong ionic-covalent bond [12]. How efficiently these impurities can diffuse to the quartz surface and be available to the reducing atmosphere is not well understood. The cations can diffuse to the lumps surface, be reduced to gaseous compounds and leave the quartz or, alternatively, the cations can remain in the quartz due to a combination of slow diffusivity, long diffusion path, (such as inability for the reducing gas to permeate the quartz cracks) or high stability to reduction into gaseous compounds. If the cracks, featured in solid quartz during heating can be invaded by reducing gases, the diffusion distance decreases considerably and the impurities are more easily exposed to reducing atmosphere. However it is not clear if the reducing gases are able to invade these cracks.

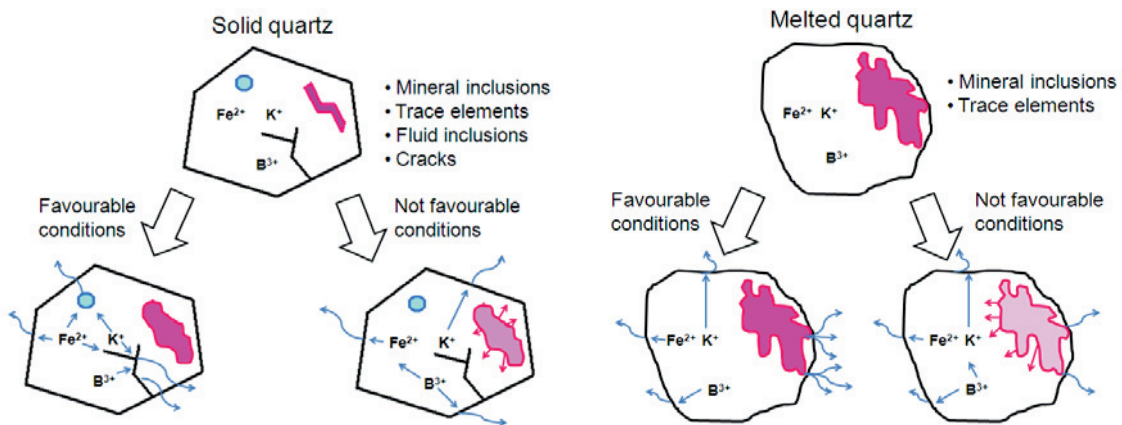


Fig.1- Possible paths of the impurities in solid and melted lumpy quartz during heating of quartz in reducing atmosphere. The conditions which enhance the formation of gaseous compounds are favourable conditions. These are: 1) interaction of trace elements with fluid inclusions and formation of gaseous Cl-based compounds which are liberated during heating of quartz; 2) short diffusion distance of the dissolved impurity to a reductive atmosphere combined with the ability to be reduced to gaseous compounds; 3) mineral at its initial composition when facing a reducing atmosphere.

The diffusivity of trace elements in solid quartz in a reducing atmosphere at temperature between 1600-2000°C (1973K -2273K) is not well documented. The only available data on the diffusivity of cations in quartz are in atmospheric air and at temperatures that are not representative of the silicon furnace [13-19]. The diffusion of Ca, Na, Li, K and Fe is fast in quartz, while diffusion of Al and Ti is significantly slower. In general, small cations diffuse more easily and voids, cracks and low density structures, such as high temperature quartz

polymorphs, enhance the cationsdiffusion[20, 21]. Geological studies on the diffusion of impurities during hydrothermal alteration of quartz show that Fe [22, 23], K [22, 24, 25] and B [25] are mobile ions in quartz.

This series of two papers examines the behavior and distribution of the impurities from quartz between reaction solid products and the gas phase. In particular the purpose of Part 1 is to understand the re-distribution of elements in solid and molten quartz and how much and which of the impurities remain in quartz after reduction. The purpose of part 2 is to investigate the concentration and form of impurities in gas and the conditions which enhance gas compounds formation.

2 Materials and methods

2.1 Materials

Hydrothermal vein quartz, quartzite, high purity SiC, and electronic grade Si (Eg-Si). The quartzite was of the common type used for the production of metallurgical silicon and Fe-Si alloys. The hydrothermal quartz is a new high purity source from a Norwegian deposit; it was examined in previous studies [27, 28]. The electronic grade silicon was supplied by Wacker, the ultra pure SiC was produced by reduction of hydrothermal quartz with high-purity carbon black. Ultra pure saccharine by Danisco AS C₁₂H₂₂O₁₂ was used as a binder in the pellet production. Quartz and silicon carbide were investigated both as pellets and lumps. The process of making pellets was described elsewhere [27].

The reactions were studied in ultra pure graphite crucibles of the isotropic type IG-110 supplied by Toyo Tanso and in ultra pure argon which contained H₂O < 3.0ppmw; O₂<2.0 ppmw. Table 1 summarizes the chemical composition of SiC, Si and graphite provided by suppliers and determined at NTNU. The graphite was analyzed by ICP-AES, SiC by GDMS while Si by ICP-MS. SiC and Si were also analyzed by ICP-MS after crushing.

Table 1. Chemical analysis (ppmw) of SiC, Si and graphite.

Trace element	B	P	K	Al	Fe	Mn	Zn	Pb
Isotropic graphite type IG-110(ref. from the supplier)	0.15	-	0.04	0.01	0.06	<0.001	-	-
Ultra pure eSiC (ref. from the supplier)	0.45	0.02	-	6.1	0.37	-	-	-
Electronic grade silicon (ref. from the supplier)	<0.001	<0.001	-	<0.001	<0.001	<0.001	<0.001	<0.001
Ultra pure SiC after crushing (NTNU)	1.43	-	-	10.9	6.8	0.44	0.07	0.01
Ultra pure SiC after milling (NTNU)	4.97	-	-	267.9	39.53	1.16	2.38	0.08
Electronic grade silicon after crushing (NTNU)	3.3	-	-	25.9	5.49	0.07	4.06	0.01

The chemical analyses of the quartz materials determined by ICP-MS at NTNU are presented in Table 2. The quartzes charged as pellets were jet milled prior to pelletizing. Hydrothermal

quartz was purer than quartzite and contained generally lower amount of B, Al, Fe, Mn, and Pb. The minerals present in the two quartz sources were identified by EPMA. Fe-rich muscovite and K-feldspar were found in hydrothermal quartz; Fe-rich muscovite, K-feldspar, clay mineral, calcite, clinocllore and carbonate were found in quartzite. Al, Fe and K were the most abundant elements in the mineral phase among the impurities studied.

Table 2. Chemical analyses (ppmw) of hydrothermal quartz and quartzite after mechanical crushing and jet milling.

Trace element	B	P	K	Al	Fe	Mn	Zn	Pb	Cr	Ni	Cu
Hydrothermal quartz after crushing	1.4	<3	<40	44	21	0.3	-	0.2	<1	<1	<1
Hydrothermal quartz after milling	3.7	-	142	199	182	1.9	1.5	0.3	<1	<1	<1
Quartzite after crushing	2.9	6.4	60	453	207	2.8	6.7	1.8	<1	<1	<1
Quartzite after milling	6.4	20.3	195	927	571	6.3	25.3	3.9	<1	<1	<1

2.2 Experimental set up and conditions

The reduction experiments were carried out in a 23 kW graphite tube furnace (model 1000-3560-FP20). The furnace chamber was 76 mm in diameter, and 153 mm in height. The experimental set-up is schematically presented in Fig.2. A crucible containing the charge materials was connected to a gas ducting tube 500 mm long and 10 mm in inner diameter. The tube end outside the furnace was connected to a two-way valve. A type C thermocouple with hafnium oxide insulator was inserted from the side of the furnace to measure the temperature close to the crucible wall.

Table 3. Experimental matrix. C represents carbon contained in the binder used for manufacturing pellets.

# Exp	Charge mixture	Temperature	Charge type	Quartz Type	SiO ₂	SiC	Si	C
2	SiO ₂ +SiC	1650°C 1923K	lumps	Hydro	1mol	1mol	-	-
2				Quartzite				
2			pellets	Hydro	0.9mol	0.9mol	-	0.3mol
2				Quartzite				
1		1850°C 1923K	lumps	Hydro	1mol	1mol	-	-
1				Quartzite				
1			Pellets	Hydro	0.9mol	0.9mol	-	0.3mol
1				Quartzite				
2	SiO ₂ +Si	1650°C 1923K	lumps	Hydro	1mol	-	1mol	-
2				Quartzite				
2			Pellets of SiO ₂	Hydro	0.9mol	-	1mol	0.5mol
2				Quartzite				
1		1850°C 2123K	lumps	Hydro	1mol	-	1mol	-
1				Quartzite				
1			Pellets of SiO ₂	Hydro	0.9mol	-	1mol	0.5mol
1				Quartzite				

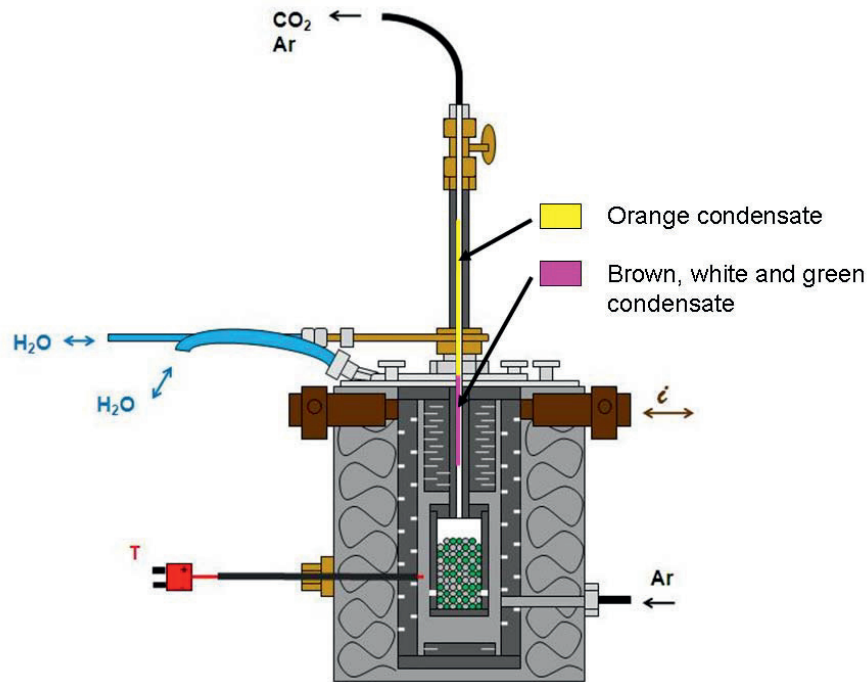


Fig.2- Experimental set in a graphite tube furnace. The condensate was collected in two regions represented in the picture in pink and yellow. Pink: mixture of white, brown and green condensate sticking on the tube surface; yellow: orange condensate in flaky-powdery form non-sticking on the tube.

The charge was directly heated to the targeted temperature at 60 °C/min when lumps were used. The charge with pellets was first heated to 1000 °C (1273 K) and kept for 10 minutes, in order to ensure the complete volatilization of the binder, and then heated at 60°C/min to the targeted temperature. The furnace was cleaned prior to the experiments by heating to 1900°C (1173 K) for 3 hours purging argon at 1 l/min (16.6 cm³/s). Argon passed through a tube furnace containing steel wool at 400°C (673 K) before entering the graphite furnace in order to flush out any oxygen impurity. The furnace was evacuated to 4x10⁻² mbar before purging argon to remove any adsorbed moisture and CO₂ from the graphite parts of the furnace. The outer surface of the graphite tube was coated with superglue, in order to ensure good hermetic condition. The furnace leakage was measured by keeping the furnace at vacuum for 1 day and was estimated to be 1.1mbar/h. The temperature along the ducting tube decreased sharply outside the chamber and as a result, a condensate deposited on the inner surface of the tube. The condensate eventually blocked the tube. The experiment was terminated when the overpressure in the chamber, due to the condensate blockage reached approximately 50 kPa.

2.3 Sample characterisation

Four analytical methods were used for the analysis of the samples after reaction: Inductively Coupled Plasma Mass Spectrometry(ICP-MS); X-Ray Diffraction (XRD); Electron Probe Micro-Analysis (EPMA) and Leco TC 600.

Single phases were taken, where possible, from the reacted charge mix and analyzed by ICP-MS. It was not possible to detach silica from silicon carbide in the mixture “pellets SiO₂+SiC”

after reaction, therefore the analysis for this experimental series refers to the mixture of SiC and SiO₂.

EPMA, JEOL model 8500F was used to identify the trace minerals as inclusions in quartz and to investigate the reacted minerals qualitatively by mapping and quantitatively by point analysis. Standard microanalysis reference materials Astimex 53 Minerals Mount MINM25-53 were used for the calibration of the instrument [30].

D8 Advance XRD, BRUKER-EVA was used to analyze the reacted quartz.

A Leco TC600 oxygen and nitrogen analyser was used to determine the oxygen content in the reacted sample. The free carbon content of the charges reacted at 1650 °C (1923 K) was measured by combustion method. The procedure was based on the Australian Standard for the ash content in coke [31]: powdery sample was heated in air to 815 °C (1088 K) in a muffle furnace for 180 min, and the carbon content was calculated from the mass change after incineration.

2.4 ICP-MS analysis: problems with SiC dissolution

Two procedures of digestion were applied in this work. If a sample contained SiC, the procedure of digestion was: 20-40 mg sample in a mixture 0.5ml concentrated HNO₃ + 0.5ml concentrated H₂SO₄ + 0.5ml concentrated HF at 255 °C (518 K) for 1 hour. It should be mentioned that complete digestion of SiC was not achieved. A sample which did not contain SiC, was digested in a mixture 0.5ml HF + 1.5ml HNO₃ at 250 °C for 1 h. The solution was digested in PTFE containers in a digestion bomb.

The addition of H₂SO₄ in the dissolution improved the recovery of the elements. The major effects were on B (+15%), P (+5%), Al (+10%) and K (+9%). Fe, Mn and Pb were less affected (+2%). Therefore the results were normalized accordingly.

Standard materials DIABASE W-2, BCS-CRM 313/1, NIST 57b (Si) and JCRM R 021 (SiC) were used for the ICP-MS calibration. Three scans were run for each sample with an average error of 4%.

Tests on standards W-2 and NIST 57b showed that the B and P concentrations were very close to the reference values. This means that the losses of B and P were negligible during digestion of samples in an autoclave, and the analyses of B and P were reliable.

The gaseous products containing mainly SiO(g) and CO(g) condense/react to a mixture of Si, SiC and SiO₂ which will be discussed further in part 2 of this publication. Gaseous compounds other than SiO(g) and CO(g), were suggested to end up in the SiC, Si, or SiO₂. Since SiC was not fully digested, an accurate quantification of those elements is questionable. Silicon carbide is very difficult to digest. The dissolution process is extremely slow because what is really dissolved is not the SiC itself but a very thin layer (around 100 nm (Presser et al. 2008)) of cristobalite formed on the SiC surface. After the first silica layer had dissolved, a new layer forms by thermal oxidation. Since the condensed SiC is in the form of β:SiC (as will be shown in Part2), which among the SiC polytypes has a relative open structure and therefore easier to digest, a completely recovery of SiC in the condensate is assumed.

3 Results

3.1 Morphology of the reacted charge

Table 4 summarizes the morphology of the reacted charge for the different experimental conditions. The morphology of the samples containing hydrothermal quartz was structurally very similar to samples with quartzite. The pictures in Table 4 represent samples with hydrothermal quartz. The experimental time, which was limited by tube blockage by the condensate is also indicated in the table.

Analyses of the oxygen and carbon content in pellets reduced at 1650°C (1923K) showed that silica reacted mainly with carbon in the binder. This series of experiments is not representative for the reaction between silica and silicon carbide but provides some information for comparison of reactions with quartzite and hydrothermal quartz.

It is worthy to note that at 1650°C (1923 K), the charge mix “lumps SiO₂+SiC” took more time to block the tube with condensate than the charge mix “lumps SiO₂+Si”. The situation was the opposite at 1850°C (2123 K). This qualitative result agrees with Andersen [32] who studied the reactions between SiO₂+SiC and SiO₂+Si. He observed that the rate of conversion of the SiO₂-SiC mixture was two times higher in comparison with the SiO₂-Si mixture at 1650°C (1923 K) and nine times higher at 1850°C (2123 K).

Microstructures of reacted quartz depended on the reaction temperature, charge mix and initial size.


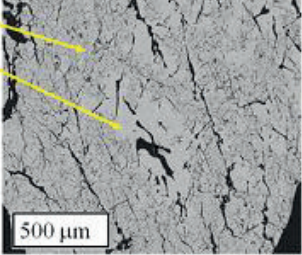

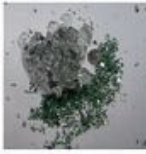
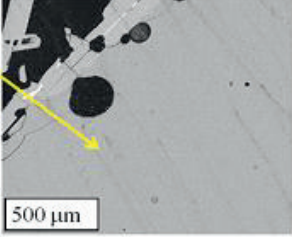


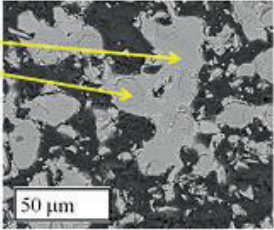

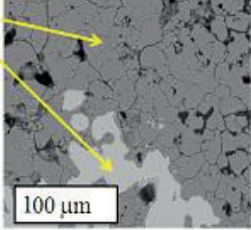

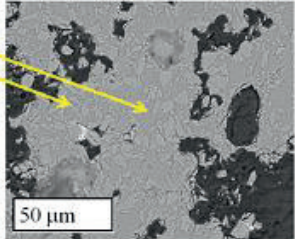

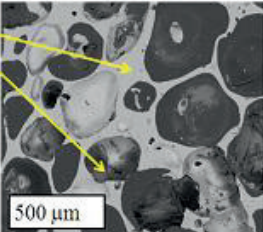
Reacted lumpy quartz (1-2 in Table 4) at 1650°C (1923 K) was still solid and was characterized by a thick network of microns-wide cracks. Cracks in the quartz before and after heating are shown in the micrographs in Fig.3. The distance between cracks was approximately 50 µm. The reacted quartz was white and visibly porous. Quartzite, originally with a brownish/reddish resemblance, changed to white after reduction. Quartz was crystallized to cristobalite. A few areas of intermediate amorphous phase appeared near the cracks.

Reacted lumpy quartz (3-4 in Table 4) melted at 1850°C (2123 K) and cracks disappeared. Melted SiO₂ lumps were in the form of numerous spherical aggregates when reacted with SiC, while fused to a single piece when reacted with Si and cavities, previously filled with silicon are also visible.

Reacted pellets of quartz (5-6 in Table 4) sintered at 1650°C (1923 K) regardless of the charge mix used. Sintering decreases the initial porosity of the charge. Cristobalite in the pelletized charge was the major phase detected by XRD.

Reacted pellets (7-8 in Table 4) melted at 1850 °C (2123 K). 7) The charge mix “SiO₂+SiC” at 1850°C (2123 K) is characterized by a matrix of amorphous SiO₂ containing SiC pieces. 8) The charge mix “SiO₂+Si” resembled a quartz sponge stretched structure characterized by openings of 250-500 µm size. This quartz spongy structure was so fluid that it partially ran out of 2 mm holes in the bottom of the graphite crucible which were present to allow the Ar to flow in to the crucible. Silicon diffused and reacted into the graphite crucible, reacted with the quartz, and only a small amount was found in the reacted charge.

Table 4. Reacted charge morphology for the different experimental conditions: visual observations and backscattering analyses. Major focus is on the quartz charge. The cases 1-2 and the cases 3-4 show the same backscattering microstructure of quartz, therefore only one representative picture for the two cases is shown.

<p>1) Lumps - $\text{SiO}_2 + \text{SiC}$ - 5h at 1650°C</p> <p>Crystalline quartz Amorphous quartz</p>  	<p>2) Lumps - $\text{SiO}_2 + \text{Si}$ - 2h at 1650°C</p> <p>Amorphous quartz</p>  <p>Quartz microstructure similar to case 1)</p>
<p>3) Lumps - $\text{SiO}_2 + \text{SiC}$ - 20 min at 1850°C</p> <p>Amorphous quartz</p>  	<p>4) Lumps - $\text{SiO}_2 + \text{Si}$ - 1h at 1850°C</p> <p>Quartz microstructure similar to case 3)</p> 
<p>5) Pellets - $\text{SiO}_2 + \text{SiC}$ - 40 min at 1650°C</p> <p>Amorphous quartz SiC</p>  	<p>6) Pellets - $\text{SiO}_2 + \text{Si}$ - 40 min at 1650°C</p> <p>Sintered quartz particles Silicon</p>  
<p>7) Pellets - $\text{SiO}_2 + \text{SiC}$ - 10min at 1850°C</p> <p>Amorphous quartz SiC</p>  	<p>8) Pellets - $\text{SiO}_2 + \text{Si}$ - 10 min at 1850°C</p> <p>Melted quartz Pores</p>  

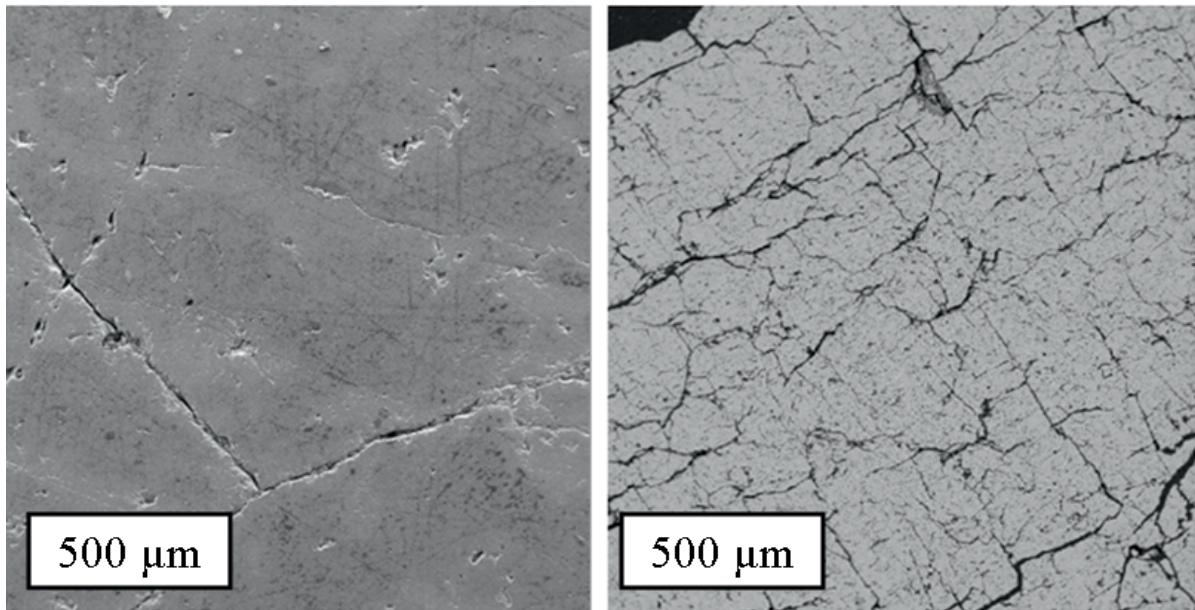


Fig.3 On the left: micro cracks, grain boundaries and porosity in the original quartz sample. On the right: cracks developed in the sample during heating.

3.2 *Impurities in reacted quartz*

Chemical analysis of the reacted hydrothermal quartz and quartzite was compared with their initial composition.

Fig.4 shows the change Δ in the impurity concentration (ppmw) for the initially charged quartz and the reacted quartz. The parameter Δ depends on both the reduction of the impurity to the gas phase, and the change in the SiO_2 mass or $\text{SiO}(\text{g})$ production.

Table 4 compares concentrations of impurities before and after reaction in hydrothermal quartz and quartzite presented as a ratio (mass). Quartzite was more polluted than hydrothermal quartz both before reduction and after reduction. However the difference in concentrations decreased after reaction, particularly for the pellet charge SiO_2+SiC reduced at $1650\text{ }^\circ\text{C}$.

P values are not reported because the values were under the detection limit (3.4 ppmw). The most consistent trends in change in the concentration were observed for Pb, Mn, B, Zn and Al. Pb, Mn, Zn and B had preferentially negative Δ values, meaning that these impurities were removed from quartz more effectively than loss SiO_2 in reduction. Al had positive Δ value meaning that it was removed less effectively or remained unaltered in the charge. The change in K concentration was scattered with uncertain trend. Δ values for Fe were more negative for lumps in comparison with pellets, meaning that Fe was more effectively removed - or less

unaltered in the quartz when pellets instead of lumps were used, in particular when hydrothermal quartz was used.



Fig.4- Impurity variation from after quartz reduction compared to the original quartz composition. Values not shown correspond to values below the detection limits or to high concentration in the blanks used as reference.

Table 4-Comparison of the impurity content in quartzite and hydrothermal quartz presented as a ratio of concentration in quartzite to the concentration in hydrothermal quartz. Average values in the reacted charge are based on eight analyses.

Quartzite/hydrothermal	B	K	Fe	Al	Mn	Pb
Lump initial charge	1.8	2.6	10.0	10.2	8.5	10.5
Average reacted lumpy charge	1.6± 0.5	2.6± 2.1	6.6± 3.2	4.4± 4.0	7.7± 3.8	\
Pellets initial charge	1.5	1.4	3.1	4.7	3.3	11.9
Average reacted pellet charge	1.1± 0.4	1.2± 0.9	1.9± 0.5	2.0± 1.4	1.0± 0.8	2.8± 3.2

Table 5 – Chemical analyses of reacted silicon after heating “SiO₂+Si” mixtures compared to the initial composition (Eg-Si = electronic grade silicon).

	B	Pb	Al	Mn	Fe	Zn
Eg-Si in the charge material	100 %	100%	100 %	100 %	100 %	100 %
Eg-Si after heating to 1850°C with lumps of hydrothermal quartz	79 %	\	146 %	2476 %	759 %	6 %
Eg-Si after heating to 1850°C with pellets made of quartzite	175 %	\	168 %	25115%	2560 %	9 %
Eg-Si after heating to 1650°C with pellets of hydrothermal quartz	436 %	236%	1048 %	7174 %	2075 %	100 %
Eg-Si after heating to 1650°C with pellets of quartzite	173 %	\	255 %	5736 %	1754 %	0 %

Impurities in Si for the “SiO₂+Si” charge were also analysed. Results presented in Table 6 show that the concentrations of B, Fe, Mn and Al in silicon increased after reaction. The phenomenon was particularly evident when pellets were used.

As described in the introduction, impurities in quartz are present in the form of trace elements in the quartz lattice and mineral inclusions. The minerals can be partially removed in a beneficiation process when quartz powder is produced; however they remain in lumpy quartz. Fig.5 illustrates the distribution of Fe, K and Al in muscovite mineral, during heating of lumpy quartz. The picture refers to hydrothermal lumpy quartz heated to 1650°C (1923 K) and 1850°C (2123 K). As shown in Fig.5, Fe, K and Al were partially dissolved into the SiO₂-matrix. K was distributed uniformly in the mineral; while distribution of Al was not uniform. The concentration of Fe in the muscovite was too low (4 at% Fe compared to 7 at% K and 15 at% Al) to describe its behavior. Two distinct liquids were formed: a Al-rich melt at the core of the mineral, and a SiO₂-rich melt at the mineral boundaries. Al and K diffused into the quartz structure at both temperature studied.

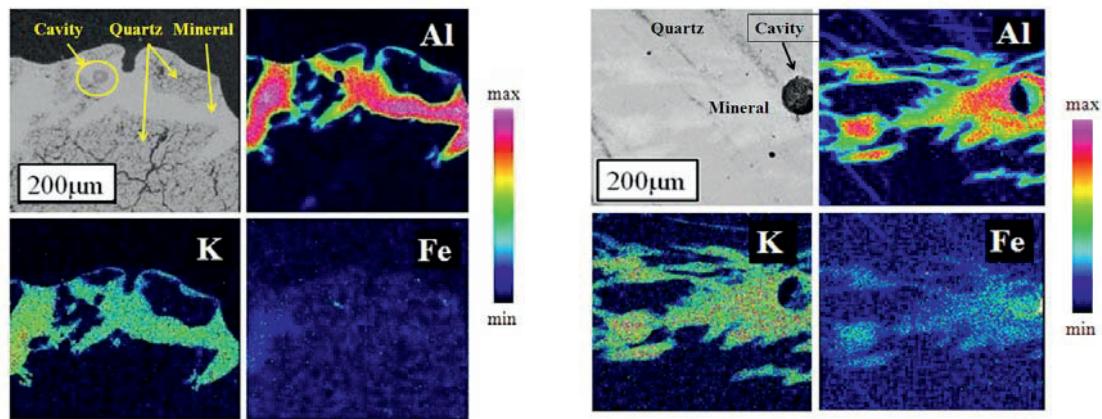


Fig.5 - EPMA mapping of muscovite in hydrothermal quartz heated to 1650°C (1923K) (left) and to 1850 °C (2123 K) (right). Muscovite melts in two immiscible liquids at temperature above 1650°C.

4 Discussion

It was, by microscopic analysis, shown that trace impurities interact with reducing gases: elements in minerals dissolve into the quartz matrix, trace elements in the matrix diffuse towards the neighbouring reacting phases or to the quartz surface where in presence of a reducing atmosphere, they can leave the quartz in form of gaseous compounds. Impurities are reduced during quartz reduction and the concentration of Mn, Zn, Al, Pb and B diminishes after quartz reduction.

Quartz microstructure during heating

XRD analyses show that the quartzes regardless the initial charge mix, are largely transformed to *cristobalite* at 1650°C (1923 K). The efficiency in cristobalite transformation may be due to the presence of argon in the atmosphere [32] or to the slow heating profile [33]. In particular, looking at the microstructure of reacted *lumps* of quartz at 1650°C (1923 K), amorphous areas can be found (Table4 Fig.1). The transformation process of quartz into cristobalite takes place right up to 1650°C (1923K) [20]. The amorphous phase which was found in the quartz lumps heated to 1650 °C (1923 K) is therefore not melted quartz, but rather the transitional intermediate phase which forms during the “reconstructive transformation” of β -quartz to β -cristobalite [20, 34, 35]. Also quartz in *pellets* was completely transformed to cristobalite at 1650 °C (1923 K). Quartz microm particles in pellets were mechanical activated by crushing and milling. During mechanical treatment of quartz (such as milling) Si-O bonds are broken and form a highly disordered silica layers (thickness from 20 to 500 nm) on the surface of the quartz fragments [36-39]. The high energy content in the activated surface area could also lead to the sintering of the quartz particles. Steinike and Balek [36, 38] observed that the direct transformation of mechanically activated quartz transforms directly into cristobalite at lower temperature (around 1200 °C (1473 K)). Cristobalite with density 2.3g/cm³ has a more open structure than β -quartz (density 2.6 g/cm³) [40]. The solubility of the impurities in cristobalite is therefore higher than in quartz, which stimulates partial decomposition of mineral phase and dissolution of its constituents into cristobalite. Kawasaki [33] reported that the

solubility of Fe^{3+} in cristobalite increases with increasing temperature. Diffusion of K, Al and Fe into the cristobalite structure is shown in Fig.5.

Muscovite mineral melts at temperatures below the quartz melting point. Melted muscovite is associated with a cavity, which was previously filled by H_2O formed by dehydration of muscovite, a phenomena referring to a process where hydrous silicates re-crystallize to an assemblage with fewer or no volatile components [9]. The dehydration reaction of mica minerals taking place at calcinations temperatures lower than the melting point of silica was also reported by Zhu [41]. In the muscovite object of this study, Fe^{3+} partly substitutes for Al according to the phengite substitution (Fe is linked to 2OH and 1 O). Fe is found concentrated at the cavity showing to have a strong affinity with the OH group. The diffusion properties of Fe with OH is reported by Fein [42].

Two distinct liquids were found in the melted mineral: a Al-rich melt at the core of the mineral, and a SiO_2 -rich melt at the mineral boundaries confirming the findings of Hammouda [8]. Fig.5 shows that Al features a typical diffusion gradient in the silicate mineral, while K has a constant profile. This gives reason to assume that Al has a slower diffusion rate than K when present in a silicate slag matrix, although it has a smaller effective ionic radii than K (Al^{3+} has an average effective ionic radius of 0.5 Å in comparison to 1.5 Å for K^+ [26]). K, is well known to be a fast diffuser in crystalline quartz due to its interstitial position [12, 14, 25].

Refining of quartz during heating quartz in reducing atmosphere

Reduction of oxides of trace elements depends on the oxides stability and volatility of reduction products. Knowledge of the stability of the oxides with respect to silica and of the boiling temperatures of the reduced volatile compounds are necessary in order to understand these trends. Oxides more stable than SiO_2 (such as Al) remained as oxides, while oxides less stable (such as B, Pb and Mn) were reduced during reduction of quartz. Al is a very stable oxide, as consequence it remained primarily in the silica; moreover, as a result of reduction of silica, concentration of aluminium in quartz after reaction increased (Figure 3). In addition Al^{3+} is a slow diffuser in quartz [16]. Opposite to the case of Al, the elements Pb, Mn and B were efficiently removed from quartz into the gas phase (Fig.4), showing to be both fast diffuser in quartz and easily reduced to gaseous compounds and/or into silicon. Thermodynamically, B, Pb and Mn are less stable as oxides than silica. The extent of removal of boron B was lower in comparison with Mn and Pb. B has an exception for the experimental condition “lumps SiO_2+SiC 1850°C” where B is not efficiently removed from SiO_2 . The experiment lasted 20 min only, which was perhaps not sufficient to allow B to diffuse from the bulk lump towards the silica surface boron reduction and removal.

Reduction of impurities in cristobalite took place on the particles surface, which created concentration gradient and diffusion of impurity element from the particle bulk to the surface.

Cracks in solid quartz are permeated by reducing atmosphere

The diffusion coefficient and diffusion distance of the impurities from the quartz bulk to the surface affects the availability of the impurities at the surface, and therefore the efficiency of impurity removal reduction. The diffusion distance was relatively short in the micron size pellets. Pellets contained 10 µm quartz particles compared to lumps of 5 mm size (in the real

industrial process 5-15 cm lumps of 5-15 cm size are used). At 1650 °C (1923 K) cristobalite particles in pellet of SiO₂+SiC sintered forming clusters of 50 µm size while lumpy quartz developed a thick network of cracks with an average distance between two cracks comparable to 50 µm. Cracks were created by thermal expansion of quartz during heating and its transformation to cristobalite (cristobalite has a density of 2.318 gr/cm³ while quartz has a density of 2.646 g/cm³ [40]). Cracks were also generated by the decrepitation of fluid inclusions which are typical in hydrothermal quartz [43]. Clusters of sintered quartz particles were separated by open spaces greater than 25 µm, while the fractures in lumps were of the order of several micrometers. Generation of cracks was essential to reaction with gaseous SiO and CO and removal of impurities in the reduction process.

It is an open question if the reducing gases can invade the cracks in crystalline quartz.

From a *theoretical* point of view, if the cracks are wider than the mean free path λ , they are invaded by reducing gases through molecular or Ficksian diffusion. The parameter λ , which is the average distance a gaseous molecule travels between collisions. The parameter was calculated according to [44] for CO₂ (input data on SiO(g) and CO(g) are not available in literature) under the temperature and pressure conditions described in this article. λ is estimated as ~1µm [44], meaning that if the cracks are wider than ~1µm, they are invaded by reducing gases through molecular or Ficksian diffusion, and if in the least probable case, cracks are smaller than 1µm, the molecules will collide with the crack wall according to Knudsen diffusion theory.

Experimental results confirm this theory. Given similar diffusion distances from quartz bulk to quartz surface in pellets and lumps for the experimental condition “SiO₂+SiC 1650 °C”, if the reducing gases can invade the micro-cracks in lumps, no significant difference between pellets and lumps should be noted after reduction. Fig.4 does not show any particular difference in impurity variation for the experimental condition SiO₂+SiC 1650 °C when quartz lumps instead of pellets are used confirming that CO(g) and SiO(g) may permeate the cracks and interact with the impurities available at the surface.

The ability of CO(g) to invade µm wide cracks, was also demonstrated in previous publications by reacting two quartzes with different initial cracks amount, at high temperature in reducing atmosphere; the quartz having the higher amount of cracks was characterized by higher weight losses [27].

5 Conclusions

This paper, which is the first of a series of two, investigated the behaviour of the impurities in quartz when quartz reacted with SiC and Si in reducing atmosphere.

The main findings of this work can be summarised as follows:

- B, Mn, Zn, and Pb were removed from quartz during heating in reducing atmosphere at temperature above 1650°C (1923K).
- Muscovite in the quartz’s mineral phase melted and formed two immiscible liquid phases: a Al-rich melt at the core of the mineral, and a SiO₂-rich melt at the mineral boundaries.
- During heating quartz in presence of silicon, Mn, Fe, Al, Zn and B diffused from quartz into the silicon, this was particularly evident when pellets were used.
- Pellets made of only quartz sintered at temperatures below 1650°C (1923K).
- During heating quartz lumps, a thick network of cracks with an average distance between cracks close to 50 µm and of the order of µm wide formed. Reducing gases can invade these cracks in quartz.

- Difference in concentration of impurities in quartzite and hydrothermal quartz decreased upon silica reduction, however contamination of quartzite remained higher than of hydrothermal quartz.

Acknowledgment

We appreciate interesting discussions with Kristian Drivenes and Jeffery Kline; this work was possible thanks to the excellent technical help of John Sharp, Xing Xing and Xiaohan Wan. Acknowledges also to Morten Raaneess and Syverin Lierhagen for the analyses. This work was partially funded by ELKEM's research fund.

References

1. Panel discussion. *Arriving at well-founded SoG-Silicon feedstock specifications*. in *Crystal Clear in the 6th framework of program of EU*. 2008. Amsterdam.
2. Yao, H., et al., *Fundamentals on vaporization behavior of trace metal compounds at different atmospheres and temperatures*. J.Jpn. I. Met., 2001: p. 256-262.
3. Wang, Q., et al., *Fuel Process. Technol.*, 2004. **85**: p. 1431-1441.
4. Garcia, M. and E.H. Myrhaug, *Revisjon av materialbalanse for sporelementer i Si-ovn basert på målekampanje på Elkem Thamshavn april 2007*. 2007, Elkem Silicon: Oslo.
5. Myrhaug, E.H. and H. Tveit, *Material Balance of trace elements in the Ferrosilicon and Silicon Processes*. Electric furnace conference proceedings, 2000. **58**.
6. Kvande, R., et al. *Solar cells manufactured from Silicon made by the Solsilc process*. in *25th European Photovoltaic Solar Energy Conference and Exhibition / Conference on Photovoltaic Energy Conversion*. 2010. Valencia, Spain.
7. Dal Martello, E., S. Bernardis, et al. *Powder Technol* , 2012 **224**: 209-216.
8. Hammouda, T. and M. Pichavant, *Eur. J. Mineral.*, 1999. **11**: p. 637-653.
9. Deer, Howie, and Zussman, eds. *An introduction to the rock-forming minerals*. 1992, Longman scientific and technical.
10. Larsen, R.B., et al., *Contrib Mineral Petr*, 2004. **147**: p. 615-628.
11. Samson, I., A. Anderson, and D. Marshall, eds. *Fluid Inclusions: Analysis and Interpretation*. Vol. 32. 2003.
12. Grimstedt, A., et al., *Chem Geol*, 2002. **182**: p. 237-247.
13. Frischat, G.H., *Ber Deut Keram Ges*, 1970. **47**: p. 364-368.
14. Verhoogen, J., *Am Mineral*, 1952. **37**: p. 637-655.
15. Frischat, G.H., *J Am Ceram Soc*, 1970. **53**: p. 357-360.
16. Pankrath, R. and O.W. Florke, *Eur J Mineral*, 1994. **6**: p. 435-457.
17. Penniston-Dorland, *Am Mineral*, 2001. **86**(5-6): p. 652-666.
18. Stock, H.D. and G. Lehmann, *J. Phys. Chem. Solids*, 1976. **38**: p. 243-246.
19. Cherniak, D.J., E.B. Watson, and D.A. Wark, *Chem Geol*, 2007. **236**: p. 65-74.
20. Chaklader, A.C.D. and A.L. Roberts, *J Am Cer Soc*, 1961. **44**(1): p. 35-41.
21. Presser, V. and K.G. Nickel, *Silica on silicon carbide*. *Crit. Rev. Solid State Mater. Sci*, 2008. **33**: p. 1-99.
22. Amington, A. and J. Balascio, *The growth of high purity low dislocation quartz*. 38th Annual Symposium on Frequency Control. , 1984: p. 3-7.
23. Muller, A., W. B.J., and M. Smith, *Mineralogical Magazine*, 2005. **69**(4): p. 381-401.
24. Larsen, R.B., F. Jacamon, and A. Kronz, *Mineralogical Magazine*, 2009. **73**(4): p. 691-707.
25. Larsen, R.B., I. Henderson, and P.M. Ihlen, *Contrib. Mineral. Petrol.*, 2004. **147**: p. 615-628.
26. Whittaker, E.J.W. and R. Muntus, *Geochim Cosmochim Ac*, 1970. **34**: p. 945-956.
27. Dal Martello, E., G. Tranell, et al. (2011). *Met. Trans. B* **42**(5): 939-950.
28. Dal Martello, E., et al., *ISIJ Int.*, 2011. **51**(9): p. 1492-1496.
29. Stoch, L., M. Laczka, and I. Waclawska, *Mineralogia Polonica*, 1985. **16**(2): p. 43-54.
30. Astimex. <http://astimex.com/com/catalog/min.html>. 2011 26th June 2011].
31. Australia, C.o.S., *Coal and Coke-Analysis and testing Part4: Coke -Proximate analysis*. 2006, Standards Australia GPO Box 476, Sydney, NSW 2001, Australia.
32. Andersen, V., *Investigation of thermal properties of quartz for the silicon industry under reducing atmosphere*, in *Department of materials science and engineering*. 2009, NTNU: Trondheim.

33. Kawasaki, T. and H. Ishizuka, *Experimental study of Fe³⁺ solubility in cristobalite and its application to a metamorphosed quartz-magnetite rock from Mt. Riiser-Larsen area, Napier Complex, East Antarctica*. J. Miner. Petr. Sci., 2008. **103**: p. 255-265.
34. Scherer, G., P.J. Vergano, and D.R. Uhlmann, Phys. Chem. Glasses, 1970. **11**(3): p. 53-58.
35. Mitra, S., Trans. J. Brit. Ceram. Soc., 1977. **76**(4): p. 71-74.
36. Balek, V., et al., Thermoc Acta, 1988. **262**: p. 209-214.
37. Benezet, J.C. and A. Benhassaine, Powder Technol 1999. **105**(1) pp 167-171.
38. Steinike, U. and K. Tkáčová, J Mater Synth Proces, 2000. **8**: p. 197-203.
39. Damn, C. and W. Peukert, Langmuir, 2009. **25**: p. 2264-2270.
40. Ford, H.M., S.M. Auerbach, and P.A. Monson, *On the mechanical properties and phase behavior of silica: A simple model based on low coordination and strong association*. J. Chem. Phys., 2004. **121**(17): p. 8415-8422.
41. Zhu Bao-zhong, S.Y.-l., Xie Cheng-we, *Spectroscopy research on the Guizhou Xingyi gangue of different calcined temperatures*. Journal of china coal society, 2008: p. 1049-1052.
42. Fein, J.B., et al., *Experimental study of iron-chloride complexing in hydrothermal fluids*. Geochim Cosmochim Ac, 1992. **56**: p. 3179-3190.
43. Gemeinert, M., et al., *On correlation of Gas-Liquid inclusion's Properties and Melting Behaviour of Different Genetic Quartzes for Production of Transparent fused Silica*. Neues Jahrbuch Miner. Abh., 1992. **165**(1): p. 19-27.
44. AA Atkins, P. and J. de Paula, eds. *Atkins' physical chemistry*. 7th ed. 2002, Oxford University Press Inc.: New York.

Article V

TRACE ELEMENTS IN THE SI FURNACE

Part 2: Analysis of condensate in carbothermal reduction of quartz

Elena Dal Martello ^a (dalmarte@material.ntnu.no),
Gabriella Tranell^a (Gabriella.Tranell@ntnu.no),
Oleg Ostrovski ^b (o.ostrovski@unsw.edu.au),
Guangqing Zhang ^d (g.zhang@uow.edu.au),
Ola Raaness ^c (Ola.S.Raaness@sintef.no)
Rune Berg Larsen^a (Rune.Larsen@ntnu.no),
Kai Tang ^c (Kai.Tang@sintef.no),
Pramod Koshy ^b (koshy@unsw.edu.au)

^aNTNU
^bUNSW
^cSINTEF
^dUOW

Silicon feedstock for production of solar grade silicon should be as pure as possible to decrease the cost of manufacturing of solar cells. Impurities in quartz, carbonaceous materials, electrodes and refractories are mostly present in the form of oxides. These oxides can be reduced to volatile gaseous compounds in presence of SiO(g) and CO(g) atmosphere and potentially leave the furnace or stay in the condensed reaction products, metal and slag.

This work investigates the conditions under which volatile impurities report to the gas phase in laboratory experiments with lumpy and pelletized mixtures of SiO₂, SiC, Si at 1923 K (1650 °C) and 2123 K (1850°C) respectively, were carried out. The volatile compounds were generated by the reduction of quartz, and collected in the form of condensate. The effects of the reaction temperature, quartz type, charge composition, pellets and lumps on the composition of the condensate were studied. The trace elements in the charge input, reacting charge and condensate were analyzed using Inductively Coupled Plasma – Mass Spectroscopy (ICP-MS) and X-ray Diffraction (XRD).

CO(g) and SiO(g), which are the major components in reduction reactions, formed four types of condensate, white, brown, green and orange. The condensate constituents were amorphous SiO₂, 3C:SiC, Si and α -quartz. Each impurity present in the quartz charge entered the gas phase during quartz reduction and was detected in the condensate. Al and Fe show limited volatility. The volatility of Mn, P and B depends on the charge mix: a higher P_{CO} enhances the concentration of these elements in the gas phase. Fluid inclusions, common in hydrothermal quartz, enhance the distribution of the contaminants to the gas phase. Industrial campaigns on Si and Fe-Si production confirm the experimental results.

1 Introduction

Reducing agents in carbothermal reduction of silica include carbon (coke and/or char), SiO(g), CO(g) and SiC. In the process of silica reduction, impurity oxides present in the charge material are also reduced. Less stable oxides than silica, such as oxides of Ni, Co, Fe, Pb, Cu, Cr, Mn, Zn, Na and K are easily reduced and partitioned between silicon, oxide and gas phases, while stable oxides of Ca, Al, Ti, and Mg are not reduced. The reduced species can be removed from quartz in the form of volatile gaseous phases. Gaseous species comprise pure metals, as well as sub-oxides and combination of metal oxides and hydroxides. The partial pressure of the gaseous species depends on the activities of elements in raw materials and reaction temperature.

Myrhaug and Tveit studied the distribution of trace elements present in the metal, “microsilica” (condensed silica fume) and off gases for a Fe-Si furnace [1] and Si furnace [2, 3]. The trace elements found in the microsilica were mainly K, Zn, Na, Mg, and Pb, while the elements found in the Fe-Si alloy were primarily Cu, Cr, P, Mn, Al, Cr, Ni, Fe, B, and Ti. The behaviour of P is dependent on the Fe content in the charge: in the Si furnace 85% of P input reports to microsilica, while in the Fe-Si furnace only 25%. Myrhaug [4] described the behaviour of trace elements in the silicon furnace with a model based on the boiling temperature of pure elements. The model assumes that an element evaporates when its boiling point is lower than the process temperature. The boiling point model refers to the case of partial pressure of the elements over the pure element p_{El}^0 equals 1 atm, when activity of the elements a_{El} equals to 1, which is not representative of the real case. Moreover the model does not take into account the fact that gaseous compounds other than the pure elements may form. Impurities found in the microsilica and in the off gases do not necessarily represent the total amount of gaseous compounds formed in the furnace: gaseous compounds may condense and circulate in the furnace, which is a process known in the manganese production (Zn(g) and K(g) react with CO(g) and CO₂(g) forming ZnO(s) and K₂CO₃(l,s) respectively [5-7]).

The formation of gaseous species is concurrent and linked with the production of SiO(g) and CO(g) in an industrial reduction furnace. The main reactions leading to the formation of SiO(g) and CO(g) are shown by equations (1) and (2) at 1873 K (1600 °C) and by equations (3-5) at higher temperatures. In particular, SiO(g) is formed at the SiO₂, SiC and Si surfaces, while CO(g) is formed at the C and SiC surfaces [8].

The main condensation reactions occurring in the system are given by equations (6-9). The reaction (6) is found to occur in the temperature range of 1873-1973 K (1600-1700 °C) [9, 10]. The reactions (7) and (9) occur at temperatures lower than 1773 K (1500 °C) [8, 11, 12]. The reaction (6) produces a brown condensate [9, 10, 13], reaction (7) produces a white condensate, while reaction (8) a green condensate [12]. Andersen et al. and Vangskåsen [10, 13] showed that the brown condensate consists of silicon spheres ranging in size from 100 to 1000 nm in a matrix of SiO₂.



This paper, which is the second of a series of two (see reference [14]), investigates the behaviour of the impurities in quartz when quartz is heated in reducing atmosphere. The major focus is on the impurities which leave the quartz during reduction and enter the gas phase.

2 Analysis of condensate and thermodynamic simulation

The experimental matrix, equipment and procedure were described elsewhere [14]. The gaseous compounds formed during the experiments were collected in a form of condensate on the inner surface of the graphite ducting tube. The different condensate phases were recovered from the inner surface of the tube using a tungsten carbide tool, mixed and collected in one sample. The sample was crushed with an agate mortar of 99.91% to the microns size needed for the analysis.

Two analytical methods were used for the analysis of the condensate samples: Inductively Coupled Plasma Mass Spectrometry (ICP-MS) and X-Ray Diffraction (XRD). The content of the impurity trace elements in the condensate was detected by ICP-MS. Details on the ICP-MS analysis are given in [14]. XRD was used to identify and quantify the phases present in the condensate. For the phase quantification, the Rietveld method was used [15]. Because the condensate contains amorphous silica, 5wt% Al_2O_3 was added as a measurement standard to find the quantity of glassy phases in samples. Firstly, contents of all the crystalline phases were calculated. Then results were re-calculated (normalised) to get a known concentration of alumina in the sample. The glassy phase content was calculated as the difference between the amount of crystalline phases and the total mass of the sample. This is a useful method to quantify amorphous phases with XRD, its disadvantage being that it is reliable only if the content of amorphous (glassy) phase is greater than 10 wt%. Electron Probe Micro Analyzer (EPMA) was used to study the morphology of the condensate.

The formation of gas compounds at equilibrium conditions was simulated using the FactSage software package, and the thermodynamic calculations were compared to the measured results. Eight experimental conditions, as described in Part 1, have been simulated: “lumps SiO_2+SiC 1650°C”, “lumps SiO_2+SiC 1850°C”, “lumps SiO_2+Si 1650°C”, “lumps SiO_2+Si 1850°C”, “pellets SiO_2+SiC 1650°C”, “pellets SiO_2+SiC 1850°C”, “pellets SiO_2+Si 1650°C”, “pellets SiO_2+Si 1850 °C”. Although two different quartzes were used in the experiments, only quartz with higher concentration of impurities was examined. The thermodynamic calculations are based on the following assumptions:

- Reactions between input materials have reached equilibrium at 1 atm total pressure.
- Carbon content in the binder of the pellet is the only difference in the simulation of pellets compared to lumps.
- Impurities are present only in the quartz, and they are treated as oxides in a mechanical mixture with quartz (i.e. activity = 1); the elements considered are B, P, K, Al, Fe, Mn, Zn, Pb with the same amount as in the quartzite .
- Oxides are reduced in the presence of $\text{SiO}(\text{g})$, $\text{CO}(\text{g})$, C and SiC.

The FACTSage (Version 6.3) pure substance database has been used to simulate the equilibrium. 100% condensation is always assumed in the equilibrium calculations.

3 Results and discussion

3.1 Condensate description

The gaseous compounds were collected in the form of condensate. Four different types of condensate (based on colour) were identified: white, green, brown and orange. The white, green and brown

condensates were found adhered in the lower part (first 6 cm) of the tube, near the crucible, and were difficult to remove. The orange condensate was found as loose flaky powder in the upper part of the tube and was easy to collect. While the white, brown and green condensates were found in all the experiments, the presence of the orange condensate varied from very high amounts in some experiments to very small amounts in others. Fig.1 shows the appearance of the condensates found in the lower part of the tube. The microstructure of the condensate in Fig.1 is illustrated in Fig.2. The condensate is characterized by an assembly of tiny spherical particles (diameters $\sim 5 \mu\text{m}$). Three main complexes were found: single Si particles in SiO_2 matrix (50 atoms% Si and 50 atoms% O), and mixtures of Si, C, and O without specific composition. The condensate has reacted with the graphite tube, forming a transitional SiC layer of $50 \mu\text{m}$ which was found at the interface condensate-tube. Mapping of the condensate for Mg, P, Ca, Fe, K, Al reveals that impurities generally are in too low concentrations to get reliable results from the EPMA. However, there is an indication that Ca and Al may partially report to the thin SiC layer formed on the tube surface. The SiC layer at the interface between the condensate and the graphite tube was difficult to remove with the WC filament and was therefore not possible to sample all of it. Between 2 g and 6 g of condensate were collected in each experiment, the exact amount varying from sample to sample.

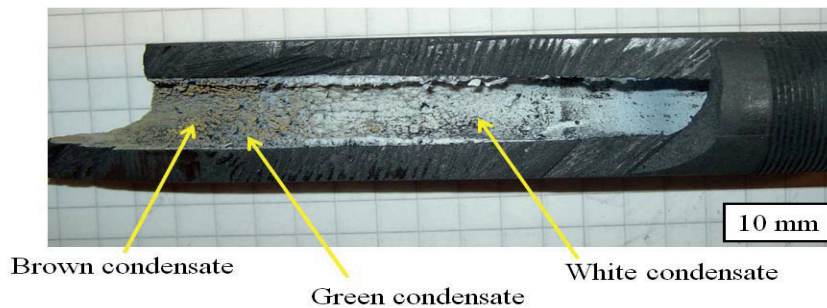


Fig.1- Appearance of the condensates collected in the graphite tube (experimental condition “pellets SiO_2+SiC 1650 °C”). Three types of condensate (white, brown, green) are sticking in the first 6 cm of the tube.

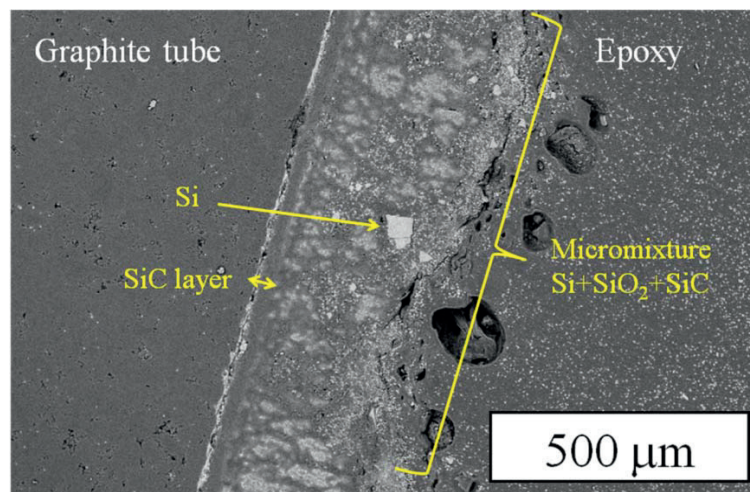


Fig.2 Backscattering image of a mixture of white and brown condensate collected in a graphite tube. The condensate has reacted actively with the graphite tube forming a thin SiC layer which is the region containing the two white lines.

The condensates produced when quartzite was used as the source of SiO_2 , were analyzed by XRD. The phases detected in the condensate were: amorphous SiO_2 , $\alpha\text{-SiO}_2$, Si and $\beta\text{-SiC}$ (products of reactions (2), (6-9)). It should be noted that XRD quantitative analysis of a system with a high amount of glassy (amorphous) phase can only be semi-quantitative. However, the relative proportions of the crystalline phases are considered accurate. The condensate composition (in mole percent) for the eight experimental conditions and the time required for the condensate to block the tube are shown in Fig.3.

Crystalline quartz, amorphous silica, SiC and Si were found in the condensate. The presence of crystalline α -quartz may be due to the re-crystallization of the amorphous silica during long term exposure at relatively high temperatures in the tube.

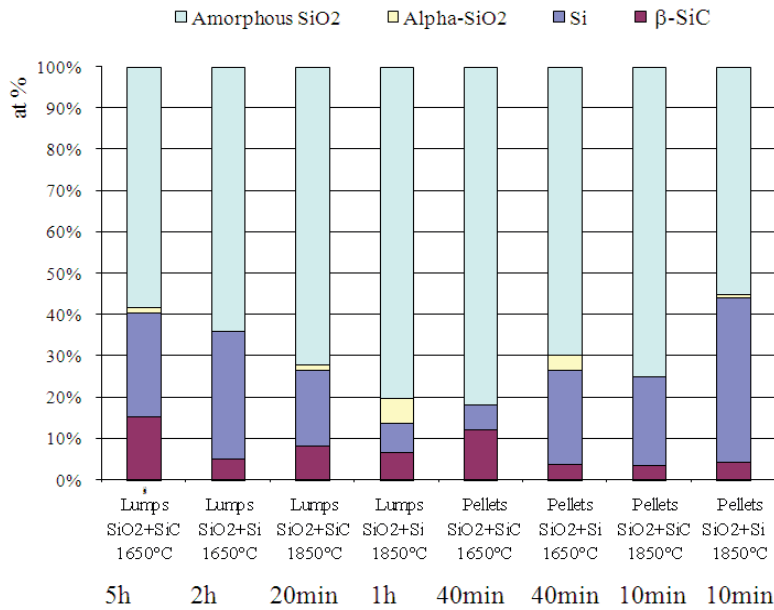


Fig.3 –Condensate composition (at%) under eight different experimental conditions. The time required for the condensate to block the tube is shown below the graphs.

The experiments stopped when the condensate derived from SiO(g) and CO(g) blocked the tube. Fig. 3 shows that less time was required to block the tube when pellets rather than lumps were used. Since the condensate phase composition does not show a significant difference between experiments with lumps and pellets, it is possible to conclude that the rate of silica reduction is faster in pellets than in lump quartz. The property of pellets to produce more SiO(g) was stated by the same author in previous publication [16].

3.2 Impurity volatility: effect of temperature and charge mix

During the heating and reduction of quartz, impurities oxides in quartz were reduced to gaseous compounds which were collected in the condensate. The degree of volatilization is defined as the ability of the impurity, denoted el , present in the quartz to report to the gas phase,

$$volatilization = m_{el, gasphase} / m_{el, chargemix} \quad (10)$$

where “ $m_{el, chargemix}$ ” is the impurity content by mass in the charged quartz and “ $m_{el, gasphase}$ ” is the impurity content by mass in the condensate.

The impurity volatilization during quartz reduction was studied both experimentally and by thermodynamic simulations and summarized in Fig.4. The experimental results refer to quartzite and hydrothermal quartz, while thermodynamic analysis refers to a quartz material having the same impurity content as the quartzite used in the experiments. The experimental conditions with pellets were simulated adding the amount of carbon present in the binder.

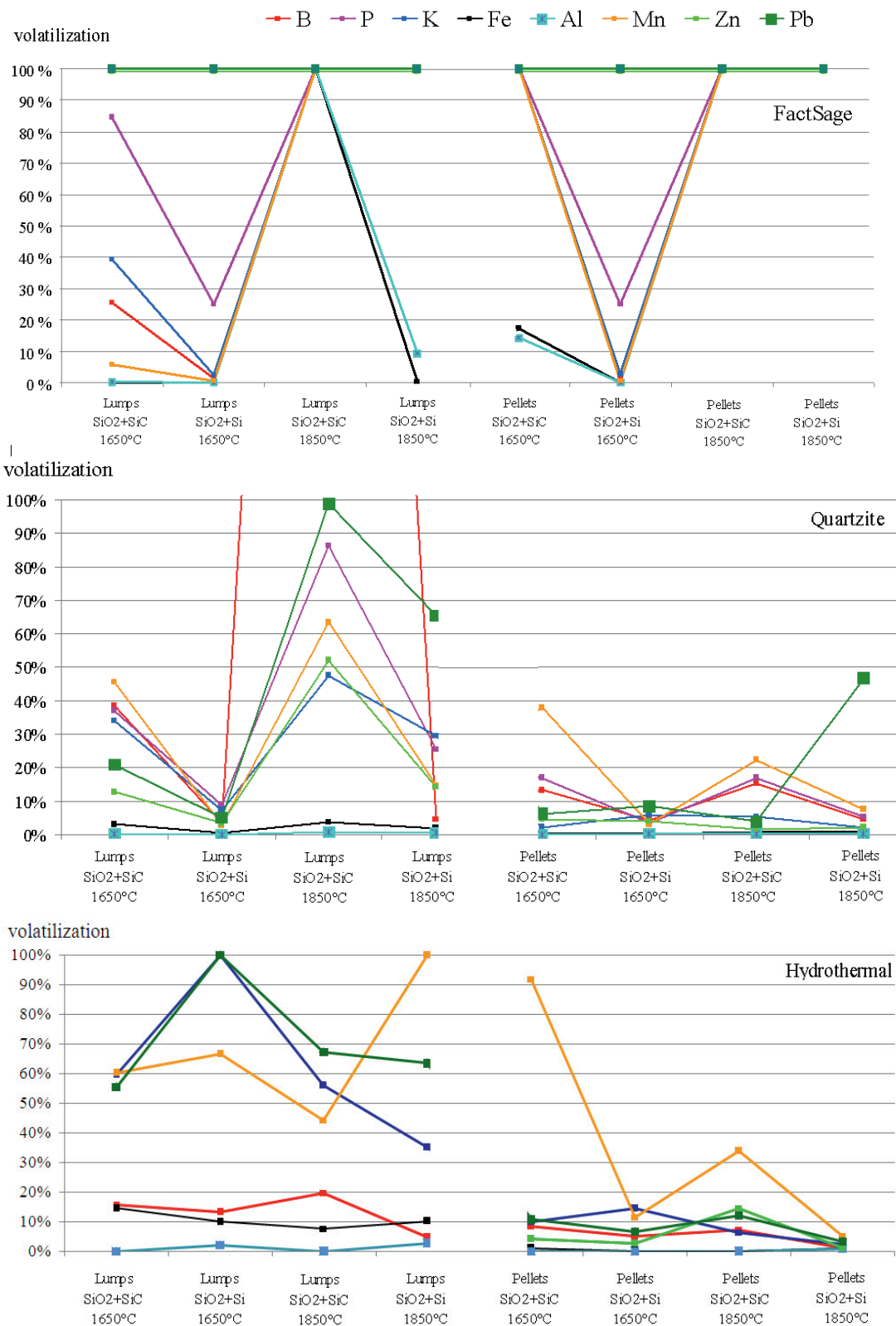


Fig.4- Volatilization of elements in mass % shown for different charge types, mixes and temperatures. Top to bottom; Thermodynamic calculations, quartzite and hydrothermal quartz. The volatility of P and Zn are not shown for all the experimental conditions in hydrothermal quartz because of the high concentration of these elements in the blank used as analytical reference.

Fig.5 shows the partial pressure of SiO and CO formed at equilibrium conditions, as calculated using the FactSage. The atmosphere created during the experiments, varies with the temperature, and the charge mix. In general, by decreasing the temperature and by increasing the amount of free carbon (i.e. by using pellets instead of lumpy charge or by using the charge mix SiO₂+SiC instead of SiO₂+Si) the equilibrium partial pressure of SiO (P_{SiO}) decreases in favour of P_{CO} . It should be mentioned that the experiments were carried out in argon, which was the main gas component in the reduction experiments ($P_{CO} + P_{SiO} < 1$).

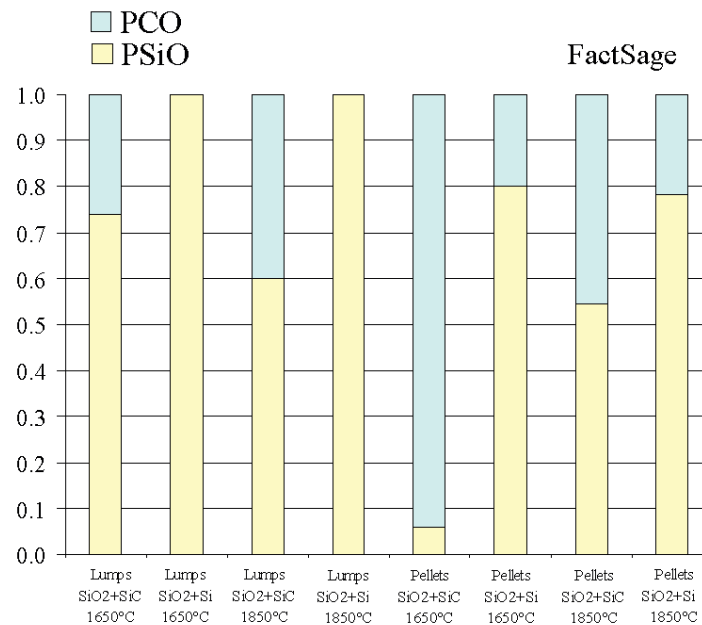


Fig.5 Partial pressure P_{CO} and P_{SiO} formed at equilibrium conditions calculated with FactSage.

Fig.4 shows that all the elements, which were found in the quartz charged, entered the gaseous phase. The volatility depends on the quartz type and the experimental conditions. The measured volatility of B for the experimental condition “Quartzite-Lumps SiO₂+SiC 1850°C” was significantly higher than 100%, which is probably a result of an analytical error.

In general, oxides more stable than SiO₂ remain in the mixed oxide/carbide/Si phase, while oxides less stable than SiO₂ are expected to reduce to pure elements or sub-oxides during the reduction of quartz. If these reduced compounds have a high partial pressure they will leave the quartz in form of gaseous compounds. Thermodynamic calculations volatilities depend both on the temperature and the charge mix: a higher volatilization is predicted at higher temperatures and higher P_{CO} .

The volatility of Fe, K, Mn and Pb for “lumps of hydrothermal quartz” lie on higher values than quartzite and pellets. *Lumps of quartzite* show a volatility profile similar to that thermodynamically predicted: higher volatility in correspondence of higher P_{CO} . *Pellets* of hydrothermal quartz and quartzite show a less pronounced dependence on P_{CO} . In general the volatility of the elements in pellets is lower than in lumps.

Experimental results show that *Al and Fe* have very low volatilities regardless the temperature, the partial pressure of CO (P_{CO}) and the quartz used. The average volatility of Al and Fe is 1 % and 4 % respectively. The low volatility of Al during quartz reduction is reflected in an increase in concentration of Al in quartz after reduction. This was confirmed in our previous paper [14] which studied the impurities in quartz after reduction. Fig.4 shows that Fe is more volatile in lumps than in pellets. This behavior is particularly evident when hydrothermal quartz is used. This finding is in agreement with Part1 which studied the impurity content of quartz after reduction: Fe was more easily removed from lumpy quartz than from pellets charge, in particular when hydrothermal quartz was used. According to thermodynamic calculations, the main Fe and Al-based gaseous compounds which

form are: Al(g) (b.p. 2792 K, (2519 °C)) and Al₂O(g) (b.p. room temperature) and Fe(g) (b.p. 3134 K (2861 °C)).

The average measured volatility for *K* is 26%. The two quartzes show the same trend when pellets are used (maximum volatility for the experimental condition “pellets SiO₂+Si 1650°C”) and a different trend when lumps are used. Quartzite lumps feature a volatility in agreement with the thermodynamic prediction. The main gaseous compound predicted by calculations is K(g) (b.p. 1032 K (759 °C)).

Experimental and thermodynamic results disagree on the behavior of *Zn and Pb*. According to thermodynamic calculations, the volatility of Zn and Pb should be 100%. Zn and Pb oxides are less stable than quartz and are easily reduced to Zn(g) (b.p. 1180 K (907 °C)) and Pb(g) (b.p. 2021 K (1748 °C)). However experimental results show that the average volatility of Zn is only 10% and of Pb 36%. A possible explanation for this behavior might be that Zn and Pb formed sub-oxides not predicted by the thermodynamic calculations.

The volatility of *Mn, P and B* depends strongly on the charge mix: at high P_{co} pressure, corresponding to the charge mix “SiO₂+SiC” the volatility of Mn, P and B increases. Mn, P and B are less stable oxides than quartz and are hence reduced to pure elements or sub-oxides having a relatively low boiling point. The main gaseous species which form according to thermodynamics are P(g) b.p. 553 K (280 °C), P₂(g), PO(g) b.p. room temperature and Mn(g) b.p. 2335 K (2062 °C). The average measured volatility of Mn, P and B is 38%, 25%, 11% respectively.

Fig.4 shows that boron has lower volatility than Mn for all the experimental conditions, and lower than Pb for most of the experimental conditions. B is generally less extracted from the charge than Mn and Pb, the reason might be that B is a more stable oxide than Pb and Mn oxides or has lower diffusivity.

3.3 Impurity volatility: effect of fluid inclusions

Fig. 6, another way of presenting the results in Figure 4, shows the volatility of each element under different experimental conditions and the quartz type (hydrothermal quartz in blue bars and quartzite in yellow bars).

Figure 6 shows that Pb, Fe, Mn, K have higher volatility in hydrothermal quartz than in quartzite when lumps are used. This trend can be attributed to fluid inclusions present in hydrothermal quartz. Fluid inclusions are only present in lumps of hydrothermal quartz; they are removed during quartz milling to the micrometres size in preparation of pellets. Fluid inclusions comprise water in solution with Na⁺, K⁺, F⁻, Cl⁻, CO₂, CH₄ and other contaminants. Fluid inclusions may have enhanced the volatilization by increasing the surface available to reduction of the quartz or by enhancing the formation of volatile Cl-based compounds.

During heating of quartz, the internal pressure of the fluid inclusions increases and they decrepitate; i.e. fissures run through the inclusions enabling removal of water vapour and CO₂ from the inclusions. Decrepitation occurs from 473 to 873 K (200 to 600 °C) depending on the fluid composition. Fluid inclusion decrepitation leaves cracks in quartz [17]. The cracks increase the surface available to reduction, reduce the diffusion distance to the surface and therefore increase the volatilization.

Fe, K, Pb and Mn in the quartz lattice or mineral impurities may react with H₂O and Cl⁻ ions in the fluid inclusions, and form volatile compounds, which are subsequently liberated during reduction of the quartz. According to Larsen [18] elements like Ca, Fe, Mg and Mn are likely to be concentrated in sub microscopic fluid inclusions. The affinity of Fe with Cl⁻ was studied in other works [19].



Fig. 6 Volatility of elements (mass %) for different experimental conditions. Note the difference in volatility scale between the individual graphs.

FactSage equilibrium calculations also indicate that addition of Cl to quartz improves the evaporation of the impurities. Calculations with the addition of 100 ppmw Cl to the system showed that main gaseous compounds formed are: AlCl₃(g), BCl₃(g), FeCl₂(g), KCl(g), MnCl₂(g), PCl₃(g), PbCl₂(g), ZnCl₂(g). The results of the thermodynamic calculations are shown in Fig.7. Two experimental conditions are studied: “Lumps SiO₂+SiC 1650 °C” and Lumps “SiO₂+SiC 1850 °C“. In both cases, the volatility increases in presence of Cl.

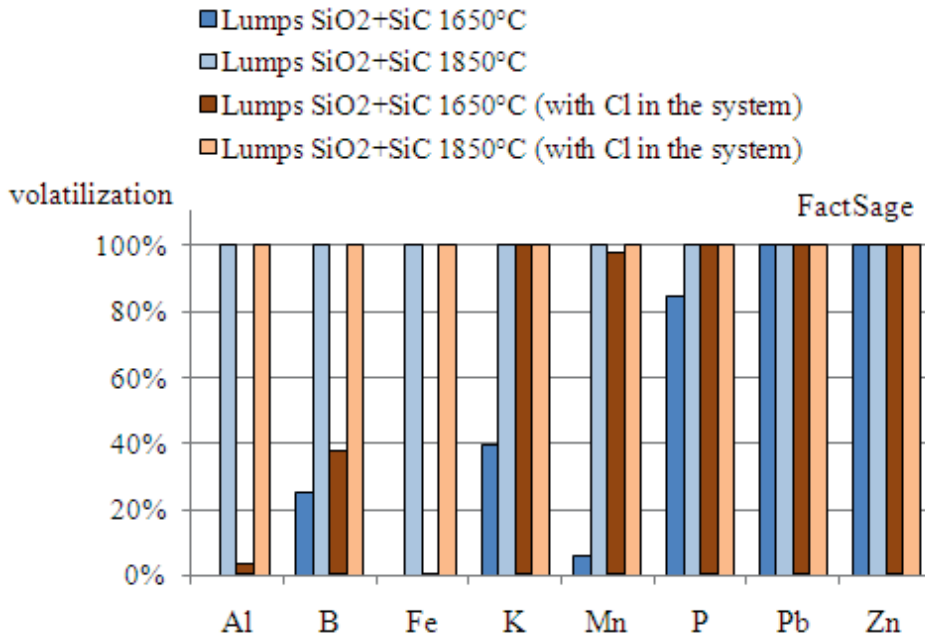


Fig. 7 Effect of chlorine on volatilization of impurities oxides in quartz during quartz reduction calculated using FactSage.

3.4 Impurity volatility: comparison with industrial measurements

Myrhaug and Garcia [2, 4] studied the distribution of contaminants between a condensed phase (metal and slag), off-gases and microsilica for a Fe-Si and a Si furnace.

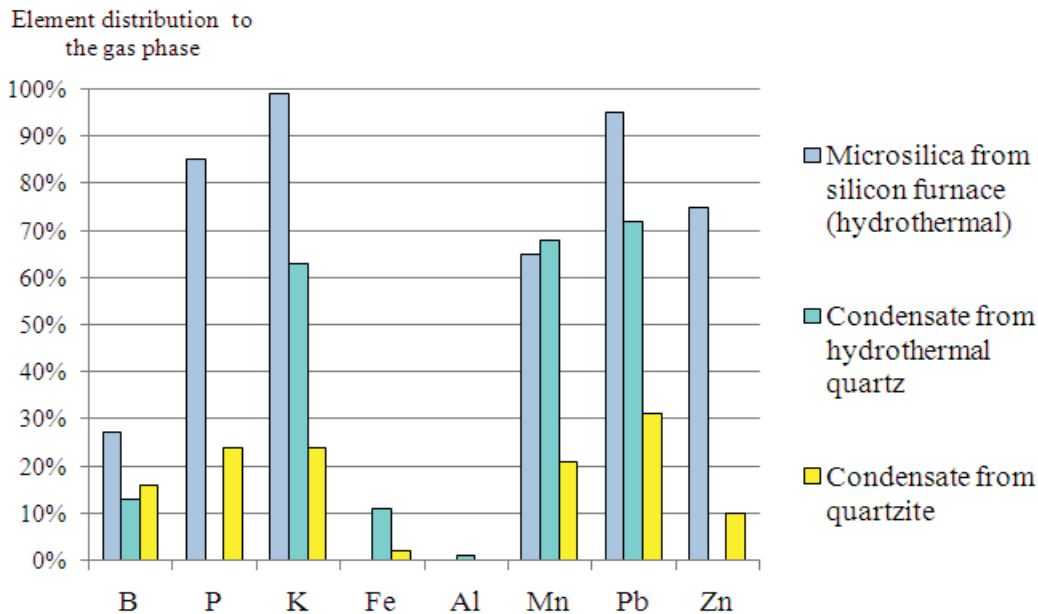


Fig. 8- Distribution of trace elements to microsilica from a Si furnace [2] (light blue bars), compared to distribution of elements to the gas phase collected as condensate (dark blue bars when hydrothermal quartz was charged) in these experiments (dark yellow bars when quartzite was considered). Lumpy charge is here considered. All numbers are in weight %. Measurements in Zn, Fe, Al are partly available.

Figure 8 compares the distribution of the impurities in the industrial arc furnace to microsilica (Myrhaug and Garcia [2]) and to condensate in reduction of hydrothermal quartz and quartzite (this experimental work). Hydrothermal quartz was used for the Si industrial production.

In the industrial case the condensation occurs between 1973 K (1700 °C) – 1273 K (1000 °C) [8] while in the experimental work discussed in this article the condensate was produced down to far lower temperatures. Contrary to expectations, Figure 8 shows that the distribution of the elements to the condensate in these experiments is generally lower than the distribution of the elements to the microsilica in industrial experiments, although trends are the same. The difference in absolute numbers may be explained by different conditions in laboratory and industry experiments.

4 Conclusion

The major findings of this work are:

- Carbothermal reduction of silica generates CO(g) and SiO(g) which form four types of condensate (based on colour). The major constituents of the condensate phase are amorphous and crystalline SiO₂, β:SiC and Si.
- All the impurities which are present in the quartz charge enter the gas phase during quartz reduction to a varying degree.
- Al and Fe have a very low volatility in comparison with other elements.
- The average measured volatilities of B, P, K, Fe, Al, Mn, Zn, Pb determined experimentally are respectively 11%, 25%, 26%, 4%, 1%, 38%, 10%, 36%.
- The volatility of Mn, P and B depends on the charge mix: a higher P_{CO} enhances the distribution of these elements to the gas phase.
- Liquid inclusions, common in hydrothermal quartz, enhance the distribution of the contaminants to the gas phase.

Acknowledgment

The authors acknowledge John Sharp, Xing Xing and Xiaohan Wan for their excellent technical help and productive discussions. This research work has been supported by ELKEM's research fund.

References

1. Myrhaug, E.H., *Non-fossil reduction materials in the silicon process-properties and behaviour*. 2003, NTNU: Trondheim, Norway.
2. Garcia, M. and E.H. Myrhaug, *Revisjon av materialbalanse for sporelementer i Si-ovn basert på målekampanje på Elkem Thamshavn april 2007*. 2007, Elkem Silicon: Oslo.
3. Tveit, H. and E. Myrhaug, *Important sub-processes in the silicon process. The behavior of trace elements*. in *Silicon for the chemical industry V*. 2000. Tromsø.
4. Myrhaug, E.H. and H. Tveit, *Material Balance of trace elements in the Ferrosilicon and Silicon Processes*. Electric furnace conference proceedings, 2000. **58**.
5. Ishak, R.J., *Reaction kinetics for reduction of manganese ore with carbon monoxide in the presence of carbon*. 2002, NTNU.
6. Lee, Y.E. and D.S. Kozak, *The Role of Zinc in the Eruption of High Carbon FeMn Smelting Furnace*. Electric Furnace Conference Proceedings, 1993: p. 145-150.
7. Sterneland, J., *Alkalis in the HCFeMn-Furnace, a mass balance of potassium oxide on the furnace no 12 at Elkem Mangan a.s. PEA*, in *Department of Metallurgy*. 1993, Royal Institute of Technology, KTH: Stockholm, Sweden.
8. Schei, A., J.K. Tuset, and H. Tveit, eds. *Production of High Silicon Alloys*. 1998, Tapir forlag, N-7005 Trondheim.
9. Førland, T. and H. Flood, eds. *Selected topics in high temperature chemistry. A collection of papers dedicated to professor Håkon Flood on his 60th birthday, 25. Septemebr 1965*. Universitetsforlaget:Oslo, 1966.
10. Andersen, V., et al., *Small scale laboratory experiments simulating an industrial silicon furnace*, in *Infacon XII*. 2010: Helsinki, Finland.
11. Poch, W. and A. Dietzel, *Ber. Dtsch. Keram. Ges.*, 1962. **39**: p. 413-426.
12. Schei, A., *Tidsskr. Kjemi Bergv*, 1967. **27**: p. 152-158.
13. Vangskåsen, J., *Condensate formation in the silicon process*. 2011, NTNU, Department of Materials Science and Engineering: Trondheim -Internal report.
14. Dal Martello, E., et al., Submitted to *Met Trans B*, June 2012.
15. Albinati, A. and B.T.M. Willis, *J. Appl. Cryst.*, 1982. **15**: p. 361-374.
16. Dal Martello, E., et al., *Met. Trans. B*, October 2011. **42**(5): p. 939-950.
17. Gemeinert, M., et al., *Neues Jahrbuch Miner. Abh.*, 1992. **165**(1): p. 19-27.
18. Larsen, R.B., I. Henderson, and P.M. Ihlen, *Contrib. Mineral. Petrol.*, 2004. **147**: p. 615-628.
19. Fein, J.B., et al., *Geochim Cosmochim Ac*, 1992. **56**: p. 3179-3190.

